## *Oligofluorene molecular wires in donor-acceptor conjugates*

Cornelia Van Der Pol

# Oligofluorene Molecular Wires

# in

# Donor-Acceptor Conjugates


## Cornelia van der Pol

**Ustinov College**





**Department of Chemistry**

**University of Durham**


A thesis submitted for the degree of Doctor of Philosophy at the University of Durham.

October 2007

## STATEMENT OF COPYRIGHT



## DECLARATION

The work described in this thesis was carried out in the Department of Chemistry at the University of Durham between October 2004 and September 2007. All the work was carried out by the author unless otherwise stated and has not previously been submitted for a degree at this or any other university.

# Table of Contents

# Abstract

## Oligofluorene Molecular Wires in Donor-Acceptor Conjugates

Cornelia van der Pol, University of Durham, 2007

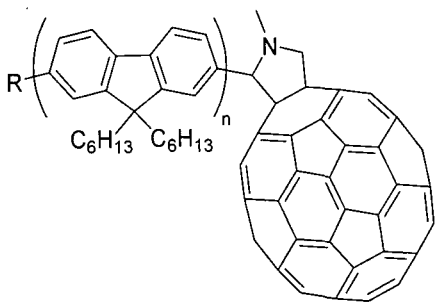


**51a,b,c** n = 2, 3, 4 R = H
**53a,b,c** n = 2, 3, 5 R = *N*-methyl pyrrolidinofullerene
**57a,b** n = 1, 2 R = *ex*TTF
**68a,b** n = 1, 2 R = Ph-ZnP-(*t*BuPh)$_3$
**74a,b** n = 2, 3 R = ZnP-(*t*BuPh)$_3$
**80a,b** n = 1, 2 R = yne-Fc
**96a,b** n = 1, 2 R = Ph-SAc

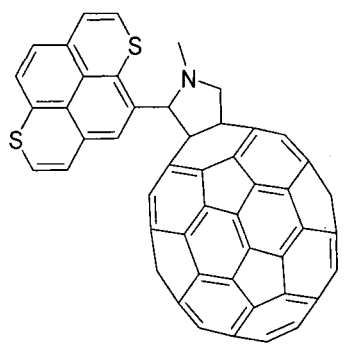


**88** DTPY-$C_{60}$

The molecular wire behaviour of oligofluorenes has been investigated by the synthesis of novel covalently bound fluorene-$C_{60}$ derivatives. Firstly, oligofluorene derivatives containing one or two pyrrolidinofullerene units at their termini (**51** and **53**) were synthesized and their electronic properties investigated. This was followed up by the preparation of donor-acceptor conjugates - using $C_{60}$ as acceptor - whereby fluorene is utilised as connecting unit. Triads containing different electron donors such as *p*-quinonoid π-extended tetrathiafulvalene (*ex*TTF), zinc(II) porphyrin (ZnP) and ferrocene (Fc) were synthesised, *i.e.* **57**, **68**, **74** and **80** respectively. The electrochemical and photophysical behaviour of **57** has been discussed, together with the electrochemical studies of **68**, **74** and **80**. Photophysical studies for the latter three are currently being undertaken. Additionally, we herein report the investigation of novel DTPY-$C_{60}$ dyad **88** and the synthesis of two thiol terminated fluorene-pyrrolidinofullerene derivatives **96a,b**.

# Acknowledgements

I would like to thank Martin R. Bryce for providing me with this 'character-building' opportunity. I am grateful to have been allowed to work on this interesting, versatile and challenging project and I have really enjoyed the multidisciplinary collaborations and conferences. Thank you very much for your advice and guidance.

Nazario Martín is thanked for welcoming me in his group for six weeks during my second year. Nazario, your advice and kind words have been greatly appreciated. Nazario's group is unbelievably friendly and I would like to thank them all for their kindness towards me. Especially Salvatore Filippone is thanked for his advice, patience and friendship. I would like to acknowledge him for his advice on the Prato reaction (Chapter 2) and his extensive help with the preparation and electrochemistry of the *ex*TTF-fluorene-$C_{60}$ systems (Chapter 3). Mª Ángeles Herranz is acknowledged for advice on electrochemistry.

Muchas gracias!

The theoretical calculations in Chapter 3 and photophysical measurements in Chapter 2 and 3 were investigated by Mateusz Wielopolski, Carmen Atienza-Castellanos and Dirk M. Guldi. They will also perform the photophysical measurements on the compounds discussed in Chapter 4 in the near future. The photophysical behaviour of the compounds discussed in Chapter 5 was investigated by Dirk M. Guldi, Fabian Spänig, Kei Ohkubo and Shunichi Fukuzumi. Thank you, Mateusz, for an enjoyable collaboration. I would like to thank Dirk for advising me to go to America; you really provided me with some 'food for thought'. In this respect, I would like to thank Guillermo Bazan for giving me a post-doc position. Gui, I look forward to joining your group and coming to America in November.

Danke schön!

I would like to thank all members (past, present and visitors) of Martin's group. I have enjoyed your company during these three years. Igor F. Perepichka is thanked for the electrochemistry and theoretical calculations on both dyads discussed in Chapter 5. David Kreher is acknowledged for his initial synthesis of DTPY-$C_{60}$ (Chapter 5). Changsheng

Wang is kindly thanked for synthesising and providing ethynylferrocene. I would like to thank the service staff at the university, especially the NMR team for their patience with the 12-24 hour long $^{13}$C-NMRs and the barely soluble samples.

Thank you very much!

For a truly wonderful time I thank all the nice people I have met during the regular conferences. Anders Madsen is acknowledged for his advice on porphyrin chemistry. Special thanks go to Bo.

Mange tak!

Lastly, I would like to thank my friends and family for their continuous support. Special thanks go to my brother Lammert and Lianne. There are no words to describe how much I appreciate the support and love I receive from my parents. Ik ben zo dankbaar voor de steun en liefde die ik van mijn ouders krijg dat het niet in woorden is uit te drukken.

Dank je wel!

The following papers are based on work described in this thesis:

- C. van der Pol, M.R. Bryce, M. Wielopolski, C. Atienza-Castellanos, D.M. Guldi, S. Filippone and N. Martín; **Energy versus Electron Transfer in Oligofluorene-$C_{60}$ and $C_{60}$-Oligofluorene-$C_{60}$ Donor-Acceptor Conjugates**, *J. Org. Chem.*, **2007**, *72*, 6662.

- C. Atienza-Castellanos, M. Wielopolski, D.M. Guldi, C. van der Pol, M.R. Bryce, S. Filippone and N. Martín; **Determination of the Attenuation Factor in Fluorene-based Molecular Wires, 2007**, DOI: 10.1039/b711678k. Published Online: 9 Oktober 2007.

- D.M. Guldi, F. Spänig, D. Kreher, I.F. Perepichka, C. van der Pol, M.R. Bryce, K. Ohkubo and S. Fukuzumi; **Contrasting Photodynamics between $C_{60}$-Dithiapyrene and $C_{60}$-Pyrene Dyads**, *Chem. Eur. J.*, **2007**, DOI: 10.1002/chem..200700837. Published Online: 28 September 2007.

# Abbreviations

| | |
|---|---|
| A | Electron acceptor |
| B | Bridge (*i.e.* connecting unit) |
| BA | Boronic acid |
| BE | Boronic ester |
| b.p. | Boiling point |
| $B_2Pin_2$ | Bis(pinacolato)diboron |
| COSY | Correlation spectroscopy |
| CV | Cyclic voltammogram |
| D | Electron donor |
| DABCO | 1,4-Diazabicyclo[2,2,2]octane |
| *o*DCB | *o*-Dichlorobenzene |
| DCM | Dichloromethane |
| DFT | Density-functional theory |
| DMF | *N*,*N*-dimethylformamide |
| DTPY | 1,6-Dithiapyrene |
| *ex*TTF | 9,10-Bis(1,3-dithiol-2-ylidene)-9,10-dihydroanthracene |
| F | Molecular fluorescence |
| Fc | Ferrocene |
| Fl | 9,9-Dihexyl-9*H*-fluorene |
| HOMO | Highest occupied molecular orbital |
| HMBC | Heteronuclear multiple-bond correlation |
| HSQC | Heteronuclear single quantum correlation |
| IC | Internal conversion |
| ISC | Intersystem crossing |
| ITO | Indium tin oxide |
| LUMO | Lowest unoccupied molecular orbital |
| NMR | Nuclear magnetic resonance |
| MALDI | Matrix-assisted laser desorption/ionisation |
| MO | Molecular orbital |

| | |
|---|---|
| m.p. | Melting point |
| MS | Mass spectrometry |
| NBS | *n*-Bromosuccinimide |
| NOESY | Nuclear Overhauser effect spectroscopy |
| OAc | Acetate |
| OD | Optical density |
| OLED | Organic light emitting diode |
| OPE | Oligo-*p*-phenyleneethynylene |
| OPV | Oligo-*p*-phenylenevinylene |
| OT | Oligothiophene |
| OTE | Oligo(thienylene-ethynylene) |
| PDI | Pyrylene-3,4:9,10-bis(dicarboximide) |
| PE 40-60 | Petroleum Ether b.p. 40-60 °C |
| PEDOT | Poly(3,4-ethylene dioxythiophene) |
| PhCN | Benzonitrile |
| PPV | Poly-*p*-phenylenevinylene |
| PSS | Poly(styrene sulphonate) |
| PT | Polythiophene |
| PTZ | Phenothiazine |
| r.t. | Room temperature |
| $S_0$ | Singlet ground state |
| $S_1$ | First singlet excited state |
| SAM | Self-assembled monolayer |
| SPM | Scanning probe microscopy |
| THF | Tetrahydrofuran |
| TLC | Thin layer chromatography |
| TMS | Tetramethylsilane |
| TOF | Time-of-flight |
| TTF | Tetrathiafulvalene |
| UV | Ultraviolet |
| yne | Alkyne |
| ZnP | Zinc(II) porphyrin |

# Chapter 1: Introduction

## 1.1 Molecular Electronics

*"I don't know how to do this on a small scale in a practical way, but I do know that computing machines are very large; they fill rooms. Why can't we make them very small...the wires should be 10 or 100 atoms in diameter, and the circuits should be a few thousand angstroms across...there is plenty of room to make them smaller. There is nothing that I can see in the physical laws that says the computer elements cannot be enormously smaller than they are now."*

Quote from physicist R.P. Feynman's lecture.

### Moore's Law

Research towards electronics has grown rapidly since the beginning of the 20th century. This was largely due to the increasing interest in radio, telephone and radar. The first transistor was developed in 1947[1] and in less then twenty years new techniques were developed to make fabrication easier.[2] The circuits were in comparison to today quite large, *e.g.* around 1965 Gordon Moore was able to integrate approximately sixty components on a chip set against 60,000 in 1975.[3, 4] The idea of scaling the integrated circuits down to a molecular level was first suggested by Richard Feynman in 1959 (see quote above).[5] At this time the capability of working on the molecular scale had not been realised. A few years later, Gordon Moore was asked to report on how integration technology would develop and he predicted that the number of transistors per $cm^2$ of silicon would double every year for the following ten years.[3] Ten years onwards his statement was remarkably close to the truth and was revised to state that the density on a chip would double every two years.[4] Currently known as Moore's Law, it should be

accurate for another ten to fifteen more years, at most, before components reach the molecular scale. Current techniques can only be scaled down to a certain level and in order to produce electronic circuits on a molecular scale new techniques will have to be developed.

## Bottom-up Approach

Scaling down conventional electronics is easier said than done, since several problems will have to be addressed before electron transfer on a molecular scale can be controlled. One of the challenges will be to tackle electromigration, which occurs as a current passes through a wire.[2] Electromigration can eventually lead to a failing connection, as it means that the current can pass its momentum onto the atoms in the framework. This is very likely to occur when high current densities are passed through the wire or at elevated temperatures, *e.g.* due to resistance produced by defects. Another problem that increases as size decreases is tunnelling, as there is less space between device components current can tunnel between them instead of travelling along them.[2] Advances in scaling down integrated circuits are made daily, but this does not change the fact that fundamental limits will be reached before achieving electron transport within molecular devices.

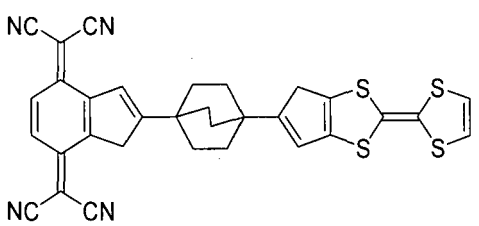


**1**

Therefore, research is focusing on obtaining a better understanding of electronics on a molecular scale. Molecules containing a function are synthesised, characterised and even assembled with other components to build an electrical device. The first efforts towards molecular electronics were made in the early 1970s. In a visionary theoretical paper Aviram and Ratner proposed the preparation of the famous compound **1** as a molecular rectifier to predict and characterise an electronic phenomenon on a molecular scale.[6] The use of single molecules as rectifiers was suggested and complex device ideas involving

molecular logic structures were discussed. This article was perhaps a bit premature, since some of the results were retracted in time.[7] Although this article has been repeatedly referenced as the earliest paper published in this field, the group of Hans Kuhn had published reproducible electrical transport measurements through organic molecules in 1971.[8, 9] A lack of analytical techniques had held research back until renewed focus onto molecular electronics was stimulated by the development of scanning probe microscopy (SPM), as this technique expanded the manipulation and measurement possibilities on a molecular scale.[10]

## Molecular Electronics

Research within the field of molecular electronics is focused on the question whether it is possible to control electronic devices on a molecular scale. Molecular electronics can be seen as technologies using only single molecules, but a slightly broader view such as devices using molecular properties is currently more appropriate. A generally accepted definition of molecular electronics is technology utilising single molecules, a small group of molecules, nanoscale metallic/semiconductor wires or carbon nanotubes to perform electronic functions.[2] In order to prepare a molecular electronic device there are some terms that should be complied with, *e.g.* for long-term use the molecules used are required to be chemically stable and show reversible electron transfer. The device units must be inert to other local molecules to avoid electromigration or tunnelling and they need to remain at the desired position. External interaction with the device in order to exchange information will also provide an interesting challenge.

Since the field is still relatively new, solutions are not readily available. Critics might ask whether a device of molecular dimensions will ever be of practical use,[11] but as research moves forward each day new discoveries are made. With time a better understanding of processes on a molecular scale is obtained and synthetic/analytical methods will be improved, which makes predicting the whereabouts of science in a hundred years time nearly impossible. Already organic materials of macroscopic proportions are utilised in devices, *e.g.* liquid crystalline materials in displays.[12]

## 1.2 Molecular Wires

Approximately a decade after the development of SPM the field of molecular electronics started to evolve rapidly. Currently, roughly fifteen years onwards, the field has expanded so vastly that this thesis can only focus on a small aspect. As photoinduced electron- and/or energy transfer processes already play vital roles in biological processes (*e.g.* in photosynthesis), it is a topic of great scientific interest in the field of molecular electronics. In this field we will mainly focus on molecular wires, which can allow and influence the transport of electrons or energy between two electron resevoirs.

### Electron- and Energy Transfer

Molecular wires are employed as a bridge (B, *i.e.* connecting unit) between two chromophoric units - *e.g.* an electron donor (D) and an electron acceptor (A) - and should enable efficient long-distance photoinduced electron transfer or energy transfer.[13] In a D-B-A system photoinduced electron- and energy transfer can be indicated as:

| | | |
|---|---|---|
| -1- | photoexcitation | D-B-A + $h\nu \rightarrow$ *D-B-A |
| -2- | (oxidative) electron transfer | *D-B-A $\rightarrow$ $D^+$-B-$A^-$ |
| -3- | (electronic) energy transfer | *D-B-A $\rightarrow$ D-B-*A |

Photoinduced electron transfer processes are followed by a charge-recombination process, which regenerates the initial ground state of the system, provided no chemical complications occur:

| | | |
|---|---|---|
| -4- | back electron transfer | $D^+$-B-$A^-$ $\rightarrow$ D-B-A |
| -5- | excited state decay | D-B-*A $\rightarrow$ D-B-A |

## π-Conjugated Wires

The bridge linking the photoactive units plays a vital role in the transfer process as its structural and chemical nature controls the electronic communication between the selected terminal moieties.[14, 15] An electron can move from the donor to the acceptor via the superexchange mechanism, where the electron jumps/hops through space to the acceptor. The rate of electron transfer ($k_{et}$) depends on the link between the electroactive substances, *e.g.* the electron would have to jump through space when the species are not linked. A σ-bridge would separate the donor and acceptor in such a way that the species do not interact or need a lot of energy to transfer to electron. In the majority of donor-acceptor systems the electron transfer rate will be closely related to the donor-acceptor distance.

A molecular wire will allow long-range hole- or electron-transfer along its conductive path of atomic orbitals for which a lower energy boost is required than for the superexchange mechanism (Figure 1.1). This is possible because the virtual bridge states are energetically comparable to the donor level. Through thermal injection into the conduction band of the bridge, the electron becomes localised within the bridge and is transported through the bridge towards the acceptor by an incoherent scattering mechanism, such as a polaron.

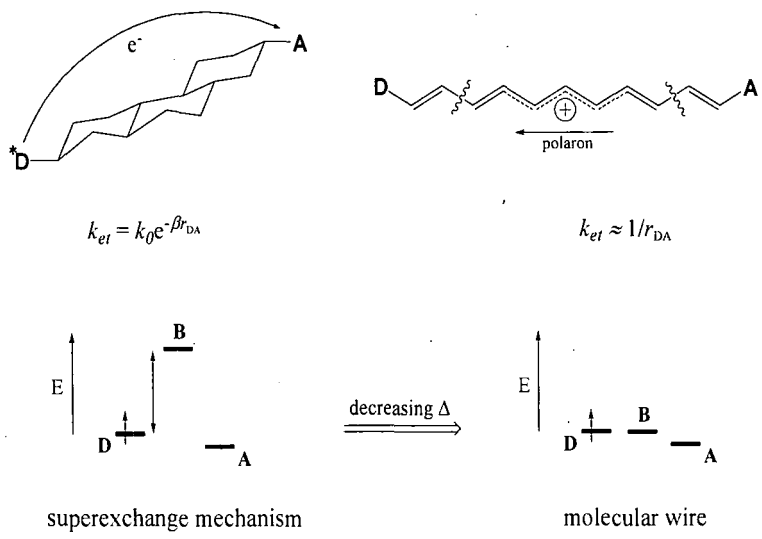


Figure 1.1: Schematic illustration of the difference between the superexchange mechanism and molecular wire behaviour. As the virtual bridge state becomes energetically comparable to the donor level the D-B-A ensemble will start expressing molecular wire behaviour.

Donor and acceptor moieties covalently attached by a rigid rodlike π-conjugated bridge have received substantial interest as dipolar chromophores due to their unique electroactive and non-linear optical properties.[16] A major advantage of these molecular systems is the possibility of tailoring the organic materials for specific applications. A conjugated oligomer bridge can be considered as a giant chromophore whose molecular orbitals are essentially delocalised over the entire bridge. The extended π-systems of conjugated oligomers qualify them as chromophores with a broad range of optical properties and as electrophores with the ability to accept or donate charges.[17] Conjugation within the oligomers with a rigid structure can limit the solubility severely, hindering sample preparation and processing. Improved solubility can be achieved by the attachment of alkyl substituents onto the chain. These alkyl chains provide a solvation shell, but any solubilising chains that do not possess extended π-systems will dilute the electronically active function of the oligomer bridge. Alkyl substitution weakens π-conjugation by inducing torsion about formal single bonds and can inhibit a tight packing of molecules in solid state.

## 1.3 Molecular Wire Efficiency

The efficiency of a molecular wire in electrochemically active systems can be determined through a range of different techniques and the method used to characterise triads is dependent upon the research group investigating their properties. Purity of the desired systems is essential before commencing any analytical, electrochemical and optical measurements. In theory any defects or impurities can affect the results and reproducibility should always be investigated. It should be noted that in this thesis covalently linked donor-acceptor systems are referred to as dyads. Donor-bridge-acceptor (D-B-A) and acceptor-bridge-acceptor (A-B-A) assemblies will herein be classified as triads.

The conductivity of molecular wires in the, herein discussed, triads will be subjected to electrochemical measurements[18-20] and photo-induced electron transfer experiments.[13, 20-24] Determination of the attenuation factor (β) will provide an indication of the wire-like behaviour of the bridge connecting the donor and acceptor moieties. Computational

chemistry[25, 26] (*e.g.* DFT calculations) can be used to aid the prediction and/or interpretation of experimental observations.

### 1.3.1 Electrochemical Measurements

Cyclic voltammetry is often used for the characterisation of electrochemically active systems, since it provides information on thermodynamic and kinetic data of electron transfer reactions and allows a precise analysis of multistep redox mechanisms.[18, 20] The electrochemical technique uses microelectrodes and an unstirred solution so that the measured current is limited by analyte diffusion at the electrode surface. Cyclic voltammetry consists of the same principles as linear sweep voltammetry, but with the main difference that a reverse scan is included in the experiment. In linear sweep voltammetry the potential of the working electrode is varied over time linearly between two values. While the potential changes continuously an uninterrupted level of current flows. Faradaic current will flow when the potential reaches values at which the analytes can undergo electrochemical conversions. This will result in a current peak for the reduced species on the forward scan, which falls off as the concentration of the analyte is depleted close to the electrode surface.

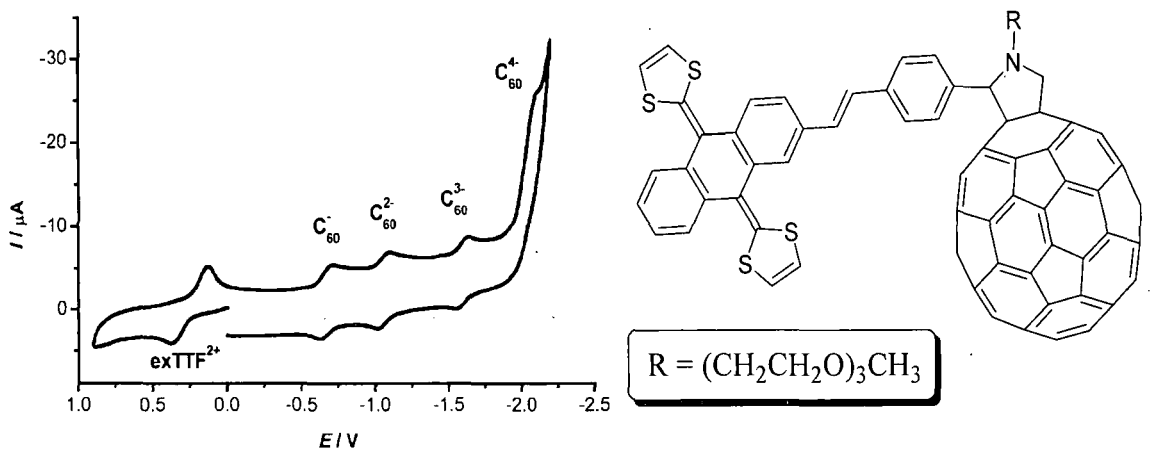


**2**

Figure 1.2: An example of a cyclic voltammogram (CV). CV of **2** with *o*DCB/$CH_3CN$ (4/1 v/v) as solvent mixture and a scan rate of 200 mV $s^{-1}$. (Taken from the literature[27]).

As for cyclic voltammetry, when the applied potential is reversed, a potential will be reached which can reoxidise the product formed in the forward scan and produce a current of the reverse polarity to the first reduction reaction. Therefore, stable species should have an oxidation peak with a similar shape to the reduction peak. With the use of cyclic voltammetry the reverse scan can even be swept past the initial potential and taken back to the initial value with a third linear sweep. Figure 1.2 illustrates an example of a cyclic voltammogram. Cyclic voltammetry can be used to obtain a vast amount of information, because it indicates the number of different redox states and gives qualitative information about the stability of these oxidation states and the electron transfer kinetics. For example, donor-acceptor species will display an oxidation potential shifting towards more positive values as there is a stronger interaction between donor and acceptor. Use of identical experimental conditions will ensure that redox features in related analogues can be compared.

## 1.3.2 Photophysical Measurements

### Fluorescence

The photo-induced electron transfer measurements use conjugates in which irradiation leads to the transport of an electron from the donor to the acceptor (Figure 1.3). Figure

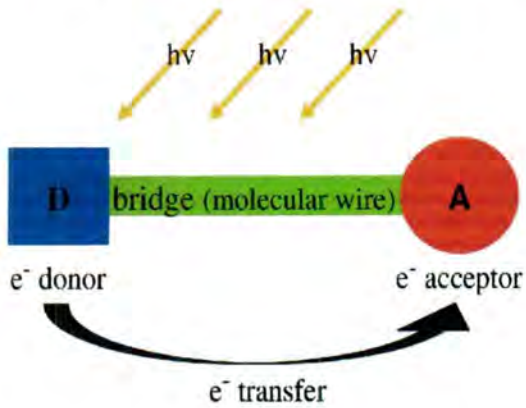


Figure 1.3a

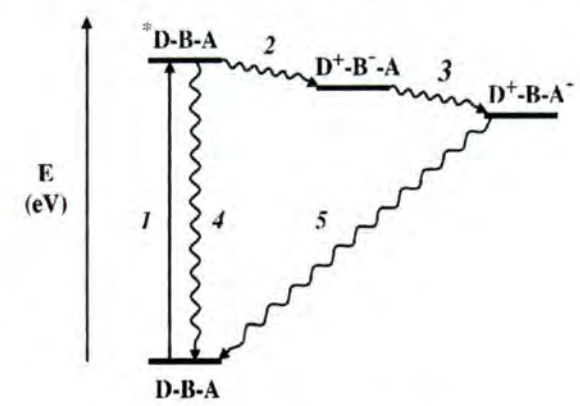


Figure 1.3b

Figure 1.3: Schematic representation (left) of the formation of a charge-separated state in a triad and its simplified schematic energy-level diagram (right).

1.3b is a simplified schematic energy-level diagram for a triad and although it is slightly more complex than herein presented, it can be used to explain the basic principle. Upon excitation of the chromophoric donor unit in a dyad to its singlet excited state $S_1$ (process 1) a rapid electron transfer to the acceptor moiety follows to form the charge-separated state (process 2 and 3), which will undergo charge-recombination (process 5) and allow the dyad to return back to the ground state ($S_0$).[13] Excitation of either the electron donor or the bridge (molecular wire) in the triad to the singlet excited state can lead to the charge-separated state. Upon transition of the electronically excited molecule to the ground electronic state light is emitted, *i.e.* luminescence. Luminescence emitted by the molecule during transitions between states of the same spin multiplicity is defined as molecular fluorescence (F).

Apart from emission of light, the excess energy can be released as heat and the two major nonradiative transitions are internal conversion (IC) and intersystem crossing (ISC), which involves transitions between states of, respectively, the same or different spin multiplicity.[21] Besides these unimolecular decay processes, the presence of a second type of molecule – able to remove the excess energy of the fluorescence species – can introduce a bimolecular decay process, *i.e.* quenching.[21]

Molecular fluorescence is recorded as a plot of fluorescence intensity versus emission wavelength. Fluorescence spectra are generally broad and cover a range of emission wavelengths, due to the existence of various vibrational (and rotational) levels in each electronic state. Fluorescence spectroscopy is an extremely sensitive technique and has a low background signal. This characterisation method will provide several physical parameters describing the performance of a triad:

| | | |
|---|---|---|
| -1- | wavelength(s) of maximum emission | $\lambda_{max}$ |
| -2- | quantum yield of charge separation | $\Phi$ |
| -3- | lifetime of charge separation | $\tau$ |
| -4- | efficiency of energy conversion | $\eta$ |
| -5- | attenuation factor | $\beta$ |

The fluorescence quantum yield is the fraction of molecules excited to the charge-separated state that decays by fluorescence. The lifetime of charge separation depends on the rate on the final charge-recombination process and the efficiency of energy conversion depends on the quantum yield and the fraction of excited state energy conserved in the final charge-separated state.

## Attenuation Factor (β)

The attenuation factor (β) is a key parameter often used as a benchmark to evaluate the wire-like behaviour of the bridge connecting the donor and acceptor units.[28] Both charge-separation and charge-recombination processes occur with kinetics defined by the electron transfer rate constant: $k_{ET} = k_0 e^{-\beta r_{DA}}$, where $k_0$ is a kinetic prefactor and $r_{DA}$ (Å) represents the donor-acceptor distance. The electron transfer rate is determined largely by the distance and the medium between the two electroactive sites, *i.e.* β ($Å^{-1}$). The smaller the β factor, the longer the distance over which charge can be efficiently conducted. The β factor is primarily dependent on the nature of the bridge unit and typical values range between 1.0 and 1.4 $Å^{-1}$ for proteins and between 0.01 and 0.04 $Å^{-1}$ for highly efficient π-conjugated oligomers.

The molecular wire behaviour can be strongly affected by other factors such as the matching energy levels of the bridge and the donor and therefore it is important to refer to the same donor and acceptor moieties in order to obtain a reliable comparison between the different π-conjugated bridges. As the wires become more and more efficient, a slight problem with this method to analyse the conjugated bridge becomes obvious. While efficient wires increase the electron transfer rate almost towards the limit for the redox moiety in question, the attenuation factor β approaches the theoretical minimum from an electrochemical conversion standpoint. As this occurs the transfer rates exceed a level that can be measured by common electrochemical methods.[19]

### Steady-State Fluorescence Spectroscopy

Steady-state fluorescence is the most-commonly used fluorescence technique, in which the solution containing the fluorescence species (*e.g.* a triad) is continuously illuminated by a stable excitation light source. Due to the constant intensity of the excitation light, the rate of photoexcitation and of charge-recombination is constant and the steady-state concentration of charge-separated molecules can be established. The fluorescence intensity is constant and is plotted in a fluorescence spectrum as a function of the emission wavelength ($\lambda$).

### Time-Resolved Fluorescence Spectroscopy

Time-resolved fluorescence allows for the determination of the fluorescence lifetime of the system. As it also provides an independent determination of some of the information obtained from steady-state fluorescence the two overlapping and complementary techniques should both be used to provide a complete profile of the investigated system. Time-resolved pulse techniques, unlike steady-state techniques, employ a short flash of excitation light to generate an initial population of the excited state. This population immediately begins to decay and as this population is directly proportional to the fluorescence intensity it decays with the same kinetics. The fluorescence intensity is measured as a function of wavelength at several given times after the excitation pulse, providing time-resolved fluorescence spectra. This technique requires a fast excitation pulse and fast electronics, as fluorescence decays occur mostly in the order of ns or ps.

## 1.4 Organic Solar Cells

### Fullerene $C_{60}$

Fullerene $C_{60}$ **3** was discovered by Kroto *et al.* in the laser vaporisation of graphite in 1985.[29] The demonstration of the large-scale synthesis[30] of fullerenes soon afterwards initiated extensive research efforts towards exploring their properties and applications.[17, 31-

[37] The delocalisation of charges – both electrons and holes – within the spherical carbon framework together with the rigid, confined structure of the aromatic π-sphere, offers unique opportunities for stabilising charged entities. Multi-electron reduction (*i.e.* up to six electrons) can be observed for fullerenes, which is illustrated in Figure 1.4. For unsubstituted $C_{60}$ the six reversible reduction steps are all equally separated from each other by *ca.* 450 mV.[32, 38-40] As for some photochemical features, pristine $C_{60}$ shows weak fluorescence at 700 and 660 nm[41] and its fluorescence lifetime has been reported as 1.2 ns.[42] The quantum yield of $C_{60}$ is as low as $3.2 \times 10^{-4}$, which can be attributed to the forbidden transition due to the closed shell with high symmetry.[42] The fluorescence quantum yield increases roughly threefold when the symmetry is broken by the introduction of a functional group.[43] Upon nanosecond laser irradiation, pristine $C_{60}$ shows a clear absorption band at 750 nm as the triplet excited state is formed almost quantitatively.[33]

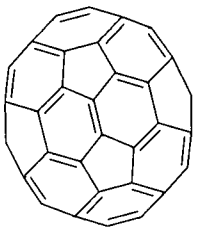

**3**

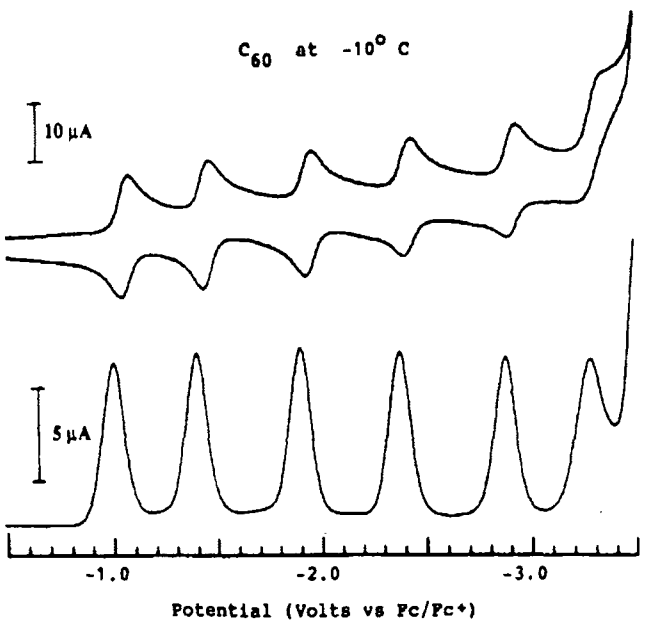


Figure 1.4: CV (top) and differential pulse voltammograms (bottom) of pristine $C_{60}$ in $CH_3CN$/toluene. (Taken from the literature[40]).

## π-Conjugated Polymer-$C_{60}$ Approach

It is the uniquely small reorganisation energy that fullerenes exhibit in electron transfer reactions (*i.e.* compared to planar acceptors), which renders this carbon allotrope particularly suitable for photovoltaic applications.[44-46] An ultimate goal is to design and assemble artificial systems which can efficiently process solar energy, replicating the natural analogue. Considering the limited absorption cross-section of $C_{60}$ in the visible range of the solar spectrum, the integration of larger light harvesting arrays is needed to store eventually larger fractions of photonic energy in the charge-separated state.[47]

Towards this goal, blends of semiconducting π-conjugated organic polymers, including poly-*p*-phenylenevinylenes (PPVs) and polythiophenes (PTs) with $C_{60}$ afford new types of plastic solar cells with energy transformation efficiencies which are promising although the values are comparatively moderate (*i.e.* relative to silicon-based solar cells).[31] It is crucial to realise that electron transfer events between the electron donating polymers and the electron accepting fullerenes within these composite materials evolve with ultrafast dynamics and high quantum efficiencies. However, the tendency of $C_{60}$ to phase separate from the polymer and to crystallise is one of the prime concerns: it imposes unrealistic measures for its solubility in conjugated polymer matrices.[48, 49]

## π-Conjugated Oligomer-$C_{60}$ Approach

The reported ultrafast photoinduced electron transfer results of electron donating polymer and $C_{60}$ blends have initiated efforts to replace the polymers with different well-defined π-conjugated oligomers.[37] Fullerenes blended with monodisperse π-conjugated oligomers that function as integrative photoexcited state electron donors have provided new types of plastic solar cells with promising energy transformation efficiencies.

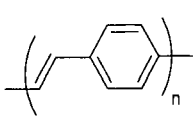


OPV

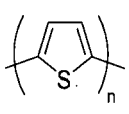


OT

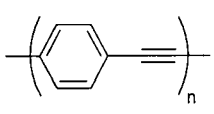


OPE

More recently, the "oligomeric" approach[16, 50, 51] (*i.e.* construction of π-conjugated oligomer functionalised fullerene derivatives) has received increasing interest as a result of the breakthroughs in metal-catalysed cross-coupling synthetic methodologies.[52] Important in this context is that π-conjugated monodispersed oligomers combine the following features: suitable size, electronic and optical properties of the more complex polymer structures, excellent solubility and structure–function relationships. Not surprisingly, systems such as oligo-*p*-phenylenevinylenes (OPVs), oligothiophenes (OTs), oligo-*p*-phenyleneethynylenes (OPEs), *etc.*, have been used as donor components in a wide range of electron donor–acceptor systems.[37, 53, 54] Used as artificial photosynthetic systems to produce chemical energy from sunlight,[55, 56] these oligomer functionalised fullerene derivatives can be terminated with a thioacetate group or an electroactive donor species, *e.g.* TTF.[36, 57]

## 1.5 Reported Conjugates

The aim of this thesis is to investigate oligofluorene molecular wires in donor-acceptor conjugates using $C_{60}$ as the accepting moiety. Hitherto, derivatives in which oligofluorene is covalently bound to $C_{60}$ had, to the best of our knowledge, not been investigated. Therefore, in this section we will discuss conjugates reported in the literature utilising alternative oligomers. As some excellent reviews already exist,[36-38, 51, 53, 58-62] the primary aim here is to discuss ensembles that are of interest in the scope of this thesis.

### 1.5.1 Oligomer-$C_{60}$ Dyads

#### Oligo-*p*-phenylenevinylene Derivatives

The first examples of OPV-functionalised fullerene derivatives were compounds **4a,b** and **5** reported by Nierengarten *et al.* in 1999.[63-65] Upon excitation of **4** and **5** on the fullerene fragment the typical pyrrolidinofullerene fluorescence and triplet-triplet transient absorption spectra were observed, which indicates that the excited state properties of the

$C_{60}$ core are

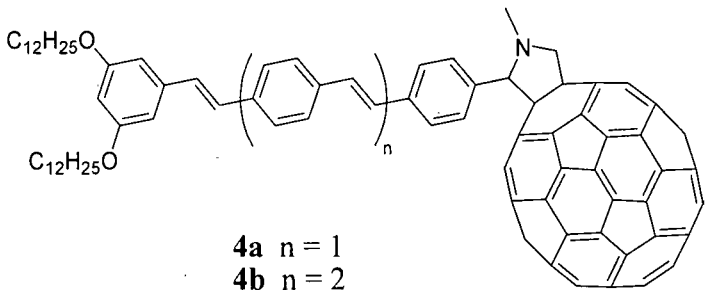


**4a** n = 1
**4b** n = 2

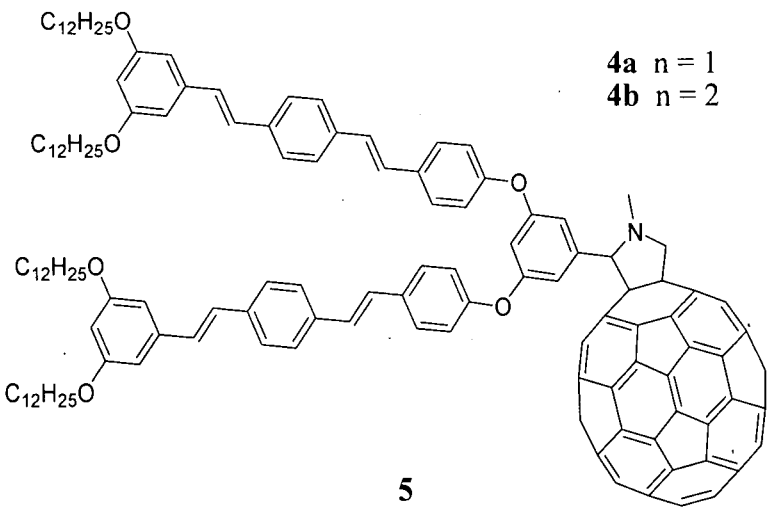


**5**

not affected by the presence of nearby OPV moieties.[64, 65] Excitation of **4** and **5** on the OPV allowed the observation of intercomponent processes. The typical fluorescence band of the pyrrolidinofullerene fragment (at *ca.* 710 nm) was observed instead of the intense fluorescence band of the OPV moiety. Nierengarten *et al.* observed quantitative occurrence of singlet-singlet energy transfer from the OPV unit to the $C_{60}$ core in **4** and **5**. The formation of the competing charge separating state is not observed and model calculations suggested that the rate of the energy transfer step is too fast for the electron transfer step to occur.[64, 65] This has important consequences for the efficiencies of photovoltaic devices prepared from **4** and **5**. The main part of the light energy absorbed by the OPV moiety is conveyed to the fullerene by energy transfer and not electron transfer, which means that electron-hole pairs cannot be generated any more. Thus, only a small part of the absorbed light is effectively contributing to the photocurrent.[63, 65]

Similar results for **4** and **5** were observed in toluene, DCM and PhCN. The photophysical properties of **6** have been systematically

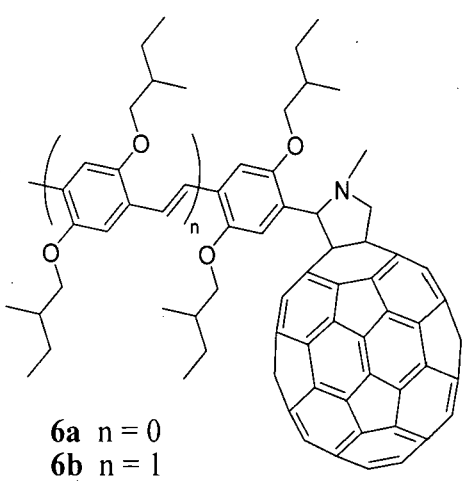


**6a** n = 0
**6b** n = 1
**6c** n = 2
**6d** n = 3

investigated with solvents of different polarities (Figure 1.5).[66] Ultrafast energy transfer from OPV towards $C_{60}$ was observed, followed by a nearly quantitative intersystem crossing (ISC) to the $C_{60}$ triplet state in the non-polar solvent toluene. However, the photoexcitation of the OPV moiety in a more polar solvent (*o*DCB) resulted in electron transfer from OPV to $C_{60}$ and, thus, formation of the charge-separated state. Calculations suggest that in toluene the charge-separated state is higher in energy than the fullerene singlet and triplet excited states. In a more polar solvent the energy of the charge-separated state drops below the first fullerene singlet excited state, this allows the occurrence of electron transfer after the initial singlet energy transfer event. Similar photophysical behaviour was observed for **7**.[67]

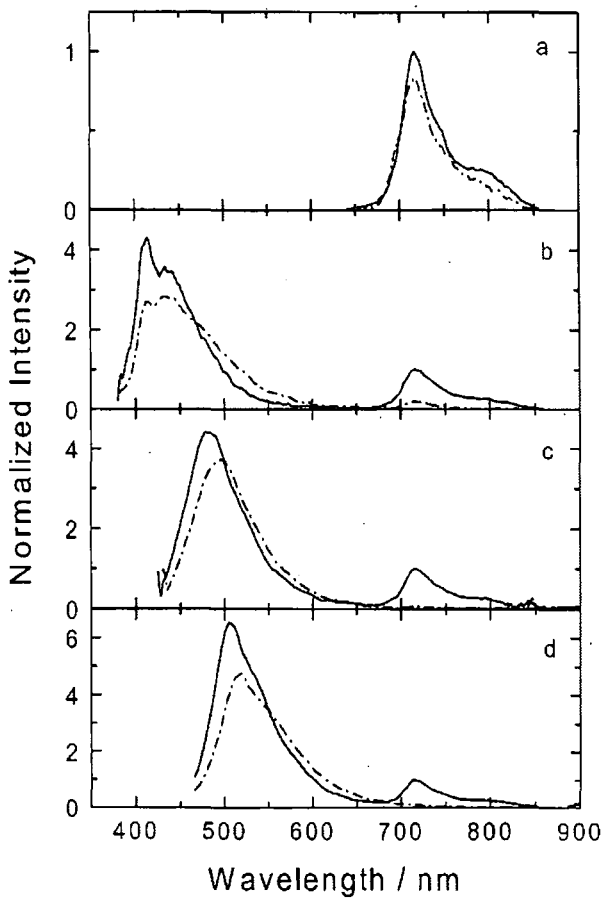


Figure 1.5: Fluorescence spectra of **6** in toluene (solid spectra) and *o*DCB (dash-dotted spectra), recorded at 295 K: (a) **6a**, $\lambda_{ex}$ = 330 nm; (b) **6b**, $\lambda_{ex}$ = 366 nm; (c) **6c**, $\lambda_{ex}$ = 415 nm; (d) **6d**, $\lambda_{ex}$ = 443 nm. All fluorescence spectra were normalised to the fullerene emission at 715 nm. For **6b-d** the residual OPV emission can be seen in the 400-600 nm range and a nearly complete quenching of the fullerene emission is observed in *o*DCB, whereas the OPV emission decreases only slightly. (Taken from the literature[66]).

The excited-state properties of **8** and **9a,b** are more complex due to the electron donating ability of the pyrazoline ring.[67-69] For these compounds quantitative singlet-singlet energy transfer from OPV to $C_{60}$ was observed, which was followed by an efficient electron transfer from the N lone pair of the pyrazoline ring.

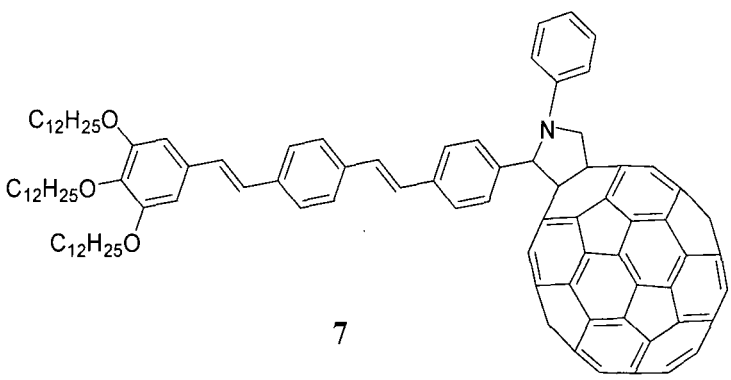


**7**

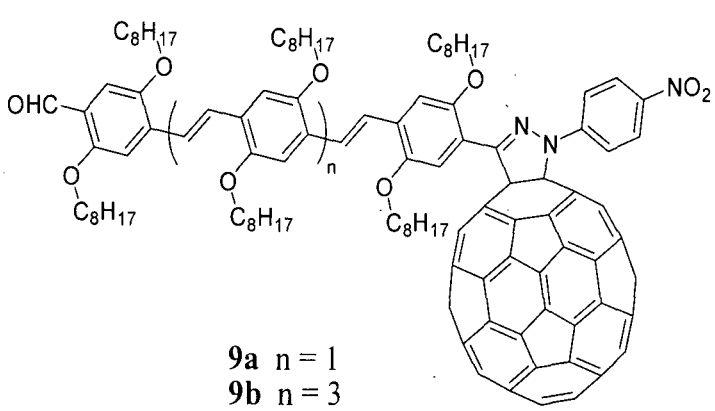


**9a** n = 1
**9b** n = 3

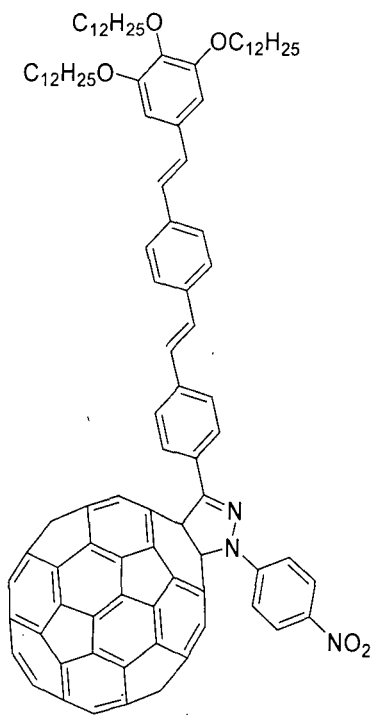


**8**

## Oligothiophene Derivatives

The first examples of OT-functionalised fullerene derivatives were compounds **10a-d** reported by Yamashiro *et al.* in 1999.[70] No interaction between OT and $C_{60}$ was observed in the ground state and, similar to **4**, photoinduced energy transfer (*i.e.* OT → $C_{60}$) in the excited state was observed for **10** in toluene. Interestingly, dual fluorescence was observed for **10b,c** from both the $C_{60}$ core and the OT chain. Due to increased separation between the two component centres (*i.e.* OT and $C_{60}$) retardation of energy transfer was observed, resulting in additional OT fluorescence, although energy transfer is still predominant. Similar to **6**, the photophysical decay process associated with **10** is solvent-dependent and electron transfer - and thus charge-separated state formation - was observed in more polar

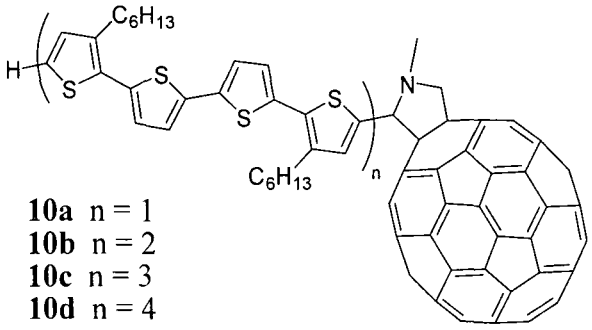

**10a** n = 1
**10b** n = 2
**10c** n = 3
**10d** n = 4

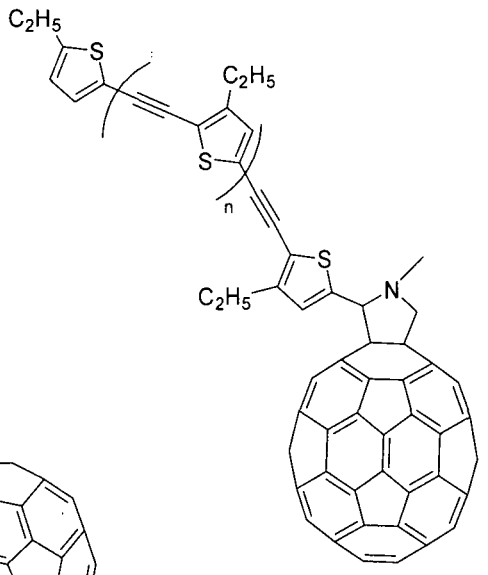

**11a** n = 3
**11b** n = 7

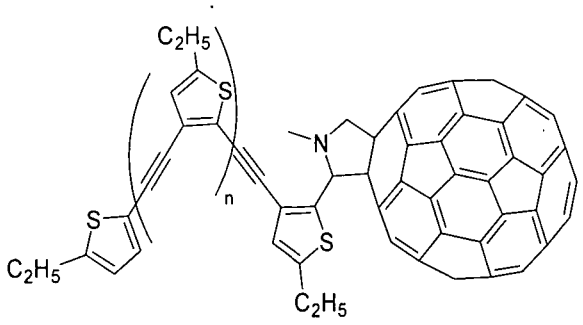

**12a** n = 3
**12b** n = 7
**12c** n = 11

solvents, such as PhCN and THF.[71, 72] Different from energy transfer, the electron transfer occurs rapidly as the OT chain length increases in **10b**, because the lower oxidation potential of the longer OT is more effective in lowering the energy level of the charge-separated state.[72]

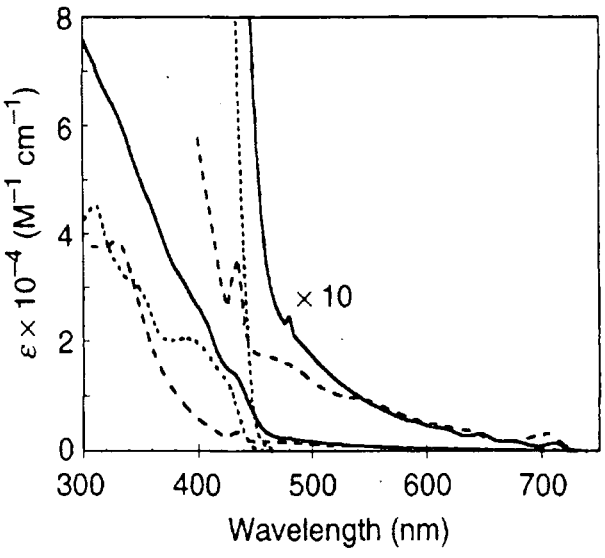


Figure 1.6: Electronic absorption spectra of **12a** (solid line), the corresponding OTE oligomer (dotted line) and *N*-methylpyrrolidine-$C_{60}$ **54** (structure shown in Chapter 2, dashed line). Slight red shifts of the absorption bands are observed in the 600-750 nm range compared to **54**, which indicates the presence of a weak through-space electronic interaction between the OTE and $C_{60}$ units. (Taken from the literature[74]).

The same groups who investigated **10**, studied the photophysical behaviour of oligo(thienylene-ethynylene) (OTE) dyads **11** and **12**.[73, 74] The electronic interaction in the ground state for **11** was quite weak. The absorption spectra indicated a stronger through-space electronic interaction between OTE and $C_{60}$ for **12** than for **11**, due to the closer arrangement as a result of the zigzag structure of OTE in **12** (Figure 1.6). For both systems the formation of charge-separated states was observed, even in toluene. They found that the charge recombination rate constant ($k_{CR}$) was larger for the linear oligomer chain (**11**) than for the zigzag structure of **12**, indicating the influence of the molecular structure.[73]

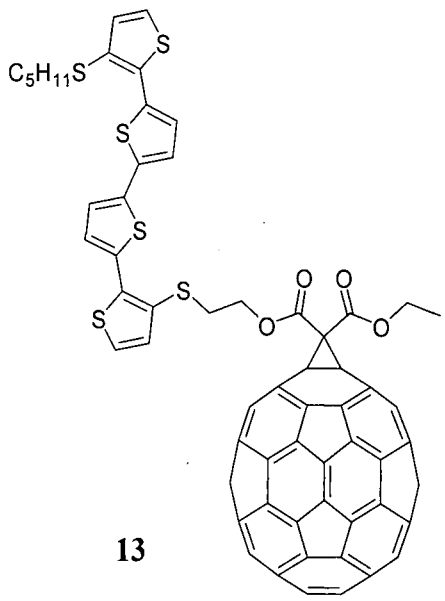


**13**

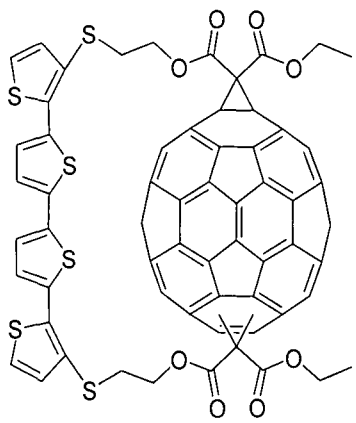


**14**

The influence of structure was also investigated with quaterthiophene dyads **13** and **14**.[75] Indirect charge transfer leading to the charge-separated state, following the singlet-energy transfer reaction, was in both cases observed in toluene. In a more polar solvent (*i.e.* *o*DCB) both indirect and direct charge transfer was observed, the latter can now occur due to the reduced activation energy barrier. It was shown that the intramolecular energy- and electron transfer occurs faster for **14**, compared to **13**, as a consequence of the imposed face-to-face orientation of the donor and acceptor moieties. In solution, the $k_{CR}$ of both dyads are higher than the rate of their formation. However, the lifetime of some charges created in the solid state increase into the micro- and millisecond time domain, due to the avoidance of intramolecular recombination of positive and negative charges and their migration to adjacent dyad molecules.[75, 76]

Guldi *et al.* investigated the photophysical behaviour of **15**, **16** and **17**.[77, 78] Energy transfer was found for all four dyads in toluene. In polar PhCN, direct electron transfer was observed for **16** and for **17**, where the oxidation potential is raised (*i.e.* the charge-separated state energy is close to that of the $C_{60}$ singlet excited state) and both electron and energy transfer was observed. In sharp contrast, instantaneous formation of the singlet excited state was observed for **15** and followed by subsequent ISC, possibly due to unfavourably raised energies of the charge-separated state. Photovoltaic devices of **16** showed white light efficiencies up to ~0.2%.[78] The synthetic and electronic properties of oligo(phenothiazine)-ethynyl-hydro-$C_{60}$ series **18** was reported in 2006 and photophysical studies are currently in progress.[79] Upon UV excitation the phenothiazinyl fluorescence is considerably quenched, something presumed to indicate charge separation by an intramolecular photo-induced electron transfer from phenothiazine to $C_{60}$.

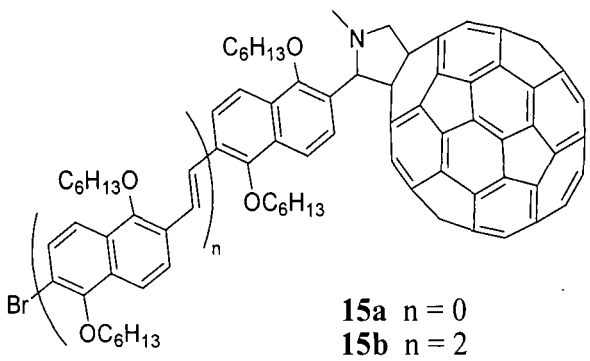


**15a** n = 0
**15b** n = 2

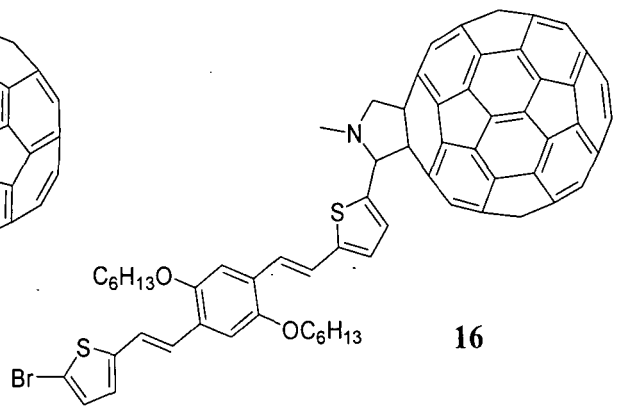


**16**

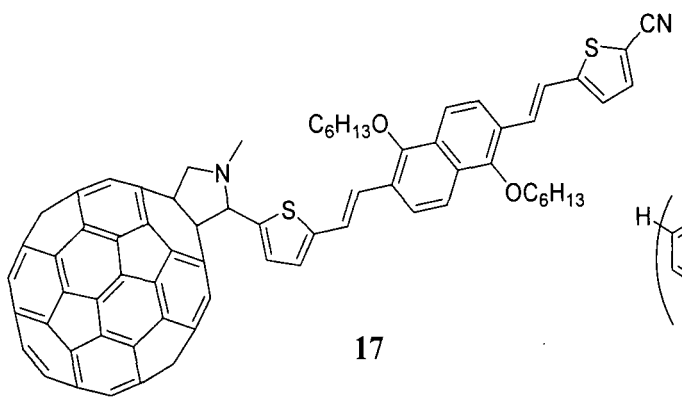


**17**

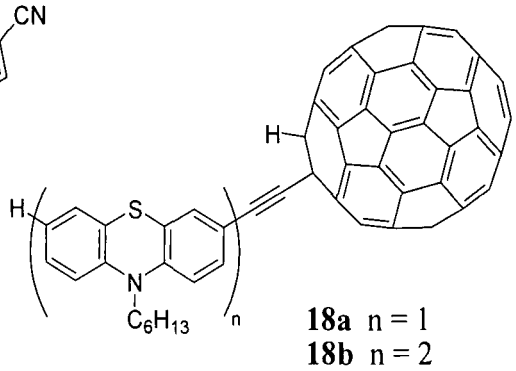


**18a** n = 1
**18b** n = 2
**18c** n = 3

An alternative thiophene-containing oligomer-$C_{60}$ dyad series **19** was prepared by Roncali and co-workers in 2002.[80, 81] The dyad series - containing two fullerene units - **20** was simultaneously investigated. In *o*DCB the intramolecular charge-separated state is formed

in a two-step mechanism involving a fast singlet energy transfer followed by electron transfer (observed for **19a,b** and **20c**). In toluene ISC followed by triplet energy transfer was observed in a competing manner next to the electron transfer for **19b**. Dyad **19a** showed no electron transfer, while triad **20c** showed the same behaviour as in *o*DCB.

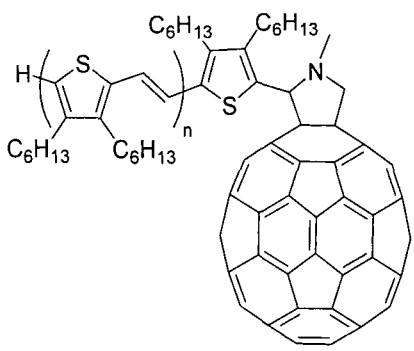

**19a** n = 1
**19b** n = 2
**19c** n = 3
**19d** n = 5

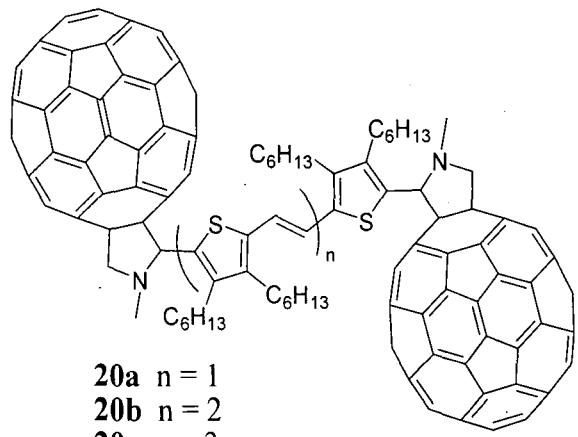

**20a** n = 1
**20b** n = 2
**20c** n = 3
**20d** n = 5
**20e** n = 7

## 1.5.2 $C_{60}$-Oligomer-$C_{60}$ Triads

### Oligothiophene Derivatives

The first $C_{60}$-based dumbbell (*i.e.* $C_{60}$-OT-$C_{60}$ triads) ensembles **21** were reported by Janssen in 2000.[82] The formation of its radical pair whose lifetime - in the range of

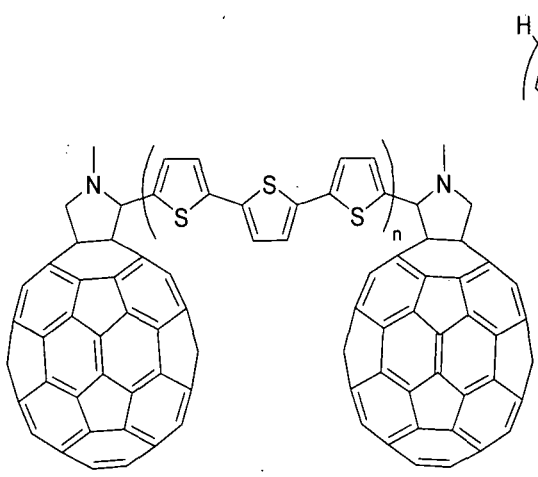

**21a** n = 1
**21b** n = 2
**21c** n = 3

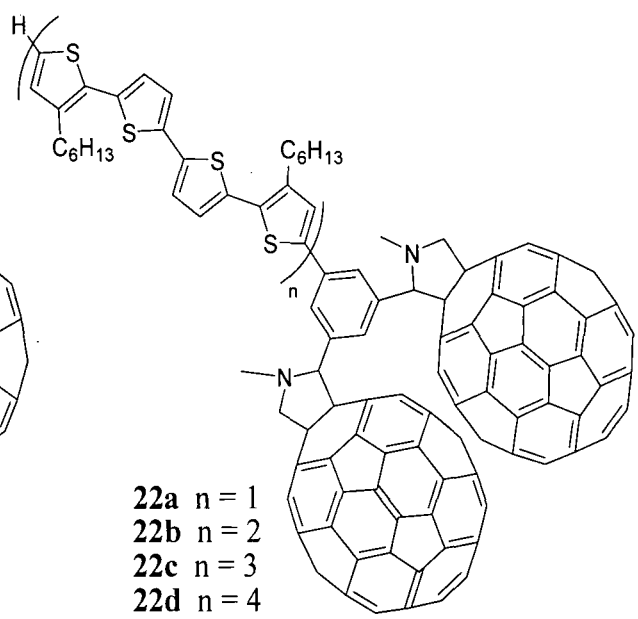

**22a** n = 1
**22b** n = 2
**22c** n = 3
**22d** n = 4

subnanoseconds - was shown by photophysical studies to strongly depend on the solvent polarity. Significantly higher values - milliseconds in an intermolecular fashion - for the lifetimes of **21b,c** were observed during the photoexcitation in solid state. Oligothiophene triads **22** were also prepared by Otsubo *et al.*[83] and the increased number of pendant $C_{60}$ cages increases the quenching of the OT emission, compared to **10**. Photovoltaic devices based on **22** demonstrated that the presence of a second $C_{60}$ enhances the interactions among the fullerene units creating a more ordered network, which increased the power efficiencies. Comparing series **10** and **22**, the photovoltaic cell with the highest performance was prepared from **22d**.[58]

## Oligo-*p*-phenyleneethynylene Derivatives

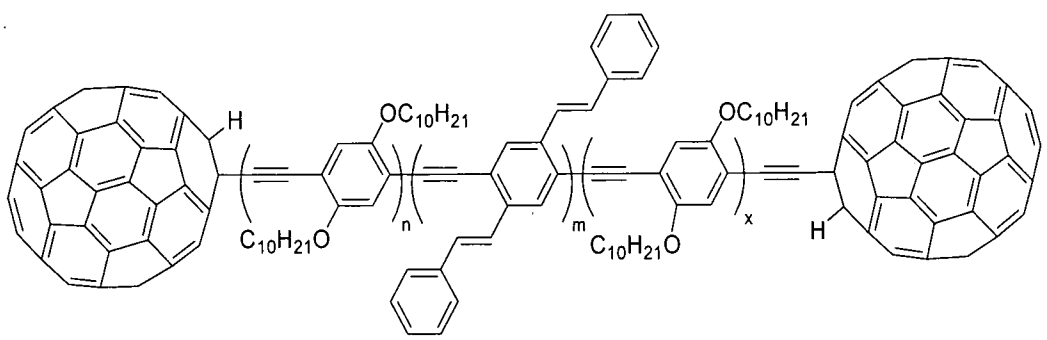


**23a** n = 1 m = x = 0
**23b** n = 2 m = x = 0
**23c** n = 3 m = x = 0
**23d** n = 5 m = x = 0

**24a** n = x = 1 m = 1
**24b** n = x = 2 m = 1

Tour and co-workers published two articles on OPE bridged fullerenes **23** (synthetic procedure reported by Komatsu *et al.*),[84] which provided evidence of a synergistic interaction between the conjugated OPE backbone and the terminal fullerenes.[85, 86] This

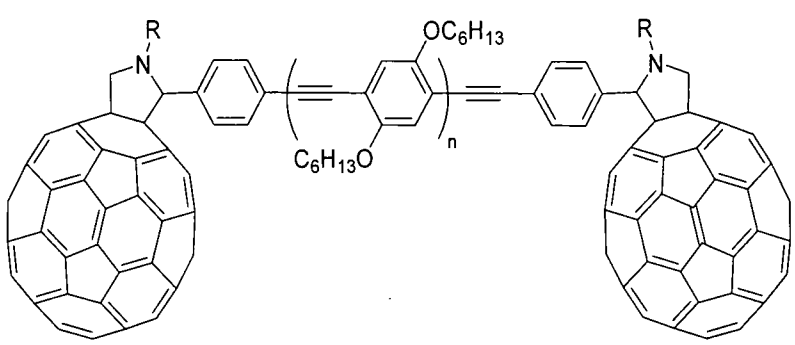


**25a** n = 0 R = $CH_3$
**25b** n = 5 R = $CH_3$

**26a** n = 0 R = $C_8H_{17}$
**26b** n = 1 R = $C_8H_{17}$
**26c** n = 3 R = $C_8H_{17}$

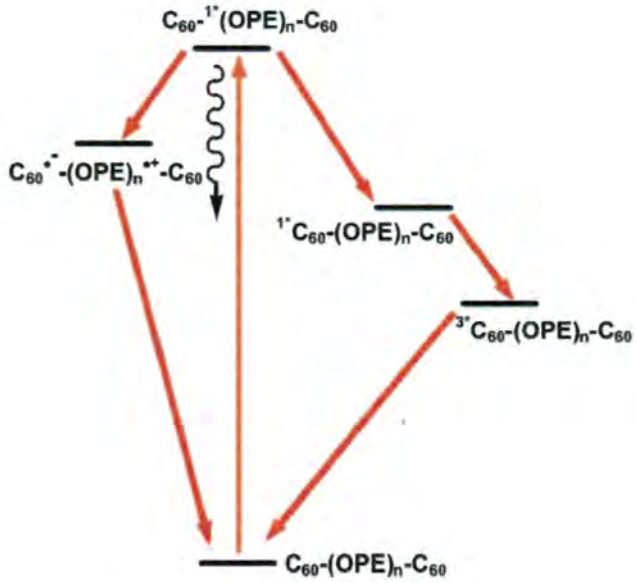


Figure 1.7: Schematic illustration of the reaction pathways in photoexcited compounds **25b** and **26b,c**. (Taken from the literature[59]).

suggests the formation of a charge-transfer species in which excited electrons are passed from OT to $C_{60}$. Similar species (**25** and **26**) were also prepared Martín and co-workers,[87] whose transient absorption spectroscopy experiments demonstrated an efficient intramolecular energy transfer from the photoexcited oligomer to the covalently linked $C_{60}$ (Figure 1.7). However, they did note that a weak competitive electron transfer could also operate the deactivation process (Figure 1.7). Preliminary results on the photophysical properties of the related OPE-$C_{60}$ dyads (structures not shown) indicated the occurrence of an intramolecular decay process.[88-90] Interestingly, most systems discussed so far showed no (or only weak) electronic interaction in the ground state, but triads **24a,b** showed quite different electrochemical properties.[91] The origins of the observed irreversible reduction processes are not well understood, but are suggestive of electronic interactions between the cruciform oligomer and $C_{60}$. Substantially quenched fluorescence does indicate rapid photoinduced intramolecular energy/electron transfer.

The dumbbell equivalent of **15**, **16** and **17** (*i.e.* the Br- and CN- functionalities were replaced with pyrrolidinofullerene, structures not shown) were also synthesised by the same group.[92, 93] The main advantage of the photophysical behaviour of the $C_{60}$-oligomer-$C_{60}$ series over the behaviour of the mono-fullerene substituted derivatives is the increased stability of the product and enhanced yield of charge-separation.[92]

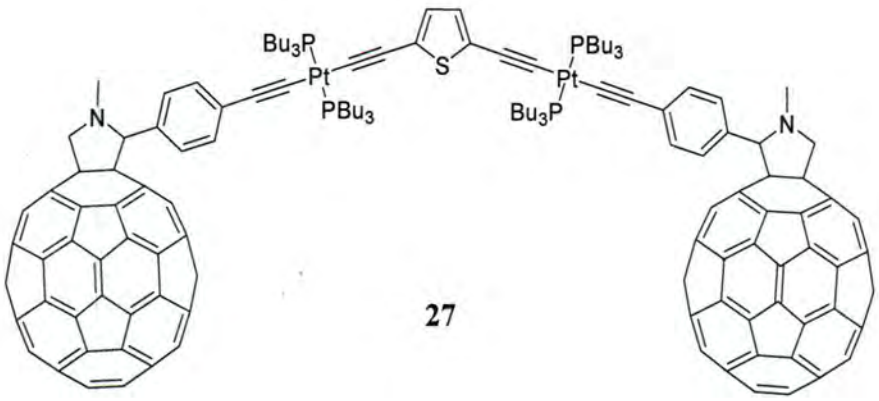


**27**

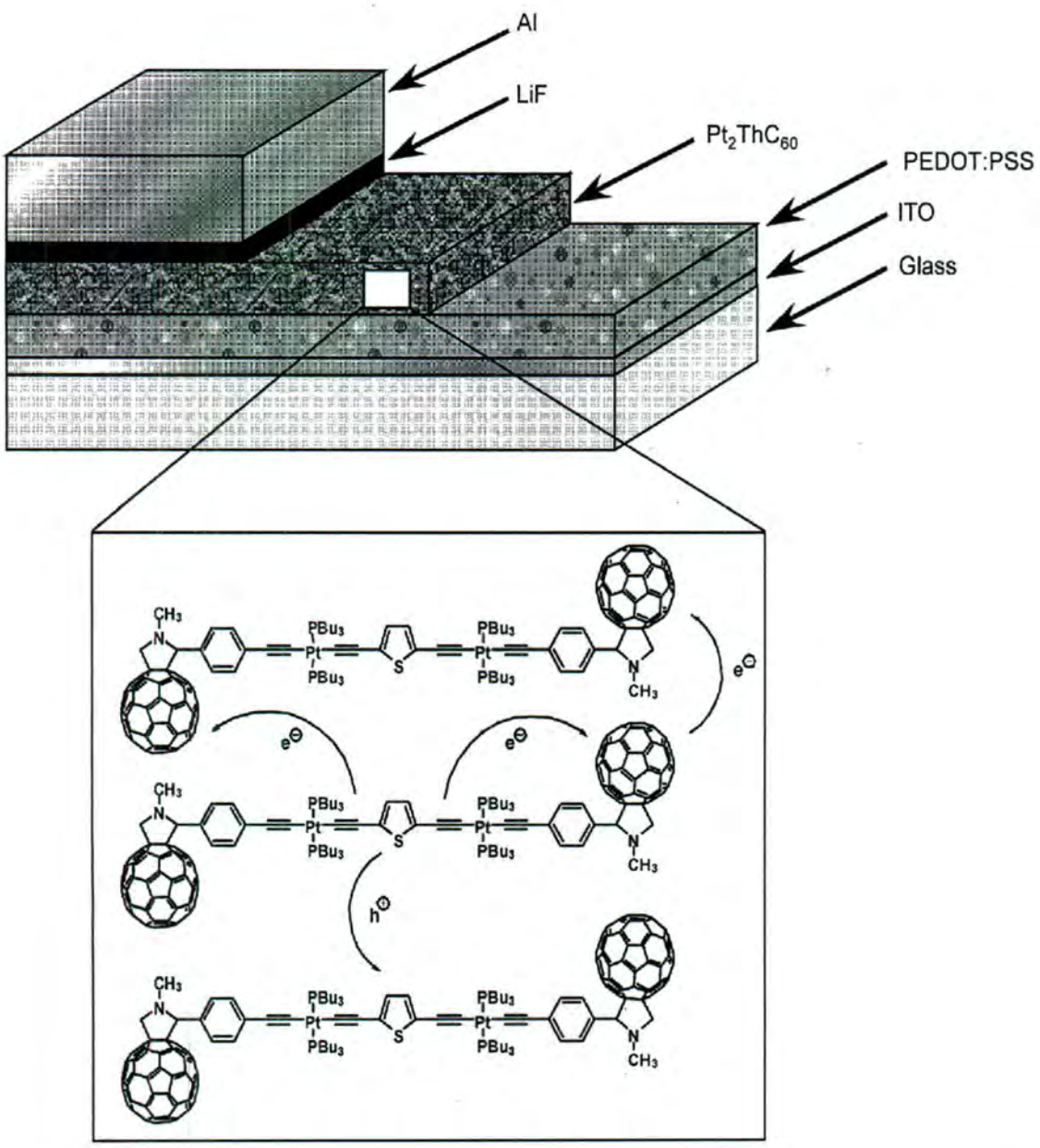


Figure 1.8: Example of a photovoltaic device configuration based upon **27** and an illustration of intra- and intermolecular charge transfer in the active layer. (Taken from the literature[94]).

Recently, pyrrolidinofullerene end-capped platinum-acetylide triad **27** was published.[94] The novel triad was subjected to photophysical methods and photovoltaic device testing. Although quantitative assessment of the contributions of the singlet and triplet electron transfer pathways was not possible, the authors believe that the photoinduced charge transfer occurs mainly from the triplet state. Despite the suggestion that the radical ion pair is in a triplet spin state, the charge-separated state decays rapidly. The organic voltaic devices of **27** operated with modest efficiency (Figure 1.8).

## 1.5.3 Donor-Oligomer-$C_{60}$ Triads

### Tetrathiafulvalene Derivatives

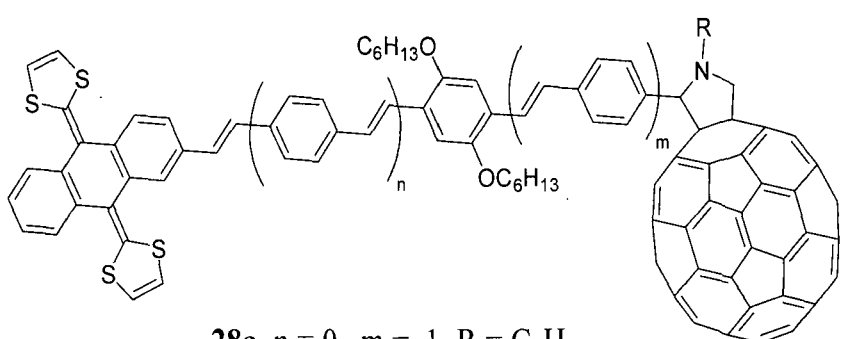


**28a** n = 0 m = 1 R = $C_8H_{17}$
**28b** n = 1 m = 1 R = $CH_3$
**28c** n = 2 m = 2 R = $(CH_2CH_2O)_3CH_3$

Several $C_{60}$-TTF derivatives have been synthesised[36, 59, 61] and emphasis on the oligomer aspects of this field brings us to the first *ex*TTF-oligomer-$C_{60}$ triads synthesised in 2004, namely a series of oligo-*p*-phenylenevinylene bridged ensembles (**28**).[27, 95, 96] The investigation revealed a lack of significant electronic communication in the ground state and formation of the photoinduced charge-separated state (*i.e.* *ex*$TTF^+$-OPV-$C_{60}^-$). For these compounds wire-like behaviour was observed over distances of up to 50 Å. The matching HOMO energies of $C_{60}$ and OPV result in an exceptionally small attenuation factor ($\beta$ = 0.01 ± 0.005 $Å^{-1}$). Paraconjugation of the $\pi$-conjugated oligomer into the *ex*TTF-donor - with coupling constants (V) of ~5.5 $cm^{-1}$ - was realised by the strong

electronic coupling between the donor and acceptor moieties. Electron/hole transfer is here limited by distance and the nature of the $C_{60}$/OPV linkage.

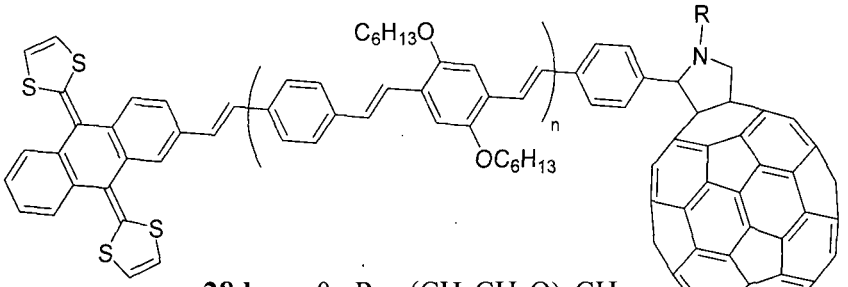


**28d** n = 0 R = $(CH_2CH_2O)_3CH_3$
**28e** n = 3 R = $C_8H_{17}$

Subsequently, the same groups studied *ex*TTF-$C_{60}$ triads linked by an OPE bridge (**29**).[97] With this series, the influence of the bridge on the electron transfer becomes clear. The structure of **28** and **29** is essentially the same (*i.e.* donor, acceptor, solubilising chains and linkage to $C_{60}$) and the main difference is the exchange of C=C double bonds with C≡C triple bonds. However, the photoinduced excited state behaviour was very different, as the attenuation factor (β) for **29** was reported to be 0.2 ± 0.05 $Å^{-1}$. Thus, mere weak molecular wire behaviour was observed for the OPE bridge, which could be attributed to different factors. The HOMO energy of OPE (*i.e.* between -8.9 and 8.4 eV) is slightly lower than those of OPV (*i.e.* between -8.4 and 7.9 eV), which might diminish interactions with $C_{60}$. DFT calculations revealed that the HOMO of the OPE triad is localised on the *ex*TTF moiety, while in the OPV system the HOMO reaches into the bridge (Figure 1.9). It is believed that the injection of an electron into the bridge is facilitated through better orbital overlap.

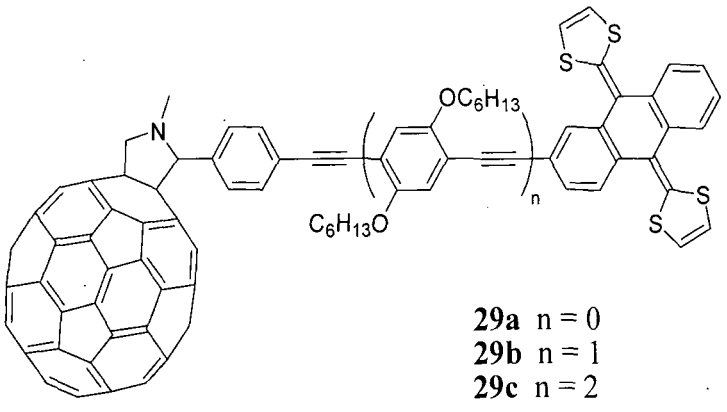


**29a** n = 0
**29b** n = 1
**29c** n = 2

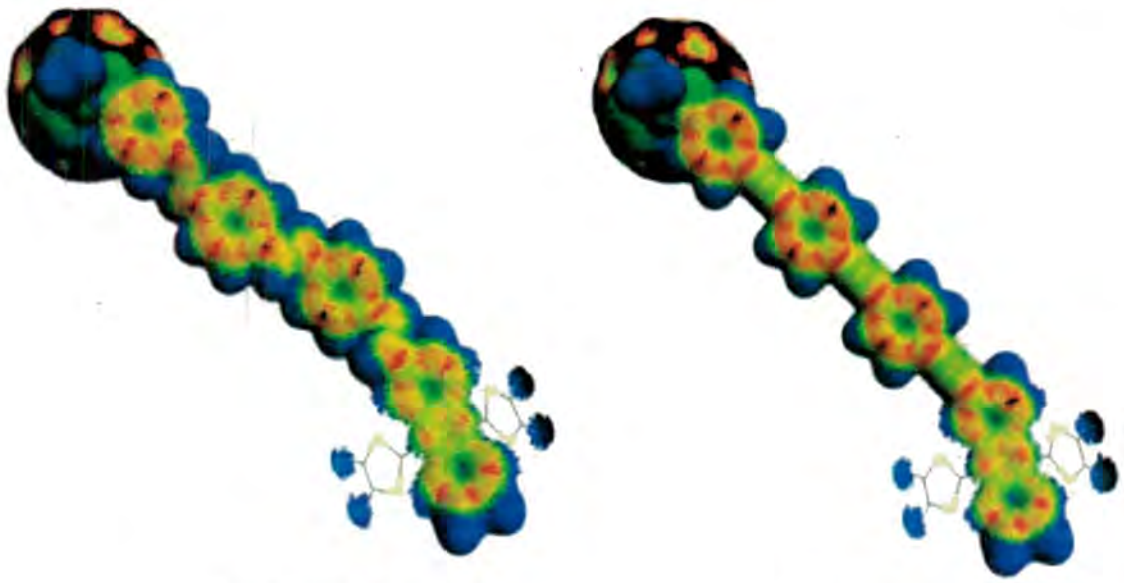

*ex*TTF-$(OPV)_3$-$C_{60}$ *ex*TTF-$(OPE)_3$-$C_{60}$

Figure 1.9: Electron affinity maps of *ex*TTF-OPV-$C_{60}$ (left) and *ex*TTF-OPE-$C_{60}$ (right) as computed with Parasurf A07[98] and viewed with Tramp 1.1d[99]; from blue to red: low to high. (Taken from the literature[97]).

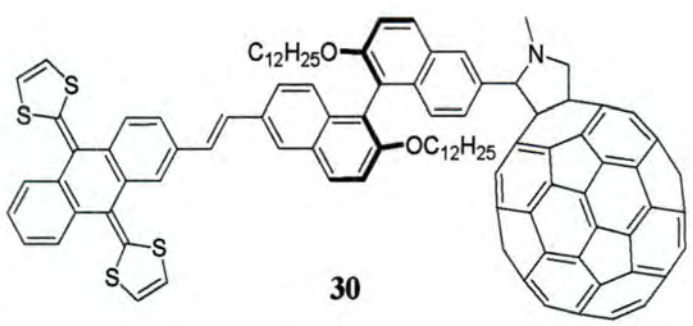


**30**

The influence of the bridge was further investigated with the use of triads **30** and **31**.[100] For these two triads, whose main difference is the degree of conjugation, the charge-recombination dynamics in both solution phase and solid film were explored. The process was found to be slower for **30** ($\tau$ = 25 μs) in solution, which is consistent with the expected stronger electronic coupling in **31** ($\tau$ = 0.7 μs). In contrast, solid films demonstrated faster recombination dynamics for **30** ($\tau$ = 2.1 μs) than for **31** ($\tau$ = 7 μs). The faster dynamics of **30** were assigned to the enhanced electronic coupling between the *ex*$TTF^{\bullet+}$ and $C_{60}^{\bullet-}$ radical pairs in the solid film. The increase of lifetime for **31** is attributed to π-orbital stacking favouring efficient radical pair dissociation to yield free carriers, which requires favourable intermolecular acceptor-acceptor and/or donor-donor interactions.

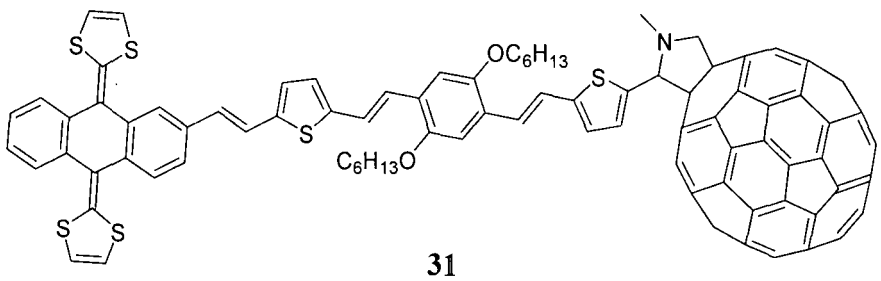

**31**

In the series of oligothiophene-$C_{60}$ assemblies (*i.e.* **10**, **21** and **22**), TTF derivative **32** was published in 2006.[58, 101] The results indicated efficient intramolecular charge transfer leading to long-range charge-separation, *i.e.* $TTF^{+}$-OT-$C_{60}^{-}$. Their photovoltaic cells showed somewhat higher photocurrents in comparison with the OT-$C_{60}$ series (**10**), indicating that a covalently attached TTF moiety can enhance the photoinduced charge separation and/or charge migration.

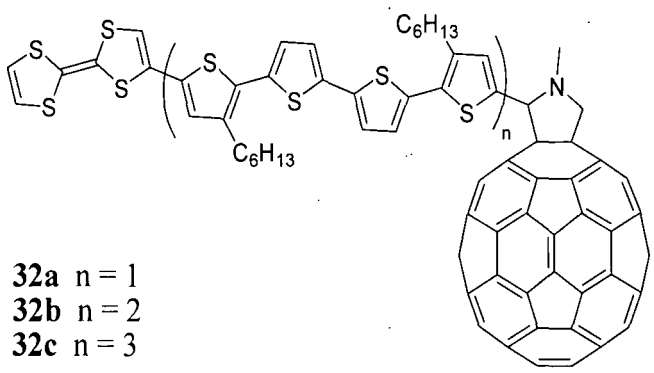

**32a** n = 1
**32b** n = 2
**32c** n = 3

## Ferrocene Derivatives

The investigation into oligothiophene molecular wires (*i.e.* **10**, **21**, **22** and **32**), was followed up with the preparation of two series of ferrocene derivatives (**33** and **34**).[102, 103] Similar to compound **30**, for **34** the conjugation was broken by the insertion of a trimethylene unit. In non-polar solvent (*i.e.* toluene) energy transfer from the OT chain to $C_{60}$ was observed for both dyads. In PhCN electron transfer was observed together with different behaviour for the two triads. The charge-separated state for **33** was formed immediately upon photoexcitation of the OT unit and the radical cation was delocalised on both donor moieties (*i.e.* $(Fc\text{-}OT)^{+}$-$C_{60}^{-}$). The lifetimes increased as the length of the

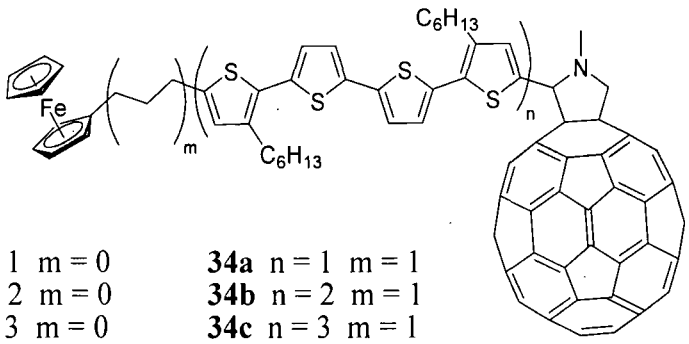


**33a** n = 1 m = 0
**33b** n = 2 m = 0
**33c** n = 3 m = 0

**34a** n = 1 m = 1
**34b** n = 2 m = 1
**34c** n = 3 m = 1

oligomer increased, that is **33a** ($\tau$ = 0.08 ns) → **33b** ($\tau$ = 2.7 ns) → **33c** ($\tau$ = 50 ns). As the conjugation between Fc and OT is broken, the three units act independently. This means that the formation of the charge-separated state $Fc^{+}$-spacer-OT-$C_{60}^{-}$ occurs via radical cation delocalisation on the OT chain state (*i.e.* Fc-spacer-$OT^{+}$-$C_{60}^{-}$), which was formed via an energy transfer process. The prevention of $\pi$-conjugation between the donor and bridge moiety was more effective in the extension of the lifetime of the charge-separated state - **34a** ($\tau$ = 22 ns) → **34b** ($\tau$ = 240 ns) → **34c** ($\tau$ = 330 ns) - than the positive-charge delocalisation obtained by $\pi$-conjugation extension. Regrettably, the attenuation factor of **33** was not published, while for **34** $\beta$ was evaluated to be 0.10 $Å^{-1}$.

That the lifetime of a charge-separated state increases with the length of the oligomer and the positive influence of an electron donor on the charge-separated lifetime and efficiency was also demonstrated by studies on **35**.[104] The observed lifetime of **35a** in PhCN was < 6ns and for **35b** was 50 ns.

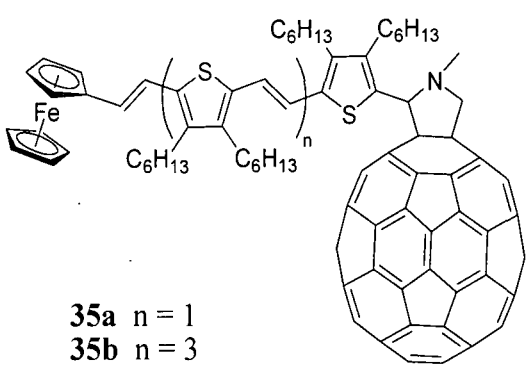


**35a** n = 1
**35b** n = 3

## Porphyrin Derivatives

In continuation of the oligothiophene theme, we now look towards the predecessor of **32**, **33** and **34**, namely porphyrin containing derivatives **36** and **37**.[58, 105-108] Interestingly, the $\beta$ factor for **36** was found to be significantly different depending upon the strength of polarity of the solvent, *i.e.* PhCN ($\beta$ = 0.03 $Å^{-1}$) and *o*DCB ($\beta$ = 0.11 $Å^{-1}$). The attenuation factor for **37** was not calculated. The positive influence of metal in the porphyrin moiety

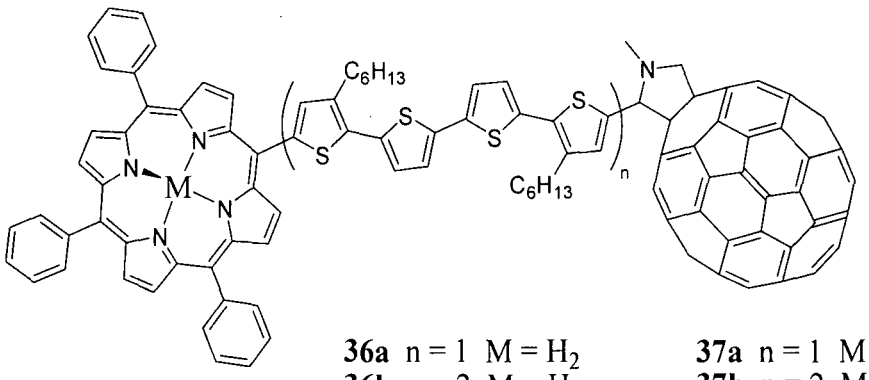

**36a** n = 1 M = $H_2$
**36b** n = 2 M = $H_2$
**36c** n = 3 M = $H_2$

**37a** n = 1 M = Zn
**37b** n = 2 M = Zn
**37c** n = 3 M = Zn

could be established by a comparison of the lifetime of the charge-separated state of **36** and **37**. In *o*DCB the lifetimes increase with length up to a maximum and decrease afterwards; **36a** ($\tau$ = 14 μs) → **36b** ($\tau$ = 27 μs) → **36c** ($\tau$ = 20 μs). The lifetimes are dramatically increased by the presence of zinc(II), *i.e.* **37a** ($\tau$ = 450 μs) and **37b** ($\tau$ = 910 μs). Not only the lifetime, but also the final charge-separated state is affected by the presence of zinc. The charge-separated state of **36** was - independent of solvent - $H_2P$-$OT^+$-$C_{60}^-$. Charge-recombination processes of **37** occur via $ZnP^+$-OT-$C_{60}^-$ in PhCN and are in equilibrium between two states (*i.e.* $ZnP^+$-OT-$C_{60}^-$ and ZnP-$OT^+$-$C_{60}^-$) for *o*DCB. It is interesting to note that Aso and co-workers have also investigated switching behaviour on similar ensembles by insertion of a moiety which can either be oxidised to the cation radical or for a complex with a cation.[109, 110] The photoinduced intramolecular electron transfer in controllable by displacing the counter ion.

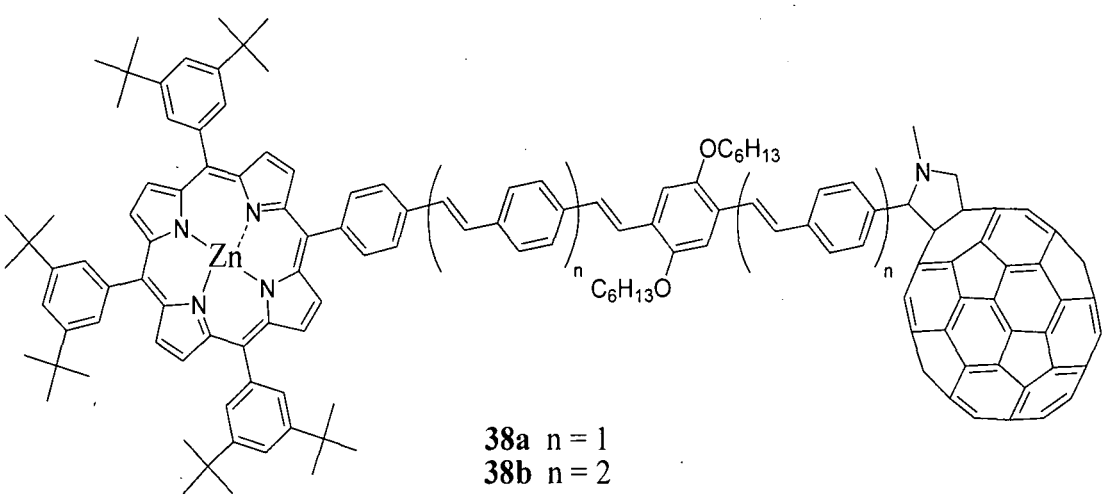

**38a** n = 1
**38b** n = 2

Earlier we discussed *ex*TTF-$C_{60}$ ensembles (**28**, **29** and **30**) investigated by Guldi, Martín and co-workers, who also reported similar triads (**38**,[111] **39**[112] and **40**[113]) wherein the *ex*TTF donor is replaced with a porphyrin moiety. The photophysical behaviour of **38** is similar to **28** with wire-like electron transfer observed over distances of up to 40 Å. Electron/hole injection is facilitated by matching HOMO energies of $C_{60}$ and OPV. Donor-acceptor coupling constants (V) of ~2.0 $cm^{-1}$ and a small attenuation factor ($\beta = 0.03 \pm 0.005$ $Å^{-1}$) were observed. Although results of **39** are still forthcoming, the β factor - which is 0.32 $Å^{-1}$ - has been published.[113] These results also indicate that OPV shows stronger molecular wire behaviour and thus they complement the previous study (**28** and **29**). Furthermore, it illustrates that the molecular wire behaviour is stronger when an *ex*TTF moiety is utilised as electron donor, *e.g.* **28** ($\beta = 0.2$ $Å^{-1}$) *vs.* **38** ($\beta = 0.32$ $Å^{-1}$).

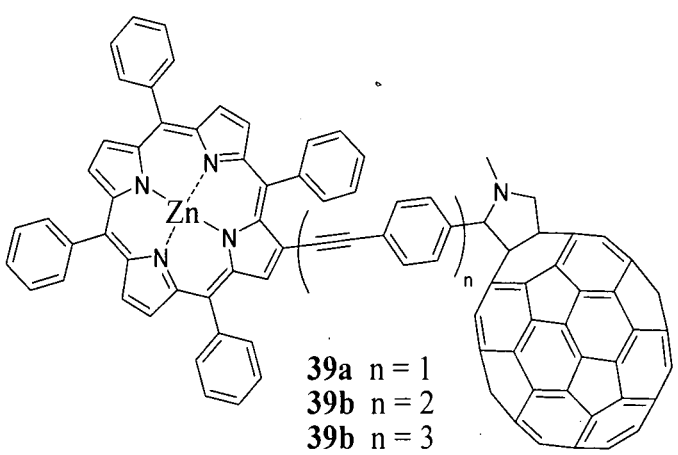


**39a** n = 1
**39b** n = 2
**39b** n = 3

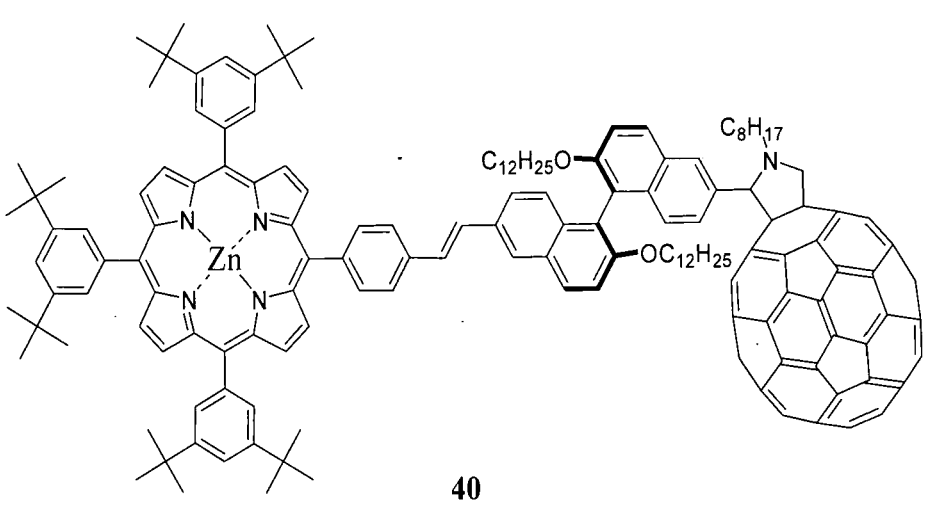


**40**

Electrochemical measurements indicated electronic communication between the different units in the ground state of **40**, which was not observed for **30**. The electronic communication of triad **40** results from the geometry which favours donor-acceptor and π-

π interactions. This through-space interaction was supported by excited-state studies and resulted in a dramatic difference in lifetimes, *i.e.* 165 μs (**30**) and 730 ns (**40**) in PhCN.

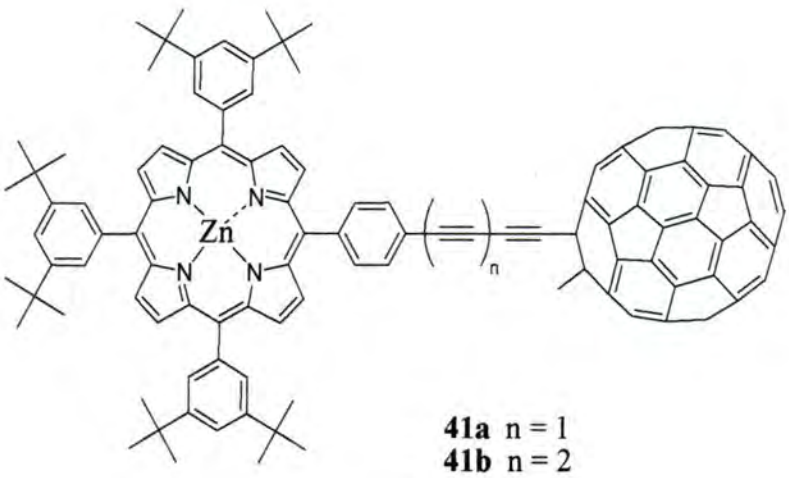


**41a** n = 1
**41b** n = 2
**41b** n = 3

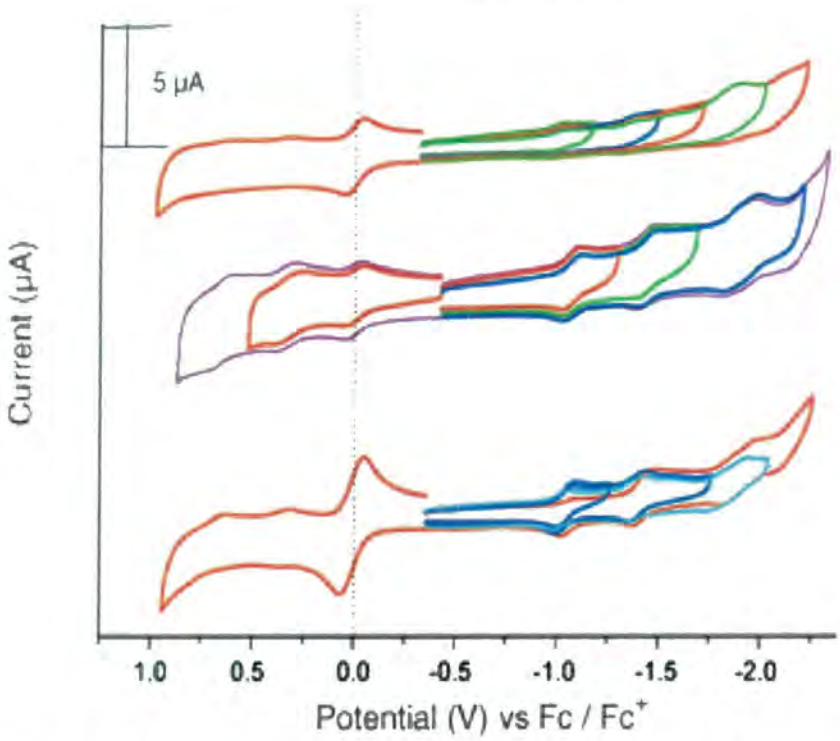


Figure 1.10: CV of **41a** (bottom spectrum), **41b** (middle spectrum) and **41c** (top spectrum). (Taken from the literature[114]).

Finally, compound **41** was reported by Vail *et al.* in 2005.[114] Cyclic and differential pulse voltammetry studies indicated electronic coupling between the donor and acceptor and that the degree of this coupling decreases with the length of the alkyne bridge (Figure 1.10). Similar to most triads described above, energy transfer was observed in toluene, while

rapid photoinduced electron transfer was observed in THF and PhCN. Electronic interaction is effectively mediated by the alkyne bridge, which is reflected by $\beta = 0.06 \pm 0.005$ Å$^{-1}$. Comparison of **41a** with **42** indicates that the linkage of the bridge to the porphyrin donor influences the lifetime of the charge-separated radical pair, *i.e.* in THF 100 ps (**42**) *vs.* 550 ns (**41a**).[115]

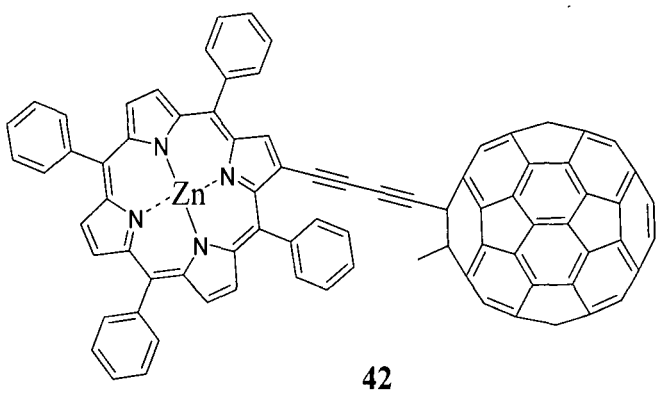


**42**

## 1.6 Conclusions

This chapter has aimed to provide a brief introduction into molecular electronics and molecular wires with the emphasis on relevant dyads and triads reported in the literature with $C_{60}$ as the end group in all cases. This overview has highlighted that most reported examples concern OPV, OT and OPE bridges and these moieties can significantly modify the wire behaviour depending on oligomer length and details of the mode of attachment to the end-groups. There is, therefore, clear scope and interest in the synthesis of alternative molecular wires and studies of their redox and photophysical properties.

# Chapter 2: Oligofluorene-$C_{60}$ and $C_{60}$-Oligofluorene-$C_{60}$ Conjugates

## 2.1 Introduction

In the previous chapter an account of the literature has been presented, which focused on the research field of oligomeric molecular wires in dyads or triads containing fullerene. Oligo- and poly-fluorenes are currently receiving considerable attention due to their excellent optical and electronic properties as materials for the preparation of organic light emitting diodes (OLEDs).[116-118] Recently, low-bandgap fluorene copolymers have also been combined with a variety of chemically modified fullerenes to form new plastic solar cells showing power conversion efficiencies as high as 2.2%.[119-122] However, to the best of our knowledge, fluorene oligomers have not been employed as the electron donor constituent in dyads or triads in the search for photo-generated charge-separated states for

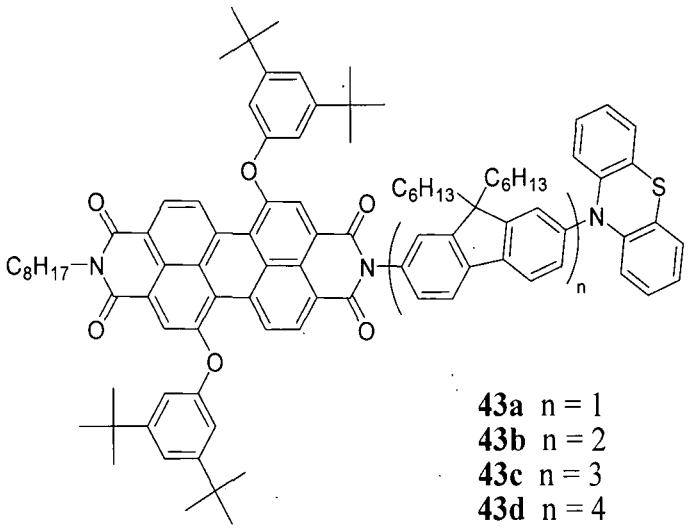


**43a** n = 1
**43b** n = 2
**43c** n = 3
**43d** n = 4

photovoltaic purposes. In this regard, Wasielewski *et al.* have recently shown that the length of oligofluorenes used as a bridge component between a phenothiazine (PTZ) donor unit and perylene bis(dicarboximide) (PDI) as an acceptor (**43**), could be modified without

significantly changing the energies of the relevant bridge states; this was a consequence of the charge localisation on the two terminal fluorene units of the oligomeric bridge.[123]

Encouraged by the findings, we have carried out a systematic study of new $C_{60}$-oligomer dyads and $C_{60}$-oligomer-$C_{60}$ dumbbell-type triads endowed with oligofluorene moieties of different lengths (*i.e.* dimer, trimer, tetramer and pentamer). This chapter will discuss the synthesis, electrochemical behaviour (studied by cyclic voltammetry) and the photophysical behaviour of these conjugate systems.

## 2.2 Results and Discussion

### Synthesis

Oligofluorenes with well-defined end-groups and chain length are predominantly made utilising the Suzuki-Miyaura reaction.[124-127] The mechanism of this reaction is generally described as a catalytic cycle involving oxidative addition-transmetalation-reductive elimination sequences in which the rate-limiting step is often the oxidative addition (Figure 2.1), but is under continuous investigation.[128-130] The relative reactivity of aryl halides decreases in the order I > Br > Cl and is influenced by the proximity of electron-donating or withdrawing groups.[131] This cross-coupling reaction proceeds smoothly when activated with suitable bases, since the reaction rate is influenced by the pH.[132]

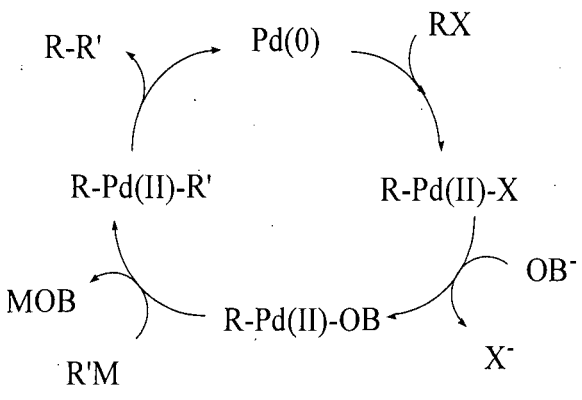


Figure 2.1: Reaction mechanism of the Suzuki-Miyaura cross-coupling reaction.

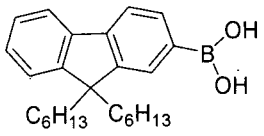

**44** Fl-BA

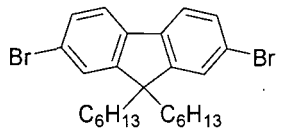

**45** Br-Fl-Br

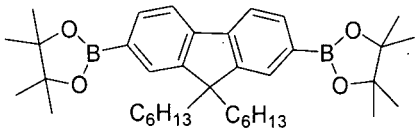

**46** BE-Fl-BE

Palladium catalysed aryl-aryl bond formation was dramatically improved by using boronic acids as the nucleophilic part of the reaction.[124] Although the preparation of boronic derivatives can be difficult, there are several advantages presented by boronic derivatives over other organometallic counterparts.[125] The compounds are easy to handle and involve lower toxicity reagents and byproducts in the reaction. The OH protons of arylboronic acids are often not visible in their $^1$H NMR spectra. This phenomenon occurs due to the ability of the acids either to form dimers through intermolecular hydrogen bonding or to lose water enabling the formation of tricyclic anhydrides, also known as boroxines.[133] Arylboronic esters can be prepared through lithiation, like arylboronic acids, or through a palladium catalysed reaction,[134] and can be more easily identified from their NMR spectra. Both boronic species possess a similar reactivity in the Suzuki methodology and are

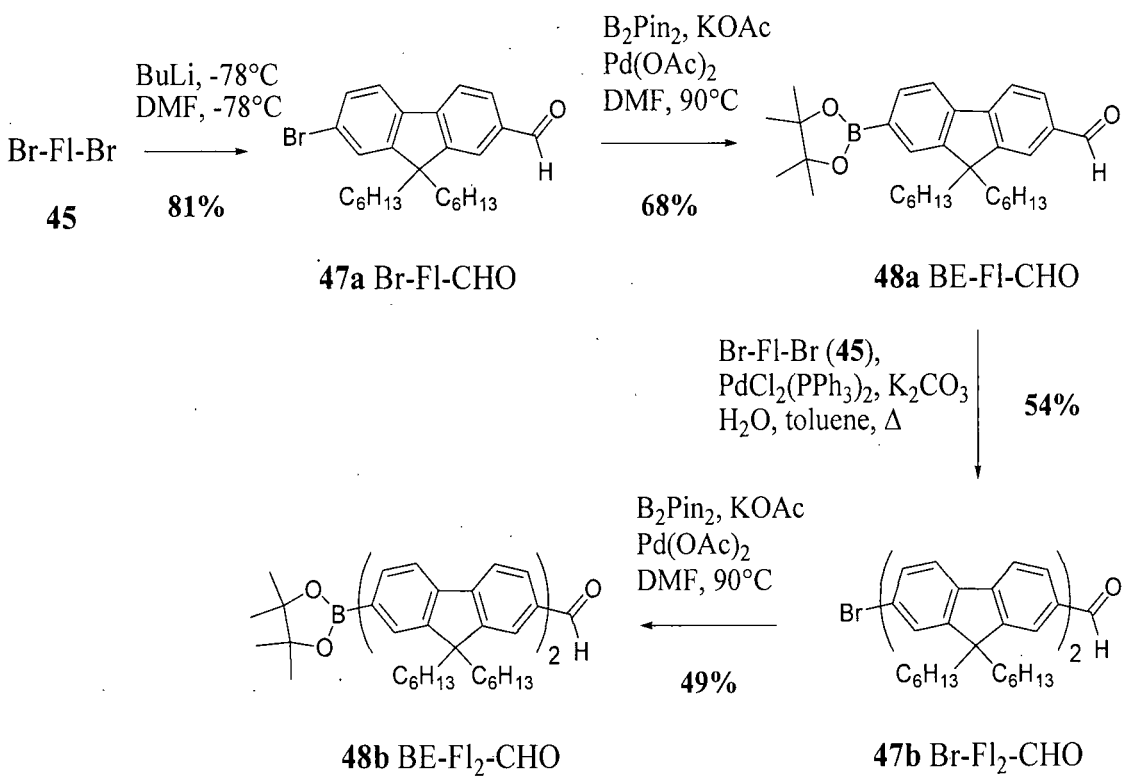


Scheme 2.1

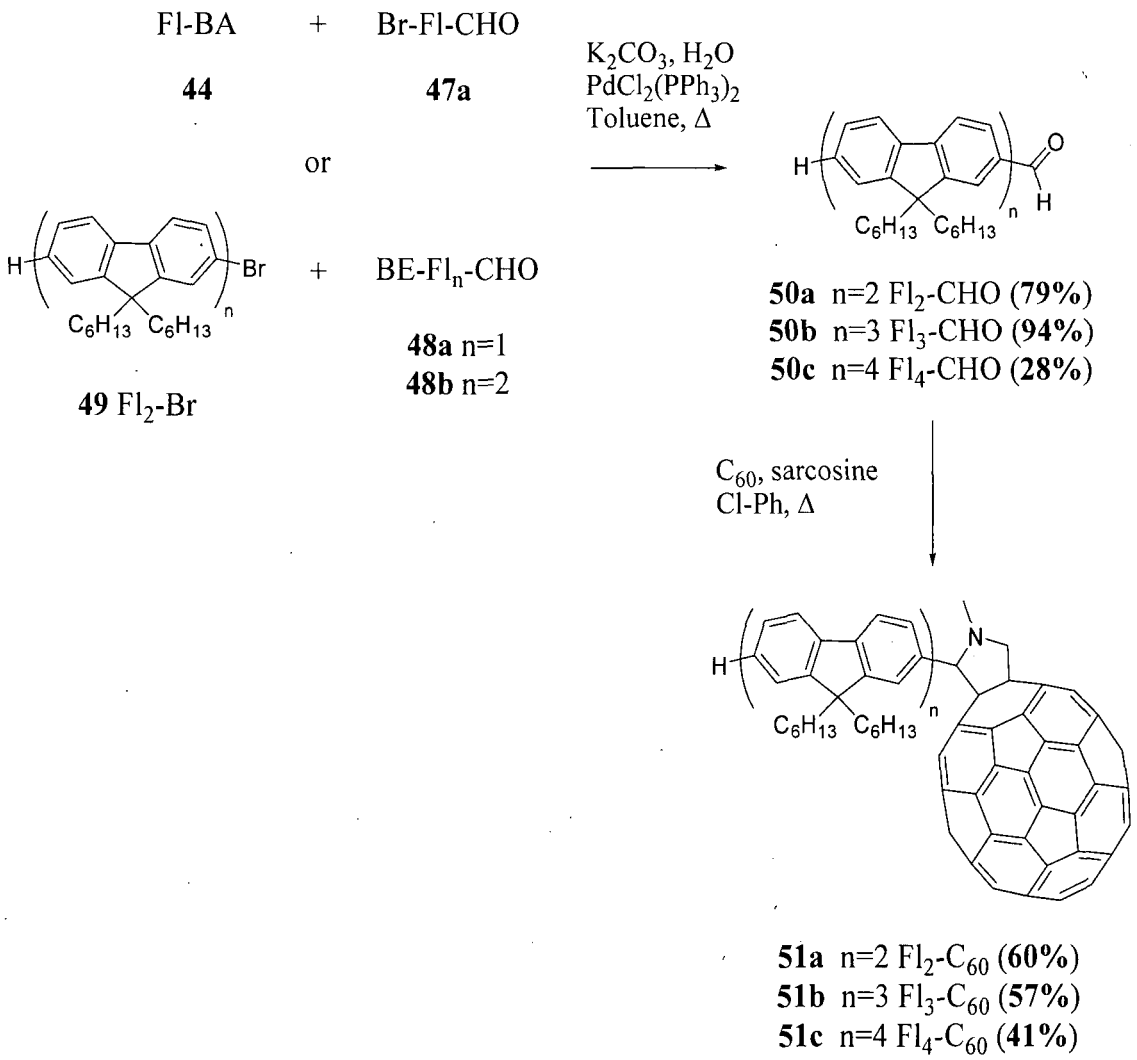


Scheme 2.2

therefore exchangeable between each other. First, fluorene monomers with two solubilising hexyl chains (**44-46**) were prepared in accordance with the literature.[126, 135, 136] Next, the oligofluorene building blocks were appended with formyl groups, to enable in the final stage the Prato reaction with $C_{60}$. Thus, monolithium-halogen exchange of **45**[136] in diethyl ether at -78 °C and subsequent quenching with DMF led to bromofluorene aldehyde **47a** in 81% yield (Scheme 2.1). The Suzuki coupling reaction has a wide tolerance towards a variety of functional groups, which includes aldehydes. Boronic acids / esters are conventionally prepared through treatment with butyllithium, which is not suitable to prepare a formyl containing arylboronate. Formylfluorene boronic ester **48a** was synthesised by heating **47a** in DMF at 90 °C with an excess of bis(pinacolato)diboron ($B_2Pin_2$) in the presence of a catalytic amount of palladium acetate (Scheme 2.1).[137]

Although not previously utilised in the presence of an aldehyde, this palladium catalysed route had been successfully used to boronate arylbromides containing electron-withdrawing groups, such as -COMe, -CN and –COOMe.[138] The literature reports that with one equivalent of the diboron ester only 10% dimer will be produced by the cross-coupling between the product and starting material,[138] but we found that for aldehyde **47a** the dimer was produced in 40-50% yield. An excess of bis(pinacolato)diboron (2.5 eq) prevented this side-reaction from occurring. Difluorene building blocks (Scheme 2.1) were prepared through the Suzuki reaction of **48a** and an excess of **45** under argon atmosphere in a mixture of $H_2O$ and toluene overnight at 110 °C together with $K_2CO_3$ and catalytic amounts of $PdCl_2(PPh_3)_2$. The bromofluorene aldehyde dimer **47b**, obtained in 54% yield, was then converted into the formylfluorene boronic ester dimer **48b** in 49% yield in similar manner as **48a**.

The fluorene building blocks were assembled into functionalised and well-defined oligomers using standard Suzuki conditions.[124, 126, 128, 135, 136, 139] In order to obtain two complementary series of oligofluorene-$C_{60}$ and $C_{60}$-oligofluorene-$C_{60}$, oligofluorenes containing one or two formyl groups at the termini, respectively, have been synthesised. Firstly, for the monoaldehyde precursors, reaction of **44**[126] with **47a** yielded dimer **50a** (Scheme 2.2) in 79% yield. Trimer **50b** and tetramer **50c** were subsequently obtained, in the same way, from the reaction between bromo difluorene **49**[136] and either **48a** or **48b** (Scheme 2.2). Secondly, for the dialdehyde precursors, dimer **52a** was obtained from **47a** and **48a** in 68% yield (Scheme 2.3). The Suzuki reaction of **46**[135] with **47a,b** gave trimer **52b** and pentamer **52c**, respectively in 59% and 41% yields (Scheme 2.4).

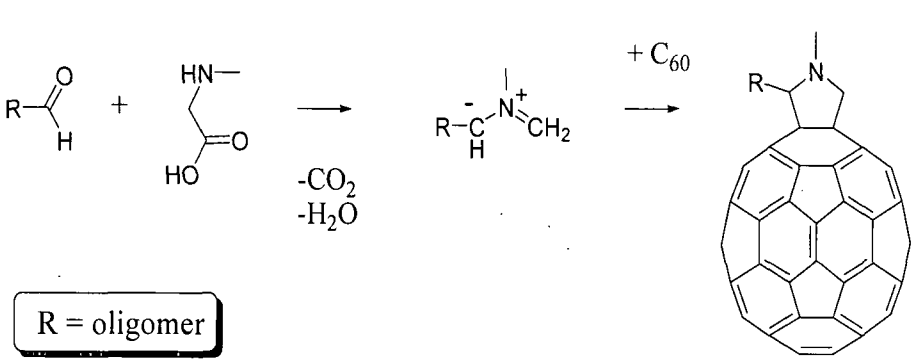


Scheme 2.3: Reaction mechanism of the 1,3-dipolar cycloaddition between an aldehyde, sarcosine and $C_{60}$.

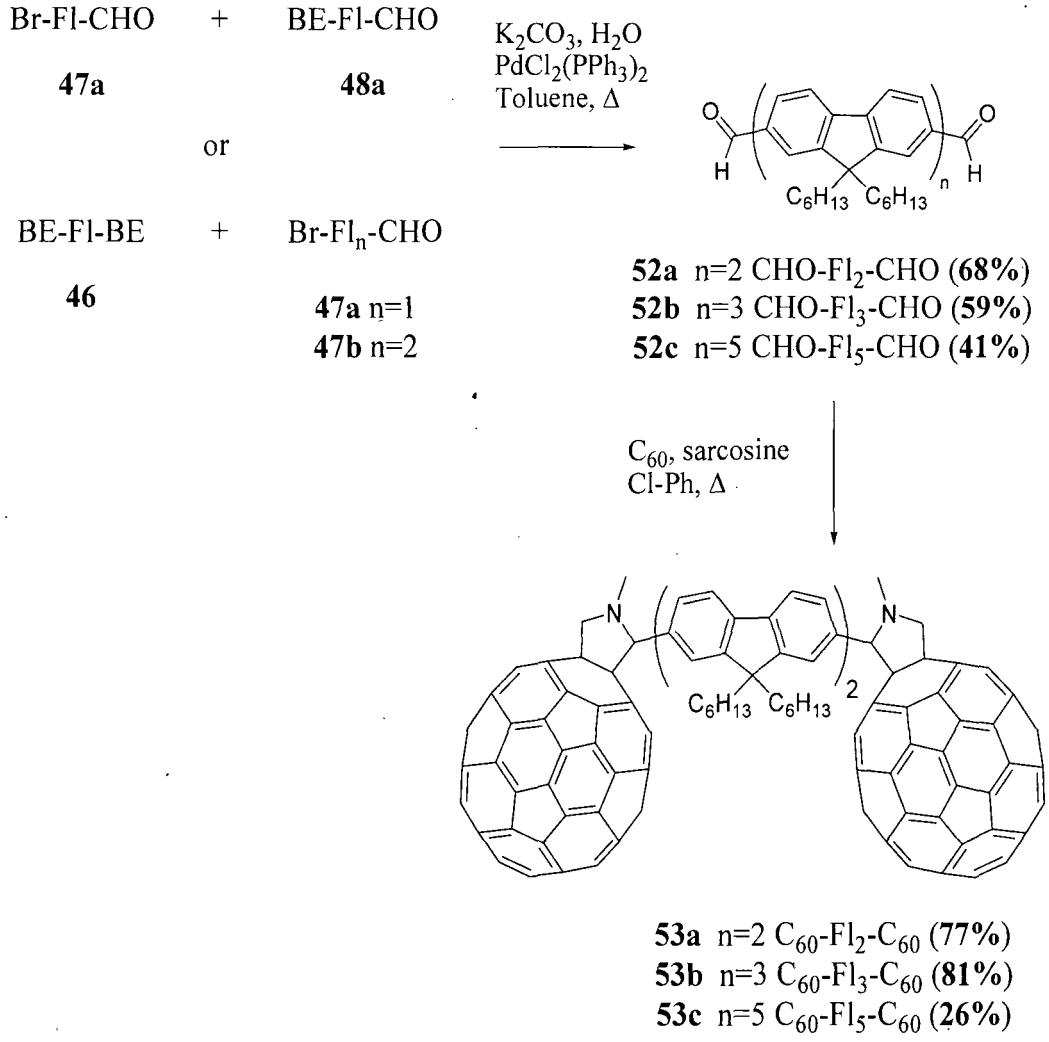


Scheme 2.4

Attachment of the [60]fullerene to the oligofluorenes has been achieved by a 1,3-dipolar cycloaddition, also known as the Prato reaction (Scheme 2.3).[140, 141] Azomethine ylides were formed *in situ* by reaction of aldehydes **50a-c** with sarcosine in refluxing chlorobenzene. Cycloadditions of these azomethine ylides with $C_{60}$ led to the formation of pyrrolidinofullerenes **51a-c** in moderate yields (Scheme 2.2). Enantiopure oligomers will yield an inseparable mixture of diastereoisomers as a stereocentre is introduced by this reaction in the pyrrolidine ring. Photophysical and analytical measurements are, however, not influenced by this stereocentre. Finally, Prato reaction of the diformyl oligofluorenes (**52a-c**) with sarcosine and an excess of $C_{60}$ afforded dumbbell-like compounds **53a,b** in good yields; pentameric analogue **53c** was obtained in lower yield (Scheme 2.4). For all Prato reactions (reported in this thesis) fullerene $C_{60}$ was used in excess, as this produces

less side-products and $C_{60}$ is readily available commercially. Unreacted $C_{60}$ is easily recovered at the end of the reaction and can be re-used in subsequent cycloadditions. NMR spectroscopy ($^{1}H$ and $^{13}C$) was used to characterise these fullerene containing materials. MALDI-TOF MS was used where possible.

## Electrochemical Studies

The electrochemical properties of **51a-c** and **53a-c** were probed by room temperature cyclic voltammetric measurements in an *o*DCB-$CH_3CN$ solvent mixture (4:1 v/v) with a glassy carbon working electrode, $Bu_4NClO_4$ as supporting electrolyte correlation and a scan rate of 100 mV $s^{-1}$. The redox potentials are collated in Table 2.1 together with those of **50a-c**, **52a-c**, pristine [60]fullerene and *N*-methyl pyrrolidinofullerene (**54**)[141] as references. At this point it should be noted that we describe the redox processes for our dyads and triads as quasireversible, since the redox process is chemically reversible for the systems discussed in this thesis (*i.e.* stable to repeated recycling). However, full agreement with the Nernst equation is not obtained, as the peak potential separation for the systems discussed in this thesis is on average 100 mV. The Nernst equation states that the peak potential separation of the reduction and oxidation wave should be equal to 59/n mV (n is the number of electron equivalents transferred during the redox process).[142]

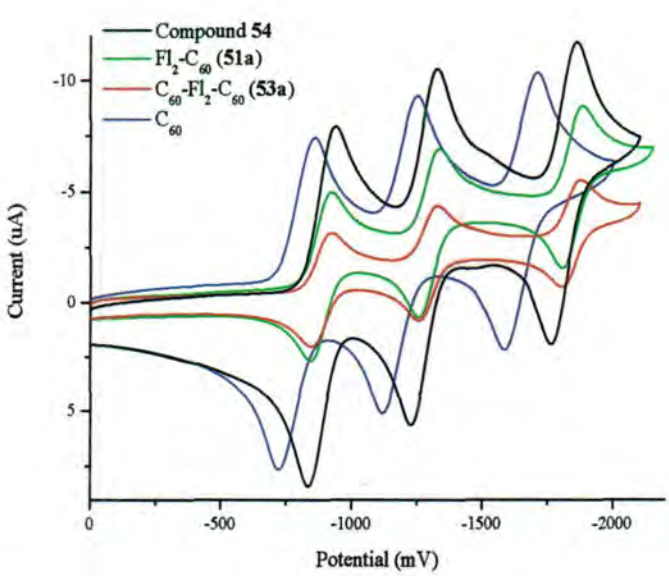



**54**

Figure 2.3: CVs of $C_{60}$, **51a**, **53a** and **54**. For conditions see Table 2.1.

Table 2.1: Redox potential values of $C_{60}$ derivatives **51a-c** and **53a-c**, together with aldehyde intermediates **50**, **52** and reference compounds (pristine $C_{60}$ and **54**).[a]

| Compound | $E^1_{red}$ | $E^2_{½, red}$ | $E^3_{½, red}$ | $E^4_{red}$ | $E^1_{ox}$ | $E^2_{ox}$ | $E^3_{ox}$ |
|---|---|---|---|---|---|---|---|
| $Fl_2$-CHO (**50a**) | -2029[b] | | | | 1295 | 1608 | 1873 |
| $Fl_3$-CHO (**50b**) | -2080 | | | | 1114 | 1332 | 1800 |
| $Fl_4$-CHO (**50c**) | -2083 | | | | 1045 | 1095 | 1572 |
| CHO-$Fl_2$-CHO (**52a**) | -2102 | | | | 1411 (1353)[b] | 1686 | |
| CHO-$Fl_3$-CHO (**52b**) | -2058 | | | | 1179 (1126)[b] | 1368[b] | |
| CHO-$Fl_5$-CHO (**52c**) | -2078 | | | | 1087 (1061)[b] | 1262[b] | 1612 |
| $C_{60}$ | -795[b] | -1191 | -1649 | -2122[b] | | | |
| **54** | -885[b] | -1280 | -1813 | -2313 | 1116 | 1687 | |
| $Fl_2$-$C_{60}$ (**51a**) | -882[b] | -1293 | -1843 | -2333 | 1170 | 1345 | 1623 |
| $Fl_3$-$C_{60}$ (**51b**) | -880[b] | -1292 | -1839 | | 1096 | 1394 | 1809 |
| $Fl_4$-$C_{60}$ (**51c**) | -879[b] | -1293 | -1848 | | 1032 | 1195 | 1555 |
| $C_{60}$-$Fl_2$-$C_{60}$ (**53a**) | -882[b] | -1294 | -1839 | -2315 | 1182 | 1545 | |
| $C_{60}$-$Fl_3$-$C_{60}$ (**53b**) | -884[b] | -1294 | -1839 | -2344 | 1123 | 1473 | |
| $C_{60}$-$Fl_5$-$C_{60}$ (**53c**) | -883[b] | -1293 | -1838 | | 1125 | 1477 | 1641 |

[a]Potentials in mV; scan rate 100 mV $s^{-1}$; glassy carbon working electrode, $Ag/AgNO_3$ reference electrode, Pt counter electrode; 0.1 M $Bu_4NClO_4$ in *o*DCB/$CH_3CN$ (4:1 v/v). [b] Half wave potential values ($E_{½}$).

As a general feature, **51a-c** and **53a-c** give rise to amphoteric redox behaviour. On the reduction side, at least three consecutive quasireversible reduction waves have been observed. Since a particularly good agreement was found with **54**, we assign these waves to the reduction steps of the fullerene core (Figure 2.3). Moreover, they corroborate the lack of electronic communication between the fullerene core and the oligomer moieties in the ground state of **51a-c** and **53a-c**.[78, 87, 92, 143] When contrasting **51** and **53** with pristine [60]fullerene, cathodic shifts to more negative values are observed. This is a clear reflection of saturating a double bond of the $C_{60}$ core as a consequence of the functionalisation and raising the LUMO energy in **51a-c** and **53a-c**.[39] A one-electron process is allocated to each reduction wave of $C_{60}$, **51** and **54**. The two $C_{60}$ units in **53** act independently: each reduction wave is, therefore, assigned to a two-electron process.

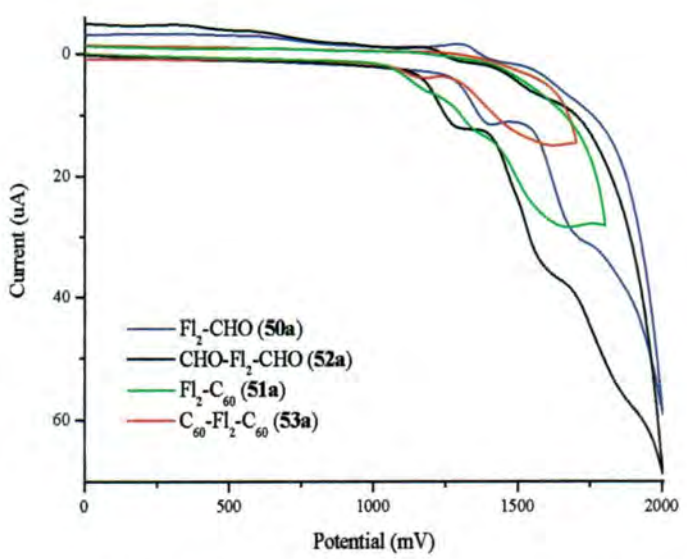


Figure 2.4: CVs of **50a**, **51a**, **52a** and **53a**. For conditions see Table 2.1.

On the oxidation side, derivatives **50**, **51**, **52** and **53** display two or, in some cases, three oxidation waves – most of them irreversible – ascribed to the oligofluorene system (Figure 2.4). The first oxidation step is subject to a notable electron withdrawing effect exerted by the aldehyde group(s). This is particularly pronounced in **50a** (*i.e.*, dimer with one -CHO functionality) and **52a** (*i.e.*, dimer with two –CHO functionalities) with anodic shifts up to 1295 mV and 1411 mV, respectively. The electron withdrawing influence of the aldehyde group decreases as the length and donor character of the oligomer increases. Figure 2.4 illustrates that substituting the formyl groups in **50a** and **52a** by $C_{60}$ shifts the anodic

oxidation to less positive values in **51a** and **53a**. This is less clearly observed for the longer oligofluorene in these series as the effect of the –CHO functionality is less pronounced to begin with. Implicit here is the loss of conjugation between the electron withdrawing formyl groups and the oligomer moieties. At the same time, going from the dimer to the trimer and pentamer (**50a** → **50b** → **50c**) sequentially raises the donor character due to a more extended π-conjugation. Consequently, the oxidation values shift cathodically: e.g. $E^1_{ox}$ 1170 mV (**51a**), 1096 mV (**51b**), 1032 mV (**51c**). A similar trend evolves for **52a-c** where the first quasireversible waves shift between $E^1_{ox}$ 1411 and 1087 mV (see Table 2.1). This trend is also observed for **53a** and **53b**, although a further cathodic shift is not seen for **53c**.

## Photophysical Studies

The photophysical properties were studied in Dirk Guldi's laboratory at University Erlangen-Nürenberg. First, the steady-state fluorescence spectra of **50a-c** and **52a-c** were recorded upon 345 nm photoexcitation. In general, all oligofluorenes fluoresce strongly throughout the visible region, which renders this particular feature extremely valuable to dissect excited state interactions with $C_{60}$ in **51a-c** and **53a-c**. Not surprisingly, when inspecting the oligofluorene fluorescence in **51a-c** and **53a-c** under identical experimental

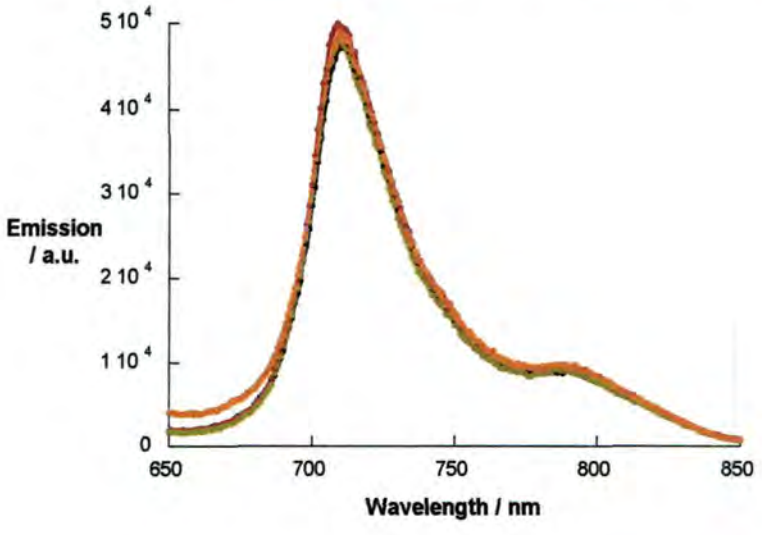


Figure 2.5: Fluorescence spectra of **54** (black line), **53c** (red line), **53a** (green line) and **53b** (orange line) in THF, with matching absorption of 0.2 at the 370 nm excitation wavelength.

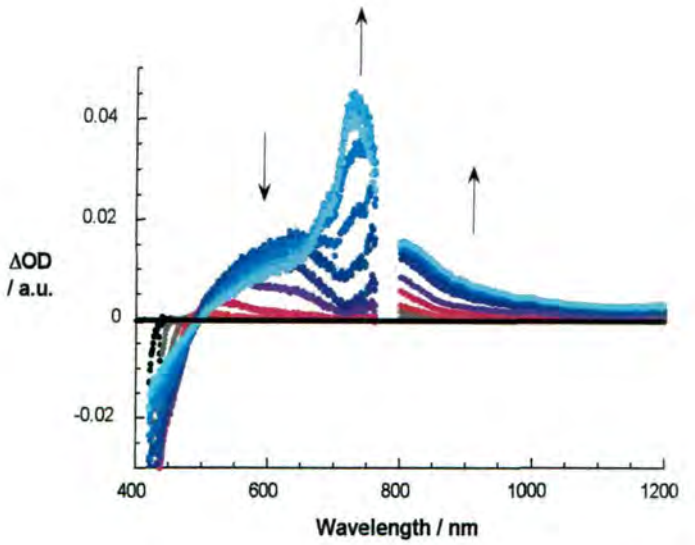


Figure 2.6: Differential absorption spectra (visible and near-infrared) obtained upon femtosecond flash photolysis (387 nm) of **52b** in nitrogen saturated THF solutions with several time delays between 0 and 20 ps at room temperature.

conditions a marked fluorescence quenching is seen. The quenching, for example, in toluene is as high as $10^3$ (*i.e.*, **53a**: 0.30 x $10^3$; **53b**: 1.47 x $10^3$; **53c**: 0.51 x $10^3$) and these values tend be higher for **53a-c** than for **51a-c**. Nevertheless, it is important that the fluorescence pattern of the oligofluorenes is still preserved, despite the presence of one or two $C_{60}$ units.

Turning to the near-infrared region of the fluorescence spectrum (Figure 2.5) the observed

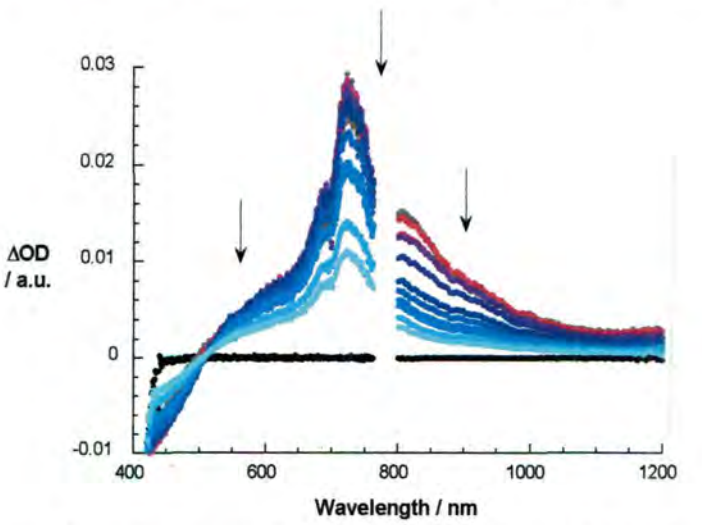


Figure 2.7: Differential absorption spectra (visible and near-infrared) obtained upon femtosecond flash photolysis (387 nm) of **52b** in nitrogen saturated THF solutions with several time delays between 0 and 1600 ps at room temperature.

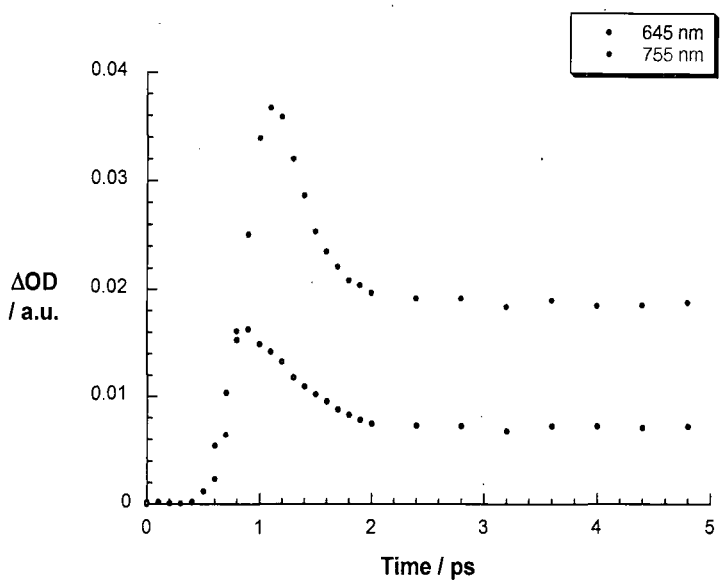


Figure 2.8: Time-absorption profiles of the spectra shown in Figure 2.7 and 2.8 at 645 and 755 nm, monitoring the formation of the singlet excited state.

features resemble those known for **54**.[27] Notably a 370 nm photoexcitation directs the light nearly quantitatively to the oligofluorenes and not to $C_{60}$. A reasonable explanation implies transduction of singlet excited state energy from the oligofluorenes (2.70 eV) to $C_{60}$ (1.76 eV). Independent confirmation for this hypothesis was obtained from excitation spectra, where the fluorescence wavelength was kept constant at 715 nm and the excitation wavelength was systematically varied (not shown). An exceptionally good agreement with the ground state absorption spectrum confirms that the $C_{60}$ fluorescence evolves, largely, from singlet energy transfer and, to a minor extent, from direct excitation. Quantification of the energy transfer reaction was possible through comparing the $C_{60}$ fluorescence quantum yields in solutions of **51a-c** and **53a-c** in toluene with that of **54** as an internal reference under exactly the same experimental conditions. Quantum yields of nearly 6.0 x $10^{-4}$ in all samples speak for a quantitative energy transfer in **51a-c** and **53a-c**.

In parallel with the steady-state experiments, the fluorescence lifetimes of **51a-c** and **53a-c** were compared to references, namely, oligofluorenes (*i.e.* **50a-c** and **52a-c**) and $C_{60}$ (*i.e.* **54**), which possessed lifetimes of the order of a few ns in the visible and near-infrared regions, respectively. In contrast, **51a-c** and **53a-c** lack any fluorescence with appreciable lifetimes in the visible range, *i.e.* the oligofluorene part. Only the near-infrared range (the $C_{60}$ part) gave rise to a detectable fluorescence with a lifetime of 1.4 ns. The rise of the $C_{60}$

fluorescence is, however, instantaneous and is masked by the instrumental time resolution of *ca.* 100 ps, preventing an accurate determination of the energy transfer dynamics.

In the final part of this investigation the oligofluorenes were studied in femto- (*i.e.* 387 nm) and nano-second (*i.e.* 355 nm) transient absorption measurements, where both constituents are nearly equally photoexcited. First, consider compounds **52a-c**. They revealed, upon photoexcitation, the nearly instantaneous generation (*i.e.* < 0.5 ps, Figure 2.6) of metastable singlet excited state transients (*i.e.* 0.8 ns, Figure 2.7). The spectral characteristics of these transients are ground state bleaching in the 400 – 450 nm range and new transient absorption in the 600 - 1200 nm range. The transient maxima vary with the length of the oligofluorene unit: 670 nm (dimer **52a**), 725 nm (trimer **52b**) and 725 nm (pentamer **52c**). Interestingly, the exciton appears to be confined in a very short conjugation length. The product of the aforementioned decay (*i.e.* 0.8 ns) is the corresponding triplet excited state of **52a-c**.

Initially upon photoexciting **51a-c** and **53a-c** transient species evolve which disclose features commonly seen in the oligofluorene references (**52a-c**), namely, transient bleach (*i.e.* below 450 nm) and transient maxima (*i.e.* around 700 nm), which can be seen in

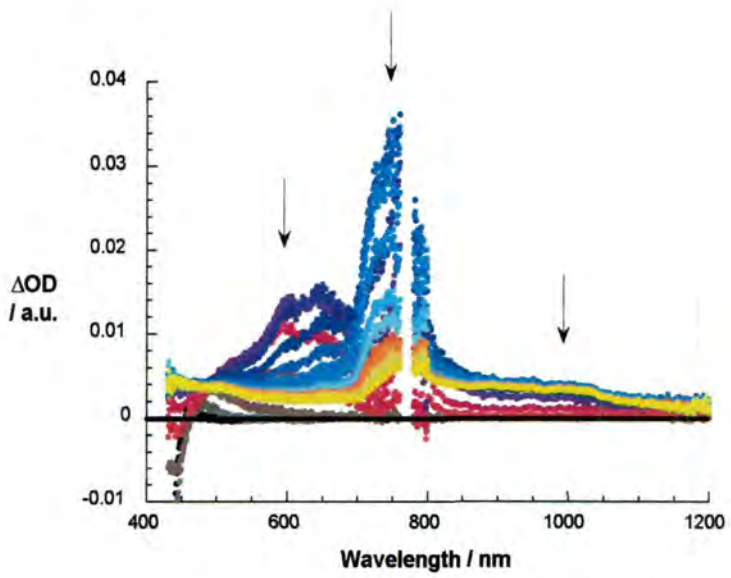


Figure 2.9: Differential absorption spectra (visible and near-infrared) obtained upon femtosecond flash photolysis (387 nm) of **53b** in nitrogen saturated THF solutions with several time delays between 0 and 2 ps at room temperature.

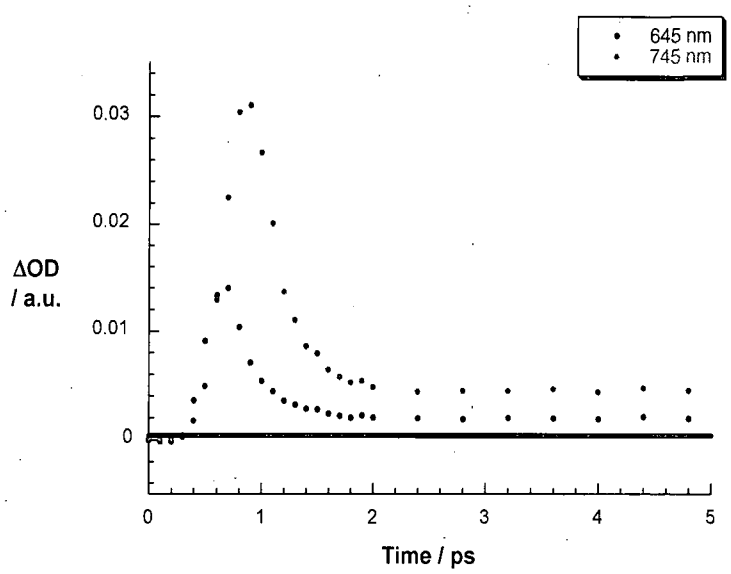


Figure 2.10: Time-absorption profiles of the spectra shown in Figure 2.10 at 645 and 745 nm, monitoring the formation of the singlet excited state.

Figure 2.9 and 2.10. Such an observation is important, since it attests - in close agreement with the ground state absorption at $\lambda_{exc}$ 387 nm - the successful excitation of the oligofluorene moieties. However, the oligofluorene singlet excited state features decay much faster than that observed for the intersystem crossing process in **52a-c**. Typical rate constants for this decay are on the order of $\sim 10^{12}$ $s^{-1}$. Such values confirm the quantitative quenching of the oligofluorene fluorescence in **51a-c** and **53a-c**. Interestingly, comparing the rate constants of oligofluorene deactivation between the **51a-c** series and the **53a-c**

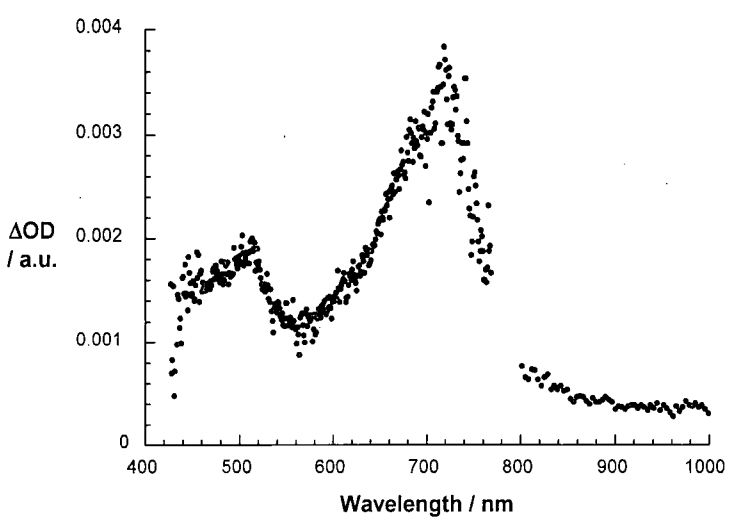


Figure 2.11: Differential absorption spectra (visible and near-infrared) obtained upon femtosecond flash photolysis (387 nm) of **53b** in nitrogen saturated THF solutions with a time delay of 3000 ps at room temperature, indicating the fullerene triplet-triplet features.

series a two-fold acceleration is seen for the latter series (*i.e.* **51a**: 0.9 ps; **51b**: 1.3 ps; **51c**: 1.9 ps; **53a**: 0.6 ps; **53b**: 0.7 ps; **53c**: 1.0 ps). In other words, placing two $C_{60}$ instead of one $C_{60}$ on the oligofluorene assists in accelerating the excited state decay. At the conclusion of the oligofluorene decay only the $C_{60}$ singlet excited state features are discernable, that is, a transient maximum at 880 nm.

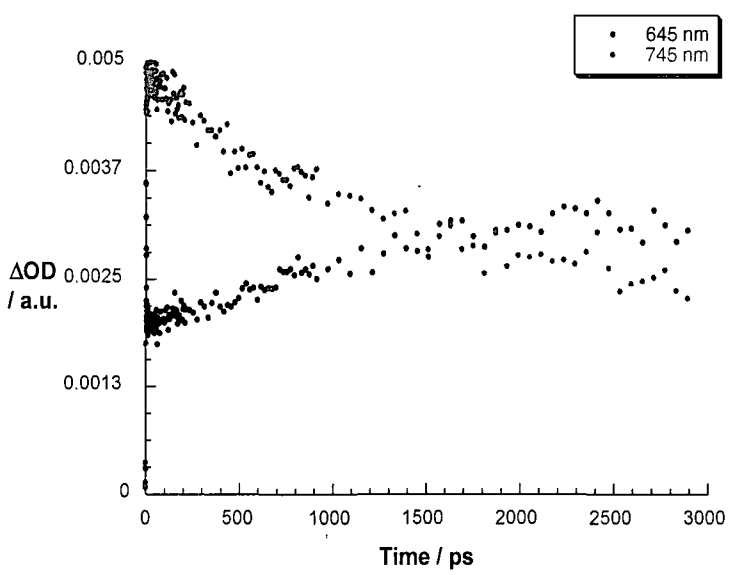


Figure 2.12: Time-absorption profiles of the spectra shown in Figure 2.12 at 645 and 745 nm, monitoring the decay of the singlet excited state and formation of the triplet excited state.

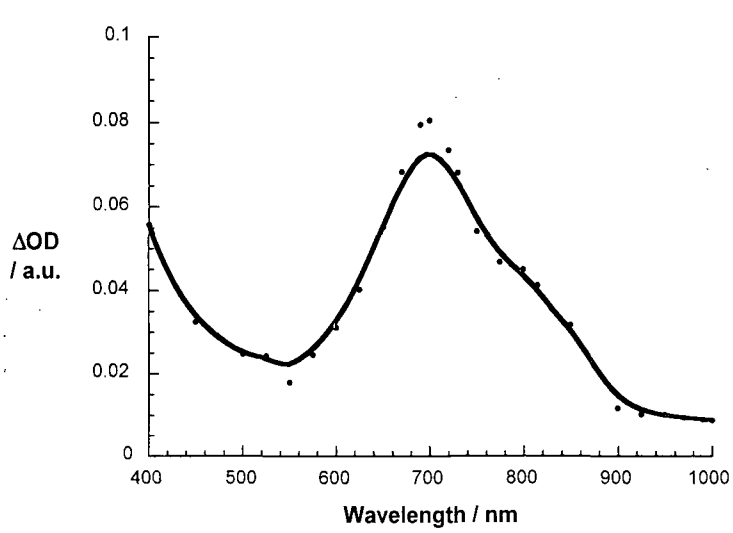


Figure 2.13: Differential absorption spectra (visible and near-infrared) obtained upon femtosecond flash photolysis (355 nm) of **53b** ($2.0 \times 10^{-5}$ M) in nitrogen saturated THF solutions with a time delay of 100 ns at room temperature, indicating the fullerene triplet-triplet features.

On a time-scale of up to 3.0 ns the $C_{60}$ singlet excited state intersystem crosses to the corresponding triplet manifold. Importantly, the kinetics of the singlet decay and the triplet growth match each other reasonably well to yield intersystem crossing rates in **51a-c** and **53a-c** of 6.5 x $10^8$ $s^{-1}$ (Figure 2.11). The most prominent feature of the $C_{60}$ triplet excited state is a 700 nm maximum as it evolves towards the end of the time-scale of the femtosecond experiments (*i.e.* 3.0 ns), which is depicted in Figure 2.12. In complementary nanosecond experiments with **51a-c** and **53a-c** the same triplet transient is seen, which in the absence of molecular oxygen, decays with multiexponential kinetics. An illustration is given in Figure 2.13.

## 2.3 Conclusions

We have carried out the rational design and synthesis of $C_{60}$-$(Fl)_n$ derivatives **51a-c** and $C_{60}$-$(Fl)_n$-$C_{60}$ derivatives **53a-c** in which 9,9-dihexylfluorene oligomers of well-defined length are attached to *N*-methyl pyrrolidinofullerene termini. The new compounds were prepared using Suzuki cross-coupling methodology to assemble oligofluorenes with terminal aldehyde units, followed by Prato 1,3-dipolar cycloaddition reactions of *in situ* generated azomethine ylides with $C_{60}$. The solution electrochemical data show amphoteric behaviour (three one-electron reduction waves of each $C_{60}$ core) and irreversible oxidations of the oligofluorene chains with no significant interaction between these electroactive partners in the ground state. Fluorescence time-resolved and steady-state experiments were carried out to determine the photophysical behaviour of the new compounds. In particular, an efficient transduction of singlet excited state energy transfer prevails from the photoexcited oligofluorene to the energy accepting fullerene. Importantly, no spectral evidence has been found that would suggest the presence of competing electron transfer reactions that would evolve from the energetically high lying singlet excited states of the oligofluorenes. The next two chapters will address D-$(Fl)_n$-$C_{60}$ ensembles where D is a strong electron donor group designed to further probe the effect of integrating oligofluorene molecular wires into donor-acceptor pairs.

# Chapter 3: *ex*TTF-Oligofluorene-$C_{60}$ Triads

## 3.1 Introduction

In Chapter 2 the synthesis and properties of oligofluorene-$C_{60}$ (**51a-c**) and $C_{60}$-oligofluorene-$C_{60}$ (**53a-c**) were discussed. In Chapters 3 and 4 we extend this work and address D-$(Fl)_n$-$C_{60}$ ensembles where D is a strong electron donor group designed to further probe the effect of integrating fluorene molecular wires into donor-accepter pairs.

Initial efforts will focus on the insertion of oligofluorene in between a *p*-quinonoid π-extended tetrathiafulvalene (*ex*TTF) donor and fullerene. The TTF derivative with π-extended conjugation possesses a strong donor character, similar to its parent TTF.[144-146] The ability of the quinonoid structure to form a new aromatic (anthracene) ring system upon oxidation rationalises the decrease of the on-site Coulombic repulsions in the charged species.[144-148] Stable dication species are produced by *ex*TTF analogues forming charge-transfer complexes with interesting electrical and magnetic properties.[144-146] Examples of *ex*TTF donors covalently linked to $C_{60}$, some including an oligomeric bridge, have been discussed in Chapter 1.

The *ex*TTF-$(Fl)_n$-$C_{60}$ triad structure we aimed to create was inspired by similar ensembles from the literature.[27, 95, 97, 149] By maintaining the basic structure and changing only the oligomeric bridge the efficiency of charge-transfer between the electron donor and acceptor by different molecular wires can be more easily compared. Therefore this chapter will discuss the synthesis of *ex*TTF-$(Fl)_n$-$C_{60}$ assemblies wherein the oligofluorene bridge is covalently linked to the fullerene cage through a pyrrolidine ring and full conjugation is obtained between the donor and the wire. These systems have been subjected to electrochemical and photophysical studies. Determination of the attenuation factor (β, Chapter 1) allowed us an insight into the molecular wire behaviour of the fluorene based bridge.

## 3.2 Results and Discussion

### Synthesis

The coupling of the *ex*TTF moiety to the oligofluorene bridge should allow extended conjugation to be achieved, to facilitate the electronic coupling between the donor and acceptor. A Suzuki cross-coupling reaction between *ex*TTF and fluorene would yield such a triad,[124, 128] where the donor is directly linked to the oligomeric bridge. In Chapter 2 the syntheses of the fluorene monomer and dimer **48a,b**, featuring two solubilising hexyl chains, a formyl group as a link to the $C_{60}$ and a boronic ester, were discussed. The palladium-catalysed reaction of these fluorene building blocks with 2-iodo-9,10-bis(1,3-dithiol-2-ylidene)-9,10-dihydroanthracene (**55**)[150] afforded compounds **56a** and **56b** in good yields (Scheme 3.1). Subsequently the presence of the formyl group

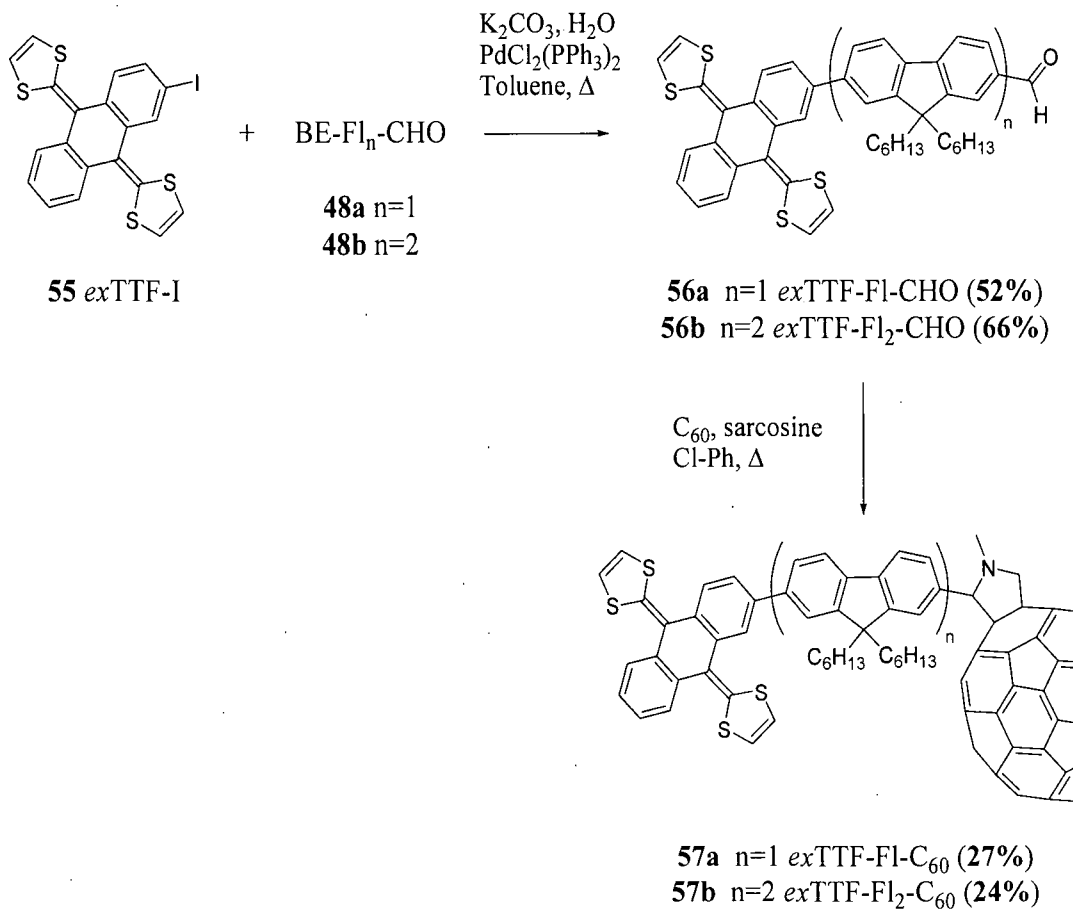


Scheme 3.1

allowed the *in situ* generation of the corresponding azomethine ylides by reaction with sarcosine in refluxing chlorobenzene (see Chapter 2), which provided the cycloadducts **57a,b** by cycloaddition to $C_{60}$ following Prato's protocol (Scheme 3.1).[140] During the work-up of **57a,b** it was noted that these triad ensembles decompose upon exposure to light and air. Characterisation of decomposed **57b** (**58**, structure shown in experimental section) revealed oxidation of the *ex*TTF unit (see Chapter 6); this sensitivity of the donor unit is observed only after the addition of $C_{60}$. Decomposition was not observed for **56a,b** and the formation of the pyrrolidine ring was not affected. For this reason, the Prato reaction was conducted under argon and in a dimly lit laboratory as a precaution. Compounds **57a,b** were obtained by purification in dim light and afterwards were perfectly stable in the solid state when stored under argon and in the dark.

In a second step we have investigated increasing the length of the fluorene wire bridging the *ex*TTF and $C_{60}$ units. As discussed in Chapter 2, dimer **48b** was prepared from monomer **47b** in two steps (Scheme 2.1). A similar method could not be employed to produce a formyl and boronic ester functionalised trimer, due to limited availability of **48b**.

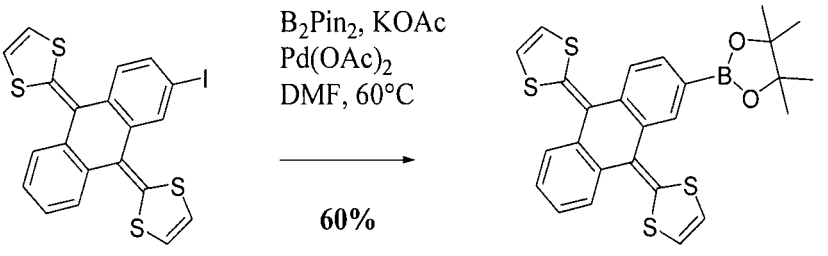


**55** *ex*TTF-I

**59** *ex*TTF-BE

Scheme 3.2

Purification of these oligofluorenes becomes more delicate as the length increases, which affects yields and this was particularly apparent during the purification of **48b**. As no oligofluorene trimer, containing both a boronic ester and a formyl group, could be synthesised, a boronic ester functionalised *ex*TTF (**59**) was synthesised, utilising the same procedure as for **48a**, in good yield from *ex*TTF-I (Scheme 3.2).

Lithiation of monomer **45** yielded monomer Br-Fl-CHO (**47a**) and we found that using 2-3 equivalents butyllithium yielded the same product, as the lithiation at one terminus affects

the reactivity of the remaining bromine. 7,7"-Dibromo-9,9,9',9',9",9"-hexahexyl-9*H*,9'*H*,9"*H*-[2,2',7',2"]terfluorene (**60**) was prepared in accordance with the literature.[151] The ample distance between the bromines at both termini of this trimer ensures that the reactivity of both bromines is the same throughout a lithiation process. Thus, monolithium-halogen exchange of **60** in diethyl ether at -78 °C and subsequent quenching with an excess of DMF led to the formation of multiple side-products and this mixture could not be successfully separated.

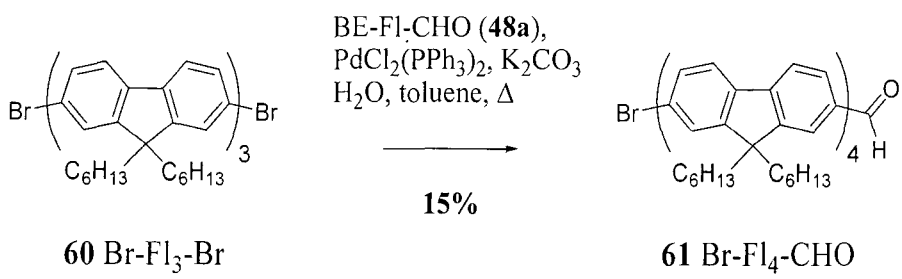


**60** Br-$Fl_3$-Br **61** Br-$Fl_4$-CHO

Scheme 3.3

In an alternative attempt to prepare a longer oligofluorene bridge for our *ex*TTF-wire-$C_{60}$ triads we reacted **48a** with **60** via Suzuki reaction and obtained the desired tetramer **61** in low yield (Scheme 3.3). Subsequent palladium-catalysed cross-coupling between **59** and **61** yielded a multi component mixture, which provided no product after purification. Finally, cross-coupling between **45** and **59** to produce *ex*TTF-Fl-Br which could have then been reacted with **48b** to provide a terfluorene bridge, was not undertaken due to the limited availability of *ex*TTF-I (**55**).

## Electrochemical Studies

The electrochemical properties of **57a,b** were probed by room temperature cyclic voltammetric measurements in an *o*DCB-$CH_3CN$ solvent mixture (4:1 v/v) with a glassy carbon working electrode, $Bu_4NClO_4$ as supporting electrolyte and a scan rate of 100 mV $s^{-1}$. The redox potentials are collated in Table 3.1 together with those of **48a,b**, **50a**, **51a**, **53a**, **56a,b**, *ex*TTF-I, pristine [60]fullerene and *N*-methyl pyrrolidinofullerene (**54**) as references.

Table 3.1: Redox potential values of triads **57a** and **57b**, together with aldehyde intermediates **48a,b**, **56a,b** and reference compounds (pristine $C_{60}$, *ex*TTF-I, **50a**, **51a**, **53a** and **54**).[a, b]

| Compound | $E^1_{red}$ | $E^2_{½, red}$ | $E^3_{½, red}$ | $E^4_{red}$ | $E^1_{ox}$ | $E^2_{ox}$ | $E^3_{ox}$ |
|---|---|---|---|---|---|---|---|
| BE-Fl-CHO (**48a**) | -1848 | | | | 1380 | | |
| BE-$Fl_2$-CHO (**48b**) | | | | | 1250 | | |
| $Fl_2$-CHO (**50a**) | -2029[c] | | | | 1295 | 1608 | 1873 |
| *ex*TTF-I (**55**) | | | | | 232 | 1643 | |
| *ex*TTF-Fl-CHO (**56a**) | -1978 | | | | 234 | 1458 | |
| *ex*TTF-$Fl_2$-CHO (**56b**) | | | | | 259 | 1280 | |
| $C_{60}$ | -761[c] | -1171 | -1632 | -2098[c] | | | |
| **54** | -863[c] | -1263 | -1802 | | 1140 | 1710 | |
| $Fl_2$-$C_{60}$ (**51a**) | -882[c] | -1293 | -1843 | -2333 | 1170 | 1345 | 1623 |
| $C_{60}$-$Fl_2$-$C_{60}$ (**53a**) | -882[c] | -1294 | -1839 | -2315 | 1182 | 1545 | |
| *ex*TTF-Fl-$C_{60}$ (**57a**) | -874[c] | -1291 | -1834 | | 215 | 1091 | 1665 |
| *ex*TTF-$Fl_2$-$C_{60}$ (**57b**) | -889[c] | -1287 | -1787 | | 281 | 1277 | 1682 |

[a] Potentials in mV; scan rate 100 mV $s^{-1}$; glassy carbon working electrode, $Ag/AgNO_3$ reference electrode, Pt counter electrode; 0.1 M $Bu_4NClO_4$ in *o*DCB/$CH_3CN$ (4:1 v/v). [b] See also Table 2.1, Chapter 2. [c] Half wave potential values ($E_{½}$).

Amphoteric redox behaviour was observed for both triads **57a** and **57b**. Electrochemical measurements provide information about the donor and acceptor strength of the different components within the synthesised triads. On the reduction side (Figure 3. 1), $C_{60}$ is by far the best electron acceptor with a first one-electron reduction potential of -874 (**57a**) and -889 mV (**57b**). The three consecutive one-electron reduction waves can be allotted to the $C_{60}$ core, since good conformity with the reduction behaviour of reference compounds **51a** and **54** is observed. The good agreement of these quasireversible waves suggests the absence of significant electronic interactions.[78, 87, 92, 143] Compared to pristine $C_{60}$, cathodic shifts have been noted for **57a,b**, which were also observed for **51a-c** and **53a-c**. Again this is consequence of the saturation of a double bond on the fullerene core and the raised LUMO energy in **57a,b**.[39]

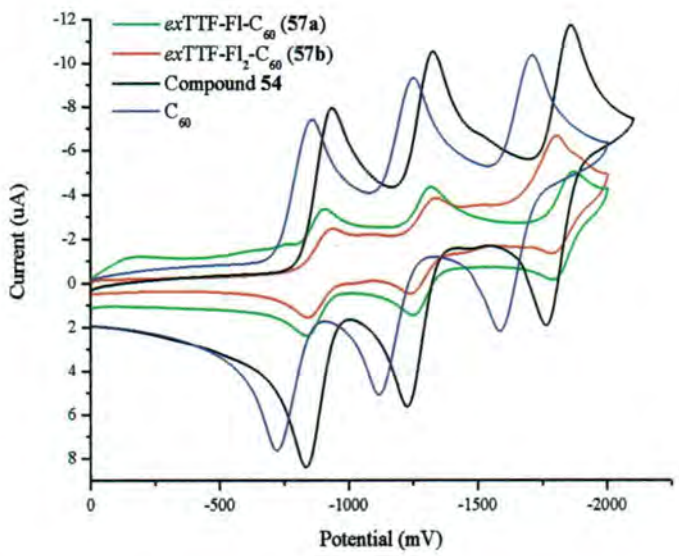


Figure 3.1: CVs of $C_{60}$, **54** and **57a,b**. For conditions see Table 3.1.

Two or three irreversible oxidation waves are observed during the oxidation of **57a,b** and the various reference compounds (Figure 3.2). As established for **50a** (Chapter 2), the aldehyde group subjects the oligofluorene system to a notable electron withdrawing effect, which can also be observed in Table 3.1 for **48a,b** and **56a,b**. The first oxidation wave of the oligofluorene system in dimer **50a** had shifted to 1295 mV, due to the electron withdrawing effect exerted by the aldehyde moiety. Similarly, the same wave is observed at 1280 mV in **56b** showing that the addition of *ex*TTF has a negligible effect on the oxidation of the oligofluorene. As discussed in Chapter 2, the influence of the formyl group increases as the oligomer decreases in length and donor character, *e.g.* **48a** (1380

mV) compared to **48b** (1250 mV) and **56a** (1458 mV) versus **56b** (1280 mV). Interestingly, a noteworthy cathodic shift is observed for **57a** and to a lesser extent for **57b**, which can be assigned to the boronic ester group. Comparison between **50a**, **56a,b** and **57a,b** suggests that the electron donating effect of this functional group decreases as the length of the oligofluorene increases.

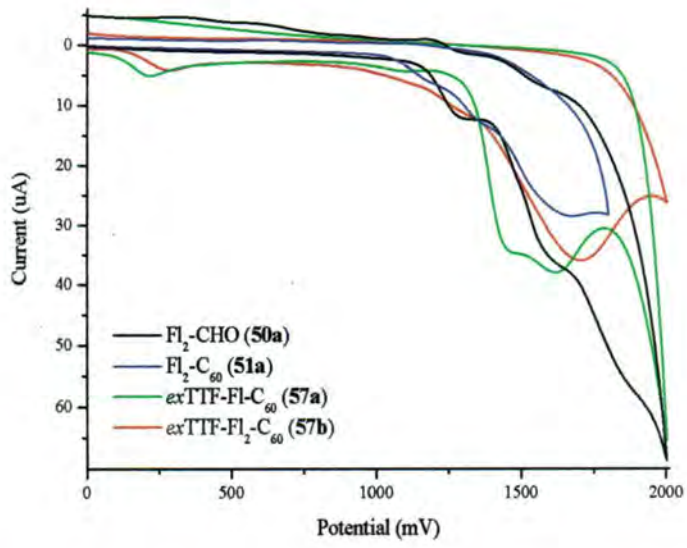


Figure 3.2: CVs of **50a**, **51a**, **57a,b**. For conditions see Table 2.1.

Finally, three irreversible oxidation waves were observed for **57a,b**. The first oxidation wave can be ascribed to the formation of an *ex*TTF dication,[144-146] indicating that *ex*TTF is the strongest donor in this triad. The two one-electron processes coincide leading to the observance of one two-electron process as the presence of the quinonoid structure leads to unstable, highly distorted, non-planar, radical cations.[152, 153] Our reference compound **55** has a slightly poorer oxidation potential than its parent *ex*TTF, due to the electronegative iodine atom.[150] Therefore, no notable anodic shift due to the formyl group is observed for **56a,b** in comparison to **55**. As the length of the oligofluorene is increased from **56a** to **56b**, the more positively shifted oxidation of **56b** cannot be allocated to the -CHO functionality. Moreover, this anodic shift to more positive values for the *ex*TTF dication is even more potent in **57b**, which was unanticipated. Interestingly, monomer **57a** did behave as expected, with the oxidation of both the *ex*TTF and oligomer moieties being at less positive values relative to **56a**, due to the loss of the electron withdrawing formyl group.

## Absorption Spectra and Theoretical Calculations

The absorption spectra of **57a,b** in toluene, THF and benzonitrile (not shown) are best described as the linear sums of the three individual constituents: *ex*TTF, fluorenes, and $C_{60}$ with the most dominant absorptions at 430 nm (*i.e.* *ex*TTF), at 345 nm (*i.e.* mono- and bifluorene) and 300 nm (*i.e.* $C_{60}$). This suggests that there is only little, if any, electronic communication in the ground state between *ex*TTF, fluorenes and $C_{60}$ in **57a,b**.

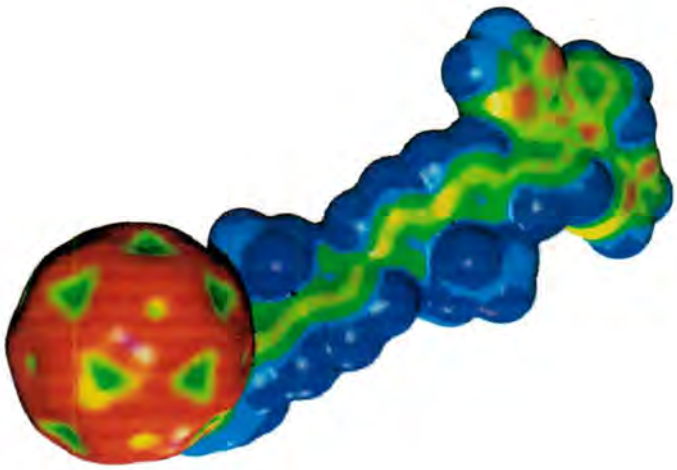

Figure 3.3: Electron affinity maps of *ex*TTF-$Fl_2$-$C_{60}$ (**57b**) as computed with Parasurf A07[98] and viewed with Tramp 1.1d[99]; from blue to red: low to high.

Prior to photophysical investigations we assessed the donor and acceptor features in the *ex*TTF-$Fl_n$-$C_{60}$ conjugates by using DFT calculations (B3LYP/6-31G*) as a reference point. The DFT calculations on the HOMO and LUMO energies of *ex*TTF, *N*-methyl pyrrolidinofullerene, the pristine fluorene oligomers and the oligofluorene-$C_{60}$ dyads reveal that the HOMO and LUMO energies *in vacuo* of *ex*TTF (-4.7 eV and -1.2 eV) closely match the energies of the oligomeric building blocks (-5.1 eV and -1.1 eV), providing good orbital overlap between the donor and the bridge, which is essential for electron transfer between the two units. Interestingly, in the oligofluorene-$C_{60}$ dyads the LUMO is lowered to an energy (-3.0 eV) that is equal to the energy of the LUMO of *N*-methyl pyrrolidinofullerene, while the HOMO (-5.1 eV) remains energetically unchanged in comparison to pristine fluorenes. Hence, this proves the electron-accepting features of $C_{60}$

and neglects electronic communication between the donor, bridge and acceptor in the ground state. Furthermore, electron affinity calculations confirm the electron-transfer pathway from the donor over the bridge to the fullerene acceptor. Figure 3.3 represents the local electron affinity map of the *ex*TTF-bridge-$C_{60}$ system **57b**. A homogenous distribution of the electron density (surface) throughout the whole molecule followed by a channel of high electron affinity through the bifluorene bridge resulting in a maximum at $C_{60}$ proves the charge-transfer features of these systems.

## Photophysical Studies

To determine the rates of charge separation and charge recombination and eventually the corresponding β factor, **57a,b** were tested in a series of photophysical assays (*i.e.* steady-state/time-resolved fluorescence and time-resolved transient absorption measurements) in Dirk Guldi's laboratory. The first insight into electron-transfer interactions came from fluorescence experiments (Figure 3.4 and 3.5). Here, in line with the earlier investigations of oligofluorene-$C_{60}$ conjugates (Chapter 2), a nearly quantitative fluorescence quenching of the oligofluorene units was observed. This is a result of an efficient transduction of singlet excited state energies to $C_{60}$. In stark contrast to the behaviour seen for oligofluorenes-$C_{60}$ (**51a-c**) and $C_{60}$-oligofluorenes-$C_{60}$ (**53a-c**), **57a,b** give rise to a number

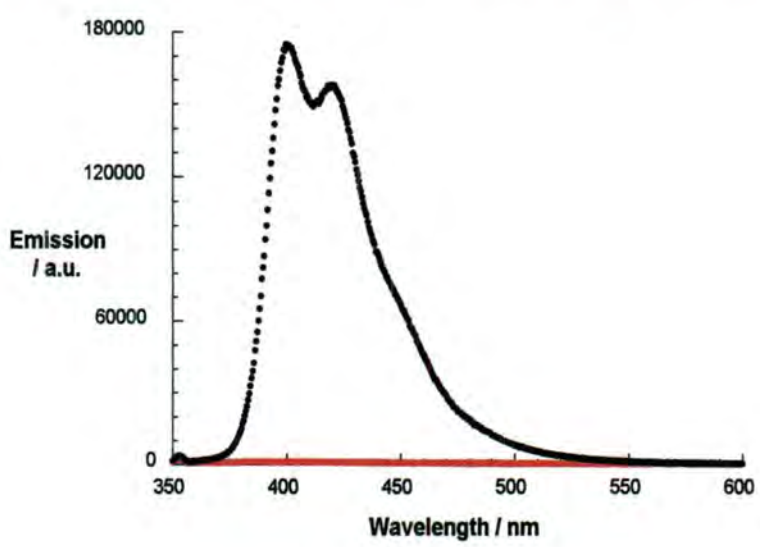


Figure 3.4: Room temperature fluorescence spectra of difluorene **50a** (black line) and *ex*TTF-$Fl_2$-$C_{60}$ **57b** (brown line) in THF recorded with solutions that exhibit optical absorptions of 0.45 at the 360 nm excitation wavelength.

of interesting trends. Firstly, the $C_{60}$ fluorescence is not quantitative with quantum yields that are typically only of the order of $0.07 \times 10^{-4}$ for the monomer **57a** and $0.90 \times 10^{-4}$ for the dimer **57b** (note that the quantum yield is $6.0 \times 10^{-4}$ for comparable $C_{60}$ references).

Secondly, a strong solvent dependence emerges, *i.e.* the $C_{60}$ fluorescence quenching intensifies gradually with increasing solvent polarity from, for example, toluene to benzonitrile. Finally, a marked distance dependence is seen. In particular, the $C_{60}$ fluorescence quenching tends to be stronger in **57a** than in **57b**. Summarising the above observations, we postulate charge transfer between the transiently formed $C_{60}$ singlet excited state and the electron accepting oxidised *ex*TTF.

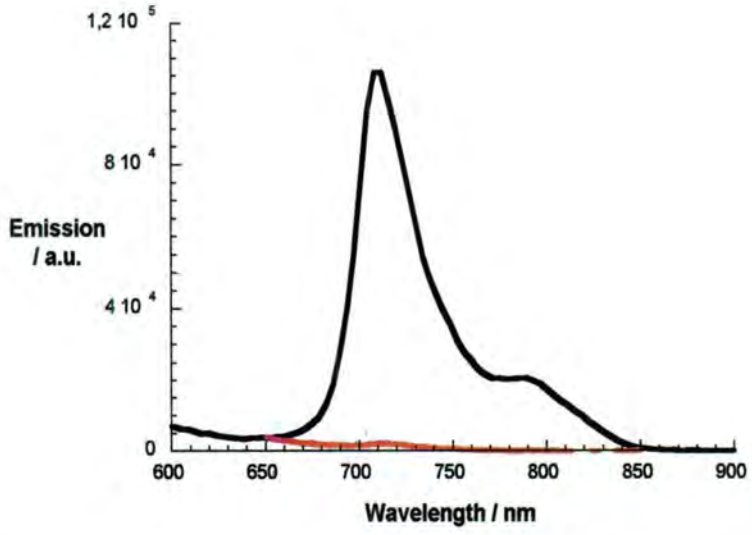


Figure 3.5: Room temperature fluorescence spectra of pristine $C_{60}$ (black line) and *ex*TTF-Fl-$C_{60}$ **57a** (brown line) in THF recorded with solutions that exhibit optical absorptions of 0.22 at the 435 nm excitation wavelength.

Conclusive evidence in support of the electron-transfer hypothesis was found in transient absorption measurements (Figure 3.6 and 3.7). Triads **57a,b** were photoexcited with short 387 nm (150 fs) and long 355 nm (5 ns) laser pulses. The short laser pulses, at a wavelength that is absorbed by both oligofluorenes and $C_{60}$, resulted in a discernable transient absorption spectrum (*i.e.* 880 nm maximum) that is attributed to the $C_{60}$ singlet excited state. Again, this results from a rapid singlet excited state transfer. This transient species intersystem crosses in the corresponding oligofluorenes-$C_{60}$ (**51a-c**) and $C_{60}$-

oligofluorenes-$C_{60}$ (**53a-c**) to form the triplet manifold on a time-scale that is typically *ca.* 1.5 ns. In **57a,b**, however, the $C_{60}$ singlet excited state features decay much faster.

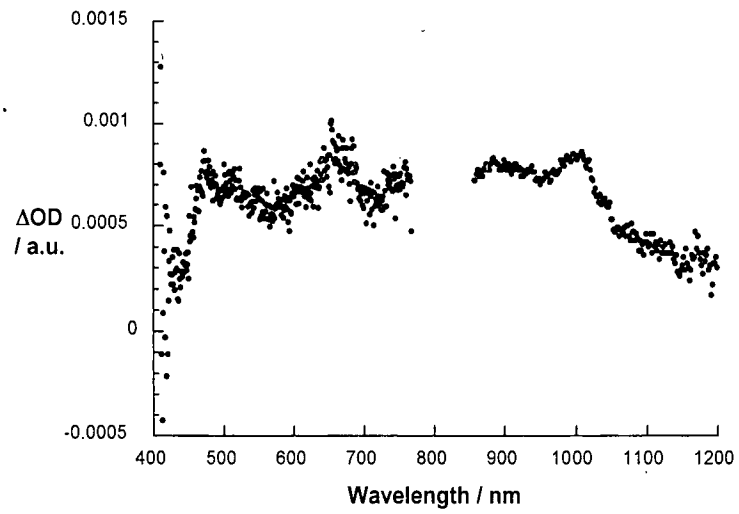


Figure 3.6: Differential absorption spectrum (visible and near-infrared) obtained upon femtosecond flash photolysis (387 nm) of **57a** in nitrogen saturated THF ($1.0 \times 10^{-5}$ M) with a time delay of 155 ps at room temperature.

Interestingly, the decay behaviour is an exact reflection of the fluorescence experiments, that is, a notable dependence on the solvent polarity and the distance ($R_{DA}$) is observed. More important is the spectroscopic characterisation of the transient species that develops synchronously with the $C_{60}$ singlet excited decay. Two features, a maximum in the visible

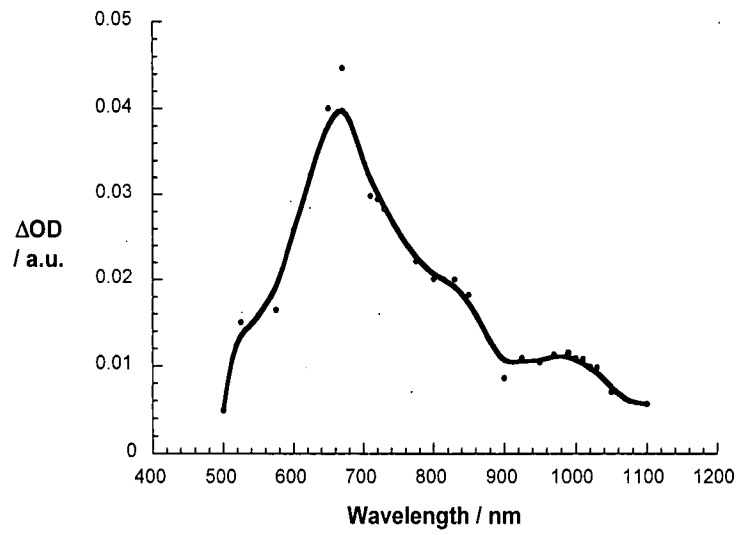


Figure 3.7: Differential absorption spectrum (visible and near-infrared) obtained upon nanosecond flash photolysis (355 nm) of **57a** in nitrogen saturated THF ($1.0 \times 10^{-5}$ M) with a time delay of 100 ns at room temperature.

region (*i.e.* 680 nm) and another maximum in the near infrared region (*i.e.* 1000 nm) confirm the intramolecular formation of the one-electron oxidised *ex*TTF radical cation (*i.e.* *ex*TTF$^{\bullet+}$)[152, 153] and the one-electron reduced $C_{60}$ radical anion (*i.e.* $C_{60}^{\bullet-}$), respectively. Fitting the singlet excited state decay and the radical ion pair formation kinetics enabled us to derive the charge separation rates, which are summarised in Table 3.2.

Table 3.2: Charge-separation and charge-recombination dynamics as determined by femtosecond and nanosecond time-resolved spectroscopic measurements for **57a** and **57b** in THF. $R_{DA}$ is the distance between the donor and acceptor.

| **Compound** | $R_{DA}$ | $k_{charge\ separation}$ | $k_{charge\ recombination}$ |
|---|---|---|---|
| *ex*TTF-Fl-$C_{60}$ (**57a**) | 16.7 Å | $8.9 \times 10^9$ [$s^{-1}$] | $7.2 \times 10^5$ [$s^{-1}$] |
| *ex*TTF-$Fl_2$-$C_{60}$ (**57b**) | 24.9 Å | $4.0 \times 10^9$ [$s^{-1}$] | $4.4 \times 10^5$ [$s^{-1}$] |

Notably, the radical ion pair states are stable on the time-scale of our femtosecond experiments and only exhibit a detectable decay in the complementary nanosecond experiments. The decays of the *ex*TTF$^{\bullet+}$ and the $C_{60}^{\bullet-}$ features are strictly first order when plotted, for example, as ln ΔOD versus time, and lead to the quantitative reconstitution of the singlet ground state without any appreciable triplet features.

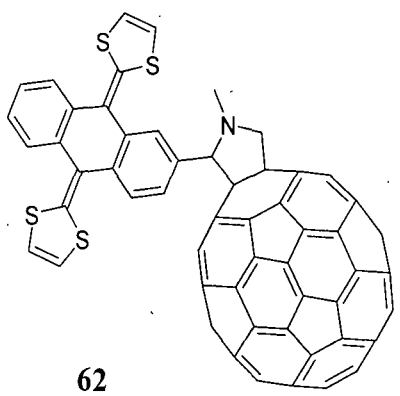


**62**

Finally, the β factor was determined by analysing the rate constants (*i.e.*, charge separation and charge recombination) as a function of donor-acceptor distance. For this the value determined for directly linked *ex*TTF-$C_{60}$ (**62**).[149] Common to both relationships is a linear

dependence from which an attenuation factor (β) of 0.09 $Å^{-1}$ (± 0.005 $Å^{-1}$) emerged. In other words, the ability of oligofluorenes to conduct charges lies between that of oligo-*p*-phenylenevinylenes (β = 0.01 ± 0.005 $Å^{-1}$)[95] and that of oligo-*p*-phenylenethynylenes (β = 0.2 ± 0.05 $Å^{-1}$).[97] Figure 3.8 represents the charge-separation and charge-recombination dynamics as a function of donor-acceptor distance in the *ex*TTF-$Fl_n$-$C_{60}$ series **57a,b** and **62**. Our attenuation factor for fluorene molecular wires matches the attenuation factor found by Wasielewski and co-workers for **43** (*i.e.* PTZ-$Fl_n$-PDI), which was 0.093 $Å^{-1}$.

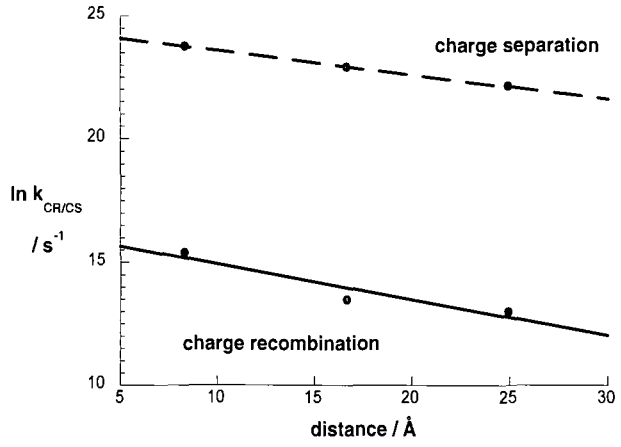


Figure 3.8: Centre-to-centre distances ($R_{CC}$) dependence of charge-separation (ln $k_{CS}$) and charge-recombination (ln $k_{CR}$) rate constants in *ex*TTF-$Fl_n$-$C_{60}$ (n = 0, 1, 2) in nitrogen saturated THF at room temperature. The slope represents β.

## 3.3 Conclusions

The synthesis of D-$Fl_n$-$C_{60}$ (n = 1, 2) ensembles was discussed in this chapter, whereby D is an π-extended tetrathiafulvalene electron donor. This strong electron donor in these novel triads is covalently attached to a 9,9-dihexylfluorene monomer or dimer with an *N*-methyl pyrrolidinofullerene terminus. Compounds **57a,b** were synthesised utilising the Suzuki cross-coupling methodology to assemble *ex*TTF-fluorenes with terminal formyl groups (**56**), followed by Prato's 1,3-dipolar cycloaddition reactions with $C_{60}$ on *in situ* generated azomethine ylides. We have discussed (unsuccessful) synthetic attempts to insert a longer oligofluorene bridge in between the *ex*TTF-$C_{60}$ conjugate for which a novel

boronic ester functionalised *ex*TTF (**59**) was prepared. The solution electrochemical data showed amphoteric behaviour (three one-electron reduction waves of the $C_{60}$ core and one two-electron oxidation wave of *ex*TTF) and irreversible oxidations of the oligofluorene chains with no significant interaction between these electroactive partners in the ground state. Fluorescence time-resolved and steady-state experiments were carried out to determine the photophysical behaviour of the novel triads. These data demonstrated that fluorene-based bridges exhibit molecular wire-like behaviour in *ex*TTF-wire-$C_{60}$ donor-acceptor systems, showing a remarkably low $\beta$ value (0.09 $Å^{-1}$).

# Chapter 4: ZnP-Oligofluorene-$C_{60}$ and Fc-yne-$Fl_n$-$C_{60}$ Triads (n = 1, 2)

## 4.1 Introduction

In Chapter 3 the synthesis and behaviour of *ex*TTF-$(Fl)_n$-$C_{60}$ (**57a,b**; n = 1, 2) were discussed. To further investigate D-$(Fl)_n$-$C_{60}$ ensembles this chapter will focus on the synthesis and electrochemistry of metal-centred electron donors, *i.e.* porphyrin and ferrocene (Fc). The compounds discussed in this chapter will be subjected to photophysical studies in the near future. A discussion of zinc(II) porphyrin (ZnP) ensembles will commence this chapter, to be followed by Fc-$(Fl)_n$-$C_{60}$ triads.

## 4.2 ZnP-Oligofluorene-$C_{60}$

### 4.2.4 Introduction

Four pyrrole-type heterocycles interconnected by four methane groups at position 2 and 5 make up the basic skeleton of a series of deep purple or red macrocycles designated as porphyrins. These macrocycles occur naturally and play essential roles in various biological processes, *e.g.* electron transfer, oxygen transfer and light harvesting.[154-159] Rich and extensive absorption features (*i.e.* $\pi$-$\pi^*$ transitions) of the porphyrinoid systems result in increased absorptive cross-sections and thus an effective use of the solar spectrum.[157] The substituents at the peripheral *meso* or $\beta$ positions and variations of the central metal ion can be used to fine-tune the excited-state properties of porphyrins.[160] Porphyrins have been frequently used as electron donors for linkage to fullerene $C_{60}$ (see Chapter 1), because they contain an extensively conjugated two-dimensional system. They are also suitable for efficient electron transfer due to the minimal structural and solvation changes

upon electron transfer.[157, 160] Some examples of ZnP-wire-$C_{60}$ ensembles have been discussed in Chapter 1.

Inspired by these findings, we decided to investigate a ZnP donor as a second strong electron moiety in our investigation towards D-$(Fl)_n$-$C_{60}$ ensembles. In the first part of this chapter we will address the synthesis and electrochemistry of novel oligofluorene-bridged zinc(II) tetraphenylporphyrin and fullerene conjugates. These triads will be subjected to photophysical studies in the near future and the determination of their attenuation factor (β) will provide us with an insight into both the molecular wire behaviour of the oligofluorene bridge and the effect of different electron donors on the electron transfer.

## 4.2.5 Results and Discussion

### Synthesis

A frequently employed porphyrin synthesis involves the tetramerisation of aldehydes and pyrroles under acid catalysed conditions.[161] The one-pot condensation in propionic acid at reflux can exhibit limitations for the preparation of sterically hindered porphyrins and Lindsey has improved the methodology for these derivatives.[162, 163] As the first porphyrin we aimed to prepare was not particularly sterically hindered, we decided to employ the classical method.[161] The non-porphyrin side-products obtained during the

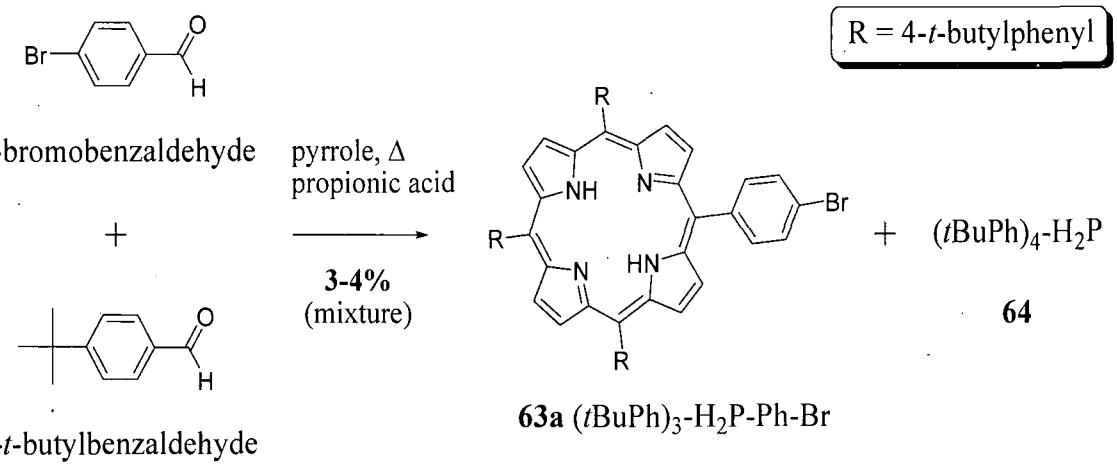


Scheme 4.1

condensation in propionic acid are slightly easier to separate from the porphyrin mixture compared to the "Lindsey condensation". The mono-functionalised porphyrin building block **63a** was synthesised by a mixed aldehyde condensation of 4-bromobenzaldehyde and 4-*t*-butylbenzaldehyde (1:3 mixture) with four equivalents of pyrrole in refluxing propionic acid (Scheme 4.1). This condensation resulted in the formation of a mixture of six porphyrins and analysis of this porphyrin-mixture **63** by MALDI-TOF MS indicated that the two main components are our desired product ($A_3B$-type porphyrin **63a**) and the $A_4$-type porphyrin **64** (Scheme 4.1 and 4.2). Unfortunately, this porphyrin mixture could not be separated by column chromatography, due to the similarities in structure and polarity of the different porphyrins. The mixture was used as obtained in the next reaction step (Scheme 4.3). Porphyrin **64** was synthesised separately as a reference compound from 4-*t*-butylbenzaldehyde and pyrrole in refluxing propionic acid (Scheme 4.2). Treatment of porphyrin **64** with zinc acetate gave zinc(II) complex **65** in high yield (Scheme 4.2).

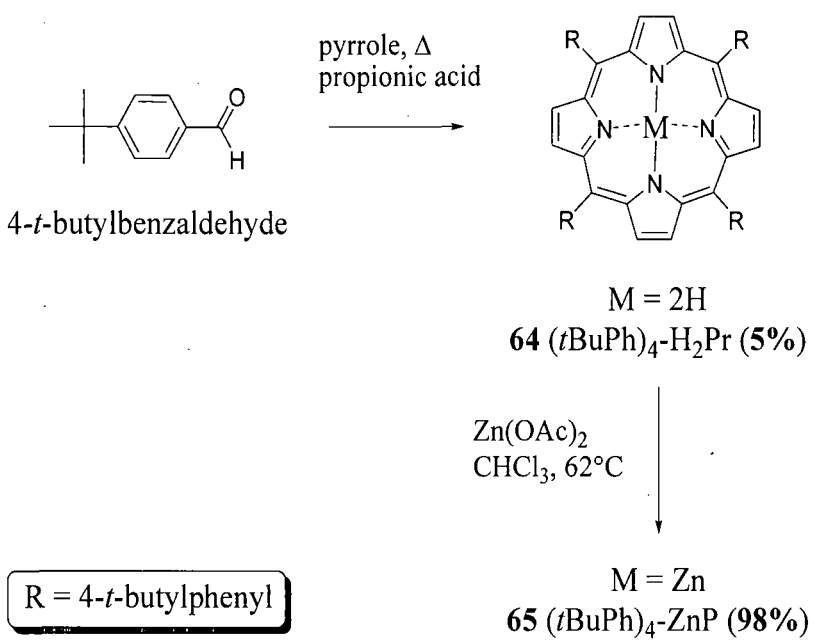


Scheme 4.2

Next, porphyrin mixture **63** was subjected to a Suzuki reaction with fluorene monomer or dimer **48a,b** (Scheme 4.3), as the porphyrin core does not need to be protected from palladium by the formation of the zinc(II) complex.[137, 164-166] We reasoned that as porphyrin **64** contains no bromine functionalities, it would be inert to this reaction and

purification of the porphyrin product mixture should become possible. Pd-catalysed cross-coupling conditions for the joining of aromatic compounds to porphyrins need substantial alterations from those employed for coupling small molecules.[166-168] Porphyrins typically have low solubility and as a consequence Pd-coupling methods, which work very well with smaller molecules at high concentrations, tend to give poor results in more dilute solutions. Unfortunately, optimisation of the Suzuki cross-coupling for our use was hampered by the fact that **63** is a porphyrin mixture. The most commonly used catalyst for Suzuki cross-couplings is $Pd(PPh_3)_4$,[137, 164-166] but several attempts (inspired by previous results from within our group[165]) utilising this catalyst (10-30 mol%) for couplings between porphyrin

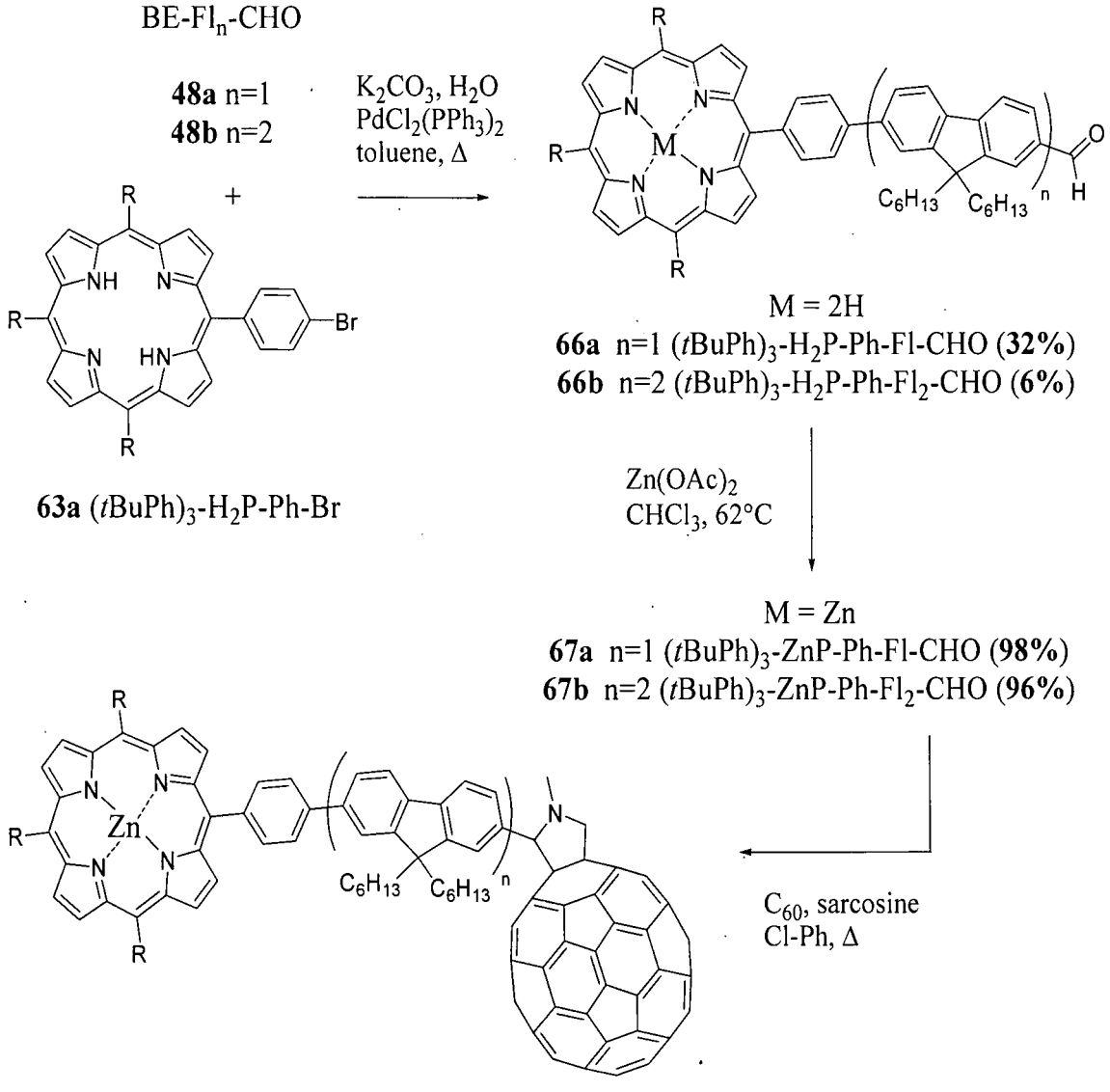


Scheme 4.3

mixture **63** and fluorene building block **48a** yielded no product. A return to the conditions used in Chapters 2 and 3 gave product **66a,b** in low yield and further optimisation was not attempted (Scheme 4.3). Compounds **66a,b** were obtained containing no impurities from previous reactions and treatment with zinc acetate yielded the zinc(II) complexes **67a,b** in nearly quantitative yields (Scheme 4.3). The presence of the aldehyde functionality allowed *in situ* generation of the corresponding azomethine ylides by reaction with sarcosine in refluxing chlorobenzene (see Chapter 2), which by cycloaddition to $C_{60}$ provided cycloadducts **68a,b** (Scheme 4.3).

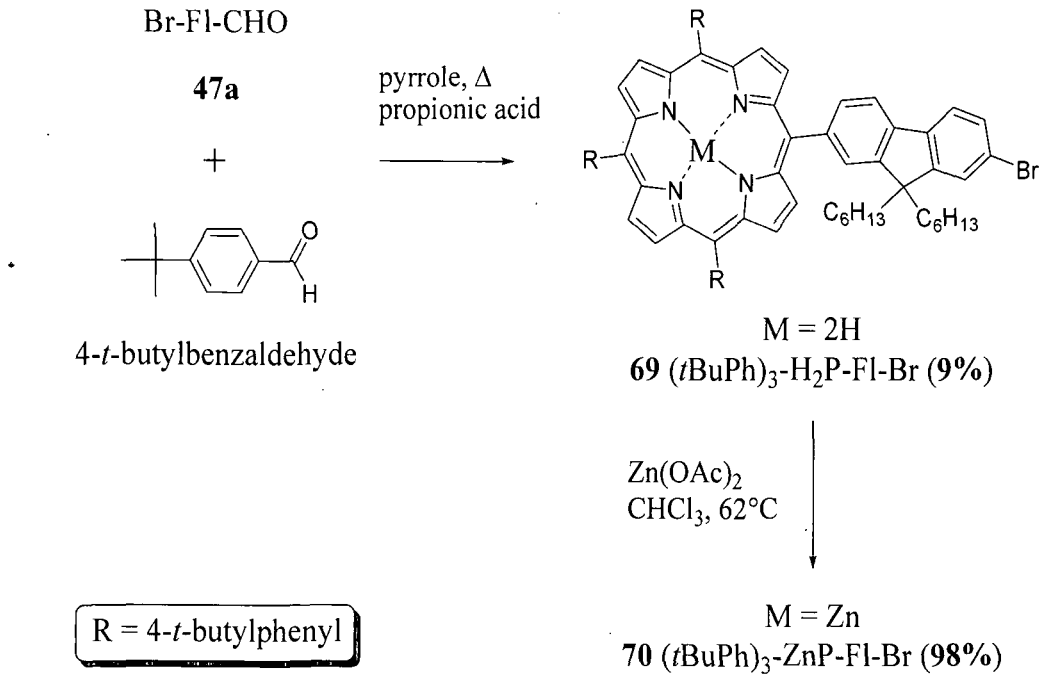


Scheme 4.4

The fact that **63** is a porphyrin mixture provided an obstacle during optimisation of reaction conditions and difficulties preparing ZnP-$C_{60}$ conjugates containing longer oligofluorene bridges. Therefore an attempt to design a novel porphyrin, which could be more easily purified, was undertaken. Fluorene-containing $A_4$-type porphyrins have been previously reported,[137, 164, 165] but to the best of our knowledge no $A_3B$-type porphyrins, where B is fluorene and A is an alternative moiety, have been previously reported. The tetramerisation of Br-Fl-CHO **47a**, 4-*t*-butylbenzaldehyde (1:3 mixture) and pyrrole under the traditional acid-catalysed conditions gave a mixture of at least 4 porphyrins

(determined by TLC), which was easily purified and the desired mono-functionalised porphyrin **69** was isolated in 9% yield (Scheme 4.4). The *n*-hexyl chains at the 9 position of the fluorene units ensure good solubility in organic solvents. The yield and solubility of the desired porphyrin in propionic acid are considerably increased compared to porphyrin mixture **63**. Evidence for the substantially higher reactivity of **47a** compared to 4-bromobenzaldehyde and 4-*t*-butylbenzaldehyde can be found not only in the increased yield but also from a closer look at the main side-product.

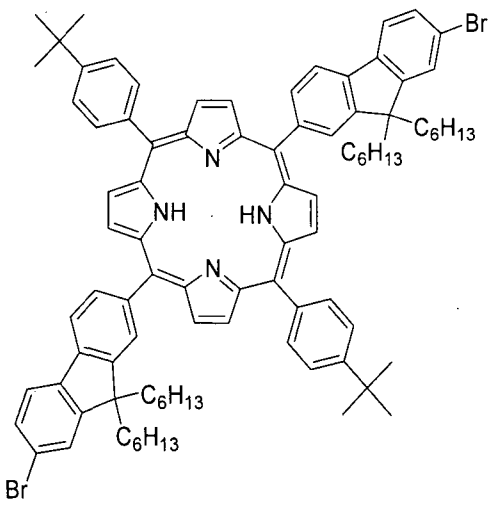


**71a**

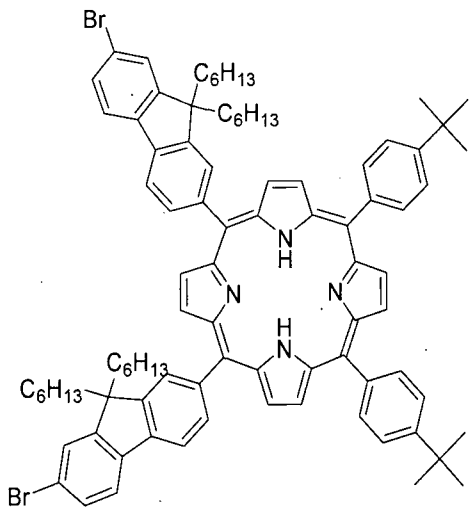


**71b**

The MALDI-TOF MS spectrum of the initial porphyrin mixture (before column chromatography) indicated that two main porphyrin products were formed. Interestingly, this time the main side-product was characterised as a $A_2B_2$-type porphyrin **71** containing two fluorene units and not the $A_4$-type porphyrin **64**. As efforts concentrated on the purification of the desired porphyrin **69**, the main side-product was not obtained pure and no further purification attempts were undertaken. However, the side-product was formed in *ca.* 6-8% yield and initial $^1$H-NMR spectra did support the $A_2B_2$-type characterisation. For clarity the side-product was indicated above as one porphyrin, but naturally an $A_2B_2$-type porphyrin has two possible structures (*i.e.* **71a** and **71b**). The $A_2B_2$-type porphyrin **71** should be considered a mixture of **71a** and **71b**, until further purification and characterisation has been carried out.

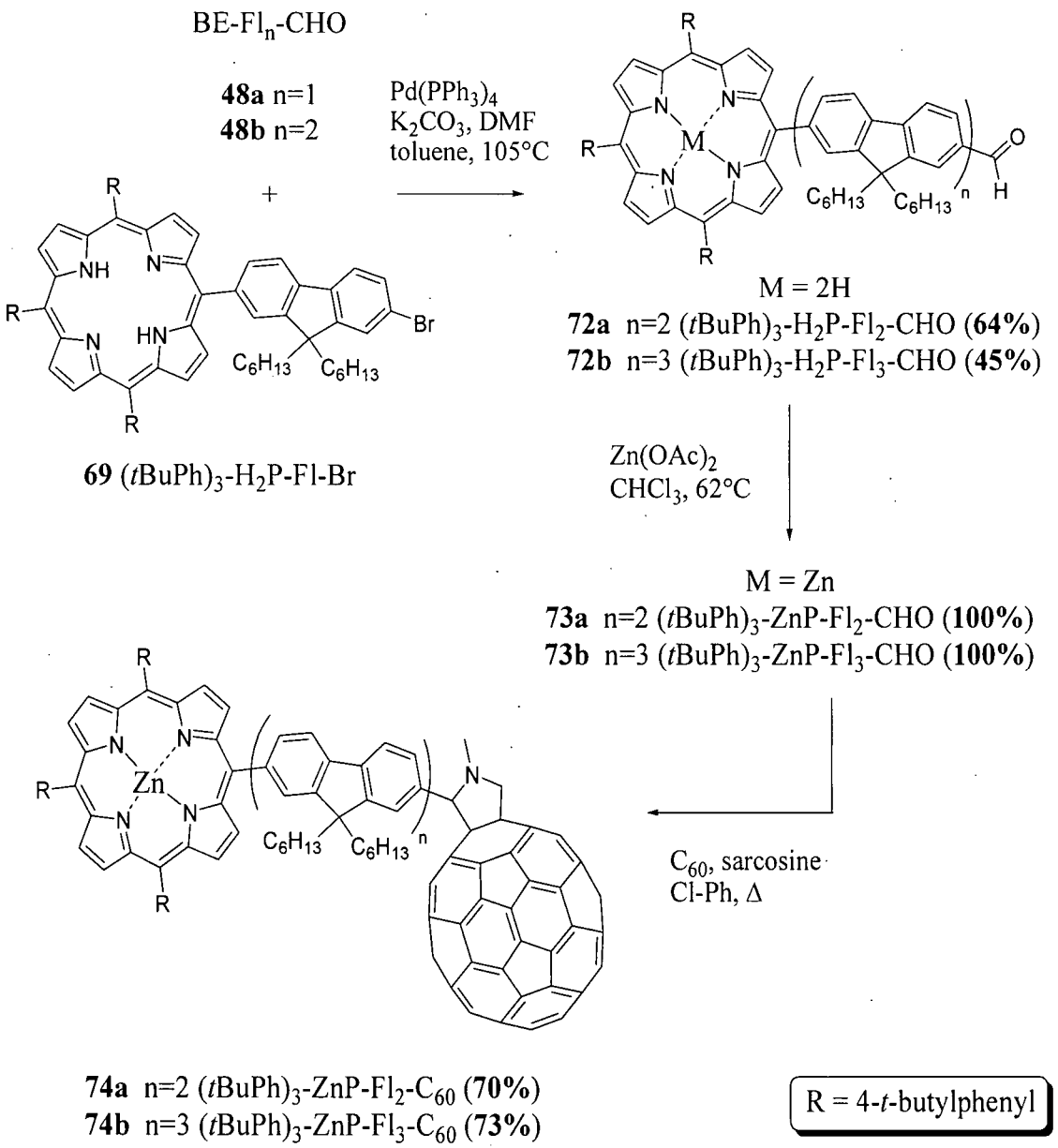


Scheme 4.5

Mono-functionalised porphyrin **69** was reacted with fluorene monomer or dimer **48a,b** utilising Suzuki methodology (Scheme 4.5).[124, 166] As porphyrin **69** was obtained pure, the Pd-catalysed cross-coupling became less complicated. However, the limited supply of porphyrin and time constraints did mean that the procedure was not optimised beyond the first reaction, which provided an acceptable yield. Toluene and DMF were chosen as the solvent mixture, since porphyrin **69** is soluble in toluene and has some solubility in DMF. The base $K_2CO_3$ has good solubility in DMF and it was found that a large excess of base (32 equivalents) is important. A fresh batch of catalyst [$Pd(PPh_3)_4$] was acquired and

utilised initially in 100 mol%, as previous attempts with 10-30 mol% $Pd(PPh_3)_4$ used in a Suzuki reaction to obtain **66a,b** were unsuccessful. Utilising this methodology bi- and terfluorene compounds **72a,b** were obtained in moderate yields (Scheme 4.5). The zinc derivatives **73a,b** were obtained upon reaction with zinc acetate in quantitative yields (Scheme 4.5). Cycloaddition to $C_{60}$ of *in situ* generated azomethine ylides from the reaction of **73a,b** with sarcosine provided cycloadducts **74a,b** (Scheme 4.5).

In summary - we have synthesised four ZnP-$C_{60}$ triads, *i.e.* **68a,b** and **73a,b**. In Chapter 3 we investigated the possibilities of lengthening the oligofluorene bridge in between the donor-acceptor conjugates. We have previously established that the synthesis of BE-$Fl_n$-CHO oligomers (n = 3 or more) is problematic, due to purification issues. Therefore any attempt to lengthen the bridge will have to be a step-wise approach, gradually adding fluorene units onto the porphyrin moiety, and for this we have attempted to replace the bromine with a boronic ester. As discussed earlier, Pd-coupling conditions used for smaller compounds (*e.g.* the methodology used for **48a,b** or **56a,b**) need adjusting before they can be applied to porphyrins. Due to limited time and availability of starting material **69**, the decision was made to try the Suzuki methodology used for **72a,b** to prepare the boronic acid species instead of trying to optimise the methodology used for **48a,b**. In the literature the highest amount of catalyst used for a Pd-coupling with porphyrins is, to the best of our knowledge, 60 mol%.[166] In this light, we reduced the amount of catalyst to 50 mol%. The reaction of **69** with 10 equivalents of bis(pinacolato)diboron yielded the desired boronic

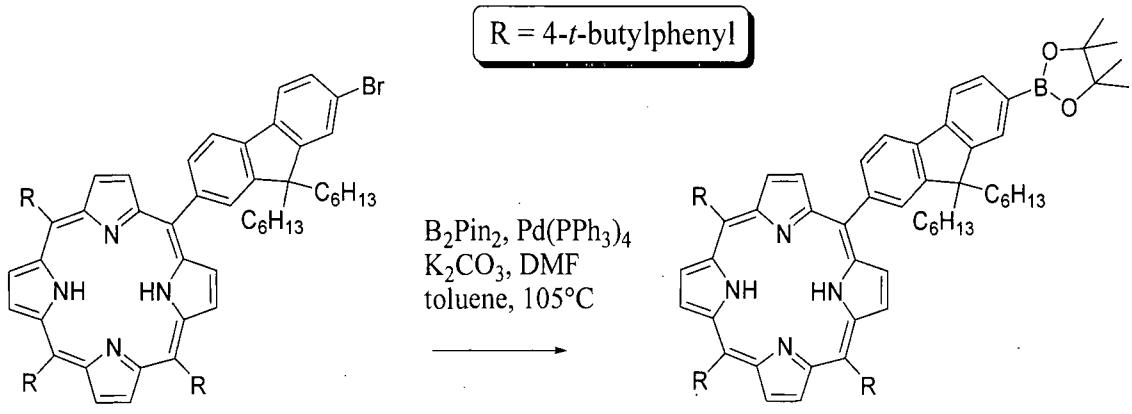


**69** ($t$BuPh)$_3$-$H_2$P-Fl-Br

**75** ($t$BuPh)$_3$-$H_2$P-Fl-BE (**32%**)

Scheme 4.6

ester species **75** in 32% yield (Scheme 4.6) and unfortunately this was not sufficient for a reaction with dibromofluorene **45**, to be subsequently followed by another Suzuki coupling with Be-$Fl_2$-CHO **48b** to produce the tetrafluorene equivalent of **72a,b**, which in the end could have been converted into a ZnP-$Fl_4$-$C_{60}$ triad.

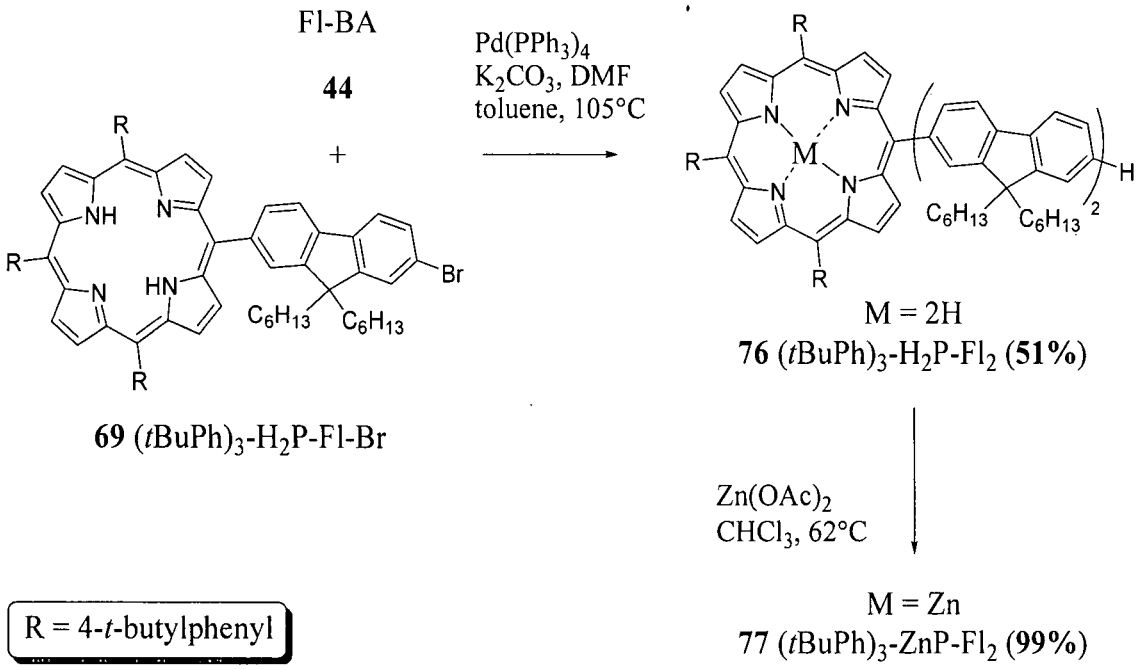


Scheme 4.7

Although the synthesis of **75** needs to be improved to provide more material, the fact that the boronic ester species can be prepared is interesting, not only for our systems, but it also opens up interesting alternative possibilities. An example of this would be the cross-coupling of **69** and **75** (or **45** with an excess of **60** or **75**) to yield two porphyrins linked together by an oligofluorene bridge. Multiporphyrin arrays are attractive constructs for light-harvesting applications.[160]

Apart from lengthening the bridge **69** also introduced the question of whether the bromine functionality could be replaced with a formyl group. If so, this would offer the possibility of a ZnP-$C_{60}$ conjugate separated by merely one fluorene unit. As this involves the use of butyllithium, the porphyrin core of **69** was protected by the formation of the zinc(II) complex **70** in 98% (Scheme 4.4). Unfortunately, monolithium-halogen exchange of **70** in

diethyl ether or THF and subsequent quenching with an excess of DMF yielded only starting material. Although these reactions were done on a small scale, all possible precautions were taken to ensure dry and inert conditions. Further attempts towards the preparation of this ZnP-Fl-$C_{60}$ conjugate were not carried out.

Finally, we have prepared a second reference compound, which consists of a porphyrin covalently linked to bifluorene and containing no functionality at the other terminus. Pd-catalysed cross-coupling between **44** and **69**, utilising the same methodology used for **72a,b** (again using 100 mol% catalyst) yielded **76** in 51% yield and subsequent reaction with zinc acetate gave reference compound **77** (Scheme 4.7).

## Electrochemical Studies

The electrochemical properties of **68a,b** and **74a,b** were probed by room temperature cyclic voltammetric measurements in an *o*DCB-$CH_3CN$ solvent mixture (4:1 v/v) with a glassy carbon working electrode, $Bu_4NClO_4$ as supporting electrolyte and a scan rate of 100 mV $s^{-1}$. The redox potentials are collated in Table 4.1 together with those of **50a,b**, **51a,b**, **65**, **73a,b**, **77**, pristine $C_{60}$ and *N*-methyl pyrrolidinofullerene (**54**) as references.

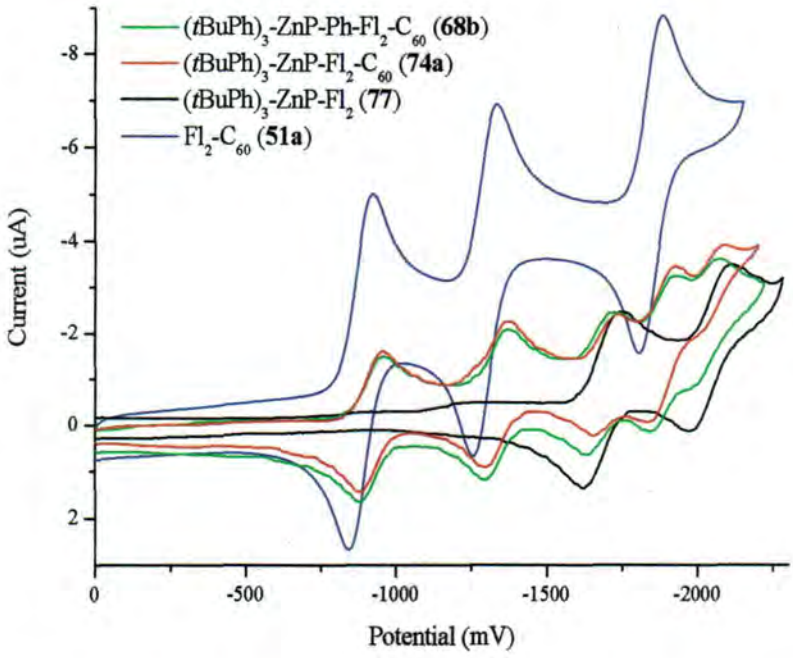


Figure 4.1: CVs of difluorene compounds **51a**, **68b**, **74a** and **77**. For conditions see Table 4.1.

Table 4.1: Redox potential values of triads **68a,b** and **74a,b**, together with aldehyde intermediates **73a,b**, and reference compounds (pristine $C_{60}$, **50a,b**, **51a,b**, **54**, **65** and 77).[a, b]

| Compound | $E^1_{red}$ | $E^2_{red}$ | $E^3_{½,red}$ | $E^4_{red}$ | $E^5_{½,red}$ | $E^1_{ox}$ | $E^2_{ox}$ | $E^3_{ox}$ | $E^4_{ox}$ | $E^5_{ox}$ |
|---|---|---|---|---|---|---|---|---|---|---|
| $Fl_2$-CHO (**50a**) | -2029[c] | | | | | 1295 | 1608 | 1873 | | |
| $Fl_3$-CHO (**50b**) | -2080 | | | | | 1114 | 1332 | 1800 | | |
| $(R)_4$-ZnP (**65**)[e] | -1691[c] | -2045[c] | | | | 503 (455)[c,d] | 884 (840)[c,d] | | | |
| $(R)_3$-ZnP-$Fl_2$ (**77**)[e] | -1684[c] | -2042[c] | | | | 518 (459)[c,d] | 903 (847)[c,d] | 1282 (1217)[c,d] | 1563 | 1803 |
| $(R)_3$-ZnP-$Fl_2$-CHO (**73b**)[e] | -1698[c] | -2158 | | | | 519 (454)[c,d] | 908 (837)[c,d] | 1394 (1323)[c,d] | 1726 | |
| $(R)_3$-ZnP-$Fl_3$-CHO (**73c**)[e] | -1693[c] | -2110 | | | | 515 (454)[c,d] | 933 (837)[c,d] | 1145 (1098)[c,d] | 1401 | |
| $C_{60}$ | -795[c] | -1191[c] | -1649 | -2122[c] | | | | | | |
| **54** | -912[c] | -1310[c] | -1849 | | | 1094 | 1545 | | | |
| $Fl_2$-$C_{60}$ (**51a**) | -882[c] | -1293[c] | -1843 | -2333 | | 1170 | 1345 | 1623 | | |
| $Fl_3$-$C_{60}$ (**51b**) | -880[c] | -1292[c] | -1839 | | | 1096 | 1394 | 1809 | | |
| $(R)_3$-ZnP-Ph-Fl-$C_{60}$ (**68a**)[e] | -911[c] | -1325[c] | -1675 | -1877[c] | -2026 | 543 (480)[c,d] | 914 (851)[c,d] | 1212 | 1480 | 1670 |
| $(R)_3$-ZnP-Ph-$Fl_2$-$C_{60}$ (**68b**)[e] | -917[c] | -1333[c] | -1674 | -1881[c] | -2026 | 528 (477)[c,d] | 915 (852)[c,d] | 1131 | 1286 | 1597 |
| $(R)_3$-ZnP-$Fl_2$-$C_{60}$ (**74b**)[e] | -922[c] | -1336[c] | -1695 | -1884[c] | -2042 | 503 (461)[c,d] | 885 (843)[c,d] | 1160 | 1492 | 1759 |
| $(R)_3$-ZnP-$Fl_3$-$C_{60}$ (**74c**)[e] | -921[c] | -1338[c] | -1696 | -1893[c] | -2065 | 520 (463)[c,d] | 899 (843)[c,d] | 1198 | 1557 | |

[a] Potentials in mV; scan rate 100 mV $s^{-1}$; glassy carbon working electrode, $Ag/AgNO_3$ reference electrode, Pt counter electrode; 0.1 M $Bu_4NClO_4$ in *o*DCB/$CH_3CN$ (4:1 v/v). [b] See also Table 2.1, Chapter 2. [c] Half wave potential values ($E_{½}$). [d] $E_{½}$ observed in partial scans. [e] R = *t*BuPh.

Analogous to triads discussed earlier, **68a,b** and **74a,b** possesses the desired bipolar character generating stable cation radicals and anion radicals, when the scan was repeated in the region between -2300 and 1100 mV. Firstly, five consecutive one-electron reduction waves (all quasireversible) have been observed on the reduction side. A good correlation with reference compounds **51a,b** and *N*-methyl pyrrolidinofullerene (**54**) allows us to assign the first, second and forth reduction waves to the reduction steps of the [60]fullerene core. The third and fifth reduction waves can be assigned to the reduction of the ZnP core, due to correspondence with reference compounds **65** and **77**. The satisfactory similarity with all reference compounds confirms the lack of substantial electronic interactions in the ground state of the zinc(II) porphyrin triads.[78, 87, 92, 143] As the first two, one-electron, reduction waves of **68a,b** and **74a,b** can be assigned to the $C_{60}$ core, the stronger electron accepting moiety in the triads is $C_{60}$. Similar to **51a-c** and **53a-c** (see Chapter 2), cathodic shifts of the $C_{60}$ reduction waves to more negative values, relative to pristine [60]fullerene, are observed for **68a,b** and **74a,b**. This is due to the saturation of a double bond on the fullerene core and the raised LUMO energy in ZnP-$C_{60}$ triads **68a,b** and **74a,b**.[39] As there is no alteration to the ZnP core in **68a,b** and **74a,b** compared to reference compound **65** no cathodic or anodic shifts are observed for its reduction or oxidation waves.

The data within Table 4.1 indicates that the second reduction wave of **73a,b** is irreversible, while the second waves of all the other compounds containing a porphyrin unit are quasireversible. For **73a,b** the reduction of the aldehyde group overlaps with the second

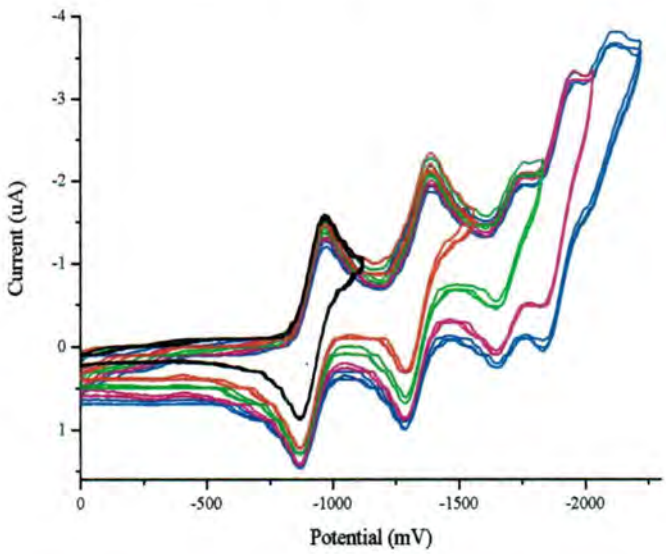


Figure 4.2: Three consecutive CVs of each reduction wave of **74b**. For conditions see Table 4.1.

reduction wave of the porphyrin moiety. On the reverse scan in the region of -2300 to 0 mV three (instead of two) one-electron oxidation waves are observed. The oxidation waves of the aldehyde functionality and the porphyrin moiety were smaller (less current) than the overlapping reduction waves and were observed separately at $E_{ox}$ -1870 and -1982 mV for **73a** and at $E_{ox}$ -1845 and -1988 mV for **73b**. Therefore, the second reduction wave of **73a,b** is observed as an irreversible two-electron process. The quasireversibility of triads **68a,b** and **74a,b** was investigated by performing several consecutive scans, *e.g.* three consecutive scans of **74c** are shown in Figure 4.2.

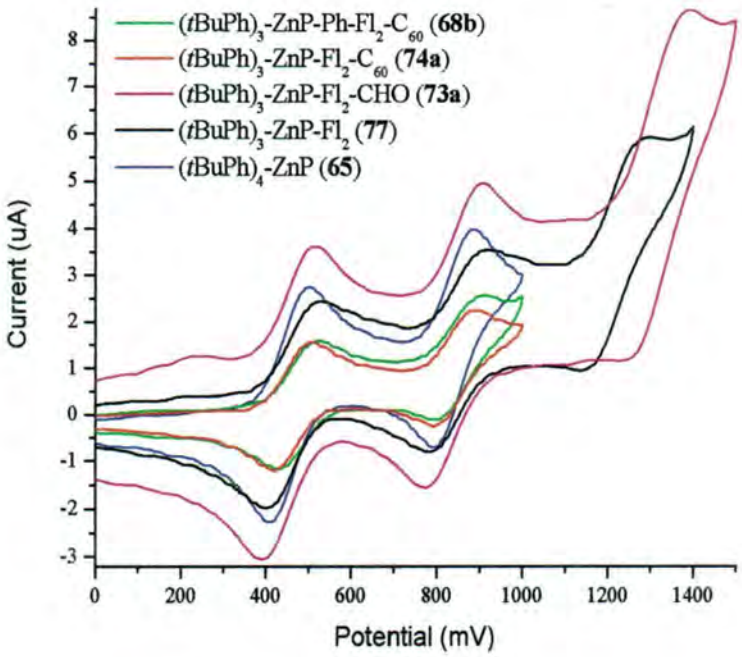


Figure 4.3: CVs of compounds **65**, **68b**, **73a**, **74a**, and **77**. For conditions see Table 4.1.

On the oxidation side, several irreversible oxidation waves are observed during the oxidation of **68a,b**, **74a,b** and the various reference compounds. Partial scans in the region of 0 - 1000 mV clearly indicate the quasireversibility of the first two waves observed in the ZnP containing compounds. These initial oxidation waves of **68a,b** and **74a,b** can be assigned to the porphyrin moiety, because a good agreement with reference compounds **65**, **77** and **73a,b** is observed. Similar to the reduction of the porphyrin moiety, no shifts in the oxidation potential were observed for the first two waves. The cation radical and dication formation of the triads are unaffected by the covalent link to oligofluorene. The additional phenyl unit in **68a,b** leaves the strongest electron donating moiety unaffected, which can

also be noted for the functionalisation of oligofluorene at the opposite termini with $C_{60}$ or a formyl group.

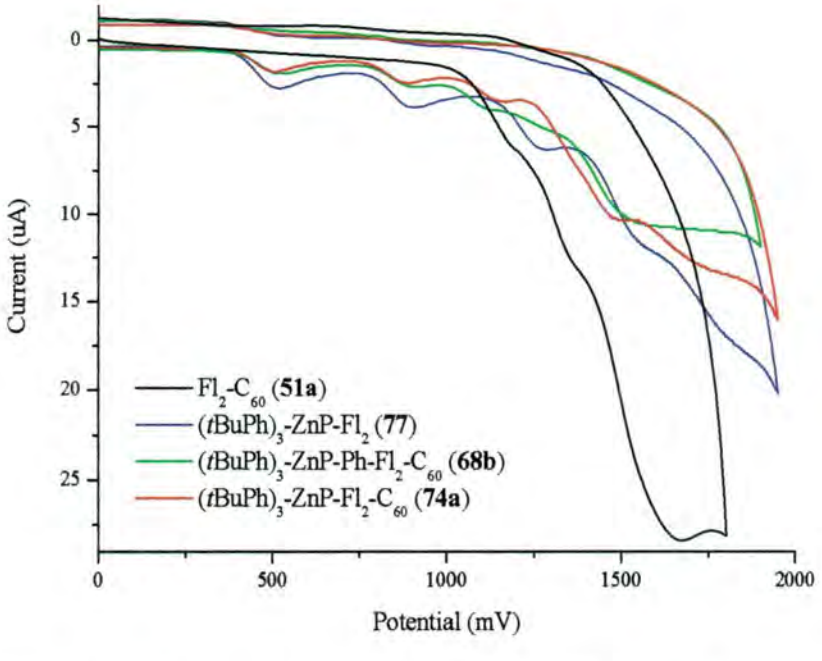


Figure 4.4: CVs of difluorene compounds **51a**, **68b**, **74a** and **77**. For conditions see Table 4.1.

Finally, the first oxidation step of the oligofluorene system in **73a,b** is subject to a notable electron withdrawing effect from the formyl group, which was first discussed in Chapter 2. Similar to previous observations, this electron withdrawing influence decreases as the length and donor character of the oligofluorene increases. Interestingly, the fluorene system of **73a** is subject to a greater electron withdrawing effect than its reference compound **50a** ($E_{ox}$ 1394 mV for **73a** versus $E_{ox}$ 1295 mV for **50a**). A closer look at reference compound **77** reveals that the oligofluorene system is subject to an electron withdrawing effect exerted by the porphyrin moiety. Similar to the influence of the aldehyde group, this effect increases as the length of the oligomer decreases. Substitution of the -CHO functionality in **73a,b** with $C_{60}$ shifts the anodic oxidation to less positive values in **74a,b**. Although still shifted to slightly higher oxidation potentials, the presence of the fullerene unit balances the electron withdrawing influence of the porphyrin unit. The raised donor character of the fluorene system, which comes from the more extended $\pi$-conjugation, compared to the monomer **68a** ($E_{ox}$ 1212 mV) shifts the oxidation potential to

less positive values in **68b** ($E_{ox}$ 1131 mV). However a similar trend is not observed as the fluorene length is increased between dimer **74a** ($E_{ox}$ 1160 mV) and trimer **74b** ($E_{ox}$ 1198 mV).

### 4.2.6 Conclusions

In the first part of this chapter we have discussed the synthesis of D-$Fl_n$-$C_{60}$ assemblies (n = 1, 2, 3), whereby D is an electron donating ZnP moiety. This strong donor is in these novel triads covalently attached to 9,9-dihexylfluorene oligomers of well-defined length with an *N*-methyl pyrrolidinofullerene termini. For this we have synthesised two different asymmetrical porphyrins both containing merely one bromine moiety (**63a** and **69**), which were reacted with formyl fluorene boronic ester via the Suzuki methodology to give **67a,b** and **73a,b**. These molecules with terminal aldehyde units were subjected to the Prato 1,3-dipolar cycloaddition reactions of *in situ* generated azomethine ylides with $C_{60}$ yielding the desired novel conjugates **68a,b** and **74a,b**. The solution electrochemical data showed amphoteric behaviour and no significant interaction between the electroactive partners in the ground state have been observed. Three one-electron reduction waves of the $C_{60}$ core and two reduction waves of the porphyrin have been observed. On the oxidation side, two one-electron oxidation waves of the ZnP core and irreversible oxidations of the oligofluorene chains were observed. Fluorescence time-resolved and steady-state experiments will be carried out in the near future to determine the photophysical behaviour of the new compounds.

## 4.3 Fc-alkyne-(Fluorene)$_n$-$C_{60}$

### 4.3.7 Introduction

Ferrocene is a metallocene (sandwich compound) with the metal atom (Fe) in between two cyclopentadienyl ligands and is an extremely stable complex.[142] Electron donating

ferrocene has been frequently used in electron-transfer systems and some examples of Fc donors covalently linked to $C_{60}$, including those with an oligomeric bridge, have been discussed in Chapter 1.

In this second part of Chapter 4 we will now address the synthesis and electrochemistry of novel oligofluorene bridged Fc-$C_{60}$ conjugates These triads will be subjected to photophysical studies in the near future and the determination of their attenuation factor ($\beta$). It is anticipated that these results will complement those obtained for the *ex*TTF-$(Fl)_n$-$C_{60}$ (**57a,b**) and ZnP-$(Fl)_n$-$C_{60}$ (**68a,b** and **74a,b**) ensembles.

## 4.3.8 Results and Discussion

### Synthesis

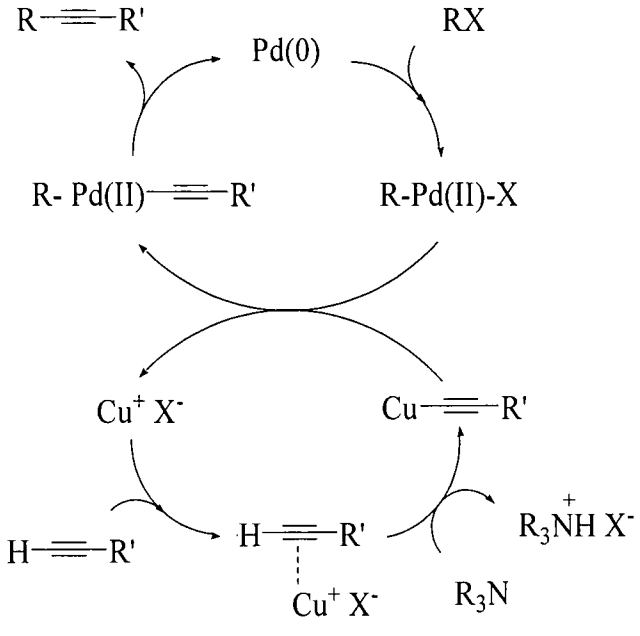


Figure 4.5: Reaction mechanism of the Sonogashira cross-coupling reaction.

Ethynylferrocene **78**[169] was used to prepare the Fc-yne-$Fl_n$-$C_{60}$ triads (n = 1, 2) as a small amount of **78** was available within our group. Due to limited time fluorene-$C_{60}$ systems

directly linked to ferrocene without the use of an alkyne moiety were not prepared. Photophysical results for the prepared triads will determine whether Fc-$Fl_n$-$C_{60}$ triads (n = 1, 2) should be prepared in the future.

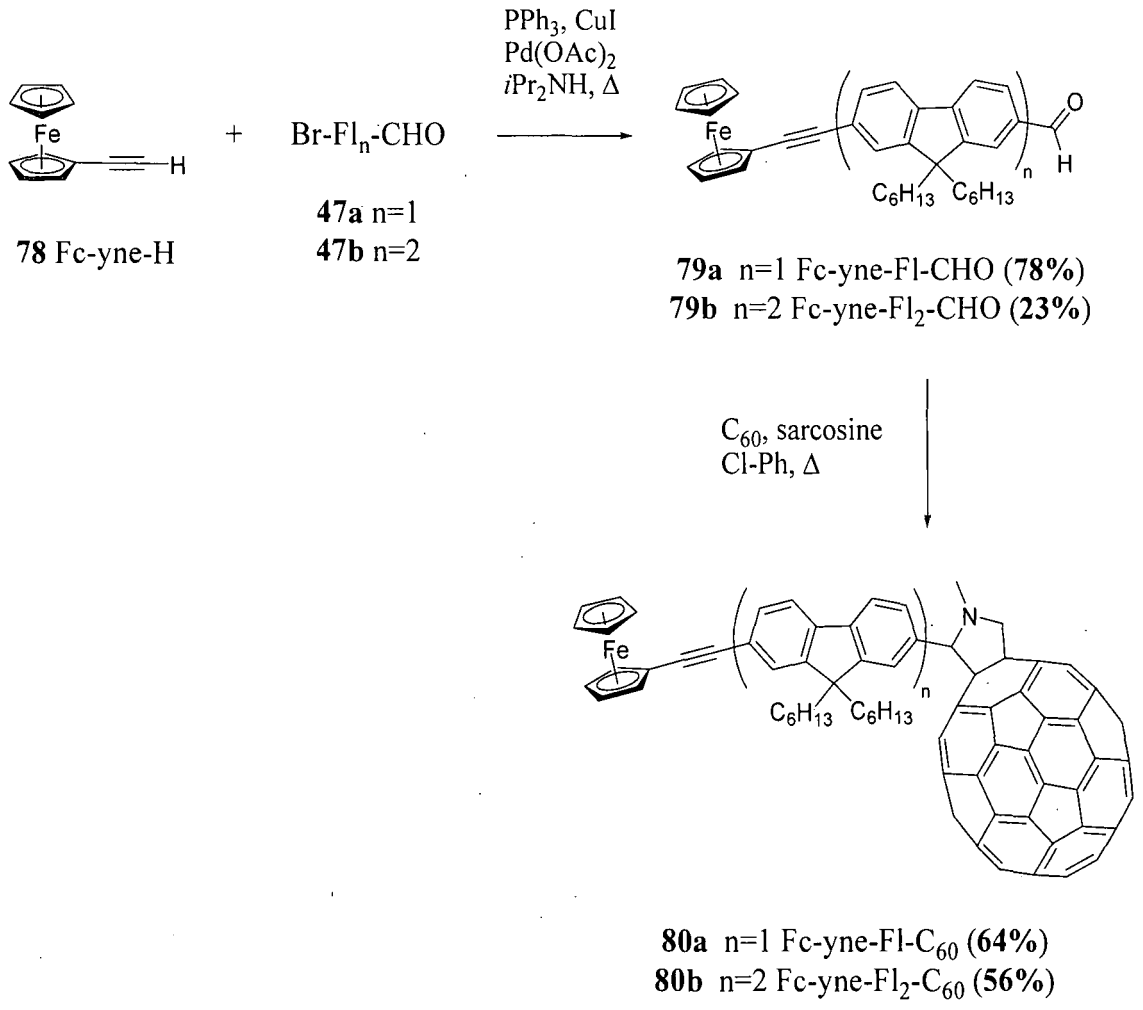


Scheme 4.8

In Chapter 2 the synthesis of the fluorene monomer and dimer **47a,b**, featuring two solubilising hexyl chains, a formyl group as a link to the $C_{60}$ and bromine, was discussed. Sonogashira coupling of these fluorene building blocks with ethynylferrocene provided compounds **79a** and **79b** (Scheme 4.8). The Sonogashira reaction is the most commonly used method for alkyne cross-coupling, due to mild coupling conditions and its tolerance to a large variety of functional groups. [170-173] Although continuously under investigation the generally accepted mechanistic pathway involves oxidative addition-transmetalation-

reductive elimination sequences (Figure 4.5).[170-173] The majority of Sonogashira cross-couplings proceed smoothly utilising the standard $Pd(PPh_3)_4$ or $PdCl_2(PPh_3)_2$ catalysts. Although $PdCl_2(PPh_3)_2$ is more stable and less expensive than $Pd(PPh_3)_4$, it is known that the use of the latter will decrease the formation of some side-products.[172] Triphenylphosphine ($PPh_3$) is the most universally used ligand as it works well in the majority of cases and is relatively inexpensive. For the Sonogashira reaction between **78** and **47a,b** the Pd-catalyst was generated *in situ* from $PPh_3$ and $Pd(OAc)_2$.

The conditions for our Sonogashira reaction were inspired by good results obtained by Wong *et al.* for the coupling of **78** with dibromofluorene (containing no alkyl chains at the 9 position).[174] For the preparation of **79a** these conditions worked well and the product was obtained in 78% (Scheme 4.8). Unfortunately, dimer **79b** was obtained in low yield (Scheme 4.8), suggesting that optimisation is needed for reactions of **44** with oligofluorenes. This was not further investigated as sufficient material of **79b** was obtained for our purposes. Reaction of **79a,b** with sarcosine in chlorobenzene at reflux (see Chapter 2), which generated corresponding azomethine ylides *in situ*, afforded cycloadducts **80a,b** by cycloaddition to $C_{60}$ following Prato's protocol (Scheme 4.8).[140] Due to limited availability of ethynylferrocene and previous experiences, no attempts were made to synthesise Fc-$C_{60}$ triads connected by a longer oligofluorene bridge.

## Electrochemical Studies

The electrochemical properties of **80a,b** were probed by room temperature cyclic voltammetric measurements in an *o*DCB-$CH_3CN$ solvent mixture (4:1 v/v) with a glassy carbon working electrode, $Bu_4NClO_4$ as supporting electrolyte and a scan rate of 100 mV $s^{-1}$. The redox potentials are collated in Table 4.2 together with those of **78**, **79a,b**, **50a**, **51a**, **53a**, ferrocene (Fc), pristine [60]fullerene and *N*-methyl pyrrolidinofullerene (**54**) as references.

Analogous to triads discussed earlier, **80a** and **80b** give rise to amphoteric redox behaviour. Firstly, three consecutive one-electron reduction waves (all quasireversible)

Table 4.2: Redox potential values of triads **80a** and **80b**, together with aldehyde intermediates **79a,b** and reference compounds (pristine $C_{60}$, Fc, **50a**, **51a**, **53a**, **54** and **78**).[a, b]

| Compound | $E^1_{red}$ | $E^2_{½, red}$ | $E^3_{½, red}$ | $E^4_{red}$ | $E^1_{ox}$ | $E^2_{ox}$ | $E^3_{ox}$ |
|---|---|---|---|---|---|---|---|
| $Fl_2$-CHO (**50a**) | -2029 | | | | 1295 | 1608 | 1873 |
| Fc | | | | | 440 (236)[c,d] | | |
| Fc-yne-H (**78**) | | | | | 480 (356)[c,d] | 1534 | |
| Fc-yne-Fl-CHO (**79a**) | -2058[c] | | | | 498 (344)[c,d] | 1228 | |
| Fc-yne-$Fl_2$-CHO (**79b**) | | | | | 402 (327)[c,d] | 1505 | |
| $C_{60}$ | -795[c] | -1191 | -1649 | -2122[c] | | | |
| **54** | -912[c] | -1310 | -1849 | | 1094 | 1545 | |
| $Fl_2$-$C_{60}$ (**51a**) | -882[c] | -1293 | -1843 | -2333 | 1170 | 1345 | 1623 |
| $C_{60}$-$Fl_2$-$C_{60}$ (**53a**) | -882[c] | -1294 | -1839 | -2315 | 1182 | 1545 | |
| Fc-yne-Fl-$C_{60}$ (**80a**) | -922[c] | -1340 | -1888 | | 380 (328)[c,d] | 1443 | |
| Fc-yne-$Fl_2$-$C_{60}$ (**80b**) | -923[c] | -1344 | -1901 | | 395 (324)[c,d] | 1488 | |

[a] Potentials in mV; scan rate 100 mV $s^{-1}$; glassy carbon working electrode, $Ag/AgNO_3$ reference electrode, Pt counter electrode; 0.1 M $Bu_4NClO_4$ in *o*DCB/$CH_3CN$ (4:1 v/v). [b] See also Table 2.1, Chapter 2. [c] Half wave potential values ($E_{½}$). [d] $E_{½}$ observed in partial scans.

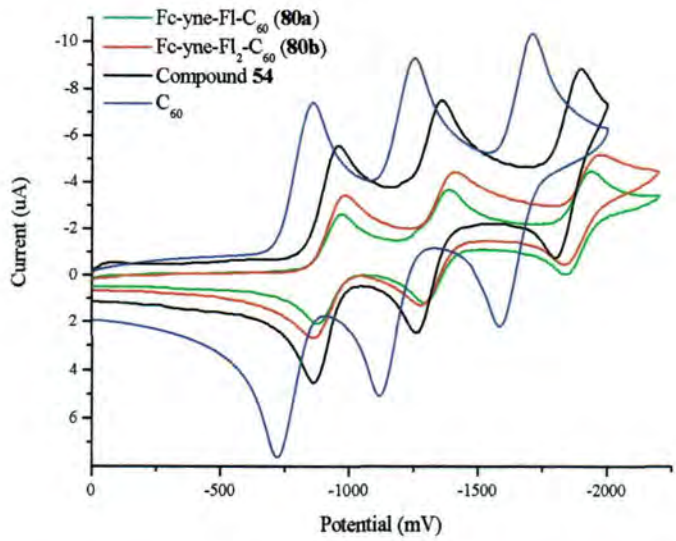


Figure 4.6: Cyclic voltammograms of $C_{60}$, **54** and **80a,b**. For conditions see Table 3.1.

have been observed on the reduction side. A good agreement with reference compounds **51a** and **54** allows an assignment of these waves to the reduction steps of the fullerene core and confirms the lack of substantial electronic interactions. As the first one-electron reduction potential of **80a** (-922 mV) and **80b** (-923 mV) can be assigned to the $C_{60}$ core, the strongest electron accepting moiety in the triads is $C_{60}$. Similar to **51a-c** and **53a-c** (see Chapter 2), cathodic shifts to more negative values, relative to pristine [60]fullerene, are observed for **80a,b**.

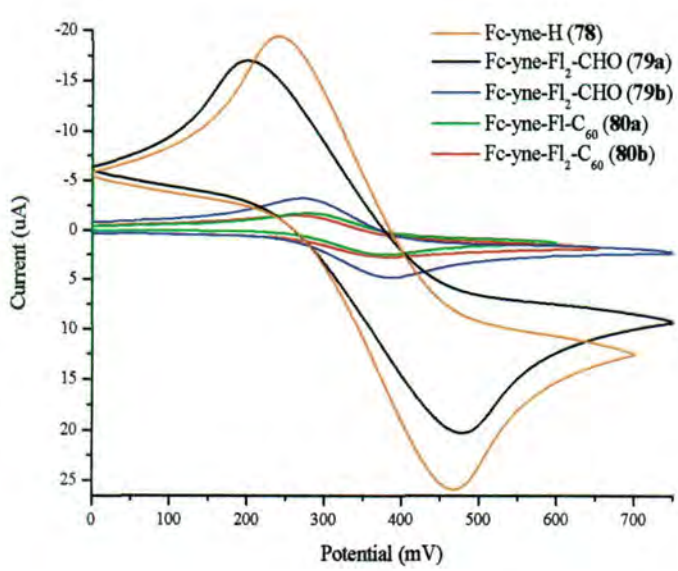


Figure 4.7: Cyclic voltammograms of **78**, **79a,b** and **80a,b**. For conditions see Table 3.1.

Several consecutive partial scans of the oxidation side in the region of 0 to 750 mV revealed that the first oxidation wave is a quasireversible one-electron process (Figure 4.7). This wave is assigned to the ferrocene donor moiety ($Fe^{2/3+}$) in the triad, due to good agreement with ethynylferrocene. The effect of the formyl group on the strongest donor is negligible in **79a,b**, which was also observed for *ex*TTF-$Fl_n$-CHO (**56a,b**, n = 1, 2) and (*t*BuPh)$_3$-ZnP-$Fl_n$-CHO (**73a,b**, n = 2, 3). Reference compounds **78** and ferrocene show that functionalisation of the ferrocene donor with an alkyne moiety shifts the oxidation of the donor to more positive values (*i.e.* reduced donor ability). Introduction of the fluorene units results in a minor cathodic shift, *i.e.* $E^1_{½}$ (ox) 356 mV (**78**) to 327 mV (**79b**). After substitution of the formyl group with $C_{60}$ the formation of the cation species remained at analogous potentials, which is 328 mV ($E^1_{½}$, ox) for monomer **80a** and 324 mV for dimer **80b**.

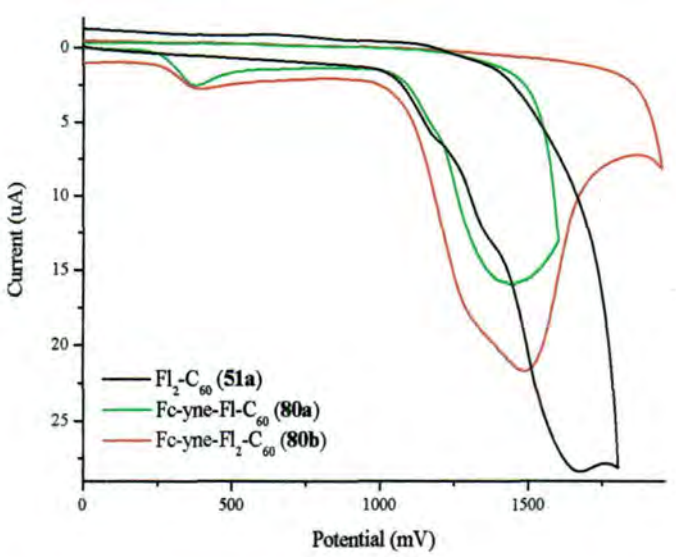


Figure 4.8: Cyclic voltammograms of **51a** and **80a,b**. For conditions see Table 3.1.

Full scans on the oxidation side illustrate that an irreversible process occurs as the oligofluorenes are oxidised (Figure 4.8); this was also observed for the ZnP triads **68a,b** and **74a,b**. The first oxidation wave of substituted fluorenes - normally between 1000 and 1300 mV (*e.g.* **50**, **51**, **53**, **56**) - is not found for **80a,b** and alternatively only a broad oxidation peak is observed, which was also observed for the *ex*TTF-$Fl_n$-$C_{60}$ (**57**) triads (Chapter 3).

### 4.3.9 Conclusions

In the second part of this chapter we have discussed the synthesis of D-$Fl_n$-$C_{60}$ (n = 1, 2) assemblies, wherein D is an electron donating ferrocene unit. In these triads ethynylferrocene is a key unit, covalently attached to a 9,9-dihexylfluorene monomer or dimer with an *N*-methyl pyrrolidinofullerene terminus. The new compounds (**80**) were synthesised utilising Sonogashira cross-coupling methodology to assemble ferrocene-alkyne-fluorenes with terminal aldehyde units, followed by Prato's 1,3-dipolar cycloaddition reactions of *in situ* generated azomethine ylides with $C_{60}$. The solution electrochemical data showed amphoteric behaviour (three, one-electron, reduction waves of the $C_{60}$ core and one, one-electron, oxidation wave of ferrocene) and irreversible oxidations of the oligofluorene chains with no significant interaction between these electroactive partners in the ground state. Fluorescence time-resolved and steady-state experiments will be carried out in the near future to determine the photophysical behaviour of the new compounds.

# Chapter 5: DTPY-$C_{60}$ and Pyrene-$C_{60}$ Dyads

## 5.1 Introduction

In the previous chapters D-$(Fl)_n$-$C_{60}$ ensembles were addressed where D is a strong electron donor group, *i.e.* extended tetrathiafulvalene, zinc porphyrin and ferrocene. Following the previous results we now report an investigation into similar triads containing a less explored electron donor, *i.e.* dithiapyrene (DTPY). In the time available for this project we were unable to synthesise DTPY-$(Fl)_n$-$C_{60}$ triads, but we have successfully synthesised and investigated the novel DTPY-$C_{60}$ conjugate. Therefore, this chapter will discuss and compare results from the DTPY-$C_{60}$ dyad with the corresponding pyrene-$C_{60}$ conjugate.

As reviewed in Chapter 1, covalently linked donor-acceptor conjugates including fullerene $C_{60}$ have attracted much attention because electron transfer reactions to $C_{60}$ are highly efficient due to the minimal changes of structure and solvation that are associated with the electron-transfer reduction.[32, 175-178] Such conjugates have been widely used in photoelectronic devices such as photovoltaic cells.[179-181] 1,6-Dithiapyrene (DTPY) is known to act as an excellent Weitz-type electron donor with a oxidation potential comparable to that of TTF.[182, 183] A key difference between DTPY and TTF is that DTPY is aromatic (18 π-electrons) in the neutral state, whereas TTF has a non-aromatic neutral state (two 7 π-electron rings) and gains aromaticity (formation of 6 π-electron dithiolium cations) upon oxidation. 1,6-Dithiapyrene has more extensive absorption in the visible region, acting as a better chromophore than TTF. However, at the outset of our work donor-acceptor dyads composed of dithiapyrene and $C_{60}$ had not been reported, despite the evident interest in combining these moieties.

We report herein the synthesis and photodynamics of a novel DTPY-$C_{60}$ dyad. The corresponding pyrene-$C_{60}$ conjugate with virtually the same geometry was synthesised to

compare the photodynamics between dithiapyrene-$C_{60}$ and pyrene-$C_{60}$ dyads. In order to confirm the photoinduced charge separation and subsequent charge recombination processes, Professor Guldi's group employed time-resolved fluorescence measurements on the picosecond timescale and transient absorption measurements on the picosecond and microsecond timescale with detections that range from the visible to the near-infrared regions. The present study provides deeper insight into the control of the electron-transfer processes by subtle changes in the redox potentials and/or solvent polarity.

## 5.2 Results and Discussion

### Synthesis

The synthesis of 1,6-dithiapyrene (DTPY) is reported in the literature.[182, 184] However, some significant changes we made to the literature methodology have persuaded us to include our procedure to prepare DTPY in detail in the experimental section. Commercially available 1,5-dihydroxy-naphthalene was reacted with 1,4-diazabicyclo[2,2,2]octane (DABCO) and *N*,*N*-dimethylthiocarbamoyl chloride to yield **81** in 66% (Scheme 5.1). This was subsequently subjected to a Kwart-Newmann rearrangement to obtain **82**, which was easily separated from the starting material by column chromatography (Scheme 5.1). Some impurities (< 5%) are difficult to remove from **82** when the reaction is done on a large scale, but these impurities do not affect the next reaction step and can then be easily removed.

In the literature[182] 1,5-bis(2,2-diethoxyethylthio)naphthalene (**84**) is obtained in an overall high yield by the hydrolysis of **82**, which provides naphthalene-1,5-dithiol **83** (Scheme 5.1), and subsequent reaction with bromoacetaldehyde diethylacetal, sodium iodide and sodium ethoxide. We have found that the hydrolysis is unnecessary and that heating **82** to reflux with bromoacetaldehyde diethylacetal, sodium iodide and sodium ethoxide over the weekend in ethanol will yield **84** in 85% yield (Scheme 5.1). Although we have not optimised this reaction, we did notice that an overnight stir yielded mostly a half-converted product (determined by TLC and $^1$H-NMR).

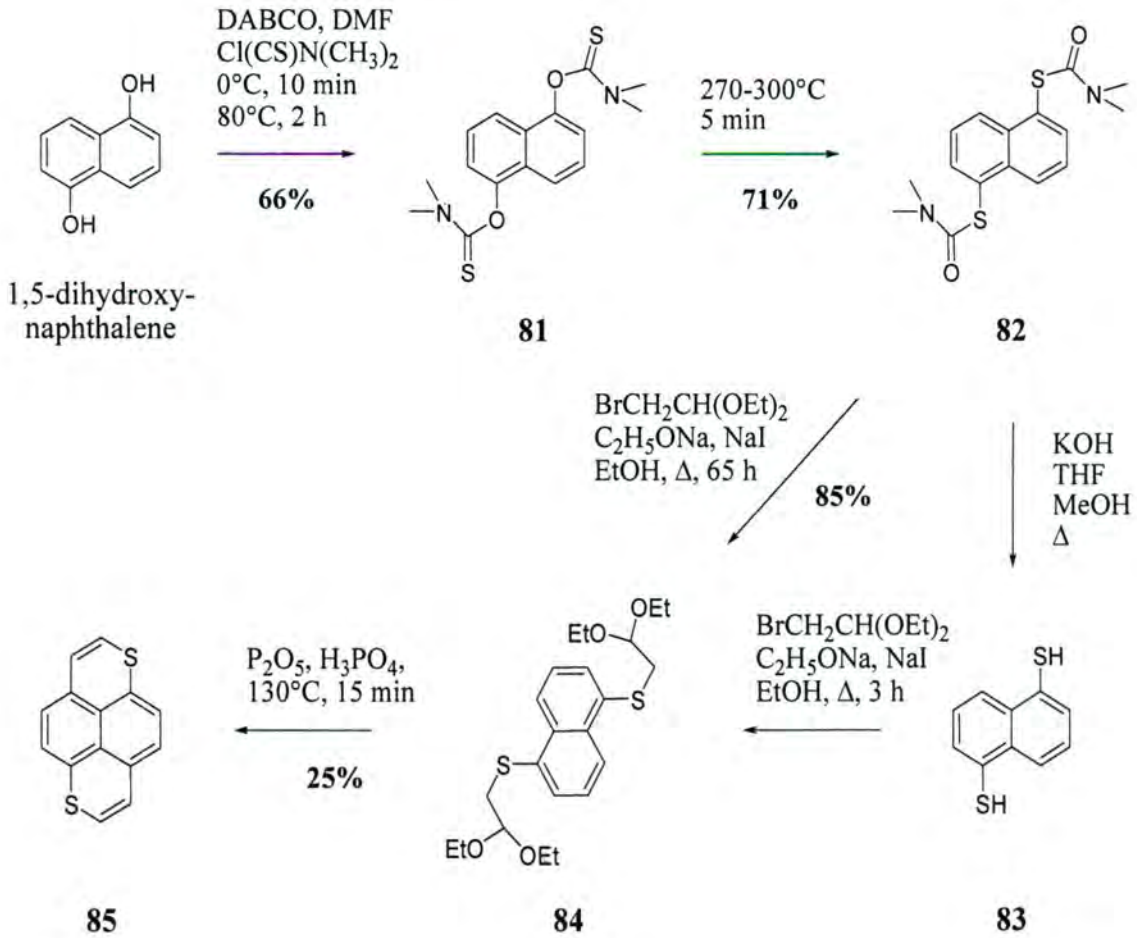


Scheme 5.1

The last and most vexatious step in the synthesis of DTPY proved to be the acid-catalysed cyclisation of **84** (Scheme 5.1). The literature originally reported a 22% yield,[182] which was later improved to 42% by the same group.[184] We have found that a lot of practise will eventually increase the yield from 0% to 25%. The key to obtaining any product is the addition of triethylamine to keep weakly basic conditions during purification and the avoidance of complete concentration of the crude reaction mixture. It is crucial that the product is cleared from all impurities produced during the reaction as quickly as possible to provide the highest yield. To obtain DTPY (**85**) in 25% yield (Scheme 5.1), this meant that the reaction and purification were completed (from start to finish) within 2 h.

Functionalisation of 1,6-dithiapyrene is essentially unexplored[182-187] and no DTPY-acceptor dyads have been reported. Derivatives of **85** functionalised only at positions 2-

and 7- are known from the literature, which are accessible through lithiation chemistry [reaction with n-BuLi followed by quenching with an electrophile, *e.g.* $C_6F_{13}I$[184] or DMF[185] resulting in 2-iodo-, 2,7-diodo- or 2-formyl- derivatives, respectively]. We have found that electrophilic substitution in DTPY opens access to 1,6-dithiapyrenes functionalised at position 5: specifically, reaction of **85** with phosphorus oxychloride and DMF under Vilsmeier conditions gave 5-formyl derivative **86** in 68% yield (Scheme 5.2). A proposed reaction mechanism is illustrated in Figure 5.1.

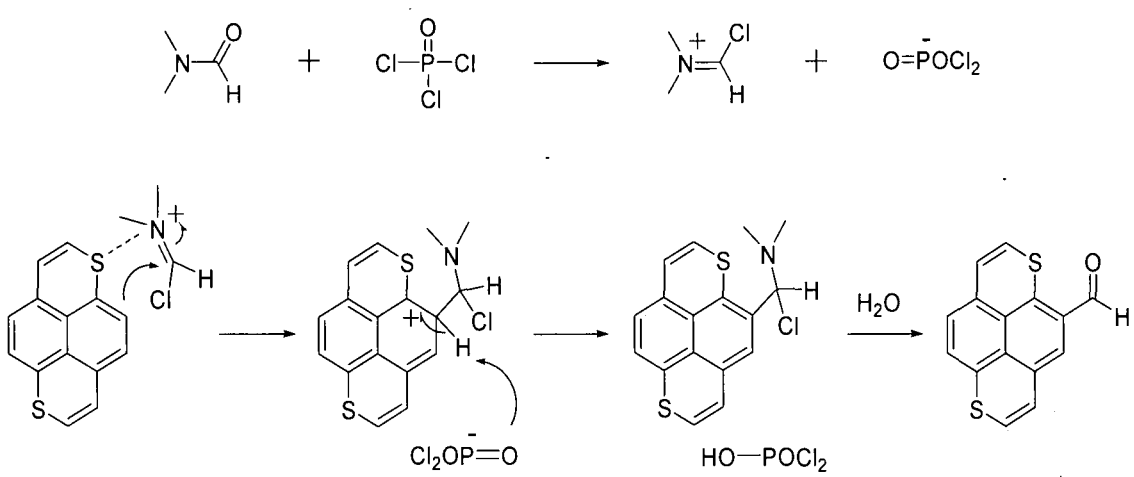


Figure 5.1: Proposed reaction mechanism for the reaction of **86**.

The new 5-formyl derivative **86** has a melting point of 255-257 °C, which is substantially different from the known 2-formyl-1,6-dithiapyrene (m.p. 215-216 °C).[185] Considering that other physical data for these two isomers are similar (*e.g.* elemental analyses, MS, number of signals in $^1H$ and $^{13}C$ NMR, and splitting in $^1H$ NMR spectra) and routine one-

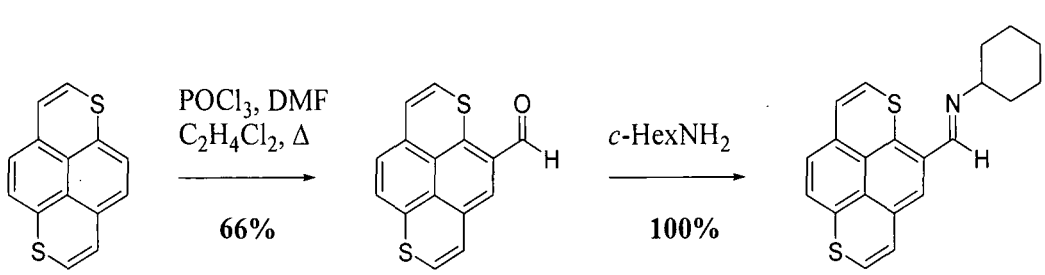


**85** DTPY **86** DTPY-CHO **87** DTPY-CHN-*c*Hex

Scheme 5.2

dimensional NMR spectroscopy did not confirm unambiguously the position of functionalisation in the 1,6-dithiapyrene ring, the structure of **86** was proved by 2D-NMR spectroscopy studies (COSY, NOESY techniques; Figure 5.2 and Appendix A). Due to the low solubility of **86** other 2D-NMR techniques, *i.e.* HSQC and HMBC were not possible. In order to provide further confirmation of this structure, aldehyde **86** was converted into the aldimine **87** (Scheme 5.2). The increased solubility introduced by the cyclohexyl moiety of **87** enabled more detailed NMR spectroscopic studies (COSY, NOESY, HSQC, HMBC techniques; Appendix B) to be preformed to unambiguously assign the structure, although **87** was not obtained analytically pure. The structure of DTPY (**85**) was assigned by 2D-NMR spectroscopy (COSY, HSQC, HMBC techniques; Appendix C) to complement the NMR studies of **86** and **87**.

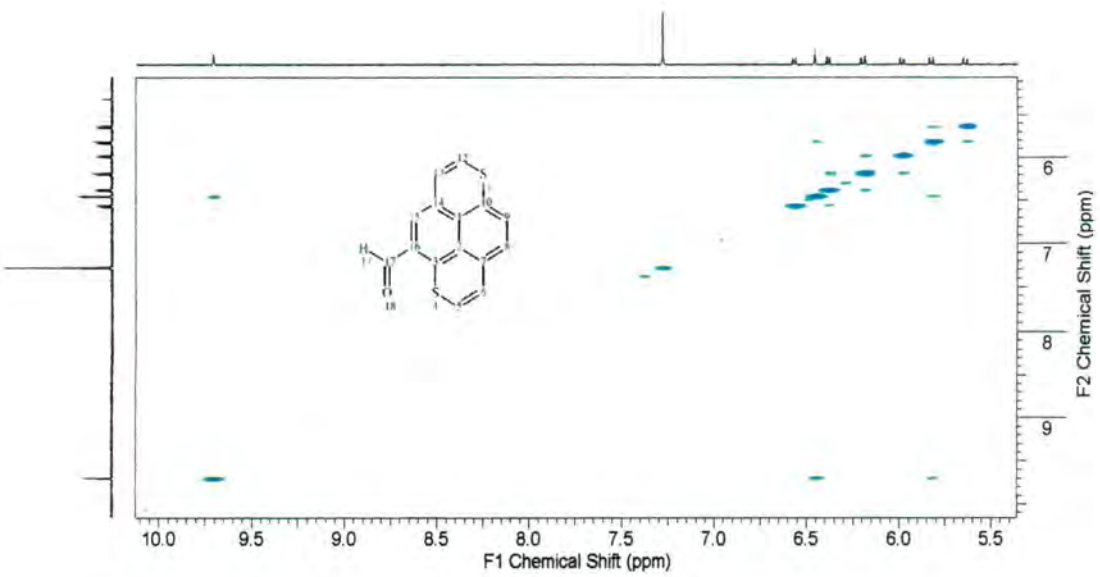


Figure 5.2: $^{1}H$-$^{1}H$-NOESY NMR spectrum of **86**; 500MHz, $CDCl_3$ containing traces of $Et_3N$.

Reaction of **86** with $C_{60}$ *via* Prato's 1,3-dipolar cycloaddition protocol[140] with an azomethine ylide generated *in situ* afforded the mono-adduct **88** in 64% (Scheme 5.3). A similar Prato reaction of pyrene-1-carboxaldehyde gave $C_{60}$-pyrene dyad **89** in 56% yield (Scheme 5.4). Electrochemical investigations on dyad **89** have recently been reported, but without any details of its synthesis or characterisation.[188] Moreover, the authors mention that additional peaks observed in the reduction region of their CV are most likely due to the presence of di- or multi-substituted $C_{60}$ side products.[188]

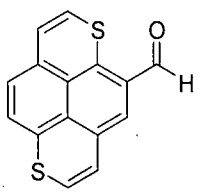

**86** DTPY-CHO

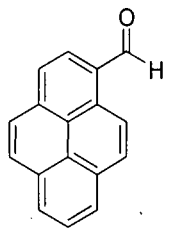

pyrene-1-carboxaldehyde

$C_{60}$, sarcosine
Cl-Ph, Δ

**64%**

$C_{60}$, sarcosine
Cl-Ph, Δ

**56%**

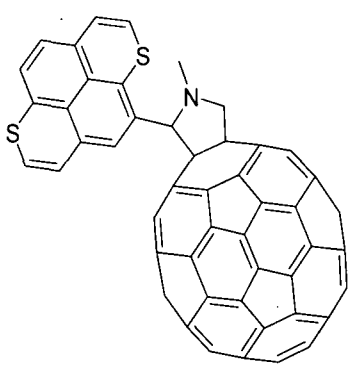

**88** DTPY-$C_{60}$

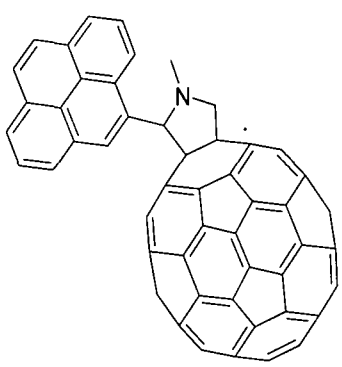

**89** Pyrene-$C_{60}$

Scheme 5.3

Scheme 5.4

Both donor-acceptor conjugates were assigned from their $^{1}$H NMR spectra, MALDI-TOF MS. Dyad **89** was additionally characterised by $^{13}$C NMR spectroscopy. The solubility of dyad **88** is too low for $^{13}$C NMR spectroscopy, but a satisfactory elemental analysis was obtained. A second rotamer is clearly visible in the $^{1}$H-NMR spectrum of dyad **89** as minor signals (Appendix D). The two rotamers are formed in a ratio of *ca.* 10:1 and are not separable by column chromatography. Due to the restricted rotation around the exocyclic C-C bond between the pyrrolidine ring and the bulky pyrene, two thermodynamically stable (at ambient conditions) rotamers are possible for dyad **89**, which according to DFT calculations are of similar energies (Appendix E).

As described in previous chapters, we aimed to investigate oligofluorene molecular wire behaviour through the preparation of D-$Fl_n$-$C_{60}$ ensembles, wherein D is a strong electron

donor. Naturally, after creating the novel DTPY-$C_{60}$ dyad we also set out to create a novel DTPY-wire-$C_{60}$ triad. Similar to the previous synthesised D-wire-$C_{60}$ assemblies, we aimed to utilise the Suzuki reaction to provide DTPY-fluorenes with terminal aldehyde units, which could then be reacted onwards with sarcosine and $C_{60}$. Therefore, a target was a halide containing 1,6-dithiapyrene derivative. As mentioned previously, the synthesis of 2-iodo-1,6-dithiapyrene has been published previously together with the synthesis and crystal structure of 2,7-diiodo-1,6-dithiapyrene.[184] The iodo functionalisation was achieved through a reaction of DTPY with *n*-butyllithium followed by quenching with $C_6F_{13}I$. However, in our hands, following the literature procedure gave only starting material and not the desired mono iodo-functionalised product.

We investigated some alternative methods in order to prepare a halide containing DTPY compound. Firstly, we attempted direct bromination by dissolving DTPY in DCM and adding one equivalent of bromine to the solution at 0 °C. Unfortunately mostly decomposition was observed and the trace amount of product that was obtained could not be identified by $^1$H-NMR spectroscopy. Another method of bromination which was explored was the use of *n*-bromosuccinimide (NBS). Thus DTPY was dissolved in DCM containing a trace of diisopropylamine and one equivalent of NBS was added at room temperature. Analysis of the obtained product by $^1$H-NMR spectroscopy revealed that it was a mixture of several different products (including some starting material), which could not be separated due to the small scale.

At this point it should be noted that due to the limited availability of DTPY, investigations towards the synthesis of a mono halide-substituted DTPY substance had to be done on a small scale (50-75 mg) and would be worth reinvestigating when DTPY can be more easily prepared and on a larger scale. It was noted that in the literature examples of the bromine functionality surviving the acid-catalysed cyclisation can be found.[189, 190] Therefore we decided that it might be worth investigating the bromination of the starting materials of DTPY (**81**, **82** or **84**). Bromination of **82** was investigated as this functionality on the naphthalene core would be less likely to react with the brominating agent than the functional group on **84**. Lithiation of **82** (500 mg) with *n*-butyllithium in dry ether at -78 °C and subsequent quenching with 1,2-dibromoethane yielded unreacted starting material. Starting material was also obtained after the attempted reaction of DTPY in DCM

containing some pyridine with NBS at 0 °C. Due to limited availability of DTPY and time, we had to abandon further attempts to prepare DTPY-$Fl_n$-$C_{60}$ ensembles.

## Theoretical Calculations and Absorption Spectra

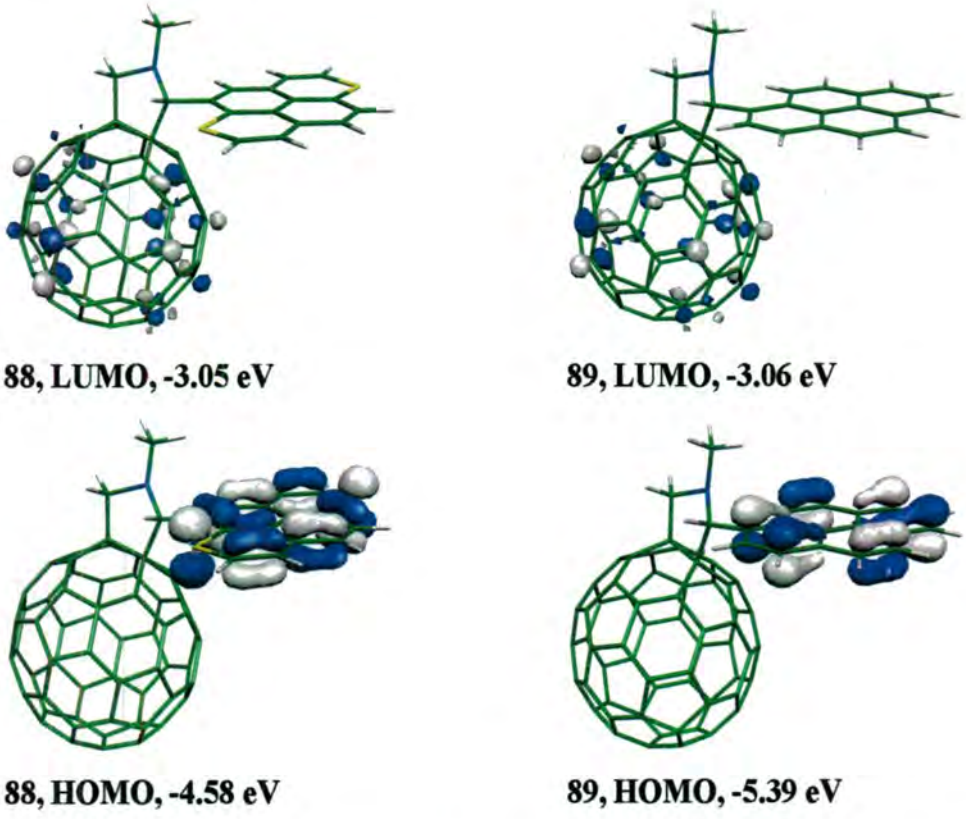

**88, LUMO, -3.05 eV** **89, LUMO, -3.06 eV**

**88, HOMO, -4.58 eV** **89, HOMO, -5.39 eV**

Figure 5.3: Localisation of HOMO and LUMO orbitals in dyads **88** (left) and **89** (right) according to DFT B3LYP/6-31G* (d) calculations.

DFT B3LYP/6-31G* (d) calculations have been employed by Dr. I. Perepichka in our group to test donor and acceptor features in DTPY-$C_{60}$ (**88**) and pyrene-$C_{60}$ (**89**). The calculations reveal that in fully optimised geometries the HOMO is exclusively delocalised over the DTPY moiety (-4.58 eV) and the LUMO over the $C_{60}$ core (-3.05 eV) in **88**. Similar delocalisation is observed in **89** with the HOMO delocalised over the pyrene moiety (-5.39 eV) and the LUMO over the $C_{60}$ core (-3.06 eV) (Figure 5.3 and Appendix E). This speaks for the lack of electronic interactions between the donor and acceptor fragments in both donor-acceptors systems, despite imminent close centre-to-centre

distances between the donor and the acceptor moieties of 8.17 and 8.30 Å in **88** and **89**, respectively.

The small effects of the donor units on the LUMO (0.17-0.18 eV) and the acceptor unit on the HOMO energy levels (0.14 eV) in DTPY-$C_{60}$ (**88**) and pyrene-$C_{60}$ (**89**) - as evident from comparison with parent DTPY (**85**) and $C_{60}$ (Figure 5.4) - are in good agreement with the lack of electronic interaction between the donor and acceptor moieties. Considering the energies of the two HOMO and LUMO levels we estimate energy gaps in the gas phase of 1.53 eV for DTPY-$C_{60}$ and 2.34 eV for pyrene-$C_{60}$ (Figure 5.4).

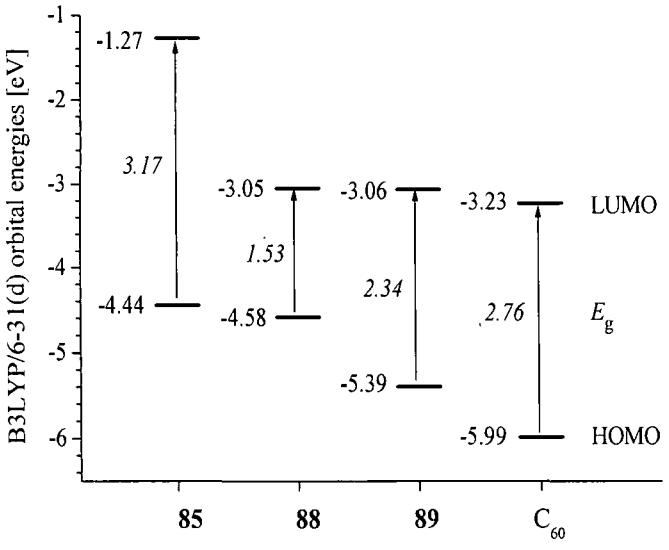


Figure 5.4: Energy levels of frontier orbitals of dyads **88** and **89** in comparison with those for DTPY (85) and C60 from DFT B3LYP/6-31G* (d) calculations in the gas phase.

The absorption spectra of **88** in toluene, THF, DCM and PhCN are best described as the superposition of that of each individual component: DTPY and $C_{60}$ with the most dominant absorptions at 430 nm (*i.e.* DTPY) and 300 nm (*i.e.* $C_{60}$). This suggests that there is only little, if any, electronic communication between DTPY and $C_{60}$ in **88**. The UV-visible spectrum of **88** is presented in Appendix G, where the spectrum of pyrene-$C_{60}$ **89** is given for comparison.

## Electrochemical Studies

The electrochemical properties of DTPY-$C_{60}$ (**88**) and pyrene-$C_{60}$ (**89**) were probed by room temperature cyclic voltammetric measurements in benzonitrile (PhCN), *o*-dichlorobenzene (*o*DCB) or their 1:1 v/v mixture with a glassy carbon working electrode, $Bu_4NPF_6$ as supporting electrolyte and various scan rates. The redox potentials are collated in Table 5.1 together with those of DTPY (**88**), pristine [60]fullerene and *N*-methyl pyrrolidinofullerene (**54**) as references.

Table 5.1: Redox potential values for Compounds **54**, **85**, **88**, **89** and $C_{60}$.[a]

| Compound | $E^1_{½,\,ox}$ | $E^2_{½,\,ox}$ | $E^1_{½,\,red}$ | $E^2_{½,\,red}$ | $E^3_{½,\,red}$ | $E^g_{CV}$[b] |
|---|---|---|---|---|---|---|
| DTPY **85**[c] | -0.06 | 0.41 | | | | |
| DTPY **85**[d] | -0.11 | 0.39 | | | | |
| $C_{60}$[c] | | | -0.92 | -1.33 | | |
| $C_{60}$[d] | | | -0.97 | -1.38 | -1.62 | |
| DTPY-$C_{60}$ **88**[c] | 0.01 | 0.45[e] | -1.03 | -1.45 | | 0.87 |
| Pyrene-$C_{60}$ **89**[c] | 0.95[e] | | -1.02 | -1.43 | -1.82[f] | 1.62 |
| **54**[c] | | | -1.01 | -1.43 | | |

[a] Potentials in V; scan rate 100 mV $s^{-1}$ (for **85**, **89** and $C_{60}$) and 500 mV $s^{-1}$ (for **88**); 0.1 M $Bu_4NPF_6$; $Ag/Ag^+$ reference electrode and standardised to $Fc/Fc^+$ couple [$E_{Fc/Fc+}$ = +0.20 V *vs.* $Ag/Ag^+$ (PhCN); +0.24 V (PhCN:*o*DCB, 1:1 v/v)]. [b] HOMO–LUMO gap, estimated from the onsets of oxidation and reduction processes in CV. [c] CV in PhCN. [d] CV in PhCN:*o*DCB, 1:1 v/v. [e] Irreversible peak ($E^1_{ox}$). [f] Irreversible peak ($E^1_{red}$).

DTPY (**85**) displayed two reversible, one-electron, oxidation waves at low potentials (Figure 5.4), due to sequential cation radical and dication formation, as described previously.[182] DTPY-$C_{60}$ (**88**), on the other hand, is highly redox amphoteric, displaying two single-electron oxidation waves from the DTPY moiety and two single-electron reduction waves from the $C_{60}$ core (Figure 5.5). Small donor-acceptor interactions in **85** result in slightly anodic shifts of the oxidation potentials of the DTPY moiety compared to

**85** (by 0.07 V for $E^1_{½,\ ox}$ and 0.02 V for $E^2_{½,\ ox}$) and little cathodic shifts of the reduction potentials of the $C_{60}$ moiety compared to **54** (by 0.02 V for both $E^1_{½,\ red}$ and $E^2_{½,\ red}$ in PhCN, Table 5.1).

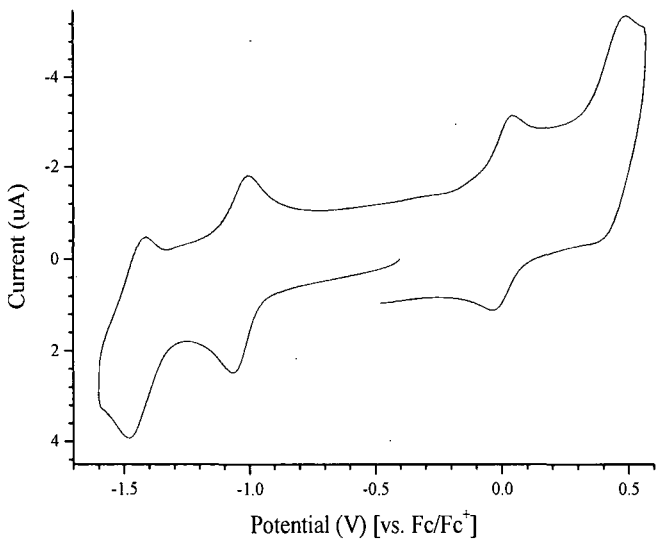


Figure 5.5: CV of DTPY-$C_{60}$ **88** (scan rate 500 mV $s^{-1}$) dyad in benzonitrile, 0.1 M $Bu_4NPF_6$.

These results are in good agreement with theoretical predictions from DFT calculations discussed above for the evolution of HOMO-LUMO energies in **88** compared to **85** and $C_{60}$. The main contribution to the cathodic shift of $E^1_{½,\ red}$ in **88** compared to pristine $C_{60}$ arises from breaking a double bond on the $C_{60}$ core; thus, a 90 mV cathodic shift of $E^1_{½,\ red}$ compared to $C_{60}$.[27] Reduction of pyrene-$C_{60}$ (**89**) occurs at almost the same potentials as for **54** and **88** thus confirming a negligible effect of the donor units on the LUMO energy level. In contrast, the oxidation of the pyrene unit in **89** is anodically shifted by 0.91 V (from comparison of their $E^1_{ox}$ potentials) compared to the oxidation of the DTPY moiety in **88** and the process is electrochemically irreversible (Figure 5.6).

Cyclic voltammetry of dyad **88** in benzonitrile at a high scan rate of 500 mV $s^{-1}$ revealed two single-electron oxidation waves from the DTPY moiety ($E^1_{½,\ ox}$ and $E^2_{½,\ ox}$; the first oxidation is reversible and the second oxidation is a quasi-reversible process) and two reversible single-electron reduction waves ($E^1_{½,\ red}$ and $E^2_{½,\ red}$) from the $C_{60}$ moiety (Appendix F). When the scan rate was decreased to 100 mV $s^{-1}$ the second reduction wave ($E^2_{red}$) became broader and revealed two overlapping redox processes (Appendix F).

Further decrease in the scan rate to 20 and 10 mV $s^{-1}$ improved the separation of these two waves demonstrating the appearance of two closely-spaced reduction processes (Appendix F). This is clearly seen from the deconvoluted CV (Appendix F). This unexpected observation is not understood at present, and we have not studied the origin of these split redox processes, which probably include some intermolecular interactions during the CV experiments at low scan rates. It is well known that pristine $C_{60}$ undergoes multistep (up to six) single-electron reduction processes to form radical anion → dianion → radical trianion → ... → hexaanion species, with relatively constant separation between any two successive reductions of *ca.* 450 ± 50 mV.[39, 191] This is not always the case for substituted $C_{60}$ derivatives: ($E^1_{red}$ - $E^2_{red}$) and ($E^2_{red}$ - $E^3_{red}$) gaps vary somewhat depending on the molecular structure, but generally both gaps are quite large, ~350-650 mV, *i.e.* much higher that the difference between the two overlapped waves for dyad **88** at low scan rates (100 mV, Appendix F).[192-201]

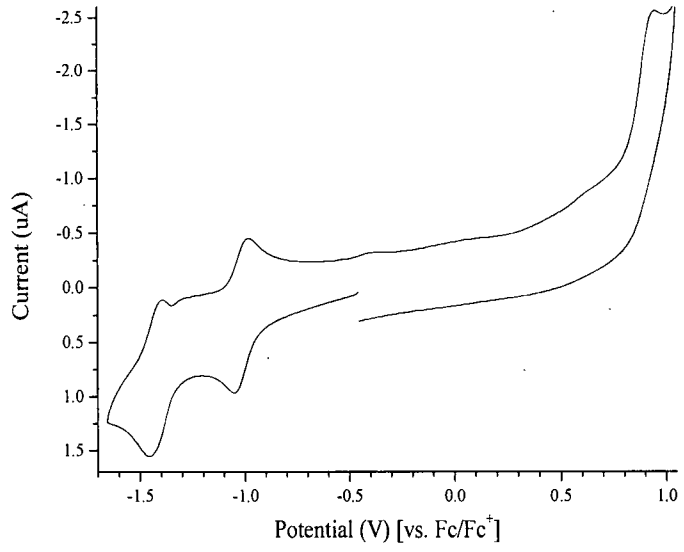


Figure 5.6: CV of pyrene-$C_{60}$ **89** (scan rate 100 mV $s^{-1}$) dyad in benzonitrile, 0.1 M $Bu_4NPF_6$.

## Photophysical Studies

Preliminary insights into conceivable donor-acceptor implications were gained from steady-state fluorescence experiments (Figure 5.7 and 5.8). Hereby, the fluorescing features of DTPY and pyrene are particularly useful, since they enable the deactivation of

the DTPY (2.43 eV) and pyrene (3.22 eV) singlet excited states in the references, as well as in DTPY-$C_{60}$ **88** and in pyrene-$C_{60}$ **89**, to be followed with ease. Specifically, fluorescence quantum yields of close to unity and fluorescence lifetimes of the order of tens of nanoseconds are sensitive markers. Notably, both sets of systems, *i.e.* **88** and **89**, exhibit dual fluorescence. Besides the strong fluorescence of DTPY and pyrene in the visible part of the spectrum, $C_{60}$ derivatives exhibit weak fluorescence in the near-infrared part of the spectrum (650 - 850 nm). In fact, the $C_{60}$-reference compound **54** (1.78 eV) reveals nearly solvent-independent fluorescence quantum yields of 6.0 x $10^{-4}$ and fluorescence lifetimes of 1.5 ns.

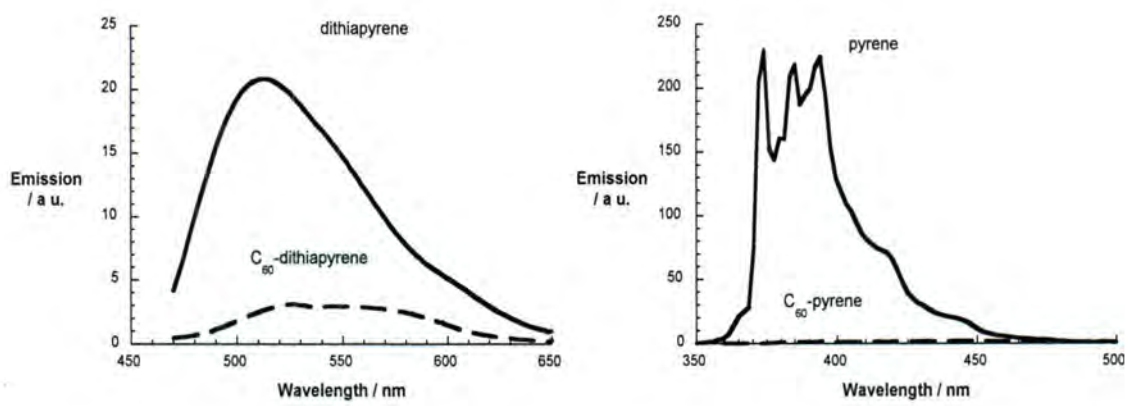


Figure 5.7: Fluorescence spectra (left) of DTPY (solid line) and DTPY-$C_{60}$ **88** (dashed line) in toluene with matching absorption at the 460 nm excitation and fluorescence spectra (right) of pyrene (solid line) and pyrene-$C_{60}$ **89** (dashed line) in toluene with matching absorption at the 335 nm excitation.

Relative to the strong fluorescence of the reference (0.75), the pyrene fluorescence in **89** is nearly quantitatively quenched. Notably, the quenching is stronger in THF (*i.e.* 0.003) than in toluene (*i.e.* 0.005). Instead, the familiar fullerene fluorescence spectrum was found with a characteristic *0-0 transition around 715 nm, despite exclusive excitation of the pyrene moiety. To unravel the mechanism of producing the $C_{60}$ fluorescence, an excitation spectrum was taken. The excitation spectrum of pyrene-$C_{60}$ was an exact match of the ground state absorption of the pyrene reference with maxima at 360 nm and 412 nm, respectively. This implies that there is a rapid transfer of singlet excited state energy from the photoexcited pyrene to the covalently linked $C_{60}$. Determining the quantum yield (6.0 x

$10^{-4}$) of the $C_{60}$ fluorescence shows that its formation is quantitative, despite the exclusive excitation of the pyrene moiety.

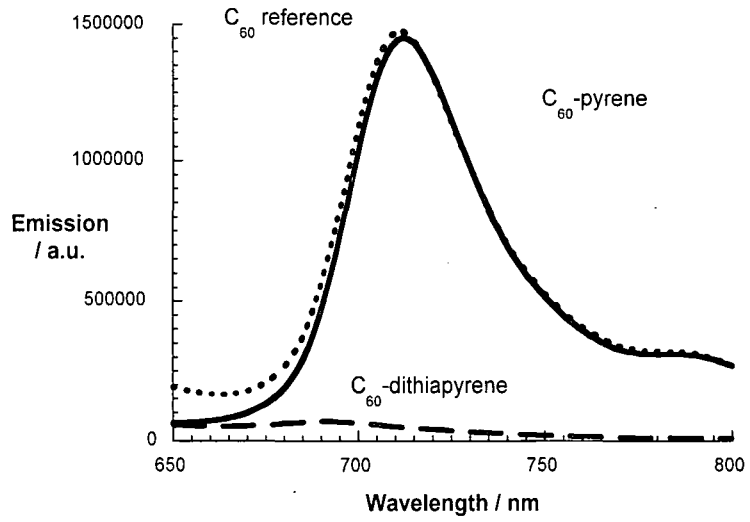


Figure 5.8: Fluorescence spectra of compound **54** (dotted line), DTPY-$C_{60}$ **88** (dashed line) and pyrene-$C_{60}$ **89** (solid line) in toluene with matching absorption at the 325 nm excitation.

Like in pyrene-$C_{60}$ **89**, the DTPY fluorescence (*i.e.* 0.023) in DTPY-$C_{60}$ **88** is subject to a marked fluorescence quenching that intensifies with the solvent polarity (*e.g.* toluene: 0.003; THF: 0.002). However, for **88** no particular $C_{60}$ fluorescence (*i.e.* $<< 10^{-5}$) was seen in the near-infrared region at all.

To complement the fluorescence studies, the photophysics of DTPY-$C_{60}$ **88** and pyrene-$C_{60}$ **89** were probed by means of time-resolved transient absorption spectroscopy. Femtosecond laser flash photolysis allowed for the characterisation of the dynamic processes, which are associated with the generation and the fate of photoexcited states in these novel donor-acceptor conjugates, but more importantly, these data helped to shed light on the nature of the photoproduct, that is, an excited state or charge-separated state evolving from an intramolecular energy or electron transfer process, respectively.

First, the reference compounds should be discussed. In femtosecond-resolved transient absorption measurements, the pyrene reference gave rise to an instantaneously formed (*i.e.*

within ~2 ps), broadly absorbing transient with a maximum around 475 nm (Figure H.1 in Appendix H). On the timescale of up to 3000 ps no significant decay of the excited state absorption was observed. It is only on the hundreds of nanosecond timescale that the pyrene singlet excited state converts slowly (*i.e.* $4.3 \times 10^6$ $s^{-1}$) to the corresponding triplet manifold, for which the following features were determined in our experiments: a transient maximum at 430 nm.

Similarly, DTPY reveals on the femtosecond timescale the rapid formation (*i.e.* within ~2 ps) of a singlet excited state, for which a maximum evolves at 530 nm (Figure H.2 in Appendix H). This state is metastable and another process follows, whose outcome on a timescale of 1500 ps is the formation of a distinct, new species, which is characterised by bleaching around 475 nm and a set of maxima at 515 and 550 nm. This absorption is in excellent agreement with that found upon nanosecond excitation, from which we infer that the underlying reaction is an intersystem crossing (*i.e.* $2.3 \times 10^9$ $s^{-1}$) from the DTPY singlet to the energetically lower lying triplet excited state. The triplet decays (*i.e.* $3.6 \times 10^5$ $s^{-1}$) to the ground state.

Lastly, $C_{60}$-reference compound **54** should be discussed (Figure H.3 in Appendix H). The singlet excited state of compound **54** displays a distinctive singlet-singlet transition around 880 nm. The lifetime of the singlet-singlet intermediate state is relatively short, as $C_{60}$ and most of its derivatives convert rapidly to the much longer-lived triplet excited state with nearly unit yield. The process is a spin-forbidden intersystem crossing (*ISC*) with a high rate of $5.0 \times 10^8$ $s^{-1}$ driven by an efficient spin-orbit coupling. The spectral characteristics of the triplet excited state are maxima at 360 and 700 nm, followed by a low-energy shoulder at 800 nm.[202]

In the context of the current investigations, important features of the electron donors (*i.e.* DTPY and pyrene) and the electron acceptor (*i.e.* $C_{60}$) are their corresponding radical cation and radical anion spectra, respectively. Thus, we have employed radiation chemical means to determine the spectral characteristics of the DTPY radical cation, the pyrene radical cation and the fullerene radical anion. The following peaks evolve for the pyrene radical cation: 450, 500 and 575 nm.[203] For the DTPY radical cation, on the other hand, peaks were noted at 560, 630 and 770 nm.

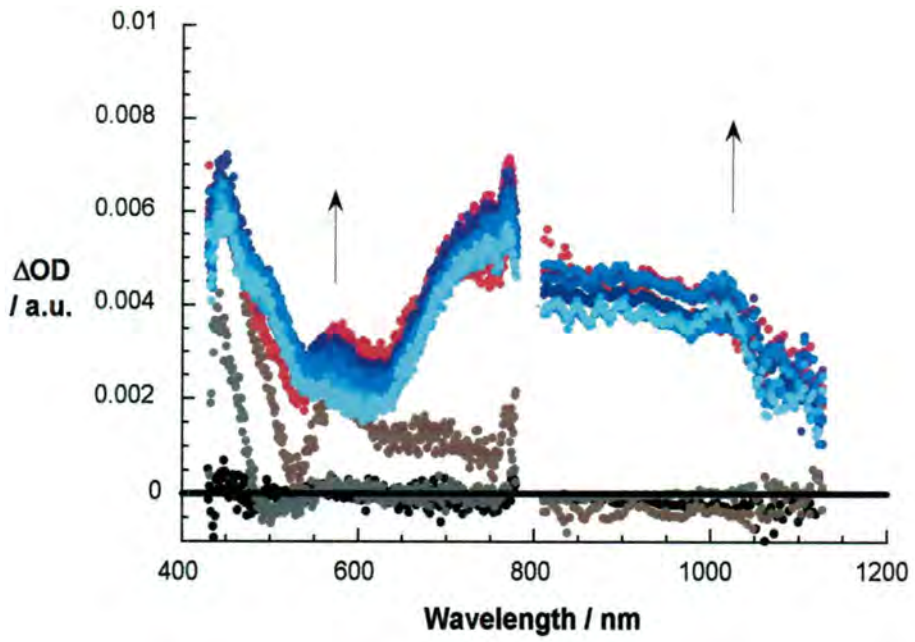


Figure 5.9: Differential absorption spectra (visible and near-infrared) obtained upon femtosecond laser flash photolysis (355 nm) of ~$1.0 \times 10^{-5}$ M solutions of pyrene-$C_{60}$ **89** in deaerated THF at different delay times; excitation at 380 nm with OD = 0.6.

Following the conclusion of the femtosecond excitation (*i.e.* 355 nm) of pyrene-$C_{60}$ **53** a transient intermediate is seen that - at first glance - resembles mostly that of the $C_{60}$ reference. As Figure 5.9 shows the same broad maximum around 880 nm, which is indicative of the $C_{60}$ singlet excited state, is seen regardless of the solvent (*i.e.* toluene and THF). This singlet excited state decays over the time course of 3000 ps and concomitant with this decay a maximum at 700 nm grows in. The latter is a clear attribute of the $C_{60}$ triplet excited state. A closer inspection reveals, however, features that the $C_{60}$ reference does not exhibit: maxima in the visible at 450, 510 and 575 nm and in the near-infrared at 1010 nm. Upon referral to the pulse radiolytic section we conclude that the 450, 510 and 575 nm features correspond to the pyrene radical cation, while the 1010 nm feature relates to the $C_{60}$ radical anion. Hence, we see besides singlet and triplet excited states, the formation of an intermediate radical ion pair state.

Considering the aforementioned analysis of the spectral evolution it is hardly surprising that the best global fit of the absorption time profiles comprise a bi-exponential fitting

function. In particular, in both solvents, namely toluene and THF, a short-lived and a long-lived component were found. Interestingly, the relative weight of the two contributions changes with solvent polarity. While, for example, in toluene the short-lived contribution is on the order of 5% it is nearly 50% in THF. The short lived component changes only slightly in the two solvents with values of 46 ± 6 ps and 53 ± 9 ps in toluene and THF, respectively. Contrasting these results, the long-lived component is solvent independent and, more importantly, resembles the kinetics seen in the $C_{60}$-reference **54**. This leads us to conclude that the short-lived component must reflect the charge recombination, while the long-lived component is the intrinsic intersystem crossing affording the triplet excited state (*vide supra*). From such dependence we must assume that the charge recombination dynamics in pyrene-$C_{60}$ **89** are located in the normal region of the Marcus parabola.

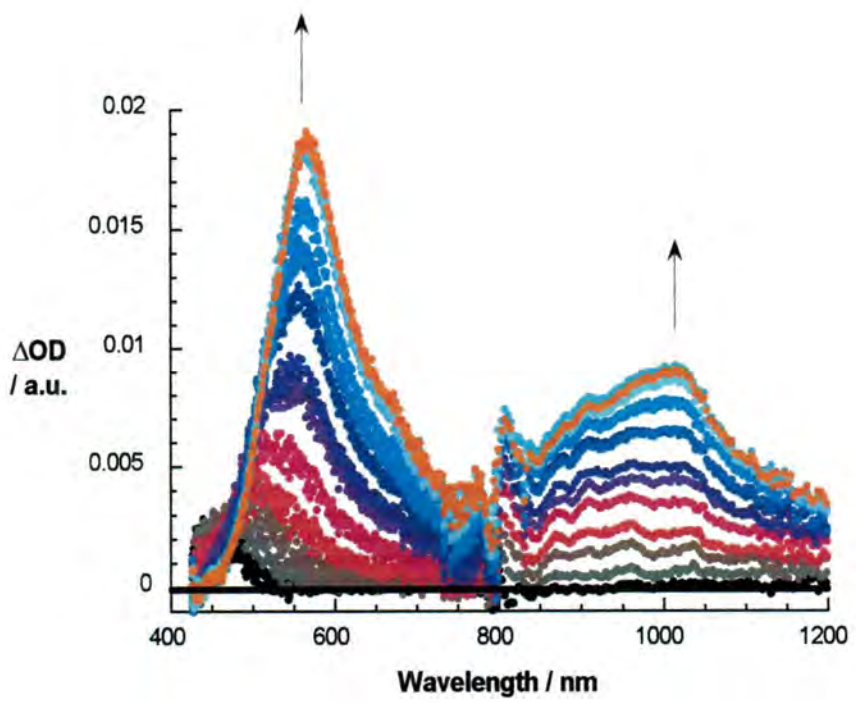


Figure 5.10: Differential absorption spectra (visible and near-infrared) obtained upon femtosecond laser flash photolysis (380 nm) of ~$1.0 \times 10^{-5}$ M solutions of DTPY-$C_{60}$ **88** in deaerated toluene at different delay times; excitation at 380 nm with OD = 0.4.

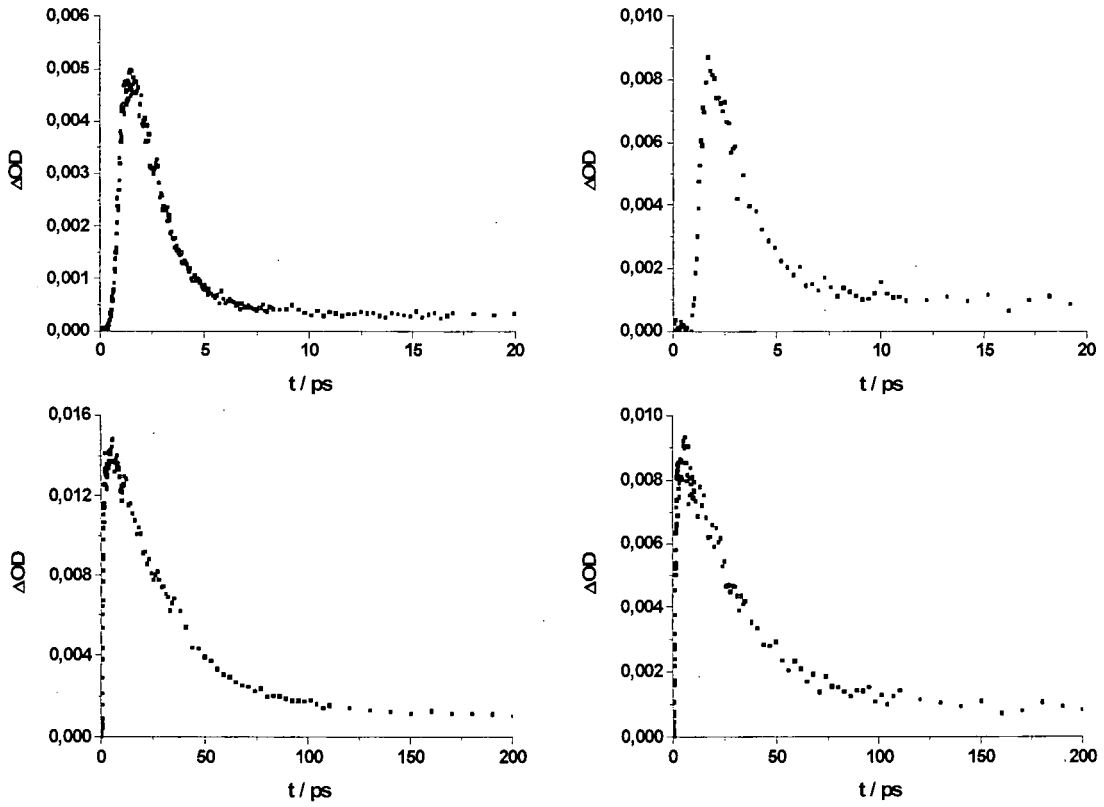


Figure 5.11: Time profiles of the transient absorption at 670 (left) and 1014 (right) nm monitoring the charge separation and recombination in DTPY-$C_{60}$ dyad **53**. Upper part in THF and lower part in toluene.

The behaviour for DTPY-$C_{60}$ **88** is very different. Most importantly, with the help of spectroscopic and kinetic analysis we identified only one photoproduct. Immediately upon 380 nm photoexcitation the DTPY singlet excited state features evolve, which attest to the successful DTPY excitation despite the presence of $C_{60}$. $C_{60}$ exerts, nevertheless, a profound impact on the singlet excited state decay. In particular, a rapid conversion ($1.3 \times 10^{12}$ $s^{-1}$) into a new transient is registered. Once the rapid disappearance of the excited DTPY absorption comes to an end (*i.e.* ~1.0 ps after the laser pulse), the following characteristics remain: maxima at 560, 630, 770 and 1010 nm (Figure 5.10). The visible maxima are ascribed to the radical cation of DTPY, because the DTPY radical cation, produced by the one-electron oxidation of DTPY **85** has absorption bands at 560, 630 and 770 nm. The absorption maximum in the near-infrared region, on the other hand, is an excellent match to the one-electron reduced fullerene. We therefore conclude that photoexcitation of DTPY-$C_{60}$ **88** yields in THF a radical ion pair state that evolves from

the DTPY and / or $C_{60}$ singlet excited state. A similar radical ion pair state is also obtained in cyclohexane, toluene and DMF. Please note that no $C_{60}$ singlet excited state features are discernable, neither in toluene nor THF, at any given time delay after the photoexcitation. On this basis we rule out any significant contribution that might evolve from a transduction of singlet excited state energy between DTPY (**85**) (2.43 eV) and $C_{60}$ (1.78 eV). The time profiles of the absorbance at 670 nm and 1014 nm in THF and toluene are shown in Figures 5.11. The lifetime is determined as $\tau_{CS} = 0.5$ ps ($2.0 \times 10^{12}$ $s^{-1}$) in DMF, $\tau_{CS} = 2$ ps ($5.0 \times 10^{11}$ $s^{-1}$) in THF, $\tau_{CS} = 27$ ps ($3.9 \times 10^{10}$ $s^{-1}$) in toluene and $\tau_{CS} = 1011$ ps ($9.8 \times 10^{8}$ $s^{-1}$) in cyclohexane.

The slower charge-recombination rate in toluene than that in a more polar solvent (THF) suggests that this process is in the Marcus inverted region, where the electron-transfer rate becomes slower with increasing driving force of electron transfer as the solvent polarity decreases.[204-206] This is demonstrated in Figure 5.12, which displays the driving force dependence ($-\Delta G^{\circ}$) for the charge recombination on the rate constant for both donor-acceptor conjugates (*i.e.* DTPY-$C_{60}$ **88** and pyrene-$C_{60}$ **89**). The parabolic fitting affords a reorganisation energy ($\lambda$) of 0.89 eV and an electronic coupling (V) of 32 $cm^{-1}$. Both of these values are well in line with recently published donor-acceptor conjugates including fullerene $C_{60}$.[32, 138, 175-181]

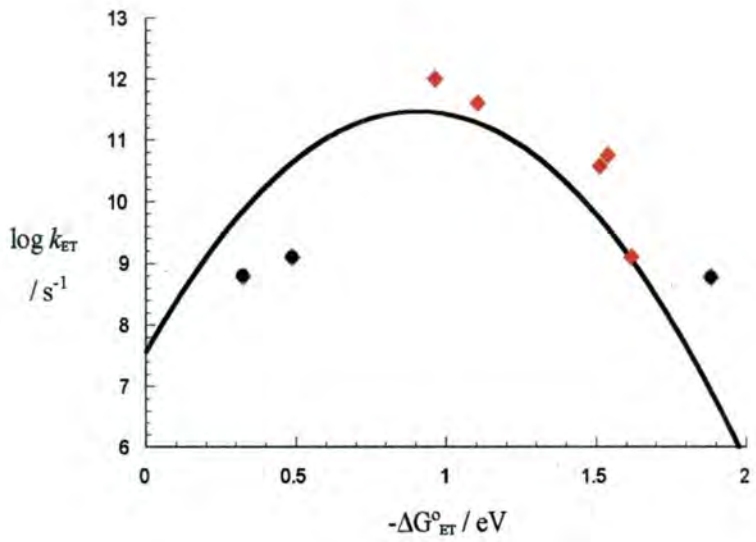


Figure 5.12: Driving force ($-\Delta G^{\circ}$) dependence of intramolecular charge recombination in DTPY-$C_{60}$ **88** (red diamonds) and pyrene-$C_{60}$ **89** (black diamonds).

In the corresponding nanosecond experiments DTPY-$C_{60}$ **88** and pyrene-$C_{60}$ **89** give rise to contrasting behaviour. While in the former case no appreciable changes were monitored on the nanosecond scale at all, in the latter case triplet characteristics were found that resemble those of the $C_{60}$ reference. A high triplet quantum yield - with a value of 0.75 ± 0.05 in toluene and THF - corroborates the efficiency of the overall energy transfer. At the same time it points to the competition between energy and electron transfer when photoexciting pyrene. The triplets in the $C_{60}$ reference and in the pyrene-$C_{60}$ donor-acceptor conjugate **89** decay similarly slowly on a time scale of up 100 microseconds to afford quantitatively the singlet ground state.

## 5.3 Conclusions

We have reported the synthesis and photodynamics of DTPY-$C_{60}$ conjugate **88** dyad. Dyads **88** and pyrene-$C_{60}$ (**89**) were synthesised through Prato's 1,3-dipolar cycloaddition reactions with $C_{60}$ on *in situ* generated azomethine ylides made from aldehyde containing DTPY (**86**) and pyrene, respectively. For this we had created and fully characterised the new 5-formyl derivative of DTPY utilising Vilsmeier conditions. Orbital analysis using DFT calculations of DTPY-$C_{60}$ (**88**) dyad confirmed the expected localisation of the HOMO on the DTPY donor moiety and the LUMO on the $C_{60}$ core. Little orbital interaction between the donor and acceptor moieties in the ground state was observed by electrochemical measurements and this was confirmed by the UV-visible absorption spectrum. The photoinduced charge separation and subsequent charge recombination processes were examined by time-resolved fluorescence measurements on the picosecond timescale and transient absorption measurements on the picosecond and microsecond timescales with detection in the visible and near-infrared regions. Quite long lifetimes (*i.e.* up 1.01 ns) were observed for the photogenerated charge-separated state in the DTPY-$C_{60}$ **88** dyad without the need for (i) a long spacer between the two moieties, or (ii) gain in aromaticity in the radical ion pair. This unexpected result raises issues of topology and aromaticity, which challenge the current views on designing $C_{60}$ derivatives with long lifetimes for charge-separated species.

# Chapter 6: Thiol Terminated Derivatives

## 6.1 Introduction

The preparation of $C_{60}$-derivatised π-conjugated ensembles that can be used to create self-assembled monolayers (SAMs) on metal surfaces is of fundamental interest and could potentially lead towards nanoscale photovoltaic devices.[207] Some thiol-terminated linear

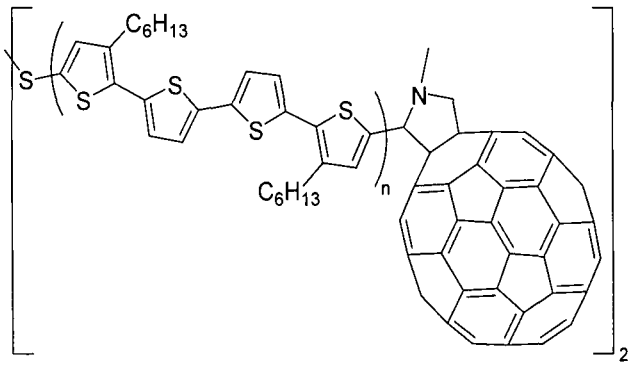

**90a** n = 1
**90b** n = 2

π-conjugated $C_{60}$ derivatives have been synthesised and their SAMs have been investigated (*e.g.* **90**,[208] **91**[209] and **92**[210]). The highest photocurrent - out of these three compounds - was observed for **92**,[210] which exhibited a current density of 3200 nA $cm^{-2}$ under 400 nm

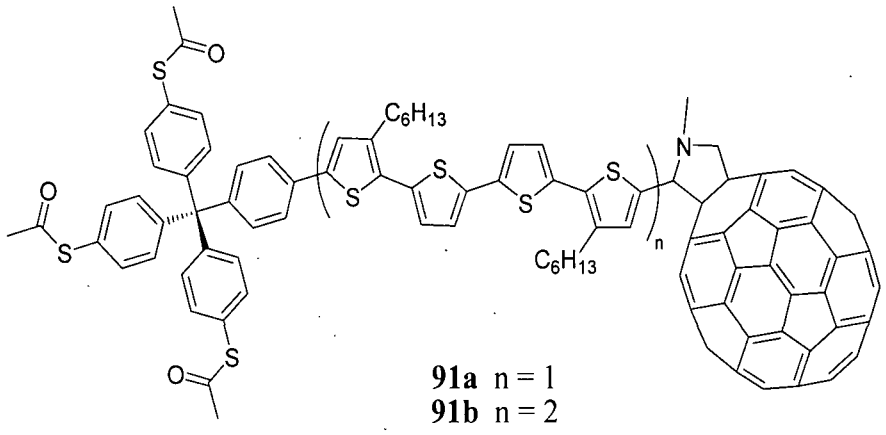

**91a** n = 1
**91b** n = 2

irradiation with 0.85 mW $cm^{-2}$ and a bias voltage of -0.10 V *vs.* Ag/AgCl.

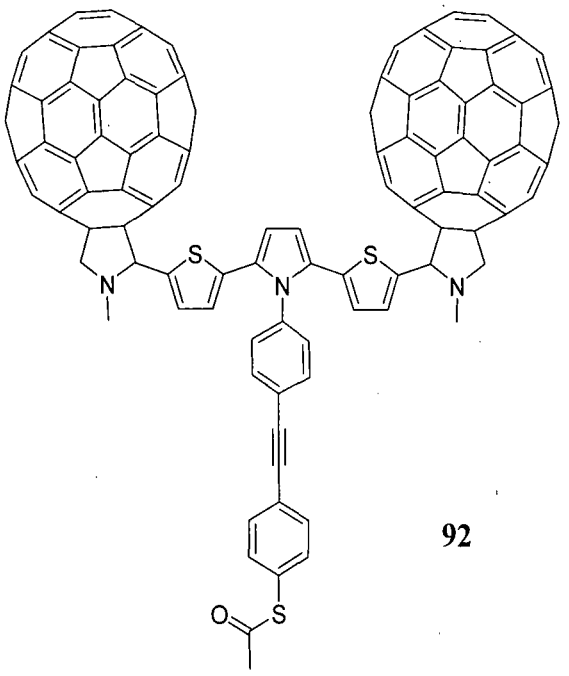

**92**

Intrigued by these findings we have synthesised two thiol-terminated fluorene-$C_{60}$ derivatives. At this point, we should note that recently Tour *et al.* reported on the complications that occur during the self-assembly of fullerene derivatives, such as multilayer formation and head-to-tail assemblies.[211] These anomalies in the SAM result from the competing strong fullerene-fullerene and fullerene-gold interactions. Considering this new finding we are currently not undertaking any investigation towards the properties of the new compounds we now report.

## 6.2 Results and Discussion

### Synthesis

Introduction of a thiol moiety onto our formylfluorene species is not straightforward, since the thiol group has a strong affinity for late transition metals. We recognised that to obtain an efficient coupling reaction more than stoichiometric amounts of the palladium species would be necessary as the thiol poisons the catalyst. It was decided to protect the free-thiol with a *tert*-butyl moiety, which is resistant towards bases and has been previously utilised in the Suzuki cross-coupling reaction.[212] Since *t*-butyl(4-bromophenyl)sulfide (**93**) is rapidly prepared from the commercially available 4-bromothiophenol,[213] no attempt was made to produce a fluorene building block with a protected thiol directly attached to it.

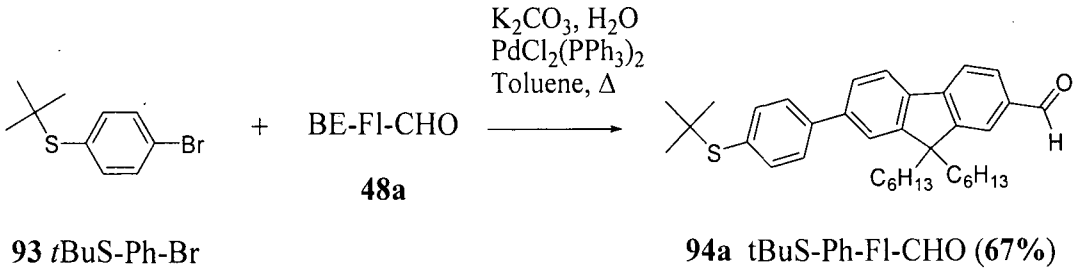


**93** *t*BuS-Ph-Br

**94a** tBuS-Ph-Fl-CHO (**67%**)

Scheme 6.1

Thiol-formyl terminated monomer **94a** was created by a Suzuki coupling of *t*-butyl(4-bromophenyl)sulfide (**93**)[213] and **48a** in 67% yield (Scheme 6.1). As **48b** had not yet been synthesised at the time of the preparation these thiol terminated compounds, the thiol-formyl terminated dimer (**94b**) was created - together with **52b** - in a multicomponent Suzuki cross-coupling between **93**, **47a** and **46** (Scheme 6.2). As expected, the separation was cumbersome and yields were not optimised as a sufficient amount of material was obtained for our purposes. Attempts to prepare longer thiol-formyl terminated oligomers were not undertaken.

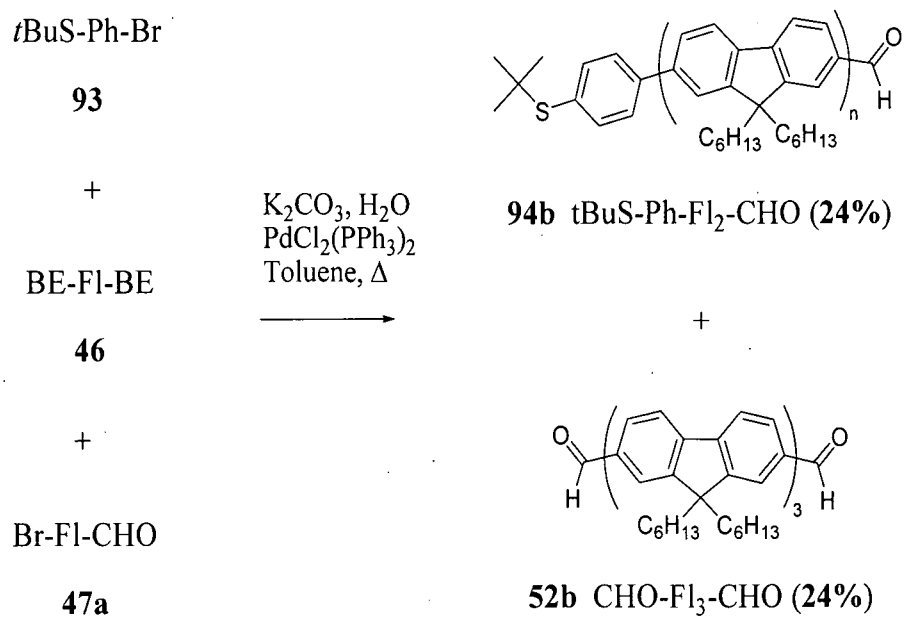


Scheme 6.2

Azomethine ylides were formed *in situ* by the reaction of aldehyde **94a,b** with sarcosine in benzene at reflux. Cycloadditions of these azomethine ylides with $C_{60}$ led to the formation of pyrrolidinofullerenes **95a,b** in moderate yields. The *tert*-butyl protecting group is very resistant and needs to be removed before the properties of these compounds can be investigated. The protecting group can readily be converted into the acetyl group[214, 215] and this labile moiety will protect the conjugated thiol against oxidation by air, while it can easily be removed *in situ* prior to experiments, *e.g.* during preparation of self-assembled monolayers. The *tert*-butyl/acetyl exchange of **95a,b** yielded **96a,b** in 68-84% yield.

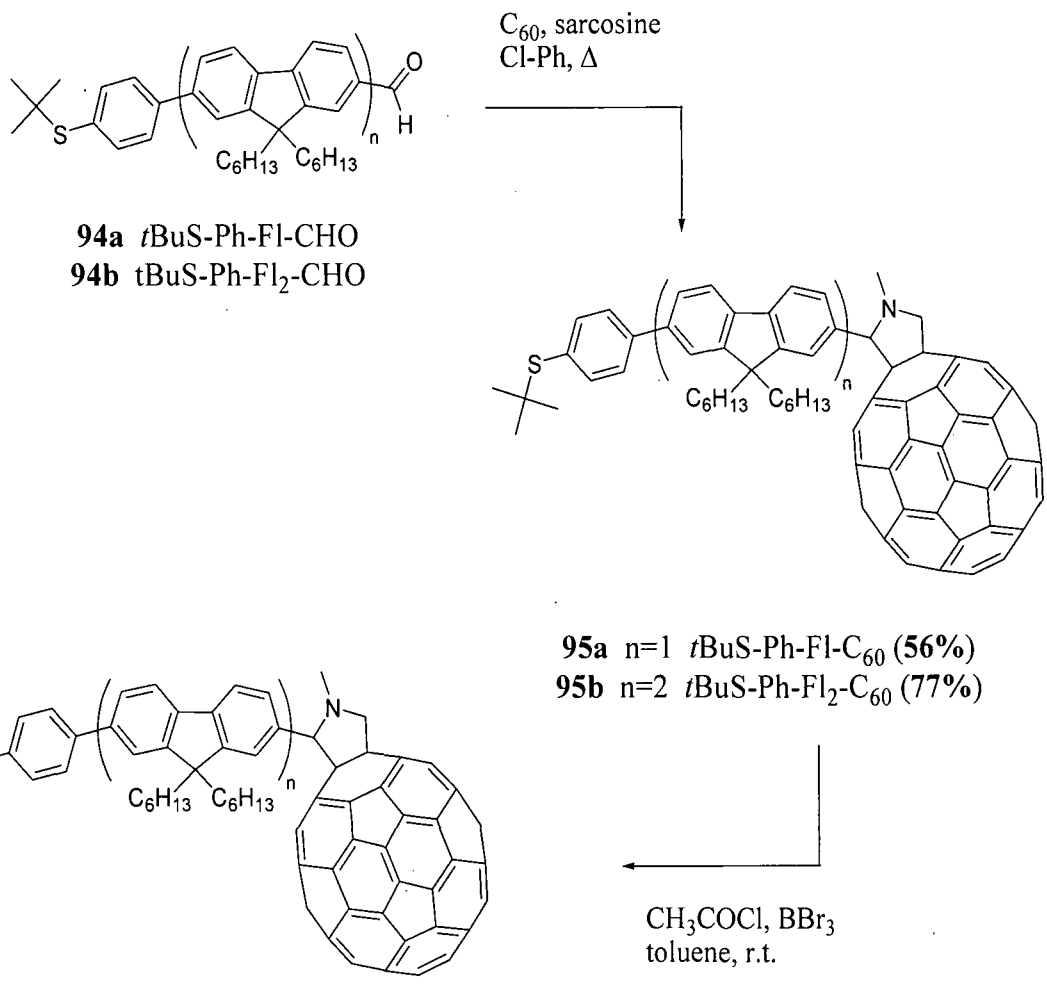


**94a** *t*BuS-Ph-Fl-CHO
**94b** tBuS-Ph-$Fl_2$-CHO

**95a** n=1 *t*BuS-Ph-Fl-$C_{60}$ (**56%**)
**95b** n=2 *t*BuS-Ph-$Fl_2$-$C_{60}$ (**77%**)

**96a** n=1 *t*BuS-Ph-Fl-$C_{60}$ (**84%**)
**96b** n=2 *t*BuS-Ph-$Fl_2$-$C_{60}$ (**68%**)

Scheme 6.3

## 6.3 Conclusions

In this chapter we have briefly discussed the synthesis of two acetyl-thiol terminated fluorene-$C_{60}$ derivatives. Thiol-terminated fluorene aldehydes **94a,b** were synthesised *via* a Suzuki reaction and converted into azomethine ylides, which were subsequently reacted with $C_{60}$ *via* the 1,3-dipolar cycloaddition. The thiol protecting group of the obtained $C_{60}$ derivatives **95a,b** was subjected to an *tert*-butyl/acetyl exchange, which provided the desired products **96a,b**. Although we are currently not undertaking any investigation towards the properties of these compounds, this remains a possibility for the future.

# Chapter 7: Experimental Section

## 7.1 General Methods

All reactions which required inert or dry atmosphere were carried out under a blanket of argon, which was dried by passage through a column of phosphorus pentoxide. Fullerene $C_{60}$ was purchased from MER Corporation Nanotubes (Tucson, USA). All reagents employed were of standard reagent grade and purchased from Aldrich, Alfa Aesar, Merck or Acros and used as supplied. Dry solvents were obtained from an Innovative Technology Inc. solvent purification system. Analytical thin layer chromatography (TLC) was performed on Merck DC-Alufolien Silica gel (60 $F_{254}$ 0.2 mm thickness) precoated aluminium plates. Column chromatography was carried out using Prolabo silica (70-230 mesh) or basic aluminium oxide (~150 mesh). Solvents for chromatography were used as supplied.

$^{13}C$ and $^{1}H$ NMR spectra were recorded on 200, 300, 400 500 and 700 MHz spectrometers operating at 300, 400 500 or 700 MHz for $^{1}H$-NMR spectra and 50, 75, 100, 125 or 175 MHz for $^{13}C$-NMR spectra. Chemical shifts are reported in ppm and TMS or the residual solvent was used as an internal reference. Elemental analyses were obtained on an Exeter Analytical Inc. CE-440 elemental analyser. Melting points were determined using a Stuart Scientific SMP3 melting point apparatus.

Cyclic voltammetry experiments were carried out with either a potentiostat/galvanostat AUTOLAB with PGSTAT30 equipped with a software GPES for Windows version 4.8 or a BAS-CV50W electrochemical workstation with positive feedback compensation. The electrochemical analyses (AUTOLAB) were carried out using a GCE (glassy carbon) as working electrode, SCE (standard calomel) as reference electrode, tetra-*n*-butylammonium perchlorate ($Bu_4NClO_4$) as supporting electrolyte, and *o*-dichlorobenzene/acetonitrile (ratio 4:1 v/v) as solvent at a scan rate of 100 mV/s. Cyclic voltammetry (BAS-CV50W) was performed in a three-electrode cell equipped with a platinum disk (∅ 1.6 or 1.0 mm) as working electrode, platinum wire as a counter electrode and a non-aqueous $Ag/Ag^{+}$

reference electrode (0.01 M $AgNO_3$ in dry $CH_3CN$). Tetra-*n*-butylammonium hexafluorophosphate ($Bu_4NPF_6$) was used as supporting electrolyte and all experiments were performed under an argon atmosphere. Electrochemical experiments were carried out in benzonitrile (PhCN), *o*-dichlorobenzene (*o*DCB) or their 1:1 v/v mixture. The potential of the reference electrode was checked against the ferrocene/ferricinium couple ($Fc/Fc^+$) before and after each experiment, which showed the following average potentials against the reference electrode: +0.201 V (*vs.* $Ag/Ag^+$ in PhCN), +0.243 V (*vs.* $Ag/Ag^+$ in PhCN/*o*-DCB, 1:1 v/v), and the values of potentials were then re-calculated versus $Fc/Fc^+$ couple.

The pulse radiolysis experiments (Chapter 5) were performed by utilising either 500 ns pulses of 1.55 MeV electrons or about 100 ns pulses of 3.8 V electrons from two different Van de Graff accelerator facilities. Details of the equipment and the analysis of data have been described elsewhere.[216]

Femtosecond transient absorption studies were performed with 387 nm laser pulses (1 kHz, 150 fs pulse width) from an amplified Ti:Sapphire laser system (Clark-MXR, Inc.). For all photophysical experiments an error of 10% must be considered. Fluorescence spectra were recorded with a FluoroMax. The experiments were performed at room temperature. Each spectrum was an average of at least 5 individual scans and the appropriate corrections were applied. Pulse radiolysis experiments were accomplished using 50-ns pulses of 8 MeV electrons from a Model TB-8/16-1S electron linear accelerator. Nanosecond transient absorption measurements were carried out using a Nd:YAG laser (Continuum, SLII-10, 4-6 ns fwhm) at 355 nm with the power of 10 mJ as an excitation source. Photoinduced events were estimated by using a continuous Xe-lamp (150 W) and an InGaAs-PIN photodiode (Hamamatsu 2949) as a probe light and a detector, respectively. The output from the photodiodes and a photomultiplier tube was recorded with a digitising oscilloscope (Tektronix, TDS3032, 300 MHz). The transient spectra were recorded using fresh solutions in each laser excitation. All experiments were performed at 298 K.

Fluorescence spectra were measured on a Shimadzu spectrofluorophotometer (RF–5000). The excitation wavelength was 422 nm in PhCN. The monitoring wavelength was

corresponding to the maximum of the emission band at $\lambda_{max}$ = 435 nm. Typically, a PhCN solution (3.0 mL) was deaerated by argon purging for 8 min prior to the measurements.

The *ab initio* computations were carried out with the Gaussian 03[217] package of programs at density-functional theory (DFT) level. The geometries were optimised using Pople's 6-31G split valence basis set supplemented by *d*-polarisation functions on heavy atoms. In the DFT calculations Becke's three-parameter hybrid exchange functional[218, 219] with Lee–Yang–Parr gradient-corrected correlation functional (B3LYP)[220] were employed. No symmetry restrictions and no constraints of bonds/angles/dihedral angles were applied and all atoms were free to optimise. Electronic structures were calculated at the same B3LYP/6-31G(d) level of theory. Contours of HOMO and LUMO orbitals were visualised using Molekel v.4.3 program.[221, 222]

## 7.2 General Experimental Procedures

These general procedures have been used throughout the remainder of the experimental section, unless stated otherwise.

### ~ General Protocol for the Suzuki-Miyaura Cross-Coupling

A mixture of the specific bromofluorene and fluoreneboronic acid derivatives was stirred under argon in $H_2O$ (5 mL, degassed) and toluene (10 mL, degassed) overnight at 110 °C together with $K_2CO_3$ (8.0 equiv.) and a catalytic amount of $Pd(PPh_3)_2Cl_2$. The organic layer was washed with brine, dried over $MgSO_4$ and the solvent was evaporated *in vacuo*. The crude product was purified by column chromatography over silica gel.

### ~ General Protocol for the 1,3-Dipolar Cycloaddition (Prato Reaction)

Fullerene ($C_{60}$, 4.0 equiv.) was heated to reflux in chlorobenzene (100 mL for 200 mg $C_{60}$). The desired fluorene-aldehyde (1.0 equiv.) and sarcosine ($\geq$ 4.0 equiv.) were added after 10 min. The mixture was heated at reflux for 4-15 h. The reaction was stopped by the evaporation of solvent *in vacuo*. The crude product was purified by column

chromatography over silica gel. Final trace impurities were removed by dissolving the product in a small amount of carbon disulfide ($CS_2$), precipitation with diethyl ether and collection of the product by centrifugation. $CS_2$ should be handled with care at all times, as it is highly flammable and toxic. $C_{60}$-derivatives were stored in the dark and under air, unless stated otherwise.

## 7.3 Experimental Procedures for Chapter 2

### ~ 7-Bromo-9,9-dihexyl-9*H*-fluorene-2-carbaldehyde (47a)

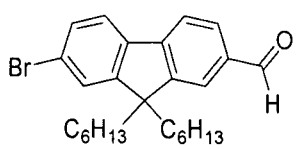


*n*-Butyllithium (4.0 mL, 2.5 M in hexane, 10 mmol) was added dropwise under argon to 2,7-dibromo-9,9-dihexyl-9*H*-fluorene[136] **45** (5.2 g, 11 mmol) in dry diethyl ether (60 mL) at -78 °C. After stirring at -78 °C for 30 min, the mixture was stirred at room temperature for 30 min. The mixture was cooled to -78 °C and DMF (1.1 mL) was added. The reaction was stirred overnight, while slowly being allowed to reach room temperature. HCl (2 M, 50 mL) was added and the mixture was stirred for an additional 2 h. The organic layer was separated and the acid layer was extracted with ether. Both organic layers were combined, dried over $MgSO_4$ and solvent was removed *in vacuo*. Purification by column chromatography (silica gel eluted by 0-25% DCM in hexane) yielded **47a** (3.80 g, 81%) as clear oily crystals, which in time turned into a white solid.

M.p.: 43-44 °C. $^1$H NMR (400 MHz, $CDCl_3$): δ 10.06 (1H, s), 7.88-7.85 (2H, m), 7.81 (1H, d, $J$ = 8.0 Hz), 7.64 (1H, d, $J$ = 8.4 Hz), 7.52-7.49 (2H, m), 2.07-1.91 (4H, m), 1.14-0.98 (12H, m), 0.76 (6H, t, $J$ = 7.0 Hz), 0.63-0.49 (4H, m). $^{13}$C NMR (75 MHz, $CDCl_3$): δ 192.2, 154.2, 151.1, 146.3, 138.5, 135.6, 130.5, 130.4, 126.4, 123.1, 122.2, 120.1, 55.6, 40.1, 31.4, 29.5, 23.7, 22.5, 13.9. HRMS, calc. for $C_{26}H_{33}BrO$ 440.1715; found 440.1714. $C_{26}H_{33}BrO$: calc. C 70.74, H 7.61; found C 70.97, H 7.61.

**~ 7-(4,4,5,5-Tetramethyl-1,3,2-dioxaborolan-2-yl)-9,9-dihexyl-9*H*-fluorene-2-carbaldehyde (48a)**

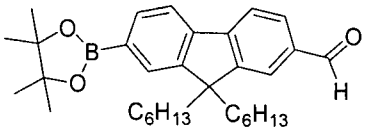

Br-Fl-CHO **47a** (0.50 g, 1.2 mmol) and bis(pinacolato)diboron (0.73 g, 2.9 mmol) were degassed in DMF (10 mL) together with KOAc (0.9 g, 9.2 mmol) for 30 min. A catalytic amount of $Pd(OAc)_2$ (*ca.* 15 mg) was added and the reaction mixture was stirred overnight at 90 °C under argon. The black precipitate was removed by filteration and ethyl acetate (40 mL) was added to the mixture. The organic layer was washed twice with $H_2O$, dried over $MgSO_4$ and the solvent was evaporated *in vacuo*. Purification by column chromatography (silica gel eluted by 0-50% DCM in hexane) yielded **48a** (0.30 g, 68%) as a clear viscous oil, which in time turned into a white solid.

M.p.: 87-88 °C. $^1$H NMR (400 MHz, $CDCl_3$): δ 10.06 (1H, s), 7.88-7.85 (4H, m), 7.78 (2H, d, $J$ = 7.6 Hz), 2.06-1.99 (4H, m), 1.40 (12H, s), 1.11-0.97 (12H, m), 0.74 (6H, t, $J$ = 7.0 Hz), 0.60-0.48 (4H, m). $^{13}$C NMR (100 MHz, $CDCl_3$): δ 192.3, 152.1, 151.3, 147.3, 142.4, 135.7, 133.9, 130.3, 129.1, 123.2, 120.4, 120.2, 83.9, 55.4, 40.0, 31.4, 29.5, 24.9, 23.7, 22.5, 13.9. HRMS, calc. for $C_{32}H_{45}BO_3$ 488.3462; found 488.3459. $C_{32}H_{45}BO_3$: calc. C 78.68, H 9.28; found C 78.39, H 9.57.

**~ Br-$Fl_2$-CHO (47b)**

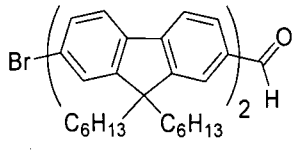

2,7-Dibromo-9,9-dihexyl-9*H*-fluorene[136] **45** (1.2 g, 2.4 mmol), BE-Fl-CHO **48a** (0.4 g, 0.8 mmol), $K_2CO_3$ (0.9 g, 6.5 mmol) and $PdCl_2(PPh_3)_2$ (0.02 g) were reacted *via* standard Suzuki-Miyaura cross-coupling and purified using 0-100% DCM in hexane as eluent to yield **47b** (0.34 g, 54%) as a white solid.

M.p.: 124-125 °C. $^1$H NMR (400 MHz, $CDCl_3$): δ 10.08 (1H, s), 7.91-7.84 (4H, m), 7.76 (1H, d, $J$ = 8.0 Hz), 7.69-7.57 (5H, m), 7.50-7.46 (2H, m), 2.12-1.92 (8H, m), 1.18-0.98 (24H, m), 0.80-0.58 (20H, m). $^{13}$C NMR (100 MHz, $CDCl_3$): δ 192.3, 153.3, 153.0, 151.8, 151.2, 147.2, 142.2, 140.5, 139.7, 139.7, 138.8, 135.3, 130.6, 130.1, 126.5, 126.4, 126.3,

123.2, 121.6, 121.5, 121.3, 121.2, 120.1, 120.0, 55.6, 55.5, 40.3, 40.2, 31.4, 29.60, 29.57, 23.80, 23.75, 22.54, 22.51, 13.98, 13.95. HRMS, calc. for $C_{51}H_{65}BrO$ 772.4219; found 772.4221. $C_{51}H_{65}BrO$: calc. C 79.14, H 8.46; found C 79.19, H 8.51.

### ~ BE-$Fl_2$-CHO (48b)

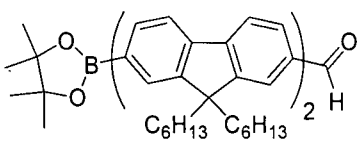


Br-$Fl_2$-CHO **47b** (0.50 g, 0.7 mmol) and bis(pinacolato)diboron (0.42 g, 1.7 mmol) were degassed in DMF (10 mL) together with KOAc (0.50 g, 5.1 mmol) for 30 min. A catalytic amount of $Pd(OAc)_2$ (*ca.* 15 mg) was added and the reaction mixture was stirred overnight at 90 °C under argon. The black precipitate was removed by filtration and ethyl acetate (40 mL) was added to the mixture. The organic layer was washed twice with $H_2O$, dried over $MgSO_4$ and the solvent was evaporated *in vacuo*. Purification by column chromatography (silica gel eluted by 25% hexane in DCM) yielded **48b** (0.26 g, 49%) as a yellow viscous oil.

$^1$H NMR (400 MHz, $CDCl_3$): δ 10.08 (1H, s), 7.92-7.58 (12H, m), 2.11-1.99 (8H, m), 1.40 (12H, s), 1.18-0.98 (24H, m), 0.79-0.58 (20H, m). $^{13}$C NMR (100 MHz, $CDCl_3$): δ 192.3, 153.0, 152.2, 151.8, 150.2, 147.3, 143.6, 142.4, 140.6, 140.5, 138.7, 135.3, 133.8, 130.6, 129.0, 126.5, 126.2, 123.2, 121.7, 121.6, 121.2, 120.4, 120.0, 119.1, 83.7, 55.4, 55.3, 40.2, 31.4, 29.60, 29.56, 25.0, 23.8, 23.7, 22.52, 22.49, 14.0, 13.9. HRMS, calc. for $C_{57}H_{77}BrO_3$ 820.5966; found 820.5967. $C_{57}H_{77}BrO_3 \cdot ½H_2O$: calc. C 82.48, H 9.47; found C 82.45, H 9.58.

### ~ $Fl_2$-CHO (50a)

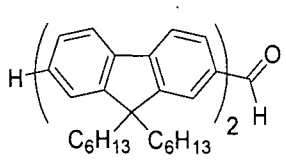


9,9-Dihexyl-9*H*-fluorene-2-boronic acid[126] **44** (150 mg, 0.40 mmol,), Br-Fl-CHO **47a** (184 mg, 0.42 mmol), $K_2CO_3$ (392 mg, 2.85 mmol) and $PdCl_2(PPh_3)_2$ (40 mg) were reacted *via*

standard Suzuki-Miyaura cross-coupling. Purification using hexane/DCM (1:1 v/v) as eluent yielded **50a** (220 mg, 79%) as a yellow solid.

M.p.: 55-58 °C. $^{1}$H NMR (400 MHz, $CDCl_3$): δ 10.08 (1H, s), 7.91-7.60 (10H, m), 7.39-7.30 (3H, m), 2.11-1.94 (8H, m), 1.15-1.00 (24H, m), 0.79-0.60 (20H, m). $^{13}$C NMR (100 MHz, $CDCl_3$): δ 192.4, 152.9, 151.7, 151.5, 151.0, 147.3, 142.4, 140.7, 140.6, 139.9, 138.6, 135.2, 130.6, 127.1, 126.8, 126.5, 126.1, 123.0, 122.9, 121.6, 121.4, 121.2, 120.0, 119.9, 119.8, 55.4, 55.2, 40.3, 40.2, 31.4, 29.7, 29.6, 23.7, 22.54, 22.51, 14.00, 13.97. HRMS, calc. for $C_{51}H_{66}O$ 694.5114; found 694.5111. $C_{51}H_{66}O{\cdot}H_2O$: calc. C 85.90, H 9.61; found C 86.17, H 9.72.

### ~ $Fl_3$-CHO (50b)

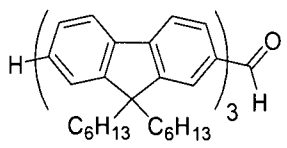


7-Bromo-9,9,9',9'-tetrahexyl-9*H*,9'*H*-[2,2']-bifluorenyl[126] **49** (200 mg, 0.27 mmol), BE-Fl-CHO **48a** (130 mg, 0.27 mmol), $K_2CO_3$ (300 mg, 2.17 mmol) and $PdCl_2(PPh_3)_2$ (0.01 g) were reacted *via* standard Suzuki-Miyaura cross-coupling and purified using 25-75% DCM in hexane as eluent to yield **50b** (260 mg, 94%) as a yellow viscous oil.

$^{1}$H NMR (400 MHz, $CDCl_3$): δ 10.08 (1H, s), 7.95-7.59 (16H, m), 7.40-7.28 (3H, m), 2.18-1.97 (12H, m), 1.30-1.00 (36H, m), 0.98-0.60 (30H, m). $^{13}$C NMR (100 MHz, $CDCl_3$): δ 192.3, 153.0, 152.0, 151.8, 151.5, 151.0, 147.3, 142.4, 140.8, 140.5, 140.4, 140.0, 139.8, 138.7, 135.3, 130.6, 127.0, 126.8, 126.5, 126.3, 126.2, 126.1, 123.2, 122.9, 121.63, 121.57, 121.5, 121.2, 120.03, 119.98, 119.9, 119.7, 55.43, 55.36, 55.2, 40.4, 40.3, 40.2, 31.5, 31.4, 29.7, 29.63, 29.58, 23.8, 22.54, 22.51, 13.98, 13.95. HRMS, calc. for $C_{76}H_{98}O$ 1026.7618; found 1026.7620. $C_{76}H_{98}O$: calc. C 88.83, H 9.61; found C 88.24, H 9.82.

### ~ $Fl_4$-CHO (50c)

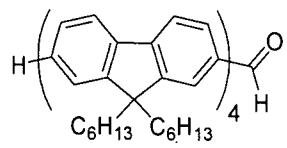

7-Bromo-9,9,9',9'-tetrahexyl-9*H*,9'*H*-[2,2']-bifluorenyl[126] **49** (115 mg, 0.15 mmol), BE-$Fl_2$-CHO **48b** (115 mg, 0.14 mmol), $K_2CO_3$ (155 mg, 1.12 mmol) and $PdCl_2(PPh_3)_2$ (0.01 g) were reacted *via* standard Suzuki-Miyaura cross-coupling and purified using hexane/DCM (1:1 v/v) as eluent to yield **50c** (53 mg, 28%) as a light yellow solid containing some impurities (≤ 5%). Due to the low yield, compound **50c** was used without further purification.

$^1$H NMR (300 MHz, $CDCl_3$): δ 10.12 (1H, s), 7.96-7.59 (22H, m), 7.40-7.28 (3H, m), 2.21-1.97 (16H, m), 1.38-1.00 (48H, m), 0.98-0.60 (40H, m). $^{13}$C NMR (75 MHz, $CDCl_3$): δ 192.3, 153.0, 151.9, 151.8, 151.5, 151.0, 147.3, 142.4, 140.8, 140.7, 140.6, 140.49, 140.46, 140.3, 140.1, 140.0, 139.9, 139.8, 138.7, 135.3, 130.6, 128.8, 127.2, 127.0, 126.8, 126.5, 126.2, 126.0, 123.1, 122.9, 121.5, 121.4, 121.2, 120.04, 119.97, 119.9, 119.7, 55.41, 55.36, 55.3, 55.2, 40.4, 40.2, 31.6, 31.4, 29.7, 29.6, 29.4, 23.8, 22.7, 22.6, 22.5, 13.99, 13.96.

### ~ $Fl_2$-$C_{60}$ (51a)

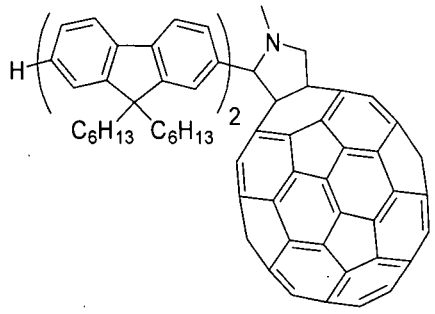


$C_{60}$ (200 mg, 0.28 mmol), $Fl_2$-CHO **50a** (49 mg, 0.07 mmol) and sarcosine (36 mg, 0.40 mmol) were reacted *via* the general 1,3-dipolar cycloaddition procedure for 4 h. Purification using 30-100% $CS_2$ in cyclohexane as eluent, followed by centrifugation yielded **51a** (60 mg, 60%) as a black solid.

$^1$H NMR (300 MHz, $CDCl_3$): δ 8.10-7.95 (1H, s, br), 7.83-7.47 (9H, m), 7.38-7.29 (3H, m), 5.07 (2H, d, $J$ = 10.0 Hz), 4.35 (1H, d, $J$ = 9.5 Hz), 2.90 (3H, s), 2.32-1.80 (8H, m, br), 0.77 (12H, t, $J$ = 7.0 Hz), 1.30-0.12 (32H, m). $^{13}$C NMR (75 MHz, $CDCl_3$): δ 156.6, 154.4, 154.10, 154.05, 152.2, 152.1, 151.4, 147.7, 146.8, 146.69, 146.66, 146.59, 146.56, 146.5, 146.4, 145.96, 145.94, 145.80, 145.75, 145.71, 145.66, 145.6, 145.1, 144.83, 144.81, 143.0, 142.7, 142.61, 142.59, 142.51, 142.47, 142.2, 142.1, 141.2, 140.77, 140.75, 140.63, 140.58, 140.3, 127.2, 126.51, 126.45, 123.3, 121.8, 121.7, 120.5, 120.3, 120.1, 84.3, 70.4,

69.5, 55.7, 55.6, 40.8, 40.5, 32.0, 31.9, 30.1, 24.29, 24.25, 24.2, 23.1, 23.0, 14.6, 14.51, 14.46. MALDI-TOF MS (*m/z*): 1443.1 ($M^+$+1).

**~ $Fl_3$-$C_{60}$ (51b)**

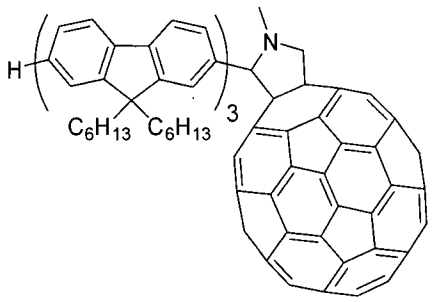


$C_{60}$ (175 mg, 0.24 mmol), $Fl_3$-CHO **50b** (62 mg, 0.06 mmol) and sarcosine (25 mg, 0.28 mmol) were reacted *via* the general 1,3-dipolar cycloaddition procedure for 4 h. Purification using 20-100% $CS_2$ in cyclohexane as eluent, followed by centrifugation yielded **51b** (60 mg, 57%) as a black solid.

$^1$H NMR (300 MHz, $CDCl_3$): δ 8.08-7.98 (1H, s, br), 7.85-7.45 (15H, m), 7.38-7.29 (3H, m), 5.07 (2H, d, $J$ = 8.2 Hz), 4.36 (1H, d, $J$ = 9.5 Hz), 2.91 (3H, s), 2.30-1.95 (12H, m, br), 0.79 (18H, t, $J$ = 6.4 Hz), 1.40-0.10 (48H, m). $^{13}$C NMR (75 MHz, $CDCl_3$): δ 152.20, 152.16, 152.1, 151.9, 151.4, 147.7, 146.9, 146.74, 146.68, 146.64, 146.58, 146.55, 146.5, 146.4, 146.2, 146.00, 145.95, 145.93, 145.88, 145.8, 145.74, 145.70, 145.66, 145.6, 145.1, 144.82, 144.80, 143.5, 143.4, 143.1, 143.0, 142.7, 142.6, 142.49, 142.47, 142.3, 142.2, 142.1, 141.2, 140.94, 140.87, 140.8, 140.7, 140.62, 140.57, 140.4, 140.3, 139.9, 136.3, 136.2, 127.4, 127.2, 126.5, 126.4, 123.3, 121.9, 121.8, 121.7, 120.5, 120.4, 120.3, 120.1, 84.3, 70.4, 69.4, 55.7, 55.6, 40.8, 40.7, 31.9, 31.8, 30.11, 30.05, 24.22, 24.18, 22.98, 22.96, 14.6, 14.5. MALDI-TOF MS (*m/z*): 1774.8 ($M^+$+1).

**~ $Fl_4$-$C_{60}$ (51c)**

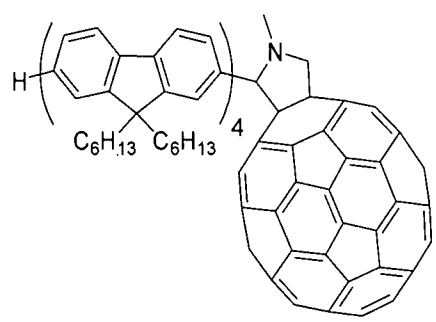


$C_{60}$ (100 mg, 0.14 mmol), $Fl_4$-CHO **50c** (47 mg, 0.035 mmol) and sarcosine (20 mg, 0.22 mmol) were reacted *via* the general 1,3-dipolar cycloaddition procedure for 4 h.

Purification using 50-100% $CS_2$ in cyclohexane as eluent, followed by centrifugation yielded **51c** (30 mg, 41%) as a black solid.

$^1$H NMR (300 MHz, $CDCl_3$ + $CS_2$): δ 8.09-8.00 (1H, s, br), 7.85-7.55 (21H, m), 7.35-7.30 (3H, m), 5.07 (2H, d, *J* = 9.0 Hz), 4.36 (1H, d, *J* = 10.1 Hz), 2.91 (3H, s), 2.31-1.97 (16H, m, br), 0.81 (24H, t, J = 6.5 Hz), 1.45-0.15 (64H, m). $^{13}$C NMR (75 MHz, $CDCl_3$ + $CS_2$): δ 152.2, 151.8, 151.4, 147.7, 147.2, 146.9, 146.8, 146.72, 146.67, 146.61, 146.57, 146.56, 146.4, 146.2, 146.1, 145.97, 145.95, 145.83, 145.75, 145.71, 145.68, 145.6, 145.1, 144.9, 144.8, 143.6, 143.4, 143.1, 143.0, 142.7, 142.6, 142.5, 142.4, 142.2, 142.1, 142.0, 141.3, 141.2, 141.0, 140.9, 140.8, 140.73, 140.65, 140.6, 140.5, 140.43, 140.37, 140.3, 139.9, 137.2, 136.3, 136.2, 127.4, 127.2, 126.6, 126.5, 123.3, 121. 9, 121.8, 121.7, 120.6, 120.43, 120.35, 120.2, 84.3, 70.4, 69.3, 55.7, 55.6, 40.9, 40.5, 32.3, 32.1, 32.0, 30.2, 24.4, 24.3, 23.1, 14.7, 14.5. MALDI-TOF MS (*m/z*): 2107.9 ($M^+$+1, 9%), 1387.6 ($M^+$-$C_{60}$+1, 100%), 1302.4 (34%).

### ~ CHO-$Fl_2$-CHO (52a)

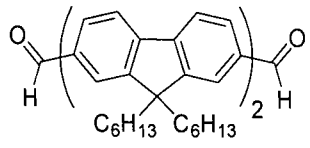


Br-Fl-CHO **47a** (350 mg, 0.79 mmol), BE-Fl-CHO **48a** (370 mg, 0.76 mmol), $K_2CO_3$ (830 mg, 6.01 mmol) and 0.01 g $PdCl_2(PPh_3)_2$ (0.01 g) were reacted *via* standard Suzuki-Miyaura cross-coupling. Purification using 50-100% DCM in hexane as eluent yielded **52a** (370 mg, 68%) as a pale yellow solid.

M.p.: 126-127 °C. $^1$H NMR (400 MHz, $CDCl_3$): δ 10.09 (2H, s), 7.93-7.81 (8H, m), 7.70 (2H, dd, *J* = 1.6 & 8.0 Hz), 7.65 (2H, d, *J* = 1.2 Hz), 2.13-2.04 (8H, m), 1.15-0.99 (24H, m), 0.76 (12 H, t, *J* = 7.0 Hz), 0.79-0.59 (8H, m). $^{13}$C NMR (100 MHz, $CDCl_3$): δ 192.3, 153.1, 151.8, 147.1, 141.9, 139.1, 135.4, 130.6, 126,6, 123.2, 121.7, 121.3, 120.1, 55.5, 40.2, 31.4, 29.5, 23.8, 22.5, 13.9. HRMS, calc. for $C_{52}H_{66}O_2$ 722.5063; found 722.5070. $C_{52}H_{66}O_2$: calc. C 86.37, H 9.20; found C 86.52, H 9.34.

### ~ CHO-Fl$_3$-CHO (52b)

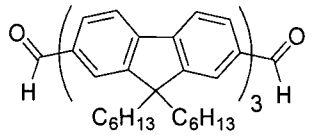

$K_2CO_3$ (140 mg, 1.01 mmol), 2,7-bis(4,4,5,5-tetramethyl-1,3,2-dioxaborolan-2-yl)-9,9-dihexyl-9*H*-fluorene[135] **46** (75 mg, 0.13 mmol), Br-Fl-CHO **47a** (140 mg, 0.32 mmol) and $PdCl_2(PPh_3)_2$ (0.01 g) were reacted *via* standard Suzuki-Miyaura cross-coupling. Purification using 10% ethyl acetate in PE 40-60 as eluent yielded **52b** (80 mg, 59%) as a yellow solid.

M.p.: 65-67 °C. $^1$H NMR (400 MHz, $CDCl_3$): δ 10.09 (2H, s), 7.93-7.82 (10H, m), 7.75-7.62 (8H, m), 2.15-2.03 (12H, m), 1.18-1.01 (36H, m), 0.93-0.62 (30H, m). $^{13}$C NMR (100 MHz, $CDCl_3$): δ 192.3, 153.0, 151.9, 151.8, 147.3, 142.3, 140.3, 140.2, 138.7, 135.3, 130.6, 126.5, 126.3, 123.2, 121.63, 121.60, 121.2, 120.1, 120.0, 55.4, 40.3, 40.2, 31.43, 31.41, 29.60, 29.57, 23.8, 22.5, 13.96, 13.93. HRMS, calc. for $C_{77}H_{98}O_2$ 1054.7567; found 1054.7566. $C_{77}H_{98}O_2$: calc. C 87.61, H 9.36; found C 86.97, H 9.39.

### ~ CHO-Fl$_5$-CHO (52c)

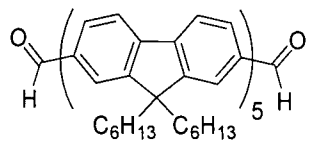

$K_2CO_3$ (140 mg, 1.01 mmol), 2,7-bis(4,4,5,5-tetramethyl-1,3,2-dioxaborolan-2-yl)-9,9-dihexyl-9*H*-fluorene[135] **46** (75 mg, 0.13 mmol), Br-Fl$_2$-CHO **47b** (250 mg, 0.32 mmol) and $PdCl_2(PPh_3)_2$ (0.01 g) were reacted *via* standard Suzuki-Miyaura cross-coupling. Purification using 10% ethyl acetate in PE 40-60 as eluent yielded **52c** (90 mg, 41%) as a light yellow viscous oil.

$^1$H NMR (400 MHz, $CDCl_3$): δ 10.08 (2H, s), 7.93-7.56 (26H, m), 7.50-7.25 (4H, m), 2.16-1.92 (20H, m), 1.20-0.96 (60H, m), 0.89-0.58 (50H, m). $^{13}$C NMR (100 MHz, $CDCl_3$): δ 129.3, 153.3, 153.0, 151.8, 151.2, 147.2, 142.2, 140.6, 139.7, 138.8, 135.4, 130.6, 130.1, 126.5, 126.4, 126.3, 123.2, 121.6, 121.5, 121.3, 121.2, 120.1, 55.6, 55.5, 40.3, 40.2, 31.4, 31.1, 29.7, 29.60, 29.57, 23.81, 23.75, 22.54, 22.51, 13.98, 13.95. HRMS, calc. for $C_{127}H_{162}O_2$ 1719.2575; found 1719.2660.

**~ $C_{60}$-$Fl_2$-$C_{60}$ (53a)**

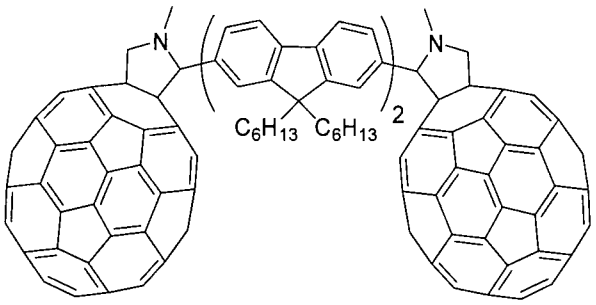


$C_{60}$ (775 mg, 1.08 mmol), CHO-$Fl_2$-CHO **52a** (108 mg, 0.15 mmol) and sarcosine (96 mg, 1.08 mmol) were reacted *via* the general 1,3-dipolar cycloaddition procedure for 15 h. Purification using 0-100% $CHCl_3$ in $CS_2$ as eluent, followed by centrifugation yielded **53a** (230 mg, 77%) as a black solid.

$^1$H NMR (300 MHz , $CDCl_3$ + $CS_2$): δ 8.10-7.90 (2H, s, br), 7.90-7.40 (10H, m), 5.04 (4H, d, $J$ = 9.2 Hz), 4.35 (2H, d, $J$ = 9.6 Hz), 2.90 (6H, s, br), 2.35-1.85 (8H, m, br), 1.30-0.10 (44H, m, br). $^{13}$C NMR (75 MHz , $CDCl_3$ + $CS_2$): δ 156.6, 154.4, 154.0, 153.9, 152.0, 147.7, 147.2, 146.9, 146.8, 146.72, 146.69, 146.64, 146.58, 146.56, 146.4, 146.2, 146.1, 146.01, 145.97, 145.9, 145.8, 145.72, 145.69, 145.6, 145.2, 144.94, 144.87, 144.8, 143.6, 143.5, 143.2, 143.1, 142.7, 142.63, 142.58, 142.5, 142.3, 142.2, 142.0, 141.8, 141.2, 140.72, 140.66, 140.4, 139.9, 137.1, 136.4, 136.3, 136.2, 126.8, 121.7, 120.7, 84.3, 70.5, 69.4, 55.6, 41.4, 40.5, 32.6, 32.5, 30.9, 30.6, 24.7, 24.6, 23.8, 23.6, 15.04, 14.96.

**~ $C_{60}$-$Fl_3$-$C_{60}$ (53b)**

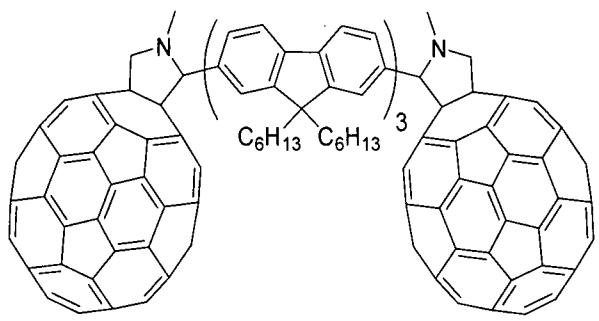


$C_{60}$ (278 mg, 0.39 mmol), CHO-$Fl_3$-CHO **52b** (47 mg, 0.045 mmol) and sarcosine (37 mg, 0.42 mmol) were reacted *via* the general 1,3-dipolar cycloaddition procedure for 15 h. Purification using 0-50% $CHCl_3$ in $CS_2$ as eluent, followed by centrifugation yielded **53b** (92 mg, 81%) as a black solid.

$^1$H NMR (300 MHz, $CDCl_3$): δ 8.14-7.92 (2H, s, br), 7.92-7.40 (16H, m), 5.07 (4H, d, $J$ = 9.6 Hz), 4.36 (2H, d, $J$ = 8.0 Hz), 2.92 (6H, s, br), 2.35-1.80 (12H, m, br), 0.79 (18H, t, $J$ = 6.4 Hz), 1.35-0.10 (48H, m, br). $^{13}$C NMR (75 MHz, $CDCl_3$): δ 156.6, 154.4, 154.0, 153.9, 152.1, 152.0, 147.7, 147.3, 147.0, 146.8, 146.72, 146.69, 146.63, 146.58, 146.56, 146.4, 146.2, 146.1, 146.0, 145.92, 145.86, 145.8, 145.73, 145.69, 145.66, 145.6, 145.2, 144.93, 144.87, 144.8, 143.6, 143.5, 143.2, 143.1, 142.74, 142.65, 142.62, 142.57, 142.5, 142.4, 142.21, 142.17, 142.0, 141.8, 141.2, 140.9, 140.7, 140.6, 140.4, 140.3, 139.9, 137.1, 136.4, 136.3, 136.1, 126.7, 121.8, 121.7, 120.6, 120.5, 84.3, 70.5, 69.5, 55.7, 41.2, 41.1, 40.5, 32.4, 32.3, 32.2, 30.4, 24.5, 23.6, 23.4, 23.3, 14.84, 14.75, 14.7.

**~ $C_{60}$-$Fl_5$-$C_{60}$ (53c)**

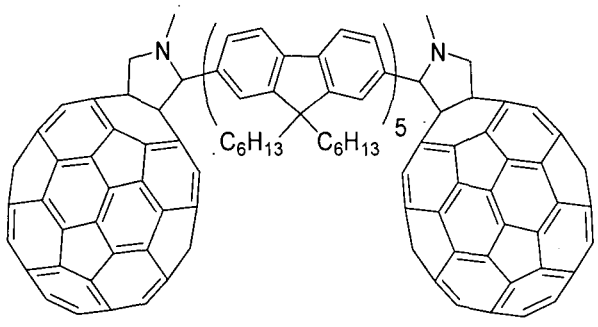


$C_{60}$ (200 mg, 0.28 mmol), CHO-$Fl_5$-CHO **52c** (60 mg, 0.04 mmol) and sarcosine (25 mg, 0.28 mmol) were reacted *via* the general 1,3-dipolar cycloaddition procedure for 15 h. Purification using 0-100% $CHCl_3$ in $CS_2$ as eluent, followed by centrifugation yielded **53c** (29 mg, 26%) as a black solid.

$^1$H NMR (300 MHz, $CDCl_3$): δ 8.10-7.90 (2H, s, br), 7.90-7.40 (28H, m), 5.05 (4H, d, $J$ = 7.8 Hz), 4.34 (2H, d, $J$ = 9.5 Hz), 2.90 (6H, s, br), 2.35-1.90 (20H, m, br), 0.78 (30H, t, $J$ = 6.8 Hz), 1.30-0.10 (80H, m, br). $^{13}$C NMR (75 MHz, $CDCl_3$): δ 154.4, 153.9, 153.6, 152.1, 151.5, 147.7, 147.2, 146.9, 146.74, 146.68, 146.64, 146.58, 146.55, 146.5, 146.4, 146.2, 145.99, 145.95, 145.92, 145.87, 145.8, 145.74, 145.70, 145.65, 145.6, 145.1, 144.82, 144.79, 143.5, 143.4, 143.1, 143.0, 142.7, 142.6, 142.49, 142.46, 142.3, 142.2, 142.0, 141.7, 141.3, 140.61, 140.57, 140.5, 140.3, 140.2, 139.8, 139.6, 137.0, 136.3, 136.2, 130.4, 126.7, 126.6, 126.5, 121.8, 121.7, 121.5, 121.4, 120.5, 120.4, 84.3, 70.4, 69.4, 55.9, 55.7, 40.9, 40.7, 40.5, 32.0, 31.8, 30.1, 30.0, 24.2, 24.1, 23.2, 23.02, 22.97, 14.6, 14.5, 14.4.

## 7.4 Experimental Procedures for Chapter 3

### ~ *ex*TTF-Fl-CHO (56a)

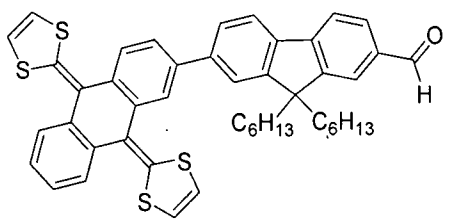

2-Iodo-9,10-bis(1,3-dithiol-2-ylidene)-9,10-dihydroanthracene[150] **55** (112 mg, 0.2 mmol), BE-Fl-CHO **48a** (98 mg, 0.2 mmol), $K_2CO_3$ (210 mg, 1.6 mmol) and $PdCl_2(PPh_3)_2$ (0.01 g) were reacted *via* standard Suzuki-Miyaura cross-coupling. Purification using toluene as eluent yielded **56a** (77 mg, 52%) as an orange solid.

$^1$H NMR (300 MHz, $CDCl_3$): δ 10.08 (1H, s) , 8.02 (1H, d, $J$ = 1.8 Hz), 7.91-7.82 (5H, m), 7.77- 7.68 (4H, m), 7.65-7.61(1H, dd, $J$ = 1.8 & 8.2 Hz), 7.33-7.29 (2H, m), 6.34 (2H, s), 6.33 (2H, s), 2.08 (4H, dd, $J$ = 7.3 & 9.0 Hz), 1.14- 1.06 (12H, m), 0.78-0.65 (12H, m).

$^{13}$C NMR (75 MHz, $CDCl_3$): δ 192.8, 153.3, 147.7, 141.8, 139.2, 139.0, 136.41, 136.37, 136.3, 135.0, 131.1, 126.7, 126.50, 126.46, 125.9, 125.4, 125.0, 124.1, 123.5, 122.6, 122.3, 122.0, 121.8, 120.4, 117.8, 117.7, 117.6, 117.5, 55.8, 40.7, 31.9, 30.1, 30.0, 24.2, 23.0, 14.4. ESI-MS (*m/z*): 765 ($M^+$+ $Na^+$).

### ~ *ex*TTF-$Fl_2$-CHO (56b)

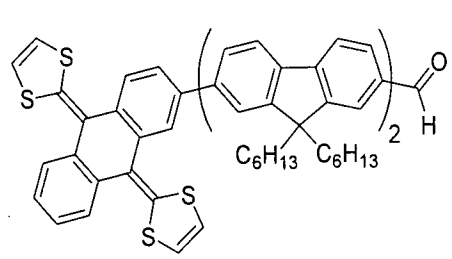

2-Iodo-9,10-bis(1,3-dithiol-2-ylidene)-9,10-dihydroanthracene[150] **55** (43 mg, 0.09 mmol), BE-$Fl_2$-CHO **48b** (70 mg, 0.09 mmol), $K_2CO_3$ (100 mg, 0.72 mmol) and $PdCl_2(PPh_3)_2$ (0.01 g) were reacted *via* standard Suzuki-Miyaura cross-coupling. Purification using 20% cyclohexane in toluene as eluent yielded **56b** (60 mg, 66%) as an orange solid.

$^1$H NMR (300 MHz, $CDCl_3$): δ 10.09 (1H, s), 8.03 (1H, d, $J$ = 1.9 Hz), 7.94-7.80 (7H, m), 7.78-7.61 (9H, m), 7.36-7.30 (2H, m), 6.35 (4H, s, br), 2.15-2.05 (8H, m, br), 1.20-1.02

(24H, m, br), 0.77 (12H, t, $J$ = 6.8 Hz), 0.84-0.64 (8H, m, br). $^{13}$C NMR (75 MHz, $CDCl_3$): δ 192.8, 153.4, 152.4, 152.2, 152.1, 147.7, 142.8, 140.8, 140.4, 140.2, 139.5, 139.1, 136.3, 135.6, 131.1, 126.9, 126.7, 126.4, 125.8, 125.4, 124.9, 123.5, 121.9, 121.6, 120.6, 120.4, 117.7, 117.6, 55.8, 55.7, 40.6, 31.90, 31.85, 30.1, 30.0, 24.3, 24.2, 23.0, 22.9, 14.43, 14.40. MALDI-TOF MS (*m/z*): 1072.5 ($M^+$).

### ~ *ex*TTF-Fl-$C_{60}$ (57a)

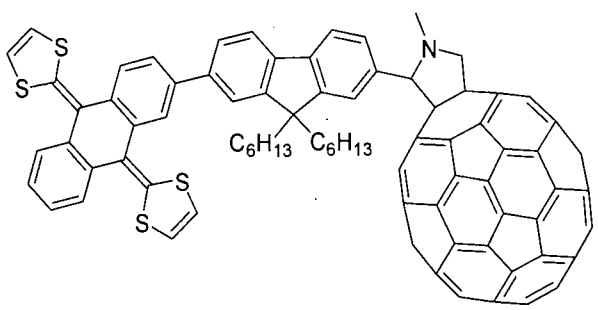


$C_{60}$ (400 mg, 0.55 mmol), *ex*TTF-Fl-CHO **56a** (100 mg, 0.13 mmol) and sarcosine (90 mg, 1.0 mmol) were reacted *via* the 1,3-dipolar cycloaddition procedure (under argon and protected against light) for 4 h. The reaction mixture was purified in the evening under dimmed light. During purification it was protected with aluminium foil against light and kept under argon as much as possible. Column chromatography using $CS_2$/cyclohexane (1:1 v/v) as eluent yielded **57a** (53 mg, 27%) as a black solid.

$^1$H NMR (500 MHz, $CDCl_3$): δ 8.02 (2H, s, br), 7.81 (1H, d, $J$ = 8.1 Hz), 7.77 (1H, d, $J$ = 7.9 Hz) 7.75 (2H, dd, $J$ = 3.1 & 5.6 Hz), 7.65 (1H, d, $J$ = 8.1 Hz), 7.62 (2H, m), 7.37 (1H, m), 7.32 (3H, m), 6.34 (4H, s, br), 5.06 (2H, d, $J$ = 10.0 Hz, br), 4.34 (1H, d, $J$ = 9.4 Hz), 2.91 (3H, s), 2.03 (4H, s, br), 1.3-0.5(22 H, m, br). $^{13}$C-NMR (125 MHz, $CDCl_3$): δ 156.2, 153.5, 151.6, 147.3, 146.8, 146.5, 146.3, 146.23, 146.20, 146.14, 146.11, 146.08, 145.9, 145.7, 145.6, 145.51, 145.49, 145.4, 145.34, 145.29, 145.25, 145.2, 145.1, 144.7, 144.4, 143.1, 143.0, 142.7, 142.5, 142.2, 142.14, 142.13, 142.05, 142.0, 141.9, 141.8, 141.7, 141.5, 141.3, 140.2, 140.1, 140.0, 139.8, 139.4, 139.0, 136.6, 135.91, 135.85, 135.8, 135.5, 135.32, 135.29, 134.2, 129.7, 128.6, 126.01, 125.98, 125.9, 125.4, 125.0, 124.4, 123.6, 122.3, 122.0, 121.3, 120.1, 117.2, 117.1, 83.9, 70.0, 69.0, 55.3, 40.6, 40.0, 31.7, 31.6, 29.8, 23.9, 22.8, 22.6, 14.1. MALDI-TOF MS (*m/z*): 1504.3 ($M^+$+1).

**~ *ex*TTF-Fl$_2$-C$_{60}$ (57b)**

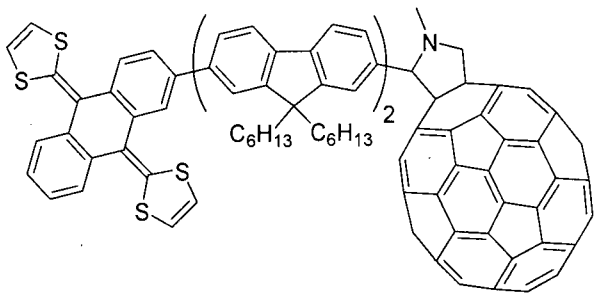


***ex*TTF-Fl$_2$-C$_{60}$ (57b)**

C$_{60}$ (280 mg, 0.4 mmol), *ex*TTF-Fl$_2$-CHO **57** (107 mg, 0.1 mmol) and sarcosine (40 mg, 0.5 mmol) were reacted *via* the 1,3-dipolar cycloaddition procedure (under argon and protected against light) for 4 h. The reaction mixture was purified in the evening under dimmed light. During purification it was protected with aluminium foil against light and kept under argon as much as possible. Column chromatography using $CS_2$, followed by toluene as eluent yielded **57b** (44 mg, 24%) as a black solid.

$^1$H NMR (500 MHz, $CDCl_3$): δ 8.03 (2H, d, $J$ = 1.7 Hz), 7.91-7.52 (15H, m, br), 7.35-7.29 (2H, m), 6.33 (4H, m), 5.06 (1H, s), 5.04 (1H, d, $J$ = 10.5 Hz), 4.33 (1H, d, $J$ = 10.5 Hz), 2.90 (3H, s, br), 2.08 (8H, s, br) 1.25- 0.98 (22H, m, br), 0.95-0.60 (22H, m, br). $^{13}$C NMR (125 MHz, $CDCl_3$): δ 154.4, 154.1, 153.9, 152.3, 152.13, 152.09, 147.7, 147.2, 146.9, 146.73, 146.67, 146.63, 146.57, 146.53, 146.50, 146.3, 146.2, 146.0, 145.94, 145.91, 145.88, 145.8, 145.72, 145.68, 145.64, 145.55, 145.1, 144.9, 144.81, 144.78, 143.5, 143.4, 143.1, 143.0, 142.7, 142.57, 142.55, 142.5, 142.4, 142.3, 142.2, 142.1, 142.0, 141.7, 141.1, 140.8, 140.60, 140.56, 140.5, 140.4, 140.33, 140.28, 140.0, 139.8, 139.6, 137.1, 137.0, 136.33, 136.31, 136.25, 136.1, 136.0, 135.8, 135.7, 134.6, 129.2, 127.6, 126.6, 126.51, 126.47, 126.4, 125.9, 125.4, 125.2, 124.9, 124.1, 122.7, 122.4, 122.0, 121.9, 121.8, 121.7, 120.5, 120.4, 117.7, 117.6, 84.3, 70.5, 69.5, 68.4, 55.73, 55.68, 41.0, 40.8, 40.5, 32.1, 32.0, 31.9, 30.2, 26.1, 24.3.

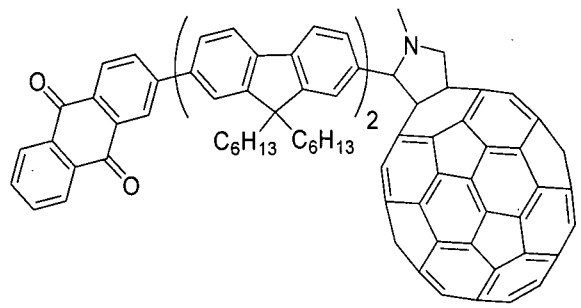


***ex*O$_2$-Fl$_2$-C$_{60}$ (58)**

Compound **58** was obtained when the reaction was exposed to light and air during the reaction and purification.

$^1$H NMR (300 MHz, $CDCl_3$): δ 8.63 (1H, d, $J$ = 1.9 Hz), 8.43-8.31 (3H ,m), 8.10 (1H, d, $J$ = 3.0 Hz), 7.87-7.60 (14H, m), 5.05 (2H, d, $J$ = 9.0 Hz), 4.34 (1H, d, $J$ = 9.0 Hz), 2.89 (3H, s, br), 2.17-2.00 (8H, m, br), 1.25-0.10 (24H, m, br), 0.74 (12H, t, $J$ = 6.0 Hz). $^{13}$C NMR (75 MHz, $CDCl_3$): δ 193.0, 183.9, 183.3, 156.6, 154.4, 154.0, 152.5, 152.4, 147.8, 147.7, 146.74, 146.68, 146.64, 146.58, 146.55, 146.5, 146.4, 145.99, 145.95, 145.9, 145.8, 145.73, 145.70, 145.65, 144.82, 144.79, 143.1, 143.0, 142.7, 142.59, 142.57, 142.49, 142.46, 142.3, 142.2, 141.8, 141.4, 140.6, 139.9, 138.3, 138.0, 134.5, 134.3, 134.13, 134.06, 132.8, 132.3, 128.5, 127.73, 127.67, 126.5, 125.9, 122.0, 121.9, 120.8, 84.3, 70.5, 69.5, 55.9, 55.8, 40.8, 40.5, 32.0, 31.9, 30.1, 24.2, 23.04, 22.97, 14.6, 14.5, 14.4. MALDI-TOF MS (*m/z*): 1647.6 ($M^+$).

### ~ 2-(4,4,5,5-Tetramethyl-1,3,2-dioxaborolan-2-yl)-9,10-bis(1,3-dithiol-2-ylidene)-9,10-dihydroanthracene (59)

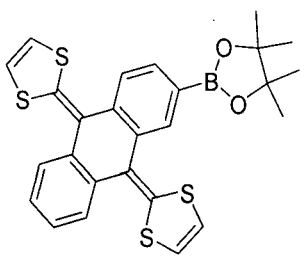


2-Iodo-9,10-bis(1,3-dithiol-2-ylidene)-9,10-dihydroanthracene[150] **55** (75 mg, 0.15 mmol) and bis(pinacolato)diboron (216 mg, 0.85 mmol) were degassed in DMF (15 mL) together with KOAc (125 mg, 1.28 mmol) for 30 min. A catalytic amount of $Pd(OAc)_2$ (*ca.* 5 mg) was added and the reaction mixture was stirred for 1 h at 60 °C under argon. The black precipitate was filtered off and ethyl acetate (40 mL) was added to the mixture. The organic layer was washed twice with $H_2O$, once with brine, dried over $MgSO_4$ and the solvent was evaporated *in vacuo*. Purification by column chromatography (silica gel eluted by 0-9% ethyl acetate in toluene/cyclohexane [4:1]) yielded **59** (45 mg, 60%) as a yellow solid containing some impurities (≤ 5%). Due to the small quantity of product, compound **61** was used without further purification.

$^1$H NMR (400 MHz, $CDCl_3$): δ 8.18 (1H, s), 7.75-7.65 (4H, m), 7.32-7.25 (2H, m), 6.32-6.26 (4H, m), 1.36 (12H, d, $J$ = 4.0 Hz). $^{13}$C NMR (125 MHz, $CDCl_3$): δ 137.8, 136.4,

135.5, 135.4, 135.2, 134.6, 132.5, 131.3, 129.0, 128.2, 125.9, 125.3, 124.9, 124.2, 122.2, 122.1, 117.4, 117.3, 117.1, 116.9, 83.7, 25.0, 24.8. HRMS, calc. for $C_{26}H_{23}BO_2S_4$ 506.0674; found 506.0677.

### ~ Br-Fl$_4$-CHO (61)

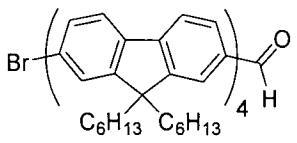


7,7"-Dibromo-9,9,9',9',9",9"-hexahexyl-9*H*,9'*H*,9"*H*-[2,2',7',2"]terfluorene[151] **60** (360 mg, 0.31 mmol), BE-Fl-CHO **48a** (135 mg, 0.28 mmol), $K_2CO_3$ (305 mg, 2.21 mmol) and $PdCl_2(PPh_3)_2$ (0.02 g) were reacted *via* standard Suzuki-Miyaura cross-coupling and purified using 0-100% ethyl acetate in hexane as eluent to yield **61** (60 mg, 15%) as a light yellow viscous oil containing some impurities (≤ 5%). Due to the low yield, compound **61** was used without further purification.

$^1$H NMR (400 MHz, $CDCl_3$): δ 10.10 (1H, s), 7.96-7.34 (24H, m), 2.22-1.88 (16H, m), 1.25-0.50 (88H, m). $^{13}$C NMR (125 MHz, $CDCl_3$): δ 192.4, 153.0, 152.3, 151.8, 147.3, 142.3, 141.9, 141.7, 141.4, 140.7, 140.5, 140.2, 140.1, 140.0, 138.7, 135.2, 132.2, 132.1, 131.9, 130.7, 128.8, 128.5, 128.4, 127.2, 126.7, 126.5, 126.3, 126.2, 123.1, 121.6, 121.5, 121.2, 120.0, 55.4, 55.3, 40.3, 40.2, 31.4, 29.63, 29.57, 23.8, 22.5, 14.0. HRMS, calc. for $C_{101}H_{129}BrO$ 1436.9227; found 1436.9225.

## 7.5 Experimental Procedures for Chapter 4

### ~ 5-(4-Bromophenyl)-10,15,20-tris(4-*t*-butylphenyl)porphyrin (63a)

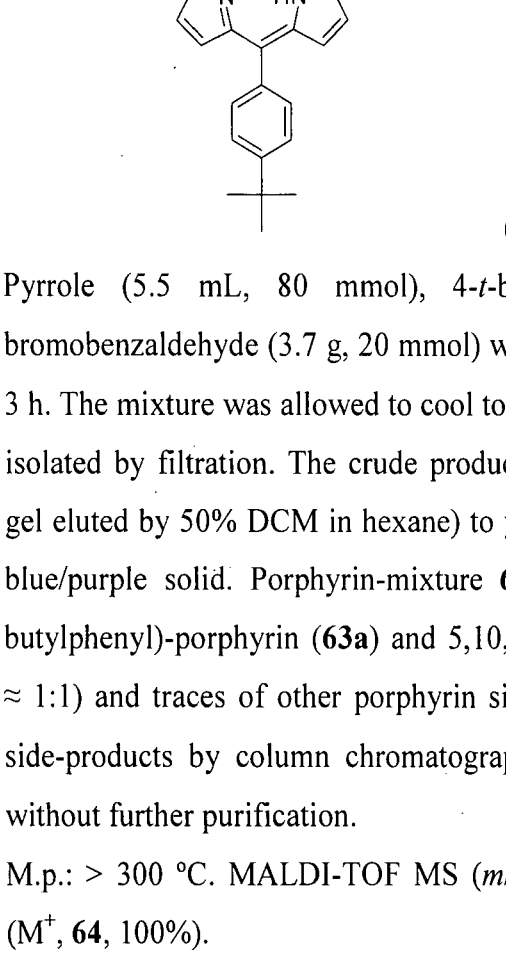


**(*t*BuPh)$_3$-H$_2$P-Ph-Br**

Pyrrole (5.5 mL, 80 mmol), 4-*t*-butylbenzaldehyde (9.7 g, 60 mmol) and 4-bromobenzaldehyde (3.7 g, 20 mmol) were heated at reflux in propionic acid (200 mL) for 3 h. The mixture was allowed to cool to room temperature and the precipitate obtained was isolated by filtration. The crude product was purified by column chromatography (silica gel eluted by 50% DCM in hexane) to yield porphyrin-mixture **63** (2.5 g, 3-4%) as a dark blue/purple solid. Porphyrin-mixture **63** contained 5-(4-bromophenyl)-10,15,20-tris(4-*t*-butylphenyl)-porphyrin (**63a**) and 5,10,15,20-tetrakis(4-*t*-butylphenyl)porphyrin (**64**, ratio ≈ 1:1) and traces of other porphyrin side-products. **63a** could not be separated from the side-products by column chromatography; therefore the mixture was used as obtained without further purification.

M.p.: > 300 °C. MALDI-TOF MS (*m/z*): 884.1 (32%), 862.3 ($M^+$+2, **63a**, 98%), 838.5 ($M^+$, **64**, 100%).

**~ 5,10,15,20-Tetrakis(4-*t*-butylphenyl)porphyrin (64)**

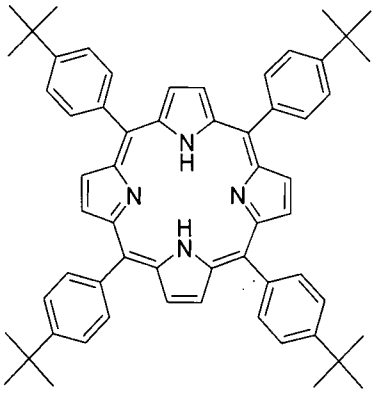

Pyrrole (0.5 mL, 7.2 mmol) and 4-*t*-butylbenzaldehyde (1.2 mL, 7.2 mmol) were refluxed in propionic acid (10 mL) for 3 h. The mixture was allowed to cool to room temperature and the obtained precipitate was filtered off. The crude product was purified by column chromatography (silica gel eluted by 50% DCM in hexane) to yield **64** (310 mg, 5%) as a dark blue/purple solid.

M.p.: > 300 °C. $^{1}$H NMR (700 MHz, $CDCl_3$): δ 8.88 (8H, s), 8.16 (8H, d, $J$ = 8.1 Hz) , 7.77 (8H, d, $J$ = 8.3 Hz), 1.62 (36H, s), -2.72 (2H, s). $^{13}$C NMR (175 MHz, $CDCl_3$): δ 150.4, 139.3, 134.5, 123.6, 120.1, 34.9, 31.7. MALDI-TOF MS (*m/z*): 838.6 ($M^+$). $C_{60}H_{62}N_4$: calc. C 85.88, H 7.45, N 6.68; found C 85.36, H 7.49, N 6.62.

**~ 5,10,15,20-Tetrakis(4-*t*-butylphenyl)porphyrin zinc(II) complex (65)**

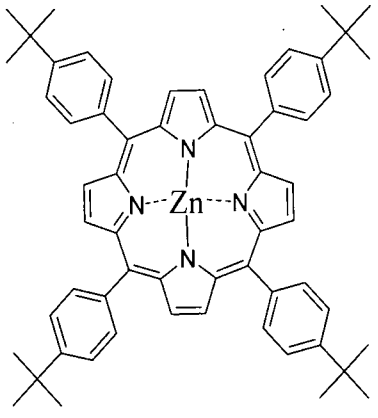

Zinc acetate dihydrate (150 mg, 0.68 mmol) and 5,10,15,20-tetrakis(4-*t*-butylphenyl)porphyrin **64** (110 mg, 0.13 mmol) were stirred together in degassed anhydrous chloroform (15 mL) at 62 °C for 3 h. The reaction mixture was filtered through

silica (eluent DCM) and removal of the solvent *in vacuo* gave **65** (115 mg, 98%) as a reddish-purple solid.

M.p.: > 300 °C. $^1$H NMR (500 MHz, $CDCl_3$): δ 8.99 (8H, s), 8.16 (8H, d, $J$ = 8.3 Hz) , 7.76 (8H, d, $J$ = 8.3 Hz), 1.63 (36H, s). $^{13}$C NMR (125 MHz, $CDCl_3$): δ 150.3, 150.2, 139.8, 134.3, 131.9, 123.4, 121.1, 34.9, 31.7, 31.6. MALDI-TOF MS (*m/z*): 900.5 ($M^+$). $C_{60}H_{60}N_4Zn$: calc. C 79.85, H 6.70, N 6.21; found C 79.68, H 6.86, N 6.12.

### ~ (*t*BuPh)$_3$-H$_2$P-Ph-Fl-CHO (66a)

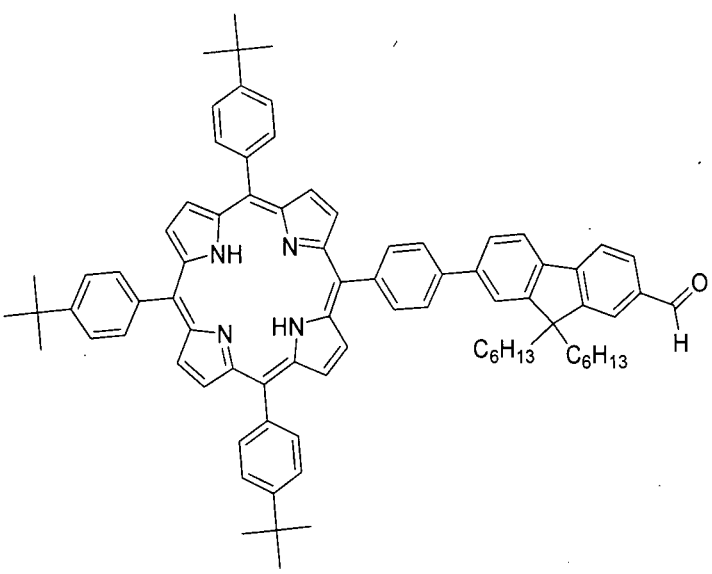


Porphyrin-mixture **63** (250 mg, excess), BE-Fl-CHO **48a** (60 mg, 0.12 mmol), $K_2CO_3$ (135 mg, 0.96 mmol) and $PdCl_2(PPh_3)_2$ (0.01 g) were reacted *via* standard Suzuki-Miyaura cross-coupling. Purification using hexane/DCM (1:1 v/v) as eluent yielded **66a** (45 mg, 32%) as a dark blue/purple solid.

M.p.: 146-149 °C. $^1$H NMR (700 MHz, $CDCl_3$): δ 10.13 (1H, s), 8.97-8.90 (8H, m), 8.36 (2H, d, $J$ = 7.8 Hz), 8.18 (6H, d, $J$ = 7.8 Hz), 8.09 (2H, d, $J$ = 7.8 Hz), 7.99-7.91 (6H, m), 7.79 (6H, d, $J$ = 7.8 Hz), 2.23-2.17 (4H, m), 1.63 (27H, s), 1.22-1.10 (12H, m), 0.82 (6H, t, $J$ = 7.2 Hz), 0.80-0.69 (4H, m), -2.67 (2H, s). $^{13}$C NMR (175 MHz, $CDCl_3$): δ 192.4, 153.2, 151.8, 150.5, 147.3, 141.7, 141.4, 140.2, 139.2, 139.1, 135.3, 135.2, 134.51, 134.48, 130.7, 126.6, 125.4, 123.61, 123.59, 123.1, 121.7, 121.5, 120.4, 120.3, 120.1, 119.3, 55.6, 40.4, 34.9, 31.7, 29.7, 23.9, 22.6, 14.0. MALDI-TOF MS (*m/z*): 1142.7 ($M^+$,100%), 1086.6 (39%). $C_{82}H_{86}N_4O{\cdot}2C_6H_{14}$: calc. C 85.79, H 8.73; found C 85.30, H 8.21.

**~ (*t*BuPh)$_3$-H$_2$P-Ph-Fl$_2$-CHO (66b)**

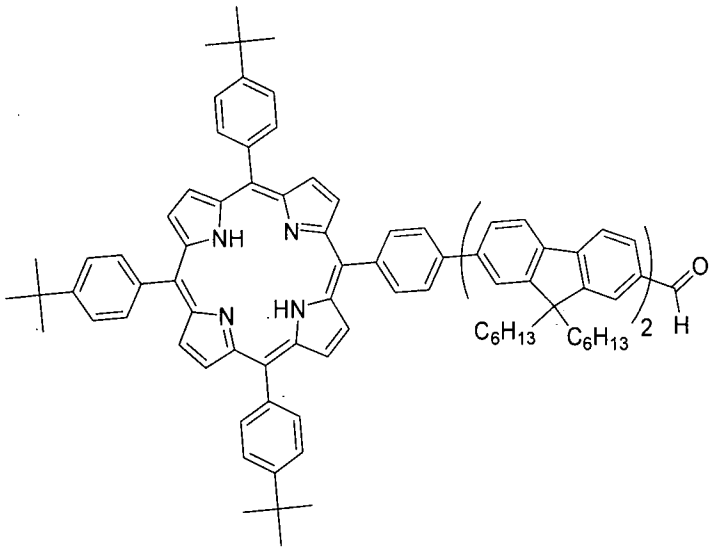


Porphyrin-mixture **63** (650 mg, excess), BE-Fl$_2$-CHO **48b** (200 mg, 0.24 mmol), $K_2CO_3$ (300 mg, 2.17 mmol) and $PdCl_2(PPh_3)_2$ (0.01 g) were reacted *via* standard Suzuki-Miyaura cross-coupling. Purification using hexane/DCM (1:1 v/v) as eluent yielded **66b** (20 mg, 6%) as a dark blue/purple solid.

$^1$H NMR (500 MHz, $CDCl_3$): δ 10.11 (1H, s), 9.01-8.90 (8H, m), 8.37 (2H, d, $J$ = 8.0 Hz), 8.21-8.16 (6H, m), 8.11 (2H, d, $J$ = 8.2 Hz), 7.99-7.87 (8H, m), 7.81-7.72 (10H, m), 2.26-2.20 (4H, m), 2.15 (4H, t, $J$ = 8.2 Hz), 1.64 (27H, s), 1.27-1.05 (24H, m), 0.90-0.66 (20H, m), -2.66 (2H, s). $^{13}$C NMR (125 MHz, $CDCl_3$): δ 192.7, 153.3, 152.2, 152.0, 150.7, 147.6, 142.6, 141.5, 140.8, 140.7, 140.6, 140.4, 140.0, 139.4, 139.0, 136.2, 135.5, 134.8, 134.7, 130.9, 130.1, 126.8, 126.6, 125.6, 123.9, 123.3, 121.9, 121.8, 121.5, 120.63, 120.60, 120.5, 120.4, 120.3, 119.7, 55.5, 55.4, 40.5, 40.2, 34.9, 31.7, 31.5, 29.8, 29.7, 29.6, 23.9, 23.8, 22.6, 22.5, 14.1, 14.0. MALDI-TOF MS (*m/z*): 1475.8 ($M^+$,100%), 1418.7 (49%).

**~ (*t*BuPh)$_3$-ZnP-Ph-Fl-CHO (67a)**

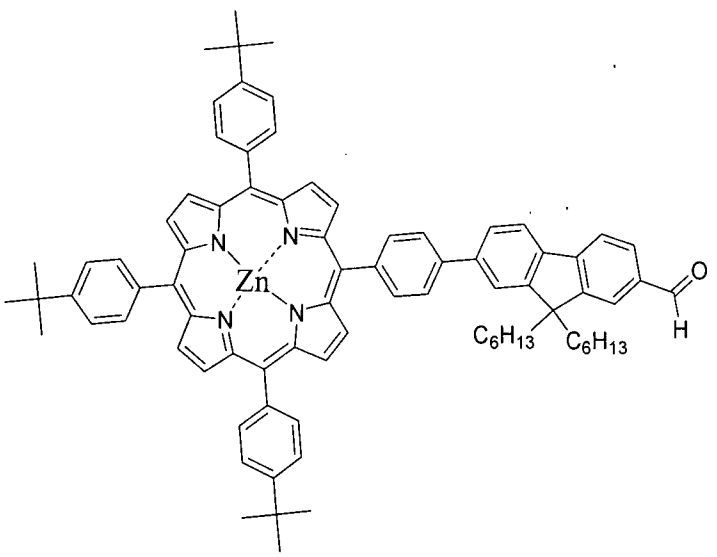


*t*Bu$_3$Ph-H$_2$P-Ph-Fl-CHO **66a** (52 mg, 0.05 mmol) and zinc acetate dihydrate (60 mg, 0.27 mmol) were stirred together in degassed anhydrous chloroform (15 mL) at 62 °C for 3 h. The reaction mixture was filtered through silica (eluent DCM) and removal of the solvent *in vacuo* gave **67a** (54 mg, 98%) as a reddish-purple solid.

M.p.: 198-201 °C. $^1$H NMR (700 MHz, $CDCl_3$): δ 10.08 (1H, s), 9.09-8.93 (8H, m), 8.36 (2H, d, $J$ = 7.1 Hz), 8.19-8.07 (8H, m), 7.98-7.90 (6H, m), 7.78 (6H, d, $J$ = 7.3 Hz), 2.22-2.15 (4H, m), 1.64 (27H, s), 1.20-1.08 (12H, m), 0.81 (6H, t, $J$ = 7.1 Hz), 0.79-0.70 (4H, m). $^{13}$C NMR (175 MHz, $CDCl_3$): δ 192.4, 153.2, 151.8, 150.4, 150.33, 150.28, 150.0, 147.3, 142.3, 141.5, 134.0, 139.8, 139.1, 135.3, 135.1, 134.3, 132.2, 132.1, 131.7, 130.6, 126.6, 125.3, 123.5, 123.1, 121.7, 121.5, 121.3, 120.1, 55.6, 40.4, 34.9, 31.7, 29.7, 23.9, 22.6, 14.0. MALDI-TOF MS (*m/z*): 1228.4 ($M^+$+$Na^+$+1, 26%), 1204.8 ($M^+$,100%), 1150.6 (19%).

**~ (*t*BuPh)$_3$-ZnP-Ph-Fl$_2$-CHO (67b)**

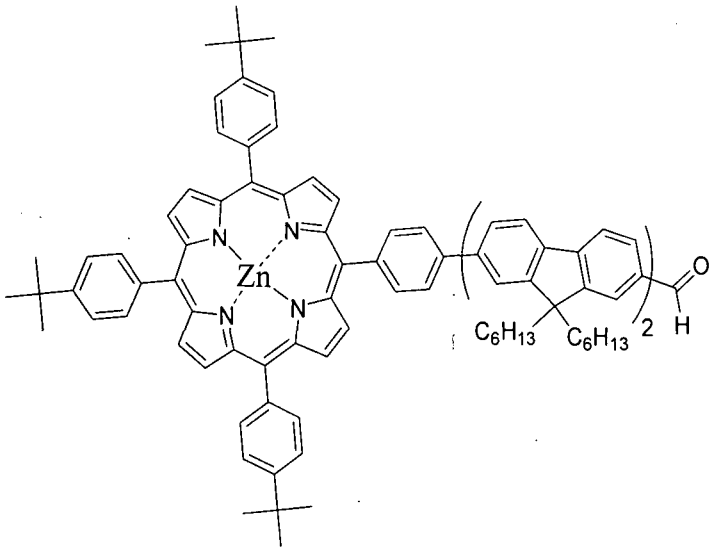


*t*Bu$_3$Ph-H$_2$P-Ph-Fl$_2$-CHO **66a** (20 mg, 0.01 mmol) and zinc acetate dihydrate (15 mg, 0.07 mmol) were stirred together in degassed anhydrous chloroform (15 mL) at 62 °C for 3 h. The reaction mixture was filtered through silica (eluent DCM) and removal of the solvent *in vacuo* gave **67b** (20 mg, 96%) as a reddish-purple solid.

$^1$H NMR (500 MHz, $CDCl_3$): δ 10.07 (1H, s), 9.09-8.92 (8H, m), 8.36 (2H, d, $J$ = 7.3 Hz), 8.22-8.09 (8H, M), 7.98-7.85 (8H, m), 7.82-7.68 (10H, m), 2.27-2.17 (4H, m), 2.13 (4H, t, $J$ = 8.2 Hz), 1.64 (27H, s), 1.27-1.05 (24H, m), 0.89-0.67 (20H, m). $^{13}$C NMR (125 MHz, $CDCl_3$): δ 192.4, 153.0, 152.0, 151.9, 151.8, 150.4, 150.3, 150.1, 147.3, 142.4, 141.9, 140.5, 140.4, 140.2, 140.1, 139.8, 138.7, 135.2, 135.1, 134.3, 132.14, 132.05, 131.7, 130.6, 126.5, 126.3, 125.2, 123.5, 123.1, 121.6, 121.2, 120.5, 120.3, 120.2, 120.0, 55.5, 55.4, 40.5, 40.2, 34.9, 31.7, 31.5, 29.74, 29.70, 29.6, 23.9, 23.8, 22.6, 22.5, 14.1, 14.0. MALDI-TOF MS (*m/z*): 1538.9 ($M^+$+2, 100%), 1482.8 (46%).

**~ ($t$BuPh)$_3$-ZnP-Ph-Fl-$C_{60}$ (68a)**

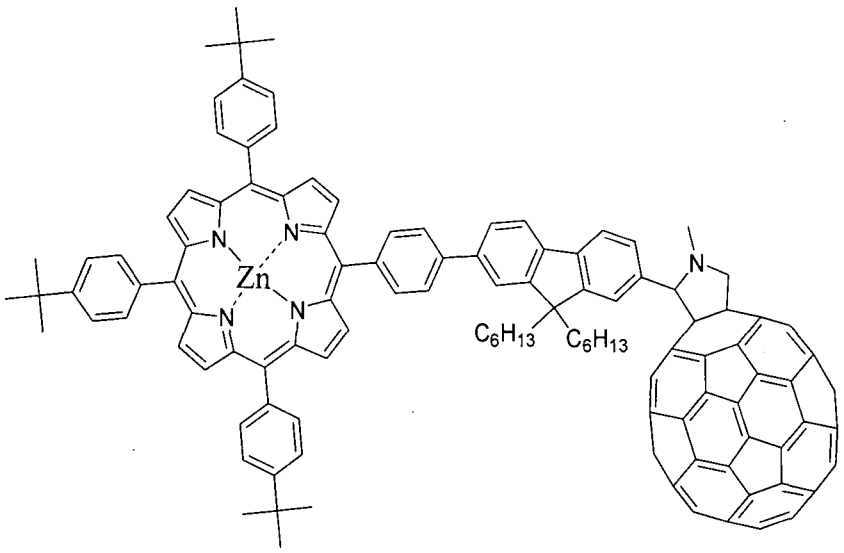


$C_{60}$ (120 mg, 0.17 mmol), $t$Bu$_3$Ph-ZnP-Ph-Fl-CHO **67a** (50 mg, 0.04 mmol) and sarcosine (20 mg, 0.22 mmol) were reacted *via* the general 1,3-dipolar cycloaddition procedure for 4 h. Purification by column chromatography using $CS_2$, followed by $CS_2$/DCM (1:1 v/v) as eluent and precipitation from hexane, yielded **68a** (50 mg, 59%) as a dark brown solid. $^1$H NMR (700 MHz, $CDCl_3$ + 3 drops $CS_2$): δ 9.07-8.90 (8H, m), 8.27-8.08 (8H, m), 8.02 (2H, d, $J$ = 7.6 Hz), 7.98-7.89 (3H, m), 7.85-7.82 (1H, m), 7.81-7.76 (7H, m), 7.49 (1H, s, br), 4.78 (2H, s, br), 4.07 (1H, s, br), 2.83 (3H, s, br), 2.34-2.00 (4H, m, br), 1.65 (27H, s), 1.34-0.75 (16H, m, br), 0.67 (4H, s, br), 0.51 (1H, s, br), 0.24 (1H, s, br). $^{13}$C NMR (175 MHz, $CDCl_3$ + 3 drops $CS_2$): δ 153.3, 153.2, 153.1, 151.8, 151.7, 150.4, 150.3, 150.14, 150.05, 146.5, 145.8, 145.5, 145.4, 145.3, 145.1, 144.8, 144.6, 144.4, 144.3, 143.9, 143.7, 142.0, 141.9, 141.84, 141.76, 141.6, 141.4, 141.3, 141.0, 140.9, 140.3, 140.1, 139.9, 139.7, 139.5, 139.0, 135.7, 135.0, 134.3, 132.1, 132.0, 131.7, 126.2, 125.1, 123.5, 121.3, 121.2, 120.5, 120.3, 83.7, 69.8, 68.5, 55.4, 40.0, 34.8, 31.7, 29.9, 24.0, 22.9, 22.7, 14.2, 14.1. MALDI-TOF MS (*m/z*): 1953.7 ($M^+$+2, 24%), 1233.8 ($M^+$-$C_{60}$+2, 46%), 1046.6 (28%), 900.5 (100%).

**~ ($t$BuPh)$_3$-ZnP-Ph-Fl$_2$-C$_{60}$ (68b)**

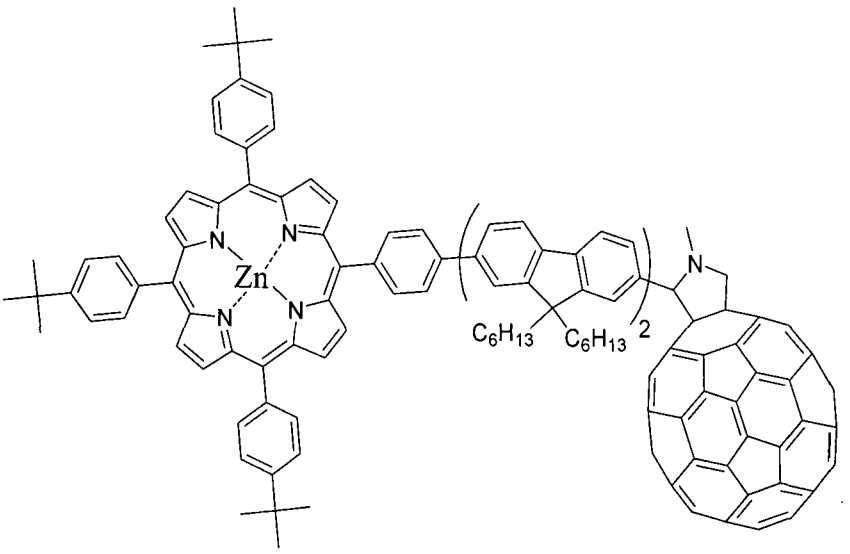


$C_{60}$ (40 mg, 0.06 mmol), $t$Bu$_3$Ph-ZnP-Ph-Fl$_2$-CHO **67b** (20 mg, 0.01 mmol) and sarcosine (10 mg, 0.11 mmol) were reacted *via* the general 1,3-dipolar cycloaddition procedure for 4 h. Purification using $CS_2$, followed by $CS_2$/DCM (1:1 v/v) as eluent yielded **68b** (25 mg, 84%) as a dark brown solid.

$^1$H NMR (700 MHz, $CDCl_3$ + 3 drops $CS_2$): δ 9.12-8.91 (8H, m), 8.36-8.29 (2H, m), 8.27-8.22 (1H, m), 8.21-8.07 (7H, m), 7.98-7.89 (4H, m), 7.86 (1H, d, $J$ = 5.6 Hz), 7.81-7.75 (7H, m), 7.74-7.59 (5H, m), 7.46 (1H, s, br), 4.87-4.76 (2H, m, br), 4.09-4.01 (1H, m, br), 2.83 (3H, s, br), 2.27-1.96 (8H, m, br), 1.65 (27H, m), 1.33-0. 57 (42H, m, br), 0.42 (1H, s, br), 0.21 (1H, s, br). $^{13}$C NMR (175 MHz, $CDCl_3$ + 3 drops $CS_2$): δ 155.7, 153.4, 153.2, 153.0, 151.9, 151.7, 151.6, 150.3, 150.2, 150.1, 146.5, 146.4, 145.9, 145.7, 145.6, 145.5, 145.39, 145.36, 145.3, 145.2, 144.8, 144.6, 144.4, 144.0, 143.7, 142.0, 141.8, 141.71, 171.68, 141.5, 141.43, 141.36, 141.2, 141.1, 141.0, 140.7, 140.5, 140.4, 140.0, 139.8, 139.7, 139.5, 139.4, 139.1, 136.3, 136.1, 135.7, 135.6, 135.2, 135.1, 135.0, 134.6, 132.1, 132.0, 131.8, 129.7, 126.3, 126.2, 126.1, 125.2, 123.5, 121.5, 121.4, 121.3, 120.5, 120.2, 120.1, 83.6, 69.8, 68.6, 55.4, 55.2, 40.6, 39.9, 34.8, 31.7, 31.6, 29.9, 24.0, 22.7, 14.2, 14.1. MALDI-TOF MS (*m/z*): 2285.9 ($M^+$+2, 18%), 1587.8 (20%), 1565.1 ($M^+$-$C_{60}$+1, 100%), 1508.9 (45%).

**~ 5-(7-Bromo-9,9-dihexyl-9*H*-fluoren-2-yl)-10,15,20-tris(4-*t*-butylphenyl)-porphyrin (69)**

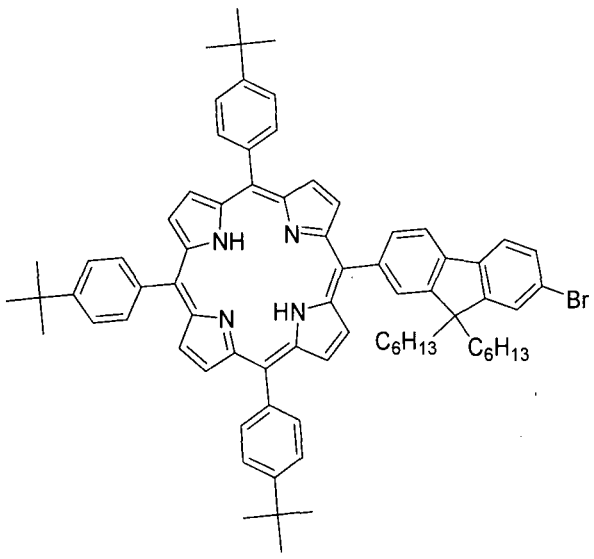


Pyrrole (2.8 mL, 40 mmol), 4-*t*-butylbenzaldehyde (5.0 mL, 30 mmol) and Br-Fl-CHO **47a** (4.4 g, 10 mmol) were heated at reflux in propionic acid (150 mL) for 3 h. After evaporation of the solvent *in vacuo*, the reaction mixture was filtered through silica (eluent DCM) to yield a crude product mixture. Purification by column chromatography (silica gel eluted by 33% DCM in hexane) yielded (*t*BuPh)$_3$-H$_2$P-Fl-Br **69** (0.95 g, 9%) as a dark blue/purple solid.

M.p.: 299-301 °C. $^1$H NMR (500 MHz, $CDCl_3$): δ 8.94-8.84 (7H, m), 8.62-8.49 (1H, m), 8.23-8.00 (9H, m), 7.84-7.74 (7H, m), 7.64-7.58 (2H, m), 2.19-2.04 (4H, m), 1.67-1.62 (27H, m), 1.26-1.13 (12H, m), 1.07-0.96 (2H, br, m), 0.96-0.86 (2H, br, m), 0.80 (6H, t, *J* = 6.9 Hz), -2.70 (2H, s). $^{13}$C NMR (125 MHz, $CDCl_3$): δ 153.5, 150.5, 148.7, 141.6, 140.0, 139.5, 139.1, 136.8, 134.4, 133.8, 130.2, 129.6, 126.3, 123.6, 121.42, 121.35, 120.32, 120.27, 120.1, 117.9, 55.7, 40.4, 34.9, 31.69, 31.67, 31.6, 29.7, 24.0, 22.6, 14.1. MALDI-TOF MS (*m/z*): 1118.6 ($M^+$+2). $C_{75}H_{81}BrN_4$: calc. C 80.55, H 7.30, N 5.01; found C 80.39, H 7.31, N 4.88.

**~ 5-(7-Bromo-9,9-dihexyl-9*H*-fluoren-2-yl)-10,15,20-tris(4-*t*-butylphenyl)-porphyrin zinc(II) complex (70)**

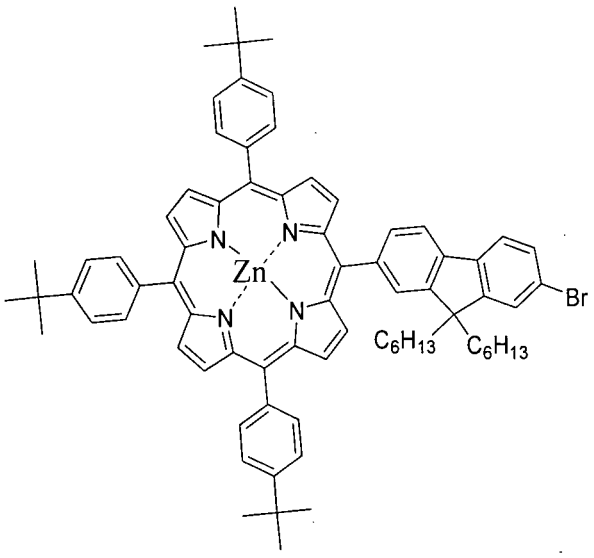


(*t*BuPh)$_3$-H$_2$P-Fl-Br **69** (122 mg, 0.11 mmol) and zinc acetate dihydrate (120 mg, 0.55 mmol) were stirred together in degassed anhydrous chloroform (15 mL) at 62 °C for 3 h. The reaction mixture was filtered through silica (eluent DCM) and removal of the solvent *in vacuo* gave **70** (126 mg, 98%) as a reddish purple solid.

M.p.: > 300 °C. $^1$H NMR (500 MHz, $CDCl_3$): δ 9.06-8.98 (8H, m), 8.24-8.15 (8H, m), 8.02-8.00 (1H, m), 7.82-7.76 (8H, m), 7.64 (1H, d, $J$ = 1.6 Hz), 7.60 (1H, dd, $J$ = 1.6 & 8.0 Hz), 2.19-2.07 (4H, m), 1.69-1.59 (27H, m), 1.28-1.15 (12H, m), 1.10-1.00 (2H, br, m), 0.98-0.88 (2H, br, m), 0.83 (6H, t, $J$ = 6.7 Hz). $^{13}$C NMR (125 MHz, $CDCl_3$): δ 153.5, 150.5, 150.32, 150.25, 150.1, 148.6, 142.2, 140.1, 139.8, 139.3, 134.3, 133.6, 132.11, 132.08, 131.7, 130.2, 129.5, 126.3, 123.5, 121.4, 121.34, 121.27, 121.1, 117.8, 55.6, 40.4, 34.9, 31.7, 31.6, 29.7, 24.0, 22.7, 14.1. MALDI-TOF MS (*m/z*): 1180.4 ($M^+$+2). $C_{75}H_{79}BrN_4Zn$: calc. C 76.23, H 6.74, N 4.74; found C 76.06, H 6.89, N 4.50.

~ **(*t*BuPh)$_3$-H$_2$P-Fl$_2$-CHO (72a)**

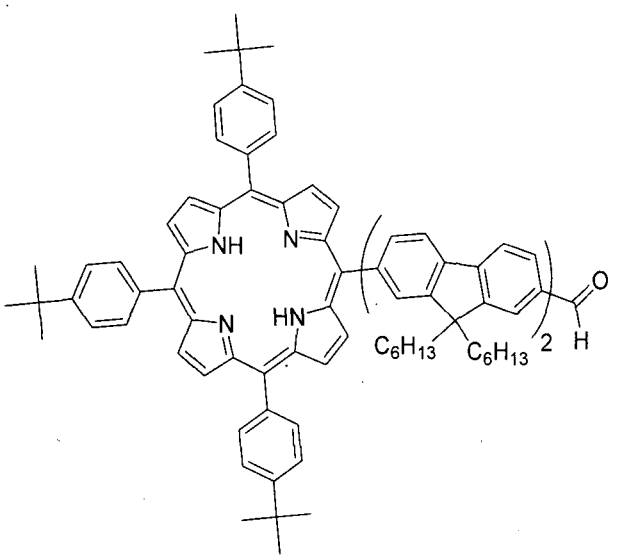


(*t*BuPh)$_3$-H$_2$P-Fl-Br **69** (75 mg, 0.07 mmol), BE-Fl-CHO **48a** (67 mg, 0.14 mmol), $K_2CO_3$ (310 mg, 2.25 mmol) and $Pd(PPh_3)_4$ (80 mg, 0.07 mmol) were stirred under argon in toluene (1 mL, degassed, dry) and DMF (2 mL, degassed, dry) at 105 °C for 6 h. The reaction mixture was filtered through silica (eluent DCM) and the solvent was evaporated *in vacuo*. Purification by column chromatography (silica gel eluted by 33-50% DCM in hexane) yielded **72b** (60 mg, 64%) as a dark blue/purple solid.

M.p.: 295-297 °C. $^1$H NMR (500 MHz, $CDCl_3$): δ 10.11 (1H, s), 8.95-8.86 (8H, m), 8.27-8.23 (2H, m), 8.21-8.14 (6H, m), 8.12 (1H, d, $J$ = 7.3 Hz), 8.07 (1H, d, $J$ = 7.7 Hz), 7.96-7.90 (4H, m), 7.84-7.74 (10H, m), 2.22 (4H, t, $J$ = 8.2 Hz), 2.15 (4H, t, $J$ = 8.6 Hz), 1.66-1.59 (27H, m), 1.26-0.65 (44H, m), -2.69 (2H, s). $^{13}$C NMR (125 MHz, $CDCl_3$): δ 192.7, 153.3, 152.4, 152.1, 150.7, 149.7, 147.6, 142.6, 141.5, 140.9, 140.6, 140.3, 139.45, 139.43, 139.0, 135.5, 134.7, 134.1, 130.9, 130.1, 126.8, 126.7, 123.9, 123.4, 121.9, 121.6, 120.7, 120.6, 120.53, 120.52, 120.3, 118.2, 55.49, 55.45, 40.5, 40.2, 34.9, 31.7, 31.6, 31.5, 29.7, 29.6, 24.1, 23.8, 22.61, 22.55, 14.1, 14.0. MALDI-TOF MS (*m/z*): 1398.9 ($M^+$). $C_{101}H_{114}N_4O$: calc. C 86.65, H 8.21, N 4.00; found C 86.63, H 8.44, N 3.77.

**~ ($t$BuPh)$_3$-H$_2$P-Fl$_3$-CHO (72b)**

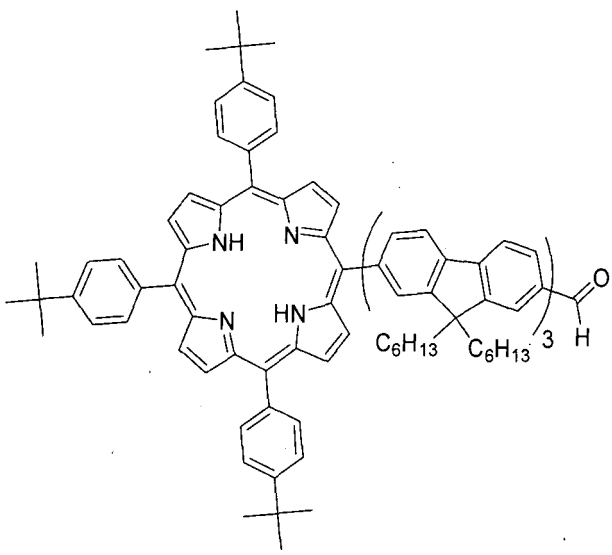


($t$BuPh)$_3$-H$_2$P-Fl-Br **69** (75 mg, 0.07 mmol), BE-Fl$_2$-CHO **48b** (220 mg, 0.27 mmol), $K_2CO_3$ (310 mg, 2.25 mmol) and $Pd(PPh_3)_4$ (80 mg, 0.07 mmol) were stirred under argon in toluene (1 mL, degassed, dry) and DMF (2 mL, degassed, dry) at 105 °C for 3 h. The reaction mixture was filtered through silica (eluent DCM) and the solvent was evaporated *in vacuo*. Purification by column chromatography (silica gel eluted by 40% DCM in hexane) yielded **72c** (52 mg, 45%) as a dark blue/purple solid.

M.p.: 260-263 °C. $^1$H NMR (500 MHz, $CDCl_3$): δ 10.10 (1H, s), 8.96-8.88 (8H, m), 8.28-8.23 (2H, m), 8.22-8.15 (6H, m), 8.12 (1H, d, $J$ = 7.5 Hz), 8.07 (1H, d, $J$ = 7.8 Hz), 7.95-7.82 (7H, m), 7.82-7.67 (13H, m), 2.30-2.05 (12H, m), 1.66-1.59 (27H, m), 1.26-1.00 (36H, m), 0.87-0.65 (30H, m), -2.67 (2H, s). $^{13}$C NMR (175 MHz, $CDCl_3$): δ 192.4, 153.0, 152.1, 151.92, 151.87, 151.8, 150.5, 149.4, 147.3, 142.4, 141.1, 140.8, 140.7, 140.5, 140.3, 140.2, 140.0, 139.9, 139.23, 139.21, 138.7, 135.3, 134.5, 133.9, 130.6, 129.8, 127.9, 126.5, 126.4, 126.3, 125.8, 123.6, 123.1, 121.62, 121.58, 121.2, 120.5, 120.34, 120.25, 120.12, 120.08, 120.0, 117.9, 55.5, 55.43, 55.41, 40.5, 40.4, 40.2, 34.9, 31.71, 31.69, 31.6, 31.47, 31.46, 29.8, 29.70, 29.67, 29.6, 24.1, 23.9, 23.8, 22.62, 22.56, 22.5, 14.1, 14.04, 13.99. MALDI-TOF MS ($m/z$): 1732.1 ($M^+$+1). $C_{126}H_{146}N_4O{\cdot}C_6H_{14}$: calc. C 87.17, H 8.87, N 3.08; found C 86.88, H 8.73, N 2.88.

**~ ($t$BuPh)$_3$-ZnP-Fl$_2$-CHO (73a)**

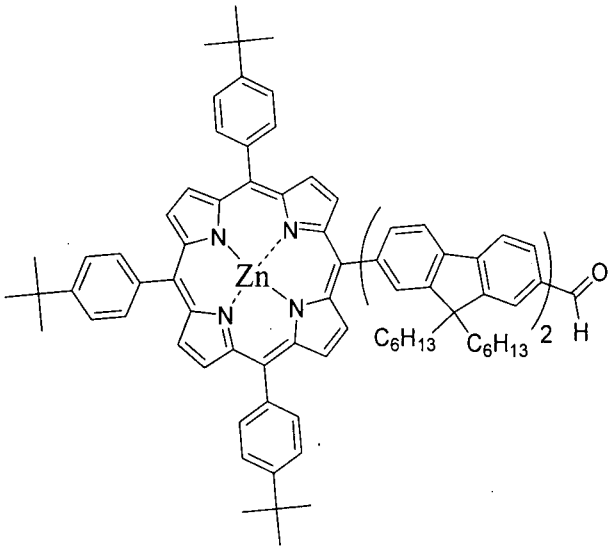


($t$BuPh)$_3$-H$_2$P-Fl$_2$-CHO **72b** (73 mg, 0.05 mmol) and zinc acetate dihydrate (57 mg, 0.26 mmol) were stirred together in degassed anhydrous chloroform (15 mL) at 62 °C for 3 h. The reaction mixture was filtered through silica (eluent DCM) and removal of the solvent *in vacuo* gave **73b** (76 mg, 100%) as a reddish-purple solid.

M.p.: 300-302 °C. $^1$H NMR (500 MHz, $CDCl_3$): δ 10.04 (1H, s), 9.09-9.01 (8H, m), 8.31-8.26 (2H, m), 8.23-8.16 (6H, m), 8.13 (1H, d, $J$ = 7.6 Hz), 8.07 (1H, d, $J$ = 7.8 Hz), 7.97-7.86 (4H, m), 7.84-7.76 (10H, m), 2.25 (4H, t, $J$ = 8.1 Hz), 2.21-2.10 (4H, m), 1.70-1.60 (27H, m), 1.30-0.65 (44H, m). $^{13}$C NMR (125 MHz, $CDCl_3$): δ 192.4, 153.0, 152.1, 151.8, 150.40, 150.37, 150.3, 150.24, 150.20, 149.3, 147.3, 142.4, 141.9, 140.8, 140.2, 139.9, 139.8, 138.7, 135.2, 134.33, 134.27, 133.6, 132.09, 132.05, 131.8, 130.7, 129.7, 126.6, 126.4, 123.5, 123.1, 121.6, 121.4, 121.31, 121.27, 120.4, 120.0, 117.8, 55.49, 55.45, 40.5, 40.2, 34.9, 31.7, 31.6, 31.5, 29.8, 29.7, 29.6, 24.1, 23.8, 22.64, 22.65, 14.1, 14.0. MALDI-TOF MS ($m/z$): 1461.7 ($M^+$+1). $C_{101}H_{112}N_4OZn{\cdot}H_2O$: calc. C 81.89, H 7.76, N 3.78; found C 82.12, H 8.08, N 3.49.

**~ ($t$BuPh)$_3$-ZnP-Fl$_3$-CHO (73b)**

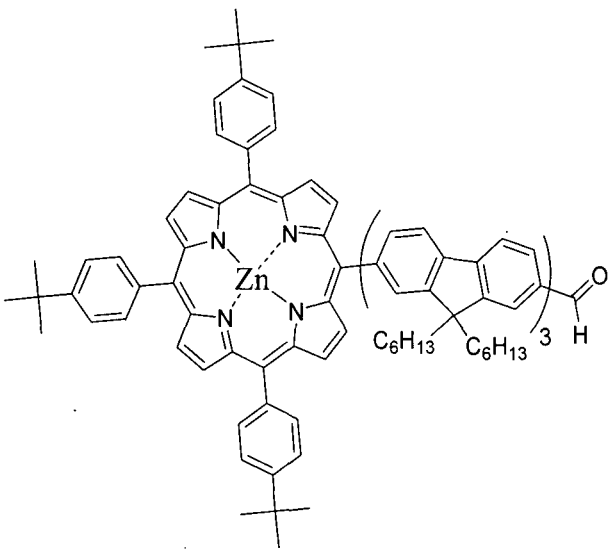


($t$BuPh)$_3$-H$_2$P-Fl$_3$-CHO **72c** (52 mg, 0.03 mmol) and zinc acetate dihydrate (33 mg, 0.15 mmol) were stirred together in degassed anhydrous chloroform (15 mL) at 62 °C for 3 h. The reaction mixture was filtered through silica (eluent DCM) and removal of the solvent *in vacuo* gave **73c** (54 mg, 100%) as a reddish-purple solid.

M.p.: 263-265 °C. $^1$H NMR (500 MHz, $CDCl_3$): δ 10.05 (1H, s), 9.09-9.02 (8H, m), 8.30-8.26 (2H, m), 8.23-8.17 (6H, m), 8.13 (1H, d, $J$ = 7.6 Hz), 8.08 (1H, d, $J$ = 7.8 Hz), 7.94-7.70 (20H, m), 2.29-2.10 (12H, m), 1.68-1.61 (27H, m), 1.29-1.01 (36H, m), 0.95-0.65 (30H, m). $^{13}$C NMR (125 MHz, $CDCl_3$): δ 192.4, 153.0, 152.1, 151.90, 151.86, 151.8, 150.39, 150.36, 150.2, 149.2, 147.3, 142.4, 141.7, 140.72, 140.68, 140.5, 140.4, 140.02, 139.98, 139.9, 139.8, 138.7, 135.2, 134.33, 134.27, 133.6, 132.1, 132.0, 131.8, 130.6, 129.7, 126.5, 126.33, 126.28, 123.5, 123.1, 121.6, 121.5, 121.3, 121.2, 120.3, 120.12, 120.07, 120.0, 117.8, 55.5, 55.4, 40.6, 40.4, 40.2, 34.9, 31.7, 31.6, 31.5, 29.8, 29.70, 29.68, 29.6, 24.1, 23.9, 23.8, 22.7, 22.6, 22.5, 14.10, 14.06, 14.0. MALDI-TOF MS ($m/z$): 1794.2 ($M^+$+1). $C_{126}H_{144}N_4OZn{\cdot}C_6H_{14}$: calc. C 84.24, H 8.46, N 2.98; found C 84.27, H 8.56, N 2.59.

~ **($t$BuPh)$_3$-ZnP-Fl$_2$-C$_{60}$ (74a)**

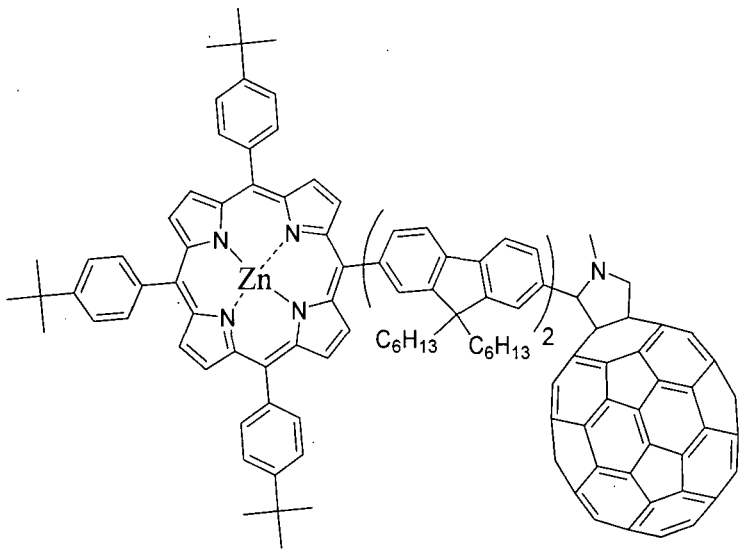


$C_{60}$ (171 mg, 0.24 mmol), ($t$BuPh)$_3$-ZnP-Fl$_2$-CHO **73b** (58 mg, 0.04 mmol) and sarcosine (25 mg, 0.28 mmol) were reacted *via* the general 1,3-dipolar cycloaddition procedure for 4 h. Purification by column chromatography using $CS_2$, followed by $CS_2$/DCM (3:1 v/v) as eluent yielded **74b** (61 mg, 70%) as a dark brown solid.

$^1$H NMR (500 MHz, $CDCl_3$): δ 9.06-8.93 (8H, m), 8.24 (1H, d, $J$ = 7.3 Hz), 8.21-8.11 (7H, m), 8.10 (1H, d, $J$ = 7.6 Hz), 8.02 (1H, d, $J$ = 7.8 Hz), 7.89 (1H, s, br), 7.84-7.64 (12H, m), 7.39 (1H, s, br), 4.65 (2H, d, $J$ = 8.2 Hz, br), 3.87 (1H, d, $J$ = 8.9 Hz), 2.79 (3H, s, br), 2.31-1.90 (8H, m, br), 1.72-1.58 (27H, m), 1.34-0.52 (42H, m, br), 0.40 (1H, s, br), 0.17 (1H, s, br). $^{13}$C NMR (125 MHz, $CDCl_3$): δ 155.5, 153.11, 153.05, 152.80, 152.77, 152.0, 151.7, 150.3, 150.24, 150.16, 149.1, 146.2, 146.13, 146.11, 145.8, 145.3, 145.1, 144.9, 144.8, 144.5, 144.4, 144.3, 144.2, 144.0, 143.9, 143.7, 143.4, 143.3, 142.4, 141.8, 141.7, 141.6, 141.4, 141.3, 141.2, 141.1, 141.00, 140.96, 140.9, 140.7, 140.6, 140.3, 139.9, 139.2, 139.1, 138.9, 136.2, 135.9, 135.6, 135.0, 134.7, 134.2, 133.3, 132.1, 132.0, 131.8, 129.7, 126.3, 126.1, 123.5, 121.5, 121.3, 120.2, 120.0, 117.7, 83.5, 69.7, 68.4, 55.4, 55.3, 40.5, 40.0, 34.9, 31.7, 31.63, 31.59, 29.8, 29.4, 24.1, 23.9, 23.8, 22.8, 22.7, 14.14, 14.07. MALDI-TOF MS ($m/z$): 2209.1 ($M^+$+1, 100%), 1570.6 (70%), 1488.0 ($M^+$-$C_{60}$, 42%).

~ **(*t*BuPh)$_3$-ZnP-Fl$_3$-C$_{60}$ (74b)**

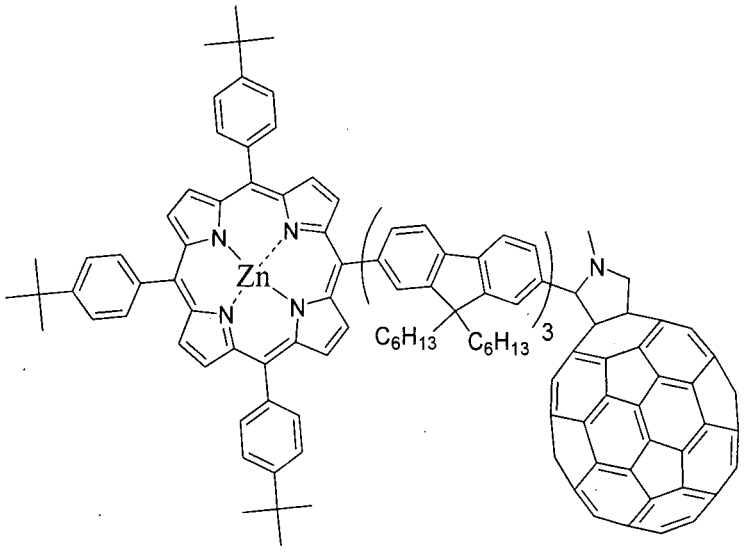


$C_{60}$ (90 mg, 0.13 mmol), (*t*BuPh)$_3$-ZnP-Fl$_3$-CHO **73c** (37 mg, 0.02 mmol) and sarcosine (15 mg, 0.17 mmol) were reacted *via* the general 1,3-dipolar cycloaddition procedure for 4 h. Purification by column chromatography using $CS_2$, followed by $CS_2$/DCM (3:1 v/v) as eluent yielded **74c** (38 mg, 73%) as a dark brown solid.

$^1$H NMR (500 MHz, $CDCl_3$): δ 9.01 (8H, s, br), 8.26 (1H, d, $J$ = 7.3 Hz), 8.24-8.10 (8H, m), 8.06 (1H, d, $J$ = 7.6 Hz), 7.96-7.58 (19H, m), 7.40 (1H, s, br), 4.75-4.60 (2H, m, br), 3.88 (1H, d, $J$ = 8.8 Hz), 2.80 (3H, s, br), 2.30-1.90 (12H, m, br), 1.74-1.58 (27H, m), 1.34-0.52 (64H, m, br), 0.39 (1H, s, br), 0.17 (1H, s, br). $^{13}$C NMR (125 MHz, $CDCl_3$): δ 155.5, 153.1, 152.8, 152.1, 151.8, 151.6, 150.4, 150.3, 150.2, 149.2, 146.23, 146.19, 145.8, 145.6, 145.4, 145.1, 145.04, 144.97, 144.84, 144.77, 144.6, 144.4, 144.3, 144.1, 143.9, 143.8, 143.5, 143.3, 142.4, 141.84, 141.79, 141.6, 141.5, 141.33, 141.29, 141.25, 141.1, 140.99, 140.96, 140.7, 140.6, 140.5, 140.4, 140.3, 140.0, 139.9, 139.2, 139.1, 139.0, 136.2, 136.0, 135.6, 135.0, 134.7, 134.2, 133.4, 132.1, 132.0, 131.8, 129.7, 126.3, 126.2, 126.14, 126.07, 123.5, 121.5, 121.3, 120.3, 120.0, 117.7, 83.6, 69.7, 68.4, 55.42, 55.35, 55.3, 40.6, 40.4, 39.9, 34.9, 31.73, 31.66, 31.5, 29.8, 29.7, 24.1, 23.9, 23.8, 22.7, 22.6, 14.2, 14.1. MALDI-TOF MS (*m/z*): 2542.4 ($M^+$+2, 100%), 1900.6 (36%), 1822.3 ($M^+$-$C_{60}$+2, 53%), 771.3 (61%).

~ **(*t*BuPh)$_3$-H$_2$P-Fl-BE (75)**

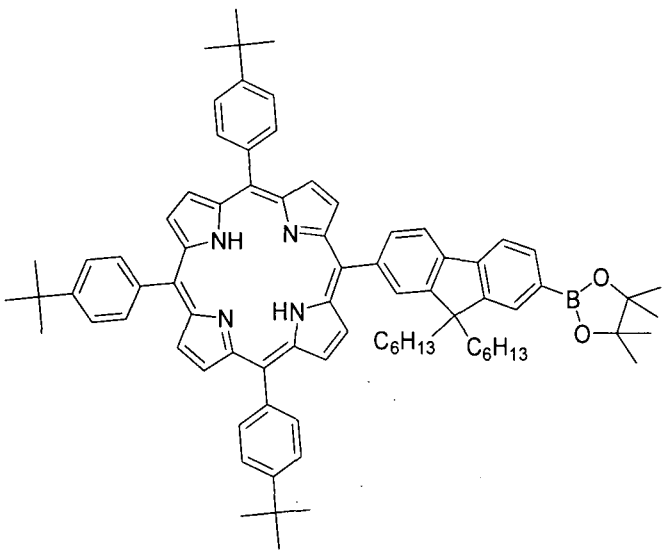


(*t*BuPh)$_3$-H$_2$P-Fl-Br **69** (200 mg, 0.18 mmol), bis(pinacolato)diboron (0.46 g, 1.81 mmol), $K_2CO_3$ (790 mg, 5.72 mmol) and $Pd(PPh_3)_4$ (105 mg, 0.09 mmol) were stirred under argon in toluene (2.6 mL, degassed, dry) and DMF (5.4 mL, degassed, dry) at 105 °C for 3 h. The reaction mixture was filtered through silica (eluent DCM) and the solvent was evaporated *in vacuo*. Purification by column chromatography (silica gel eluted by 50% DCM in hexane) yielded **75** (66 mg, 32%) as a dark blue/purple solid.

M.p.: > 300 °C. $^1$H NMR (500 MHz, $CDCl_3$): δ 8.94 (8H, s, br), 8.27 (1H, s), 8.26-8.16 (7H, m), 8.11 (1H, d, $J$ = 7.6 Hz), 8.00 (2H, s, br), 7.95 (1H, s), 7.80 (6H, d, $J$ = 7.6 Hz), 2.27-2.15 (4H, m), 1.65 (27H, s, br), 1.49 (12H, s), 1.30-0.77 (22H, m), -2.64 (2H, s). $^{13}$C NMR (125 MHz, $CDCl_3$): δ 150.5, 149.7, 144.0, 141.6, 140.4, 139.2, 134.5, 134.0, 133.7, 131.1, 129.8, 129.0, 127.7, 123.6, 120.4, 120.3, 119.4, 118.2, 83.8, 55.4, 40.4, 34.9, 31.7, 31.6, 29.7, 25.0, 24.0, 22.7, 14.1. MALDI-TOF MS (*m/z*): 1164.7 ($M^+$). $C_{81}H_{93}BN_4O_2$: calc. C 83.48, H 8.04, N 4.81; found C 83.41, H 8.21, N 4.25.

~ **5-(9,9,9',9'-Tetrahexyl-9*H*,9'*H*-[7,2']-bifluoren-2-yl)-10,15,20-tris(4-*t*-butylphenyl)-porphyrin (76)**

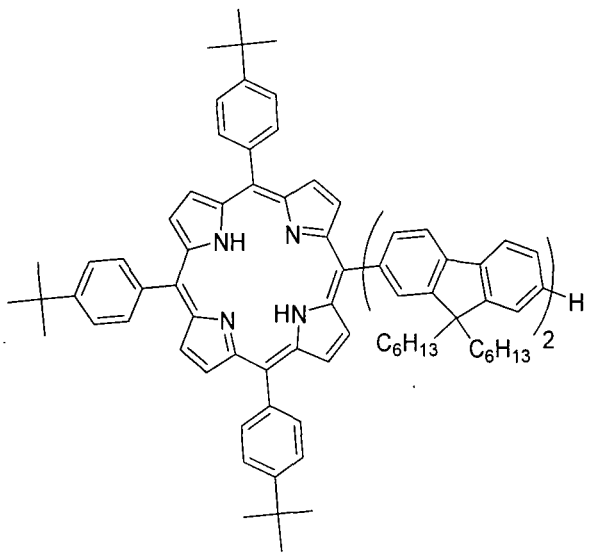


(*t*BuPh)$_3$-H$_2$P-Fl-Br **69** (100 mg, 0.09 mmol), 9,9-dihexyl-9*H*-fluorene-2-boronic acid **44** (101 mg, 0.27 mmol), $K_2CO_3$ (395 mg, 2.86 mmol) and $Pd(PPh_3)_4$ (103 mg, 0.09 mmol) were stirred under argon in toluene (1.3 mL, degassed, dry) and DMF (2.7 mL, degassed, dry) at 105 °C for 3 h. The reaction mixture was filtered through silica (eluent DCM) and the solvent was evaporated *in vacuo*. Purification by column chromatography (silica gel eluted by 33% DCM in hexane) yielded (*t*BuPh)$_3$-H$_2$P-Fl$_2$ **76** (62 mg, 51%) as a dark blue/purple solid.

M.p.: > 300 °C. $^1$H NMR (500 MHz, $CDCl_3$): δ 9.05-8.91 (8H, m), 8.33 (1H, s), 8.28 (1H, d, $J$ = 7.6 Hz), 8.27-8.19 (6H, m), 8.13 (1H, d, $J$ = 7.6 Hz), 8.06 (1H, d, $J$ = 8.2 Hz), 7.88 (1H, d, $J$ = 7.8 Hz), 7.87-7.76 (11H, m), 7.47-7.37 (3H, m), 2.28 (4H, t, $J$ = 7.7 Hz), 2.22-2.08 (4H, m), 1.67 (27H, s), 1.30-0.78 (44H, m), -2.59 (2H, s). $^{13}$C NMR (125 MHz, $CDCl_3$): δ 152.1, 151.5, 151.0, 150.5, 149.4, 141.1, 140.9, 140.8, 140.5, 140.4, 140.3, 140.2, 139.2, 134.5, 133.8, 129.8, 127.0, 126.8, 126.3, 126.1, 123.6, 122.9, 121.6, 121.5, 120.5, 120.3, 119.9, 119.7, 117.9, 55.5, 55.2, 40.5, 40.4, 34.9, 31.7, 31.6, 31.5, 29.8, 29.7, 24.1, 23.8, 22.7, 22.6, 14.11, 14.06. MALDI-TOF MS (*m/z*): 1372.0 ($M^+$+1). $C_{100}H_{114}N_4$: calc. C 87.54, H 8.37, N 4.08; found C 86.41, H 8.43, N 3.69.

~ **5-(9,9,9',9'-Tetrahexyl-9*H*,9'*H*-[7,2']-bifluoren-2-yl)-10,15,20-tris(4-*t*-butylphenyl)-porphyrin zinc(II) complex (77)**

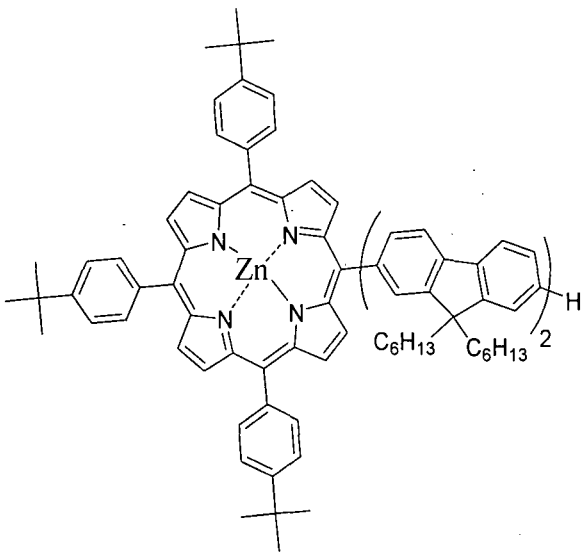


(*t*BuPh)$_3$-H$_2$P-Fl$_2$ **76** (65 mg, 0.05 mmol) and zinc acetate dihydrate (52 mg, 0.24 mmol) were stirred together in degassed anhydrous chloroform (15 mL) at 62 °C for 3 h. The reaction mixture was filtered through silica (eluent DCM) and removal of the solvent *in vacuo* gave **77** (67 mg, 99%) as a pink solid.

M.p.: > 300 °C. $^1$H NMR (500 MHz, $CDCl_3$): δ 9.09-9.00 (8H, m), 8.31-8.24 (2H, m), 8.24-8.16 (6H, m), 8.12 (1H, d, $J$ = 7.3 Hz), 8.06 (1H, d, $J$ = 7.6 Hz), 7.88-7.72 (12H, m), 7.45-7.33 (3H, m), 2.24 (4H, t, $J$ = 7.6 Hz), 2.19-2.04 (4H, m), 1.70-1.60 (27H, m), 1.30-0.65 (44H, m). $^{13}$C NMR (125 MHz, $CDCl_3$): δ 152.0, 151.5, 151.0, 150.39, 150.35, 150.2, 149.2, 141.7, 140.80, 140.78, 140.5, 140.4, 140.3, 140.1, 139.8, 134.33, 134.27, 133.6, 132.1, 132.0, 131.8, 129.7, 127.0, 126.8, 126.3, 126.1, 123.5, 122.9, 121.6, 121.52, 151.45, 121.3, 120.3, 119.9, 119.7, 117.8, 55.5, 55.2, 40.6, 40.4, 34.9, 31.7, 31.6, 31.5, 29.8, 29.7, 24.1, 23.8, 22.7, 22.6, 14.10, 14.05. MALDI-TOF MS (*m/z*): 1432.9 ($M^+$). $C_{100}H_{112}N_4Zn$: calc. C 83.68, H 7.86, N 3.90; found C 83.61, H 8.19, N 3.44.

**~ Fc-yne-Fl-CHO (79a)**

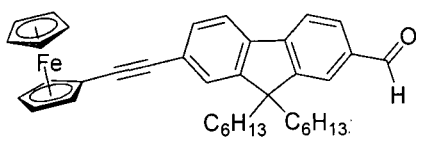


Ethynylferrocene[169] **78** (90 mg, 0.43 mmol) and Br-Fl-CHO **47a** (200 mg, 0.45 mmol) were degassed in diisopropylamine (10 mL). $Pd(OAc)_2$ (*ca.* 2 mg), CuI (*ca.* 2 mg), $PPh_4$ (*ca.* 4 mg) were added and the reaction mixture was stirred overnight at reflux under argon. The reaction mixture was filtered through silica (eluent DCM) and the solvent was evaporated *in vacuo*. Purification by column chromatography (silica gel eluted by 40% DCM in PE 40-60) yielded **79a** (142 mg, 78%) as a red viscous oil.

$^1$H NMR (500 MHz, $CDCl_3$): δ 10.06 (1H, s), 7.88-7.82 (3H, m), 7.73 (1H, d, $J$ = 8.1 Hz), 7.53-7.49 (2H, m), 4.57 (2H, s), 4.31 (7H, s), 2.09-1.95 (4H, m), 1.18-0.97(12H, m), 0.77 (6H, t, $J$ = 7.2 Hz, $CH_3$), 0.68-0.50 (4H, m). $^{13}$C NMR (125 MHz, $CDCl_3$): δ 192.3, 152.2, 151.7, 146.9, 139.1, 135.4, 130.7, 130.6, 125.8, 124.1, 123.0, 120.8, 120.2, 89.6, 86.5, 71.5, 70.1, 69.1, 55.3, 40.2, 31.5, 29.6, 23.7, 22.6, 14.0. MALDI-TOF MS (*m/z*): 570.3 ($M^+$). $C_{38}H_{42}FeO$: calc. C 79.99, H 7.42; found C 80.17, H 7.68.

**~ Fc-yne-$Fl_2$-CHO (79b)**

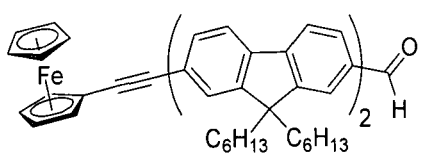


Ethynylferrocene[169] **78** (45 mg, 0.21 mmol) and Br-$Fl_2$-CHO **47b** (250 mg, 0.32 mmol,) were degassed in diisopropylamine (15 mL). $Pd(OAc)_2$ (*ca.* 2 mg), CuI (*ca.* 2 mg), $PPh_4$ (*ca.* 4 mg) were added and the reaction mixture was stirred overnight at reflux under argon. The reaction mixture was filtered through silica (eluent DCM) and the solvent was evaporated *in vacuo*. Purification by column chromatography (silica gel eluted by 40% DCM in PE 40-60) yielded **79b** (45 mg, 23%) as a red viscous oil.

$^1$H NMR (500 MHz, $CDCl_3$): δ 10.09 (1H, s), 7.91-7.87 (4H, m), 7.79 (1H, d, $J$ = 8.1 Hz), 7.72-7.62 (5H, m), 7.53-7.49 (2H, m), 4.57 (2H, s), 4.31 (5H, s), 4.29 (2H,s), 2.15-2.00 (8H, m), 1.18-1.00 (24H, m), 0.81-0.60 (20H, m). $^{13}$C NMR (125 MHz, $CDCl_3$): δ 192.4, 153.0, 151.80, 151.76, 151.0, 147.2, 142.2, 140.34, 140.26, 140.2, 138.7, 135.2, 130.63,

130.59, 126.5, 126.3, 125.7, 123.1, 122.3, 121.6, 121.5, 121.2, 120.2, 120.0, 119.7, 88.4, 86.8, 71.4, 70.1, 68.9, 55.4, 55.3, 40.3, 40.2, 31.5, 31.4, 29.7, 29.6, 23.7, 22.6, 22.5, 14.02, 13.97. MALDI-TOF MS (*m/z*): 902.7 ($M^+$). $C_{63}H_{74}FeO \cdot ½(CH_3CH_2)_2O$: calc. C 83.04, H 8.47; found C 83.16, H 8.49.

**~ Fc-yne-Fl-$C_{60}$ (80a)**

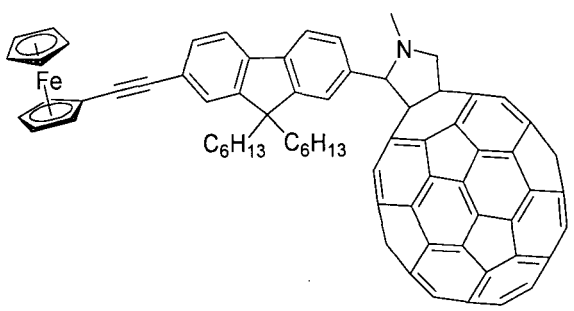


$C_{60}$ (300 mg, 0.42 mmol), Fc-yne-Fl-CHO **79a** (61 mg, 0.11 mmol) and sarcosine (40 mg, 0.45 mmol) were reacted *via* the general 1,3-dipolar cycloaddition procedure for 4 h. Purification by column chromatography using 0-1% DCM in $CS_2$ as eluent, followed by precipitation yielded **80a** (90 mg, 64%) as a black solid.

$^1$H NMR (700 MHz, $CDCl_3$): δ 7.99 (1H, s, br), 7.70 (1H, s, br), 7.63 (1H, d, $J$ = 7.9 Hz), 7.58 (1H, s, br), 7.44 (1H, d, $J$ = 8.1 Hz), 7.41 (1H, s), 5.04 (2H, t, $J$ = 4.6 Hz), 4.55 (2H, s), 4.33 (1H, d, $J$ = 9.5 Hz), 4.30 (5H, s), 4.28 (2H, s), 2.87 (3H, s), 2.18 (1H, s, br), 2.08-1.88 (3H, m, br), 1.26-0.57 (20H, m, br), 0.34 (1H, s, br), 0.16 (1H, s, br). $^{13}$C NMR (125 MHz, $CDCl_3$): δ 156.1, 153.5, 153.4, 147.3, 146.7, 146.5, 146.3, 146.23, 146.19, 146.16, 146.13, 146.10, 146.07, 145.9, 145.7, 145.53, 145.50, 145.4, 145.34, 145.29, 145.24, 145.20, 145.1, 144.7, 144.4, 144.3, 143.1, 143.0, 142.7, 142.5, 142.2, 142.14, 142.11, 142.05, 142.0, 141.9, 141.72, 141.67, 140.2, 140.1, 139.4, 136.5, 135.8, 130.5, 125.6, 119.7, 88.4, 86.8, 83.8, 71.5, 70.1, 70.0, 69.0, 55.2, 40.0, 31.7, 29.8, 23.8, 22.7, 14.14, 14.05. MALDI-TOF MS (*m/z*): 596.4 ($M^+$-$C_{60}$-1, 100%), 517.9 (38%).

**~ Fc-yne-$Fl_2$-$C_{60}$ (80b)**

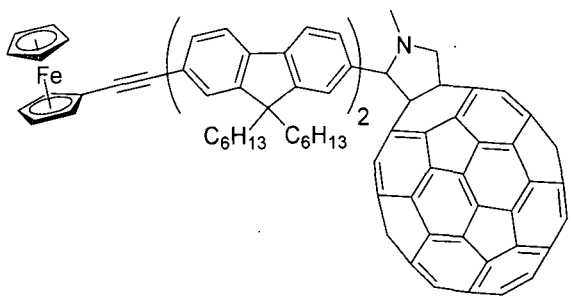


$C_{60}$ (250 mg, 0.35 mmol), Fc-yne-$Fl_2$-CHO **79b** (65 mg, 0.07 mmol) and sarcosine (40 mg, 0.45 mmol) were reacted *via* the general 1,3-dipolar cycloaddition procedure for 4 h. Purification by column chromatography using $CS_2$ as eluent, followed by precipitation yielded **80b** (67 mg, 56%) as a black solid.

$^1$H NMR (700 MHz, $CDCl_3$): δ 8.09 (1H, s, br), 7.84-7.71 (3H, m), 7.71-7.53 (6H, m), 7.53-7.45 (2H, m), 5.09-5.03 (2H, m), 4.57-4.54 (2H, m), 4.34 (1H, d, $J$ = 9.5 Hz), 4.31-4.26 (7H, m), 2.89 (3H, s), 2.23 (1H, s, br), 2.16-1.94 (7H, m, br), 1.28-0.57 (30H, m), 0.78 (12H, t, $J$ = 7.2 Hz), 0.43 (1H, s, br), 0.26 (1H, s, br). $^{13}$C NMR (125 MHz, $CDCl_3$): δ 156.2, 154.0, 153.6, 153.5, 151.7, 151.0, 147.3, 146.8, 146.5, 146.3, 146.23, 146.20, 146.13, 146.10, 146.07, 145.9, 145.7, 145.54, 145.51, 145.48, 145.4, 145.34, 145.29, 145.25, 145.2, 145.1, 144.7, 144.38, 144.35, 143.1, 143.0, 142.7, 142.5, 142.2, 142.14, 142.12, 142.06, 142.0, 141.9, 141.73, 141.67, 140.7, 140.5, 140.2, 140.1, 140.0, 139.7, 139.4, 136.60, 136.58, 135.9, 135.8, 130.5, 129.9, 128.8, 127.1, 126.2, 126.1, 125.7, 122.1, 121.37, 121.33, 120.1, 120.0, 119.6, 88.3, 86.8, 83.8, 71.4, 70.0, 69.0, 68.8, 55.3, 55.2, 40.5, 40.3, 40.1, 31.6, 31.49, 31.47, 31.4, 29.69, 29.67, 23.9, 23.8, 23.7, 22.58, 22.55, 22.5, 14.1, 14.04, 14.02, 14.00. MALDI-TOF MS (*m/z*): 929.6 ($M^+$-$C_{60}$, 100%), 862.1 (16%), 850.1 (39%).

## 7.6 Experimental Procedures for Chapter 5

### ~ *O,O*-Naphthalene-1,5-diyl bis(*N,N*-dimethylcarbamothioate) (81)

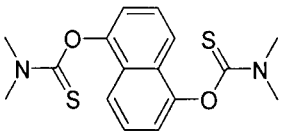

1,5-Dihydroxynaphthalene (15 g, 0.09 mol) in DMF (200 mL) was cooled to 0 °C. 1,4-diazabicyclo[2,2,2]octane (40 g, 0.36 mmol) was slowly added, then *N,N*-dimethylthiocarbamoyl chloride (29 g, 0.24 mmol) was added and the mixture was stirred for 10 min at room temperature. The reaction mixture was then heated at 80 °C for 2 h and subsequently quenched on crushed ice. After filtration, the filtrate was extracted with DCM, the organic layer was washed with $H_2O$, dried over $MgSO_4$ and the solvent was evaporated. The residue was dissolved in DCM (50 mL) and poured into hexane (400 mL). The resulting precipitate was isolated by filtration and washed with hexane to provide the slightly brownish product (*ca.* 21 g). It was purified on a short column (silica gel; DCM), hexane (*ca.* 50 mL) was then added to the DCM solution, and the solution was concentrated to a volume of *ca.* 30-40 mL by removing the solvents on a rotary evaporator. The product was precipitated by adding hexane (*ca.* 50 mL) and filtered off to yield **81** (20.8 g, 66%) as a pale yellow solid.

M.p.: 250-251 °C. $^1$H NMR (400 MHz, $CDCl_3$): δ 7.74 (2H, d, $J$ = 9.0 Hz), 7.51 (2H, t, $J$ = 8.0 Hz), 7.24 (2H, d, $J$ = 8.0 Hz), 3.53 (6H, s), 3.51 (6H, s). $^{13}$C NMR (100 MHz, $CDCl_3$): δ 188.0, 150.3, 129.1, 126.1, 120.4, 120.0, 43.7, 39.1. EI-MS (*m/z*): 334 ($M^+$). $C_{16}H_{18}N_2O_2S_2$: calc. C 57.46, H 5.42, N 8.38, S 19.17; found C 57.44, H 5.40, N 8.43, S 19.14.

### ~ *S,S*-Naphthalene-1,5-diyl bis(*N,N*-dimethylcarbamothioate) (82)

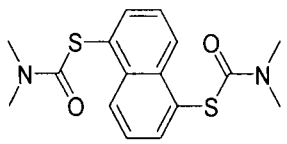

*O,O*-Naphthalene-1,5-diyl bis(*N,N*-dimethylcarbamothioate) **81** (in two separate batches: 3.89 g and 5.28 g, total 27.4 mmol) was heated in a Buchi Glass Oven to 280-300°C and

kept at this temperature for 5 min after all the material was melted. The two separate batches were cooled and combined. The product was separated from starting material and half-converted compound by a column (silica gel) using 0-10% diethyl ether in DCM as eluent. The obtained crude product (6.5 g) was used without further purification in the next reaction step. Pure product was obtained after column chromatography from a small-scale reaction (200 mg of **81**), which yielded **82** (132 mg, 66%) as a white solid.

M.p.: 216-217 °C. $^1$H NMR (400 MHz, $CDCl_3$): δ 8.48 (2H, d, $J$ = 8.5 Hz), 7.80 (2H, d, $J$ = 7.5 Hz), 7.56 (2H, t, $J$ = 8.0 Hz), 3.24 (6H, s, br.), 3.02 (6H, s, br). $^{13}$C NMR (100 MHz, $CDCl_3$): δ 166.6, 136.8, 136.2, 128.9, 127.0, 126.7, 37.3. EI-MS (*m/z*): 334 ($M^+$). $C_{16}H_{18}N_2O_2S_2$: calc. C 57.46, H 5.42, N 8.38, S 19.17; found C 57.42, H 5.39, N 8.39, S 19.13.

### ~ 1,5-Bis(2,2-diethoxyethylthio)naphthalene (84)

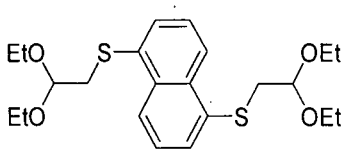


Bromoacetaldehyde diethylacetal (13.5 mL, 90 mol) was added to a mixture of *S,S*-naphthalene-1,5-diyl bis(*N,N*-dimethylcarbamothioate) **82** (10.0 g, 30 mmol), NaI (9.0 g, 60 mol) and sodium ethoxide (45 mL, 21 wt.% in EtOH, 120 mmol) in EtOH (5mL). The mixture was heated at reflux for 65 h and subsequently quenched on crushed ice / DCM (2:1), extracted with DCM, and dried over $MgSO_4$. Solvents were evaporated and the crude product was purified by column chromatography (silica gel, 0-1% diethyl ether in DCM) to afford **84** (10.8 g, 85%) as a yellow solid.

M.p.: 61-63 °C. $^1$H NMR (400 MHz, $CDCl_3$): δ 8.34 (2H, s), 7.50 (4H, m), 4.64 (2H, t, $J$ = 5.5 Hz), 3.56 (8H, m), 3.12 (4H, d, $J$ = 5.5 Hz), 1.17 (12H, t, $J$ = 7.0 Hz). $^{13}$C NMR (100 MHz, $CDCl_3$): δ 135.9, 132.2, 131.8, 126.7, 126.5, 124.6, 124.4, 123.9, 123.6, 102.9, 102.8, 55.1, 41.4, 15.4. EI-MS (*m/z*): 424 ($M^+$). $C_{22}H_{32}O_4S_2$: calc. C 62.23, H 7.60, S 15.10; found C 62.28, H 7.63, S 15.08.

### ~ 1,6-Dithiapyrene (85)

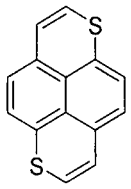

[*NOTE.* All materials needed for the purification were pre-prepared and work-up was done as quickly as possible (usually within two hours)]. $P_2O_5$ (10 g) and $H_3PO_4$ (5 mL, 85% in $H_2O$) were heated at 130 °C in an open flask. After 30 min 1,5-bis(2,2-diethoxyethylthio)naphthalene **84** (5.5 g, 12.9 mmol) was added and the mixture stirred for 15 min. The mixture was quenched into a mixture of ice-water/DCM (1:1) (*ca.* 0.5 L) and to this NaOH (6 M, 100 mL) was added. The organic layer was washed with $H_2O$, dried over $MgSO_4$ with $Et_3N$ (5 mL) added and flushed through a column (basic alumina, DCM). Toluene (50 mL) was added and this solution was concentrated *in vacuo* to *ca.* 5 mL volume. A few drops of $Et_3N$ were added and the mixture was cooled to yield 1,6-dithiapyrene (775 mg, 25%, **85**) as orange needles.

M.p.: 227-229 °C. (M.p. lit.: 228-229 °C)[182] $^1$H NMR (500 MHz, $CDCl_3$ + $CS_2$ + trace $Et_3N$): δ 6.20 (2H, d, $J$ = 7.6 Hz), 6.02 (2H, d, $J$ = 7.7 Hz), 5.74 (2H, d, $J$ = 10.1 Hz), 5.54 (2H, d, $J$ = 10.1 Hz). $^{13}$C NMR (125 MHz, $CDCl_3$ + trace $Et_3N$): δ 133.3, 130.6, 129.7, 124.8, 123.9, 121.1, 120.1. EI-MS (*m/z*): 240 ($M^+$). $C_{14}H_8S_2$: calc. C 69.96, H 3.36, S 26.68; found C 69.92, H 3.34, S 26.74.

### ~ 1,6-Dithiapyrene-5-carboxaldehyde (86)

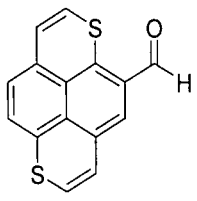

DMF (0.18 mL, 2.3 mmol) was added to a solution of 1,6-dithiapyrene **85** (180 mg, 0.7 mmol) in 1,2-dichloroethane (20 mL) under argon at 0 °C. Phosphorus oxychloride (0.10 mL, 1.1 mmol) was added, the mixture was stirred at 0 °C for 5 min, at reflux (2 h) and then left to stir overnight at room temperature. Phosphate buffer solution (15 mL, pH = 7.2) was added and after stirring for 1 h the mixture was diluted with ethyl acetate (150 mL), washed with brine (2×100 mL) and dried over $MgSO_4$. The mixture was filtered and

concentrated *in vacuo* to a volume of *ca.* 5-10 mL. This was chromatographed (silica gel, toluene) to yield **86** (110 mg, 55%) as a black (dark red/purple) solid.

M.p.: 255–257 °C. $^{1}$H NMR (400 MHz, $CDCl_3$): δ 9.70 (s, 1H), 6.56 (d, $J$ = 7.7 Hz, 1H), 6.45 (s, 1H), 6.38 (d, $J$ = 7.7 Hz, 1H), 6.19 (d, $J$ = 9.9 Hz, 1H), 5.98 (d, $J$ = 10.1 Hz, 1H), 5.82 (d, $J$ = 10.3 Hz, 1H), 5.63 (d, $J$ = 10.3 Hz, 1H). $^{13}$C NMR (125 MHz, $CDCl_3$): δ 189.0, 139.4, 134.9, 133.2, 131.6, 130.5, 129.7, 126.7, 126.0, 125.7, 124.9, 124.51, 124.48, 121.42, 120.9. EI-MS (*m/z*): 268 ($M^+$). $C_{15}H_8OS_2$: calc. C 67.14, H 3.00, S 23.90; found C 67.10, H 3.02, S 23.89.

### ~ *N*-cyclohexyl-1,6-dithiapyrene-5-carboxaldimine (87)

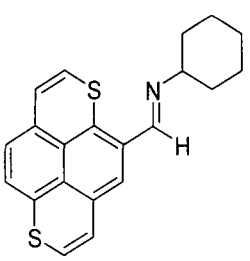


One drop of cyclohexylamine (*ca.* 25 mg) was added to an NMR tube containing 1,6-dithiapyrene-5-carboxaldehyde **86** (7 mg, suspension) in benzene-$d_6$ (0.7 mL) and a trace of $Et_3N$ (one drop of $Et_3N$ was added to 0.5 mL of $C_6D_6$ and only a small drop of this was added to the NMR tube). During 96 h at room temperature the solution became bright red and all material completely dissolved. Completion of the reaction was monitored by $^{1}$H NMR spectroscopy. Solvents were evaporated and residual red solid was dissolved in $CDCl_3$ containing a trace of $Et_3N$. Compound **87** was synthesised solely to provide additional spectroscopic proof for the structure of **86** and **87** was not further purified for these studies.

$^{1}$H NMR (500 MHz, $CDCl_3$): δ 8.14 (s, 1H), 6.59 (s,1H), 6.36 (d, $J$ = 7.81 Hz, 1H), 6.19 (d, $J$ = 7.81 Hz, 1H), 5.95 (d, $J$ = 10.01 Hz, 1H), 5.84 (d, $J$ = 10.25 Hz, 1H), 5.73 (d, $J$ = 10.01 Hz, 1H), 5.60 (d, $J$ = 10.01 Hz, 1H), 3.19-3.07 (m, 1H), 1.86-1.76 (m, 2H), 1.72-1.61 (m, 4H), 1.58-1.47 (m, 2H), 1.41-1.28 (m, 2H). $^{13}$C NMR (125 MHz, $CDCl_3$): δ 154.4, 133.5, 133.4, 132.6, 130.6, 130.2, 129.3, 127.3, 125.2, 124.9, 124.4, 123.2, 122.3, 120.09, 120.05, 70.1, 34.5, 25.6, 24.6. ESI-MS (*m/z*): 350.2 ($M^+$+1).

**~ Dithiapyrene-$C_{60}$ dyad (88)**

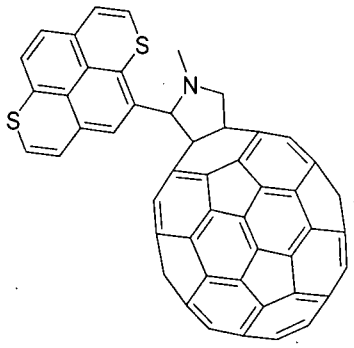


$C_{60}$ (190 mg, 0.26 mmol) was heated to reflux in toluene (80 mL). 1,6-Dithiapyrene-5-carboxaldehyde (35 mg, 0.13 mmol, **86**) and sarcosine (30 mg, 0.34 mmol) were added and the mixture was refluxed for 40 h. The solvent was removed *in vacuo* and the residue was purified by chromatography (silica, $CS_2$ + 2% $Et_3N$) to afford **88** (85 mg, 64%) as a black powder.

$^1H$ NMR (700 MHz, $C_6D_6$): δ 5.94 (d, $J$ = 7.7 Hz, 1H), 5.55 (d, $J$ = 7.9 Hz, 1H), 5.46 (d, $J$ = 10.3 Hz, 1H), 5.28 (d, $J$ = 10.1 Hz, 1H), 5.02 (d, $J$ = 10.1 Hz, 1H), 4.97 (d, $J$ = 10.1 Hz, 1H), 4.93 (s, 1H), 4.35 (d, $J$ = 9.5 Hz, 1H), 4.26 (s, 1H), 3.75 (d, $J$ = 9.3 Hz, 1H), 2.40 (s, 3H). The solubility of **88** is too low to produce an accurate $^{13}C$ NMR spectrum. MALDI-TOF MS (*m/z*): 1015 ($M^+$). $C_{77}H_{13}NS_2$: calc. C 91.02, H 1.29, N 1.38, S 6.31; found C 91.08, H 1.34, N 1.32, S 6.26.

**~ Pyrene-$C_{60}$ dyad (89)**

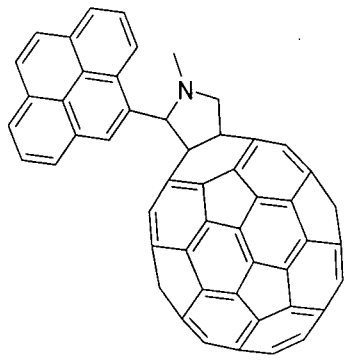


$C_{60}$ (625 mg, 0.87 mmol), pyrene-1-carboxaldehyde (100 mg, 0.43 mmol) and sarcosine (77 mg, 0.86 mmol) were reacted *via* the general 1,3-dipolar cycloaddition procedure for 4 h. Purification by column chromatography using $CS_2$ as eluent, followed by precipitation from hexane yielded **89** (25 mg, 56%) as a black solid.

$^1$H NMR (500 MHz, *o*DCB-$d_4$ + $CS_2$ (≤ 10%) + trace $C_6H_6$): δ 9.01 (d, *J* = 9.3 Hz, 1H), 8.85 (d, *J* = 7.9 Hz, 1H), 8.35 (d, *J* = 9.7 Hz, 1H), 8.14–7.95 (m, 6H), 6.23 (s, 1H), 5.14 (d, *J* = 9.6 Hz, 1H), 4.54 (d, *J* = 9.2 Hz, 1H), 2.91 (s, 3H). Due to restricted rotation around the exocyclic C–C bond between the pyrrolidine ring and the bulky pyrene ring, two thermodynamically stable (at ambient conditions) rotamers are possible for dyad **89**, which according to DFT calculations are of similar energies (Appendix E). They are formed in a ratio of *ca.* 10:1 and are not separable by column chromatography. The second rotamer is clearly visible in the $^1$H NMR spectrum as minor signals (Appendix D): δ 10.56 (d, *J* = 8.1 Hz, 1H), 8.32 (d, *J* = 9.4 Hz, 1H), 8.24 (d, *J* = 8.2 Hz, 1H), 8.20-8.17 (m, 2H), 8.14-7.95 (m, 4H), 5.71 (s, 1H), 5.18 (d, *J* = 9.4 Hz, 1H), 4.37 (d, *J* = 9.5 Hz, 1H), 2.96 (s, 3H). $^{13}$C NMR (125 MHz, *o*DCB-$d_4$ + $CS_2$ + trace $C_6H_6$): δ 156.8, 154.22, 154.15, 153.8, 147.5, 147.1, 146.9, 146.5, 146.42, 146.37, 146.3, 146.2, 146.1, 145.9, 145.84, 145.76, 145.72, 145.69, 145.6, 145.5, 145.40, 145.39, 145.3, 144.9, 144.7, 144.6, 144.5, 143.3, 143.2, 142.9, 142.8, 142.69, 142.68, 142.59, 142.56, 142.5, 142.4, 142.23, 142.18, 142.1, 142.0, 141.9, 141.72, 141.65, 140.6, 140.5, 139.8, 137.0, 136.8, 136.2, 136.0, 131.7, 131.4, 131.1, 128.3, 126.5, 126.0, 125.7, 125.5, 125.3, 123.7, 78.7, 70.5, 69.8, 40.4. MALDI-TOF MS (*m/z*): 976.1 ($M^+$-1).

## 7.7 Experimental Procedures for Chapter 6

### ~ *t*BuS-Ph-Fl-CHO (94a)

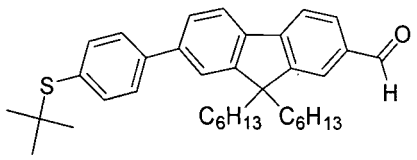


*t*-Butyl(4-bromophenyl)sulfide[214] **93** (140 mg, 0.57 mmol), BE-Fl-CHO **48a** (220 mg, 0.45 mmol), $K_2CO_3$ (510 mg, 2.17 mmol) and $PdCl_2(PPh_3)_2$ (0.01 g) were reacted *via* standard Suzuki-Miyaura cross-coupling. Purification using 0%-50% DCM in hexane as eluent yielded **94a** (160 mg, 67%) as a clear oil.

$^1$H NMR (400 MHz, $CDCl_3$): δ 10.07 (1H, s), 7.92-7.80 (4H, m), 7.71-7.56 (6H, m), 2.12-1.99 (4H, m), 1.35 (9H, s), 1.14-0.96 (12H, m), 0.75 (6H, t, $J$ = 7.0 Hz), 0.79-0.55 (4H, m).

$^{13}$C NMR (100 MHz, $CDCl_3$): δ 192.3, 153.0, 151.8, 141.5, 139.2, 137.9, 135.4, 132.1, 130.6, 127.2, 126.4, 123.1, 121.6, 121.3, 120.1, 55.4, 46.2, 40.2, 31.4, 31.0, 29.6, 23.8, 22.5, 13.9. HRMS, calc. for $C_{36}H_{46}OS$ 526.3269; found 526.3271. $C_{36}H_{46}OS \cdot ½H_2O$: calc. C 80.70, H 8.84; found C 80.11, H 8.73.

### ~ *t*BuS-Ph-$Fl_2$-CHO (94b)

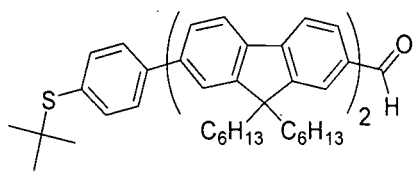


*t*-Butyl(4-bromophenyl)sulfide[214] **93** (141 mg, 0.57 mmol), 2,7-bis(4,4,5,5-tetramethyl-1,3,2-dioxaborolan-2-yl-9,9-dihexyl-9*H*-fluorene[135] **46** (402 mg, 0,68 mmol), Br-Fl-CHO **47a** (351 mg, 0.79 mmol), $K_2CO_3$ (750 mg, 5.43 mmol) and $PdCl_2(PPh_3)_2$ (0.01 g) were reacted *via* standard Suzuki-Miyaura cross-coupling. Purification using 20% DCM in hexane as eluent yielded CHO-$Fl_3$-CHO **52b** (170 mg, 24%) as a yellow solid and **94b** (350 mg, crude, *ca.* 45%). *t*BuS-Ph-$Fl_2$-CHO (**94b**) was further purified using column chromatography over silica gel with 20-50% DCM in hexane used as eluent. Some product was lost due to a human error to yield 140 mg (24%) of *t*BuS-Ph-$Fl_2$-CHO (**94b**) as a yellow viscous oil.

$^1$H NMR (400 MHz, $CDCl_3$): δ 10.08 (1H, s), 7.91-7.79 (6H, m), 7.71-7.59 (10H, m), 2.12-2.05 (8H, m), 1.35 (9H, s), 1.15-1.02 (24H, m), 0.76 (12H, t, $J$ = 7.0 Hz), 0.78-0.60 (8H, m). $^{13}$C NMR (100 MHz, $CDCl_3$): δ 192.3, 153.0, 151.9, 151.8, 147.3, 142.3, 141.9, 140.3, 140.2, 139.3, 138.7, 137.8, 135.3, 130.6, 127.1, 126.5, 126.3, 126.1, 123.1, 121.6, 121.54, 121.46, 121.2, 120.1, 112.0, 55.42, 55.37, 46.1, 40.4, 40.2, 31.4, 31.2, 31.0, 29.7, 29.6, 23.8, 22.52, 22.49, 14.0, 13.9. HRMS, calc. for $C_{61}H_{78}SO$ 858.5773; found 585.5774. $C_{61}H_{78}OS$: calc. C 85.26, H 9.15; found C 85.13, H 9.15.

**~ *t*BuS-Ph-Fl-$C_{60}$ (95a)**

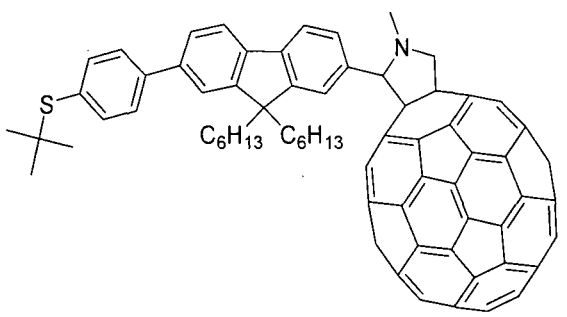


$C_{60}$ (200 mg, 0.28 mmol), *t*BuS-Ph-Fl-CHO **94a** (37 mg, 0.07 mmol) and sarcosine (50 mg, 0.56 mmol) were reacted *via* the general 1,3-dipolar cycloaddition procedure for 4 h. Purification by column chromatography using 0-50% DCM in $CS_2$ as eluent, followed by centrifugation yielded **95a** (50 mg, 56%) as a black solid.

$^1$H NMR (300 MHz, $CDCl_3$): δ 8.08-7.92 (1H, s, br), 7.90 (2H, d, $J$ = 9.0 Hz), 7.80-7.55 (7H, m), 5.07 (2H, d, $J$ = 8.5 Hz), 4.35 (1H, d, $J$ = 9.0 Hz), 2.90 (3H, s, br), 2.25-1.90 (4H, m, br), 1.35 (9H, s), 1.30-0.10 (22H, m, br). $^{13}$C NMR (75 MHz, $CDCl_3$): δ 156.6, 154.4, 154.1, 152.2, 152.1, 147.7, 146.9, 146.7, 146. 7, 146.64, 146.63, 146.58, 146.54, 146.52, 146.4, 146.2, 145.99, 145.95, 145.92, 145.88, 145.8, 145.73, 145.69, 145.64, 145.57, 145.1, 144.82, 144.79, 143.5, 143.4, 143.1, 143.0, 142.7, 142.59, 142.57, 142.49, 142.46, 142.31, 142.25, 142.2, 142.1, 140.8, 140.61, 140.57, 139.8, 139.7, 138.3, 136.3, 136.2, 131.9, 127.5, 126.4, 121.7, 120.6, 84.2, 70.4, 69.4, 55.7, 46.5, 40.5, 32.0, 31.4, 30.2, 24.3, 23.1, 14.6, 14.5. MALDI-TOF MS (*m/z*): 1272.5 ($M^+$-1).

**~ *t*BuS-Ph-Fl$_2$-C$_{60}$ (95b)**

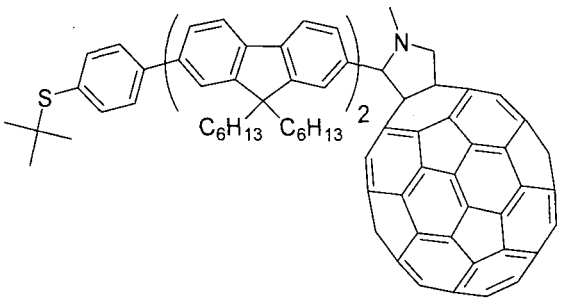


$C_{60}$ (200 mg, 0.28 mmol), *t*BuS-Ph-Fl$_2$-CHO **94b** (60 mg, 0.07 mmol) and sarcosine (35 mg, 0.39 mmol) were reacted *via* the general 1,3-dipolar cycloaddition procedure for 4 h. Purification by column chromatography using 0-20% DCM in $CS_2$ as eluent, followed by centrifugation yielded **95b** (87 mg, 77%) as a black solid.

$^1$H NMR (300 MHz, $CDCl_3$): δ 8.10-7.85 (1H, s, br), 7.80 (4H, t, $J$ = 7.5 Hz), 7.64 (11H, t, $J$ = 7.9 Hz), 5.08 (2H, d, $J$ = 9.0 Hz), 4.35 (1H, d, $J$ = 9.6 Hz), 2.91 (3H, s, br), 2.15-1.90 (8H, m, br), 1.37 (9H, s), 0.77 (12H, t, $J$ = 6.6 Hz), 1.30-0.10 (32H, m, br). $^{13}$C NMR (75 MHz, $CDCl_3$): δ 152.2, 152.1, 147.7, 147.2, 146.9, 146.74, 146.65, 146.59, 146.55, 146.5, 146.4, 146.2, 146.00, 145.96, 145.93, 145.89, 145.8, 145.74, 145.70, 145.66, 145.6, 145.1, 144.9, 144.83, 144.80, 143.5, 143.4, 143.1, 143.0, 142.7, 142.60, 142.58, 142.50, 142.47, 142.4, 142.3, 142.2, 142.1, 142.0, 141.8, 141.1, 141.0, 140.9, 140.62, 140.58, 140.4, 140.3, 139.8, 139.5, 138.3, 137.1, 136.31, 136.25, 131.9, 127.6, 126.6, 126.50, 126.47, 121.8, 121.7, 120.5, 84.3, 70.5, 69.5, 55.7, 46.5, 41.0, 40.8, 40.5, 32.1, 32.0, 31.9, 31.4, 30.14, 30.09, 24.2, 23.3, 23.04, 22.98, 14.6, 14.5, 14.4. MALDI-TOF MS (*m/z*): 1605.6 ($M^+$, 19%), 886.8 ($M^+$-$C_{60}$+1, 100%).

**~ AcS-Ph-Fl-$C_{60}$ (96a)**

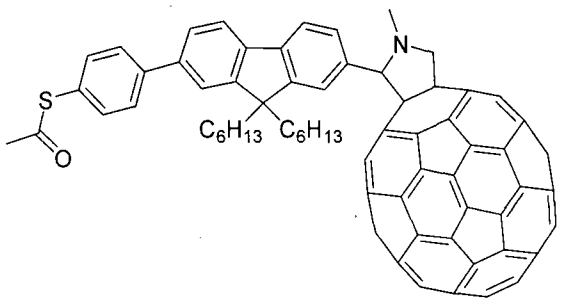


*t*BuS-Ph-Fl-$C_{60}$ **95a** (30 mg, 0.02 mmol) was stirred in dry toluene (5 mL) and acetyl chloride (2 mL). $BBr_3$ (0.4 mL, 1.0 M in DCM, 0.4 mmol) was added to the mixture, which was subsequently stirred for 2 h. The mixture was quenched on crushed ice and extracted with DCM. The organic layer was washed with $H_2O$ and dried over $MgSO_4$. Purification by column chromatography (silica gel eluted by 40% hexane in DCM) yielded **96a** (25 mg, 84%) as a dark brown / black solid.

$^1$H NMR (500 MHz, $CDCl_3$): δ 8.09-7.95 (1H, s, br), 7.76 (2H, d, $J$ = 8.0 Hz), 7.71 (2H, d, $J$ = 8.5 Hz), 7.64-7.48 (5H, m), 5.06 (2H, d, $J$ = 9.0 Hz), 4.34 (1H, d, $J$ = 9.5 Hz), 2.90 (3H, s, NC$H_3$, br), 2.47 (3H, s, COC$H_3$), 2.30-1.90 (8H, m, br), 1.40-0.10 (22H, m, br). $^{13}$C NMR (125 MHz, $CDCl_3$): δ 194.5, 156.4, 154.3, 153.8, 153.7, 152.0, 147.57, 147.56, 147.1, 146.8, 146.6, 146.52, 146.48, 146.45, 146.42, 146.39, 146.37, 146.2, 146.0, 145.83, 145.79, 145.77, 145.7, 145.63, 145.58, 145.54, 145.49, 145.4, 145.0, 144.71, 144.66, 144.6, 143.4, 143.3, 143.04, 142.96, 142.8, 142.5, 142.43, 142.41, 142.33, 142.30, 142.2, 142.01, 141.97, 141.8, 141.4, 140.8, 140.5, 140.4, 140.1, 139.7, 139.4, 136.91, 136.86, 136.14, 136.07, 135.1, 128.2, 126.8, 126.3, 121.7, 120.4, 84.1, 70.3, 69.3, 55.6, 40.8, 40.3, 32.0, 31.9, 30.5, 23.0, 24.11, 24.08, 23.1, 22.9, 14.4, 14.3. MALDI-TOF MS (*m/z*): 1260.3 ($M^+$+1).

**~ AcS-Ph-$Fl_2$-$C_{60}$ (96b)**

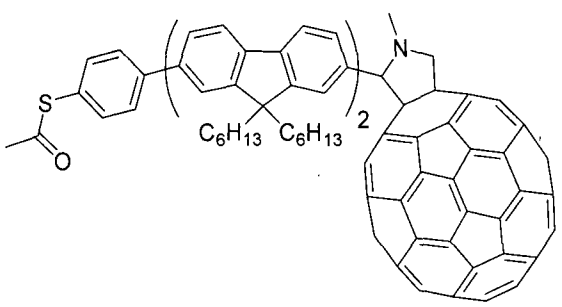


*t*BuS-Ph-$Fl_2$-$C_{60}$ **95b** (43 mg, 0.03 mmol) was stirred in dry toluene (5 mL) and acetyl chloride (0.9 mL). $BBr_3$ (0.05 mL, 1.0M in DCM, 0.05 mmol) was added to the mixture, which was subsequently stirred for 2 h. The mixture was quenched on crushed ice and extracted with DCM. The organic layer was washed with $H_2O$ and dried over $MgSO_4$. Purification by column chromatography (silica gel eluted by 40% hexane in DCM) yielded **96b** (29 mg, 68%) as a dark brown / black solid.

$^1$H NMR (400 MHz, $CDCl_3$): δ 8.07-7.94 (1H, s, br), 7.84-7.54 (13H, m), 7.54 (2H, d, $J$ = 8.0 Hz), 5.05 (2H, d, $J$ = 9.2 Hz), 4.33 (1H, d, $J$ = 9.6 Hz), 2.88 (3H, s, NC$H_3$, br), 2.46 (3H, s, COC$H_3$), 2.15-1.96 (8H, m, br), 0.75 (12H, t, J = 6.8 Hz), 1.30-0.10 (32H, m, br).

$^{13}$C NMR (100 MHz, $CDCl_3$): δ 194.5, 156.4, 154.3, 153.8, 152.1, 152.0, 151.9, 147.6, 147.1, 146.8, 146.6, 146.51, 146.47, 146.41, 146.37, 146.35, 146.2, 146.0, 145.82, 145.78, 145.76, 145.7, 145.62, 145.56, 145.52, 145.48, 145.4, 144.9, 144.7, 144.6, 143.4, 143.2, 143.1, 142.9, 142.8, 142.5, 142.4, 142.33, 142.29, 142.2, 142.0, 141.9, 140.8, 140.44, 140.40, 140.2, 140.0, 139.7, 139.1, 136.9, 136.13, 136.06, 135.1, 128.2, 126.7, 126.4, 121.9, 121.6, 121.5, 120.3, 84.1, 70.3, 69.3, 55.6, 40.8, 40.6, 40.3, 31.8, 31.7, 31.2, 30.5, 29.9, 24.0, 23.1, 22.9, 22.8, 14.4, 14.31, 14.26. MALDI-TOF MS (*m/z*): 1593.4 ($M^+$+2, 37%), 1098.6 (86%), 1053.5 (50%) 872.6 ($M^+$-$C_{60}$+1, 100%), 786.6 (69%), 800.5 (47%), 829.6 (40%).

# Appendix A: NMR Spectroscopy of DTPY-CHO (86)

Abbreviations used in Figure A.1 for proton signals:

| | |
|---|---|
| A | H-17 |
| B | H-9 |
| C | H-15 |
| D | H-8 |
| E | H-6 |
| F | H-5 |
| G | H-13 |
| H | H-12 |

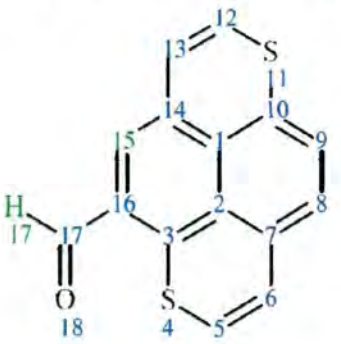


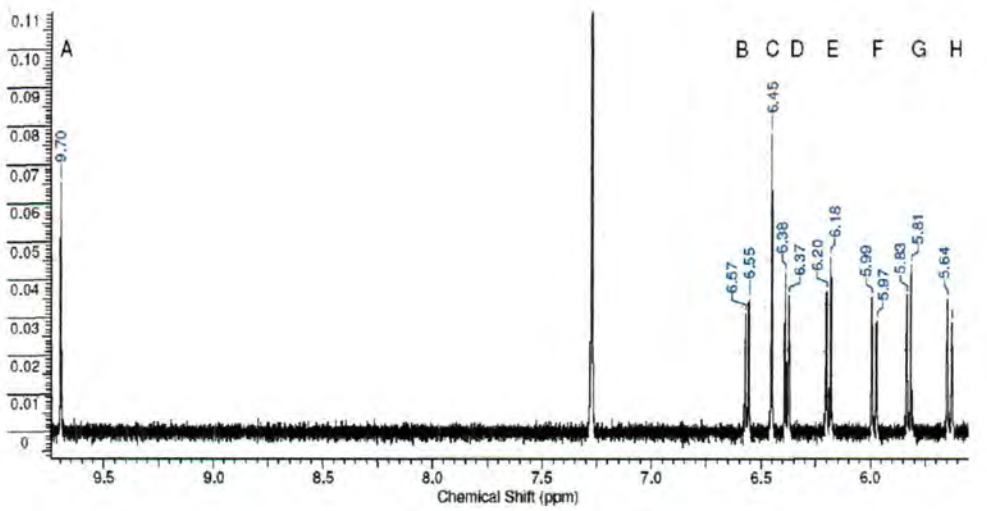


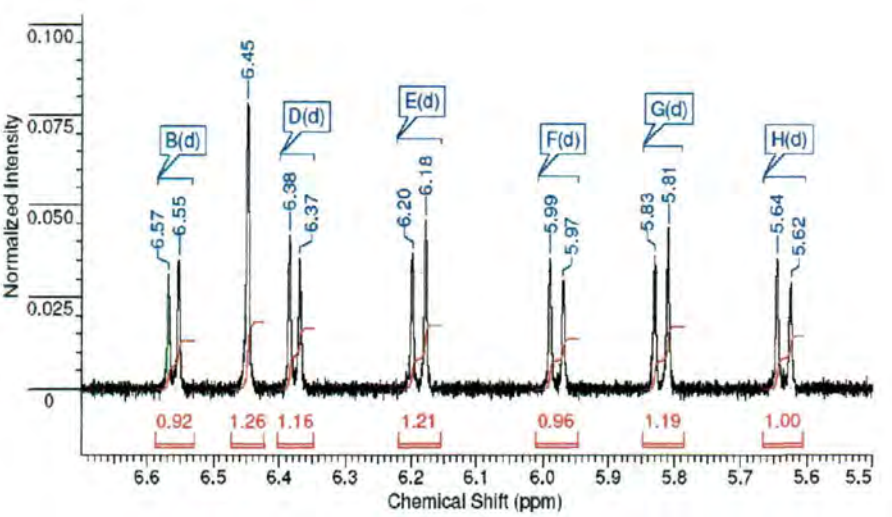


Figure A.1: $^1$H-NMR spectrum (top and bottom) of **86**; 400 MHz, $CDCl_3$ containing a trace of $Et_3N$.

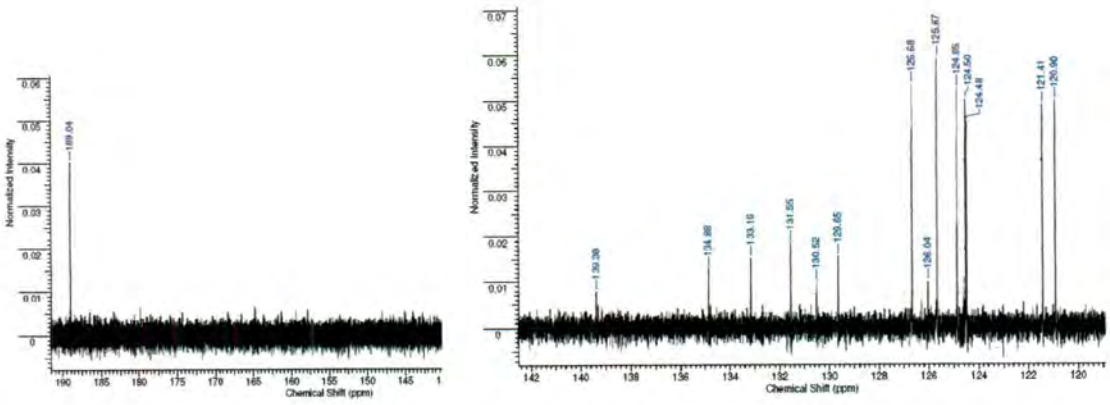


Figure A.2: $^{13}$C-NMR spectrum of **86**; 125 MHz, $CDCl_3$ containing a trace of $Et_3N$.

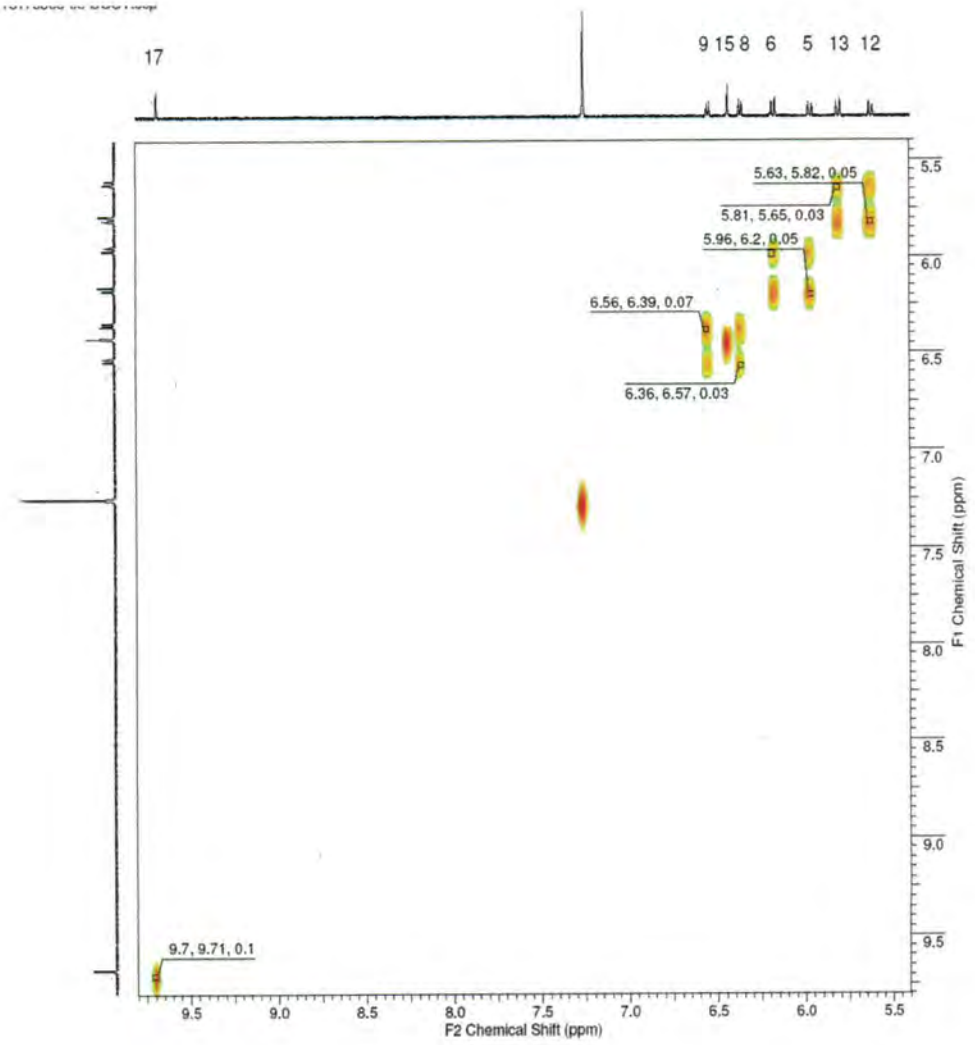


Figure A.3: $^1$H-$^1$H COSY NMR spectrum of **86**; 500/500 MHz, $CDCl_3$ containing a trace of $Et_3N$.

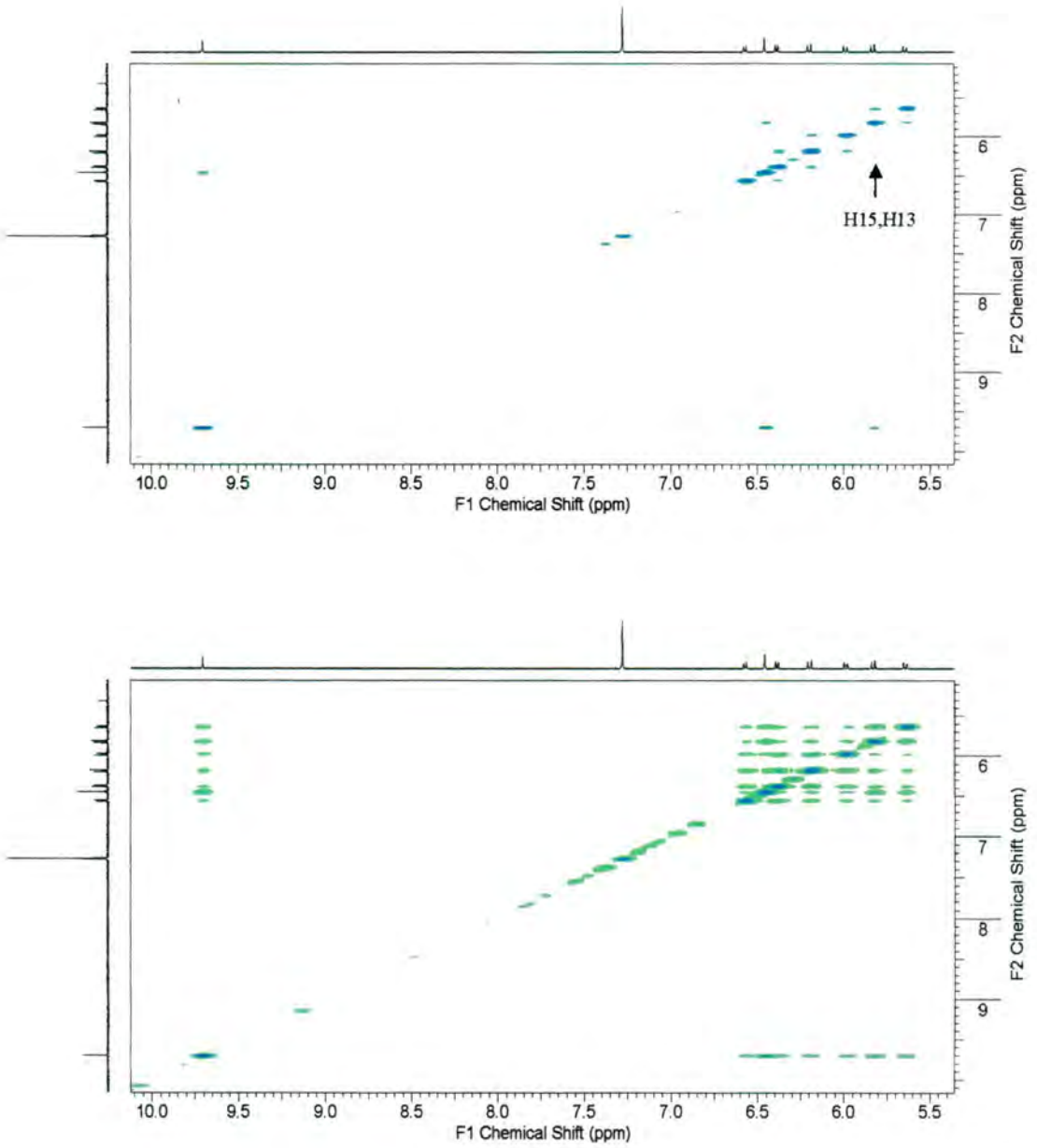


Figure A.4: $^{1}H$-$^{1}H$ NOESY NMR spectrum of **86** at different thresholds; 500/500 MHz, $CDCl_3$ containing a trace of $Et_3N$.

Although the NOESY spectrum (top) does show an interaction between H-13 and H-15, the data is not conclusive. Lowering the threshold slightly provided a very different NOESY spectrum (bottom), which showed aggregation between the molecules.

# Appendix B: NMR Spectroscopy of 87

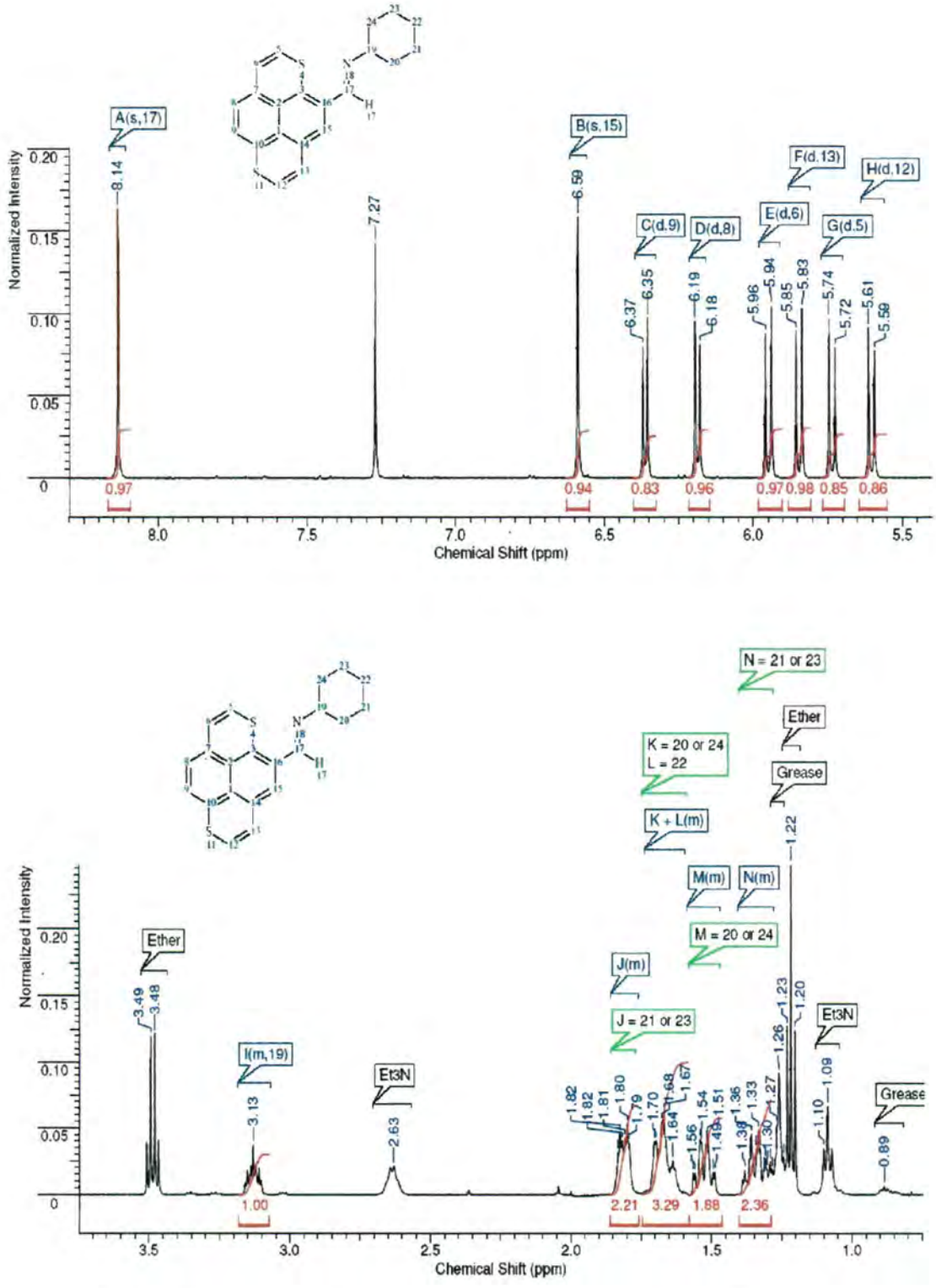


Figure B.1: $^{1}$H-NMR spectrum (top and bottom) of **87**; 500 MHz, $CDCl_3$.

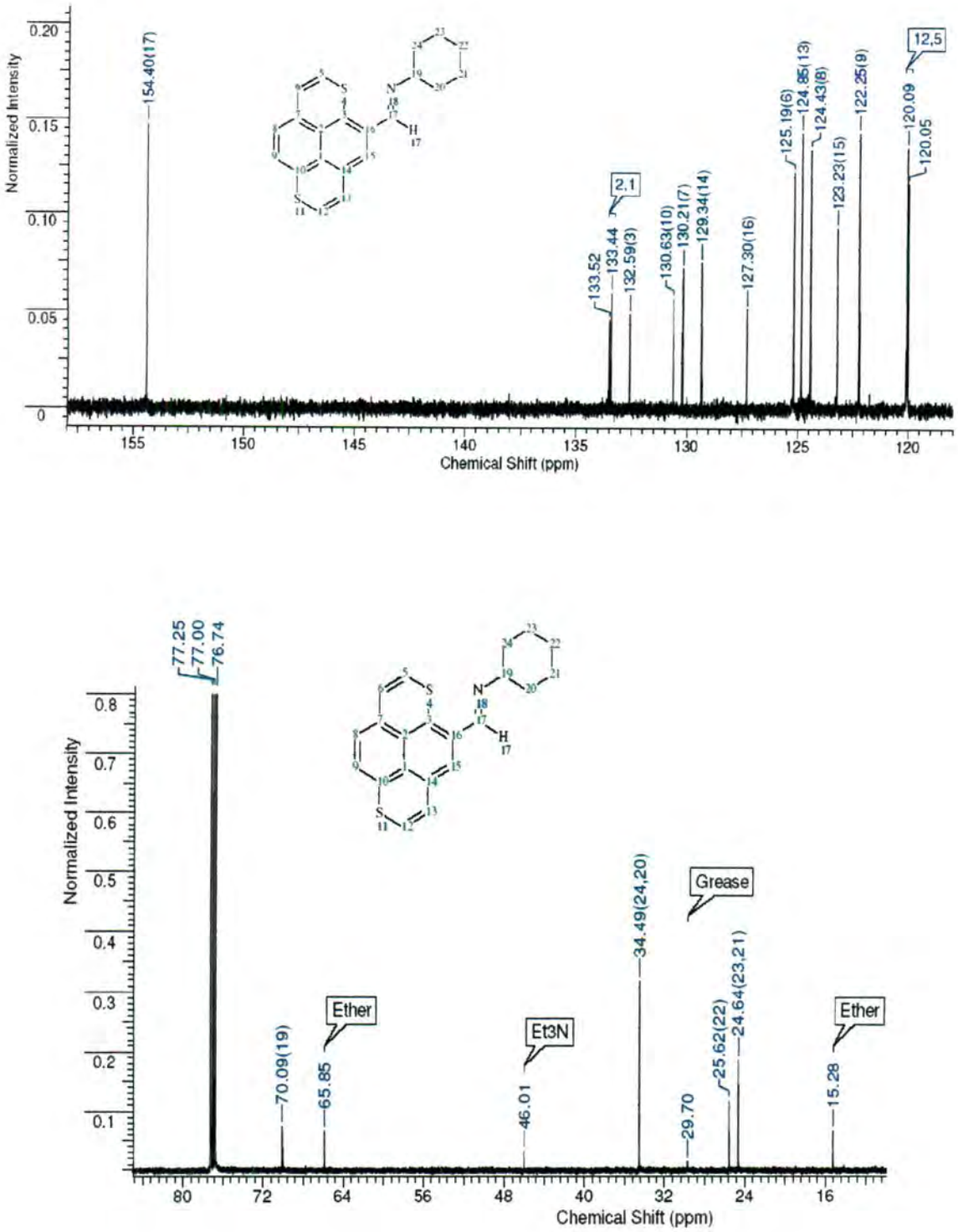


Figure B.2: $^{13}$C-NMR spectrum (top and bottom) of **87**; 125 MHz, $CDCl_3$.

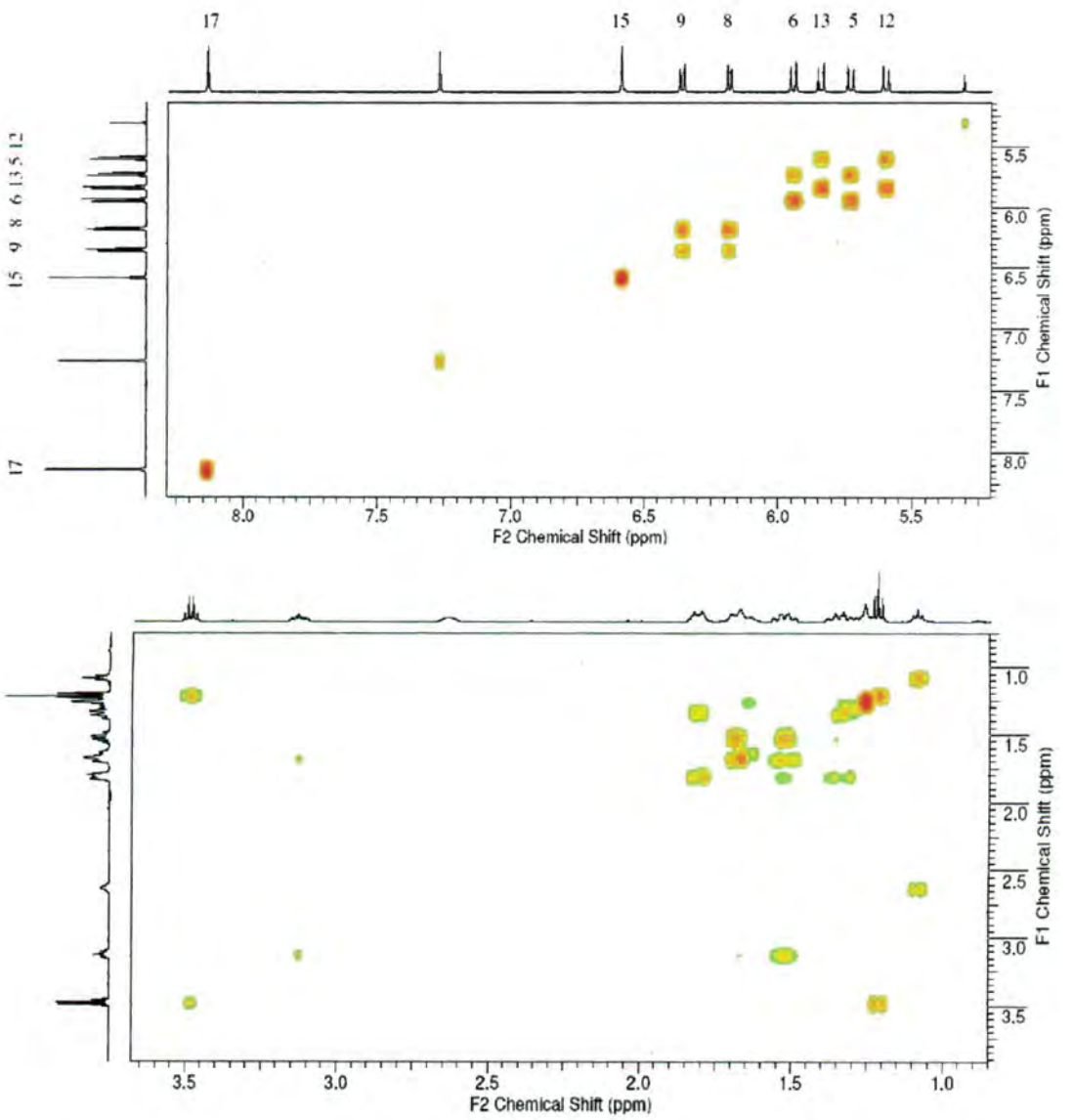


Figure B.3: $^{1}H$-$^{1}H$ COSY NMR spectrum (top and middle) of **87**; 500/500 MHz, $CDCl_3$.

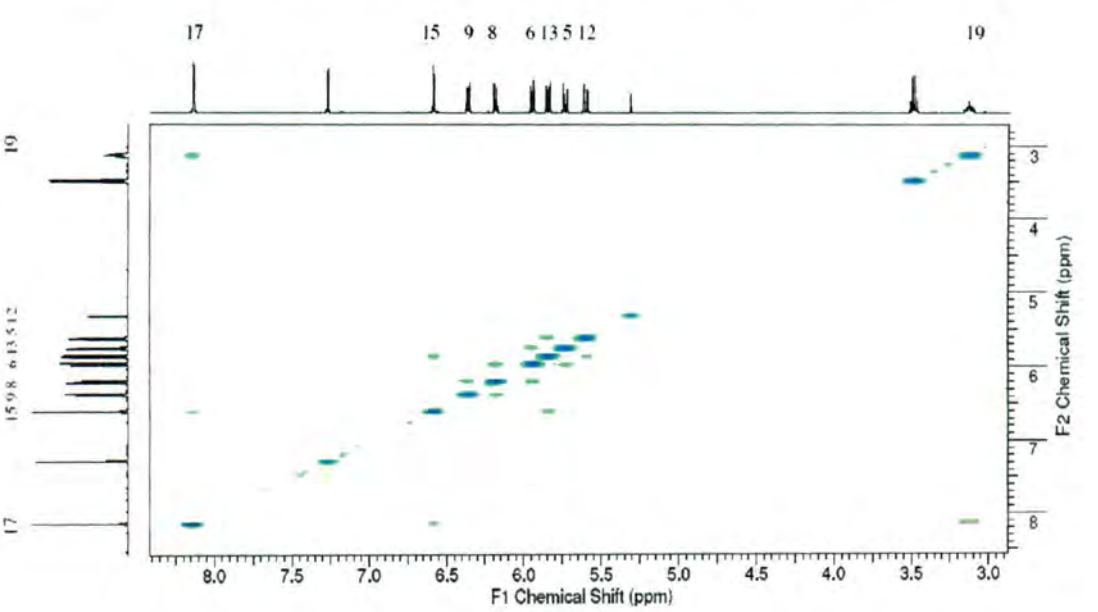

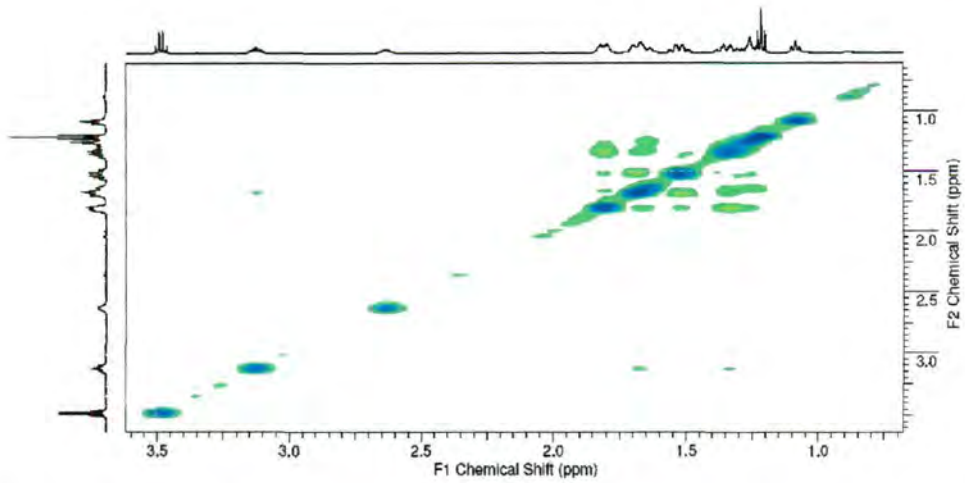


Figure B.4: $^{1}$H-$^{1}$H NOESY NMR spectrum (bottom previous page and top) of **87**; 500/500 MHz, $CDCl_3$.

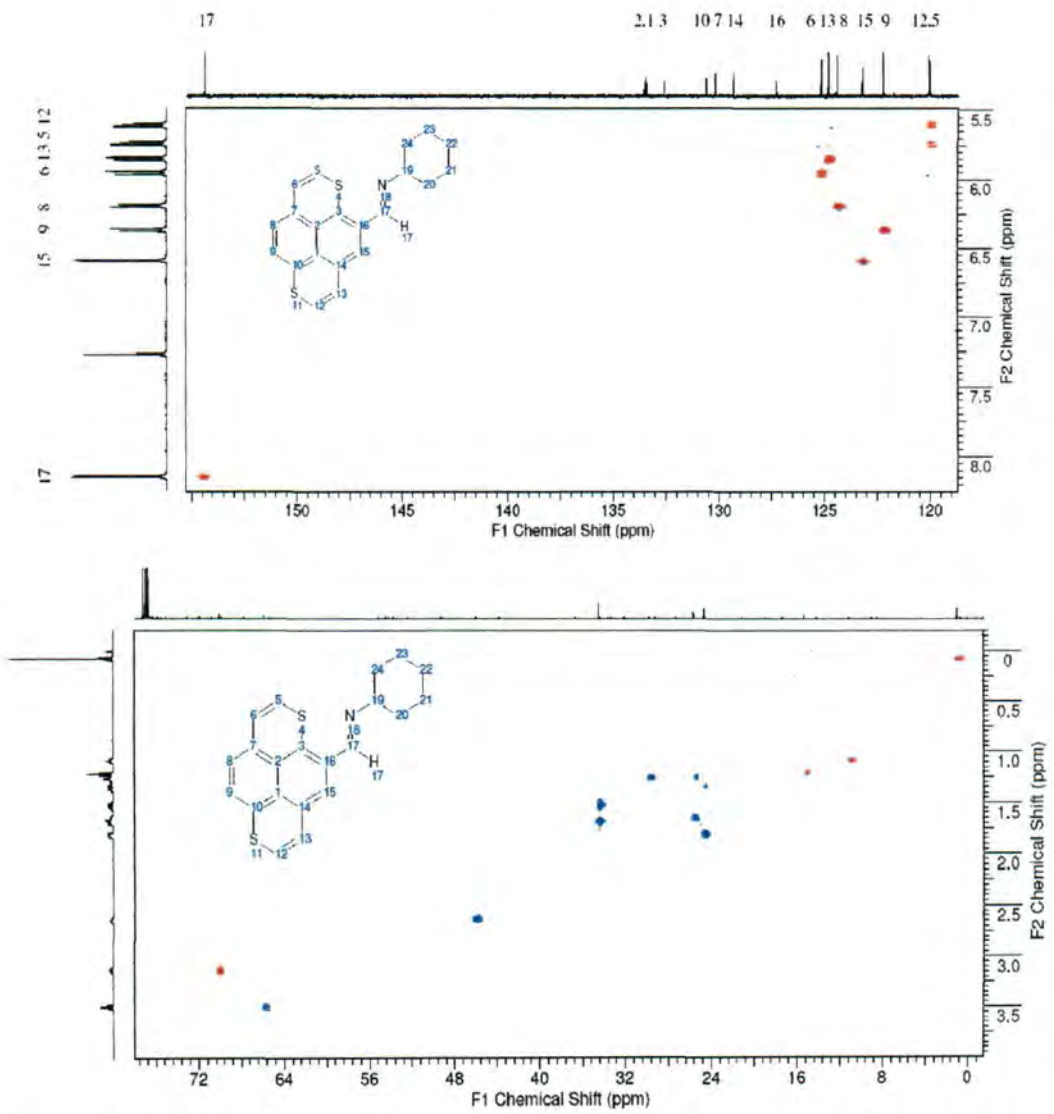


Figure B.5: $^{1}$H-$^{13}$C HSQC NMR spectrum (middle and bottom) of **87**; 500/125 MHz, $CDCl_3$.

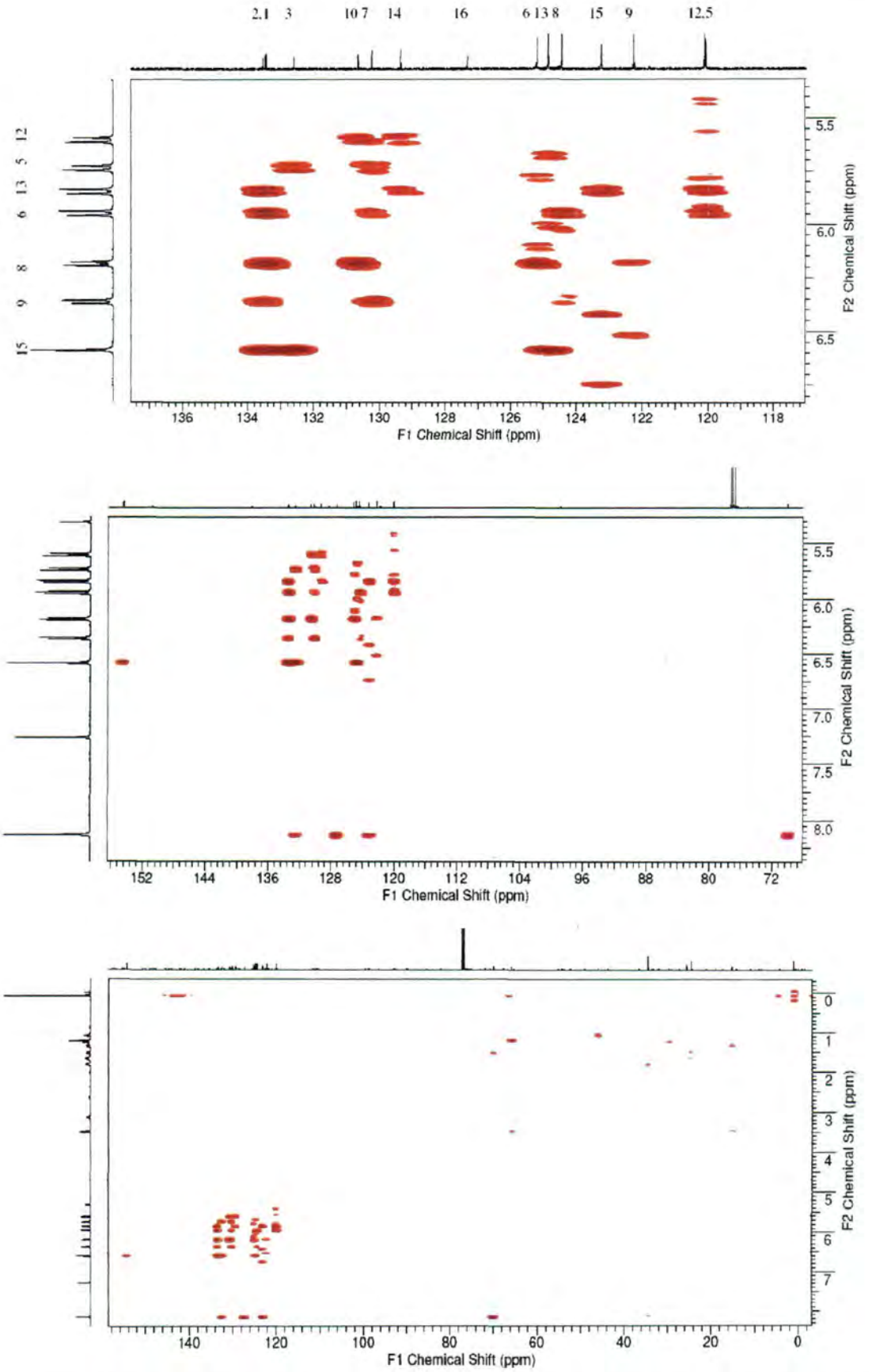


Figure B.6: $^{1}H$-$^{13}C$ HMBC NMR spectrum (top, middle and bottom) of **87**; 500/125 MHz, $CDCl_3$ (HMBC contains satellite peaks).

# Appendix C: NMR Spectroscopy of DTPY (85)

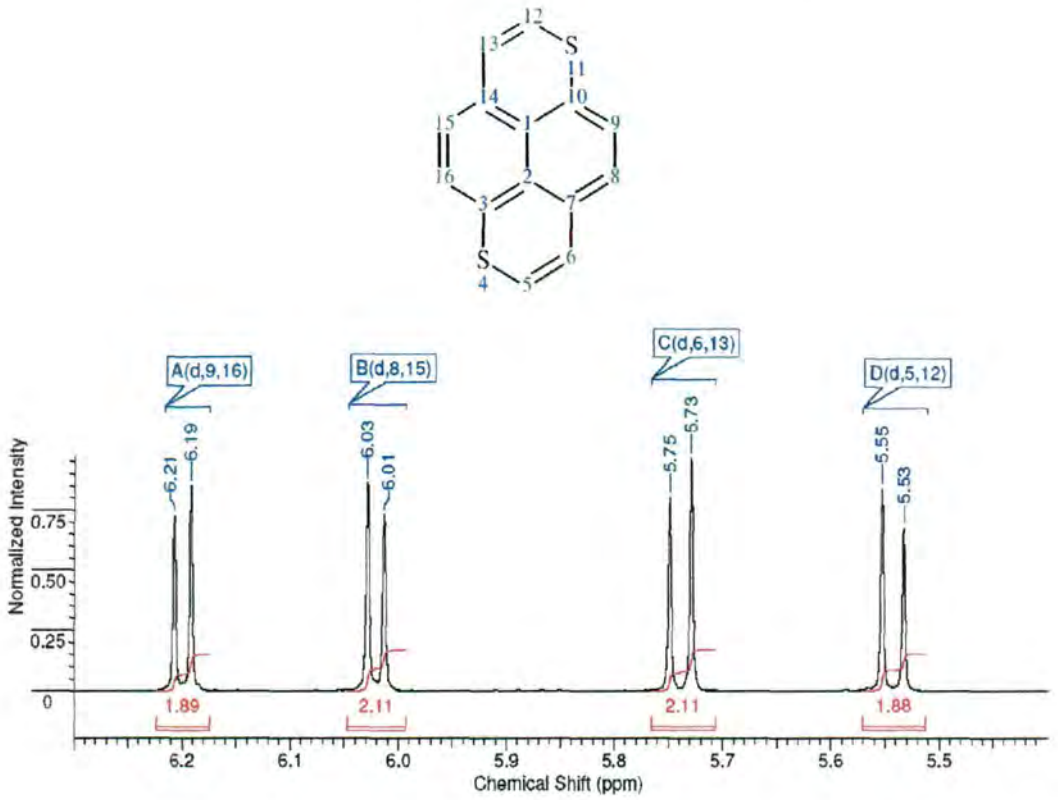


Figure C.1: $^{1}$H-NMR spectrum of **85**; 500 MHz, $CDCl_3$ containing some $CS_2$ and a trace of $Et_3N$.

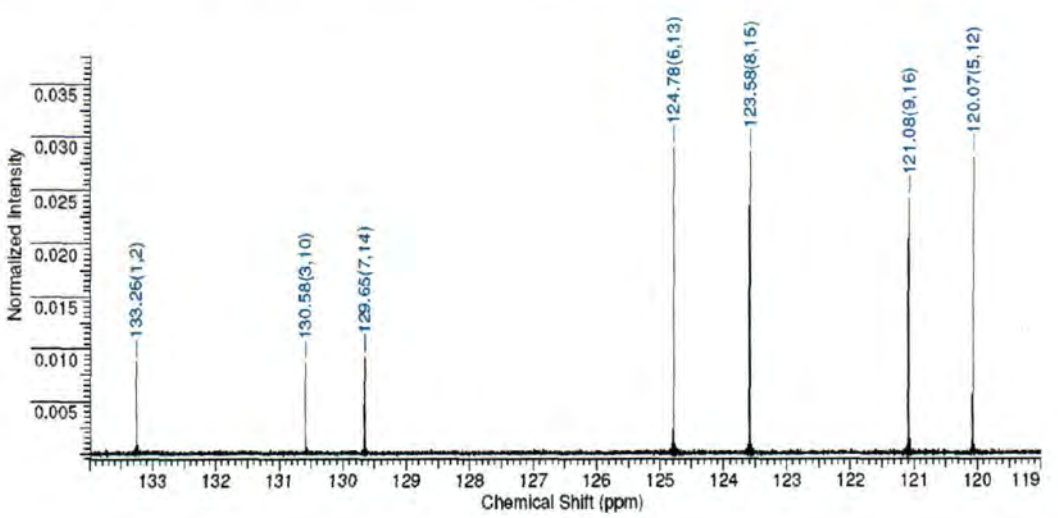


Figure C.2: $^{13}$C-NMR spectrum of **85**; 125 MHz, $CDCl_3$ containing some $CS_2$ and a trace of $Et_3N$.

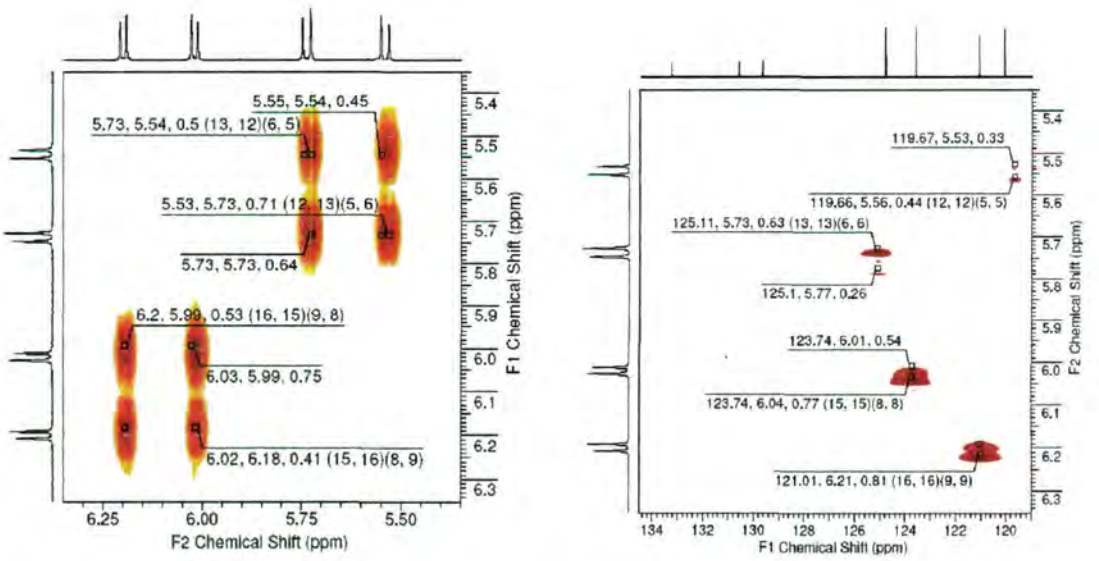


Figure C.3 and C.4: $^{1}H$-$^{1}H$ COSY NMR (left, 500/500 MHz) and $^{1}H$-$^{13}C$ HSQC NMR (right, 500/125 MHz) spectra of **85**; both in $CDCl_3$ containing some $CS_2$ and a trace of $Et_3N$.

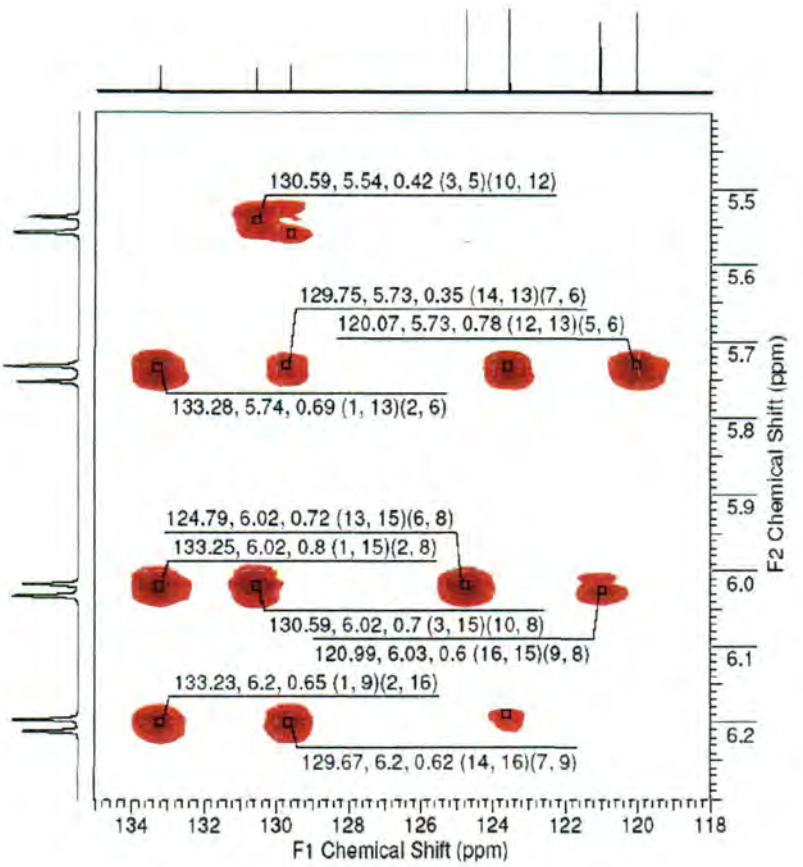


Figure C.5: $^{1}H$-$^{13}C$ HMBC NMR spectrum of **85**; 500/125 MHz, $CDCl_3$ containing some $CS_2$ and a trace of $Et_3N$.

# Appendix D: $^1$H-NMR Spectrum of Pyrene-$C_{60}$ (89)

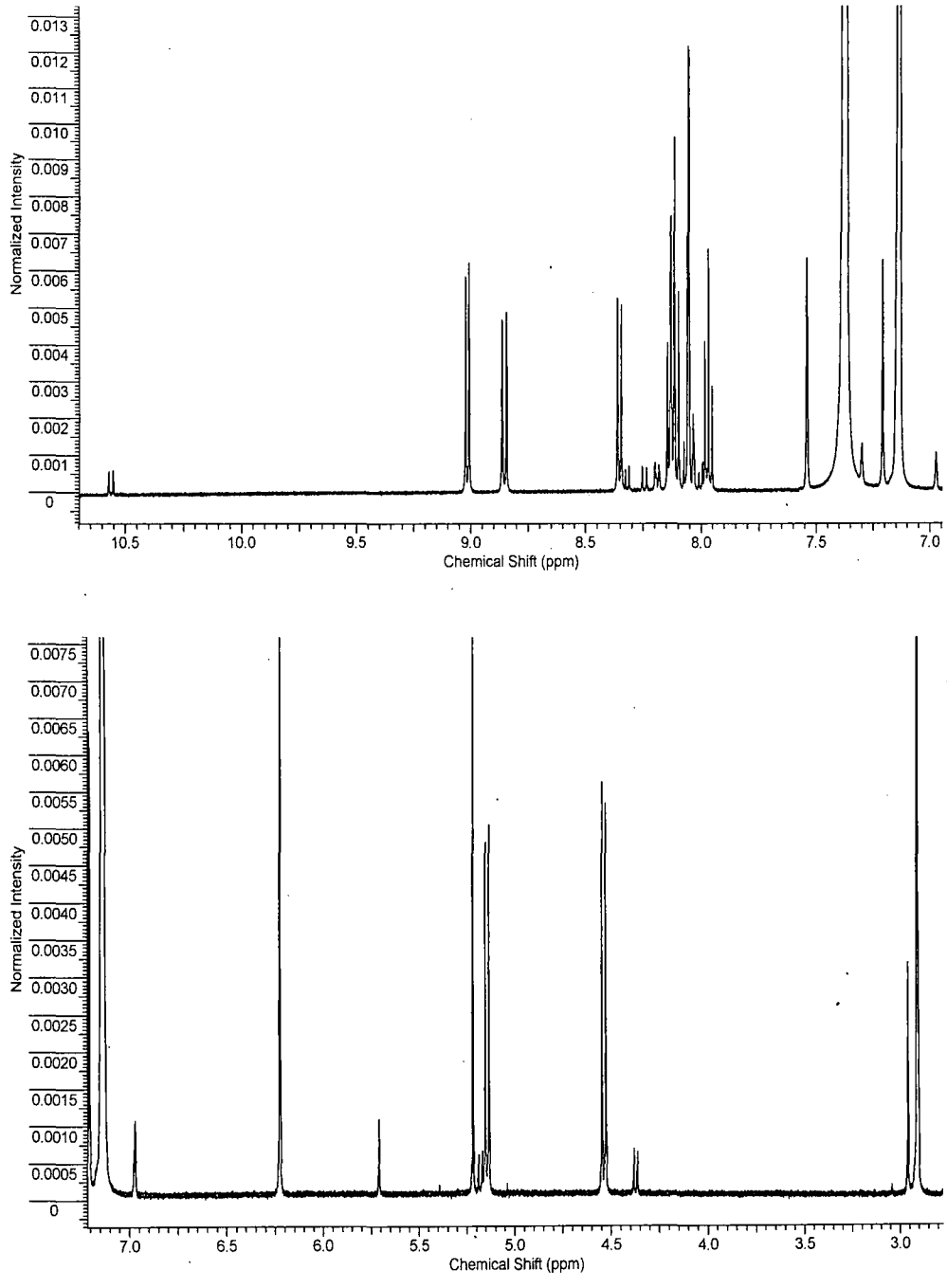


Figure D.1: $^1$H-NMR spectrum (top and bottom) of **89**; 500 MHz, *o*-DCB-$d_6$ containing some $CS_2$ and a trace of $C_6H_6$ (as internal reference).

The second rotamer is clearly visible in the $^1$H NMR spectrum as minor signals. The ratio between the two thermodynamically stable (at ambient conditions) rotamers is *ca.* 10:1.

# Appendix E: DFT Calculations

Taking into account that DFT calculations predict a low HOMO-LUMO gap for dyad **88** of ~1.5 eV (Figure E.1), we performed calculations on compound **88** at a spin-unrestricted level. The UB3LYP/6-31G(d) optimised geometry of the triplet state of **88** showed, however, higher energy than that for the singlet state. Due to the bulky donor moieties in DTPY-$C_{60}$ and pyrene-$C_{60}$ dyads being closely spaced to $C_{60}$, the rotation around the acyclic single C–C bond between the donor fragment and pyrrolidine ring is hindered. The large rotation barrier results in an existence of two rotamers, one of which differs from another by ~180° turn of the donor moieties. We optimised the geometries for both rotamers and data for the lower energy structures are discussed in Chapter 5. At B3LYP/6-31G* (d) level of theory, the calculated difference in total energies between the rotamers are 2.96 kcal $mol^{-1}$ and 6.38 kcal $mol^{-1}$ for DTPY-$C_{60}$ and pyrene-$C_{60}$ dyads, respectively (please note that the lower energy rotamers are enumerated in Chapter 5 and here in Appendix E as **88** and **89**, whereas higher energy rotamers as **88r** and **89r**). The optimised structures of both rotamers for both series of dyads (**88**, **88r** and **89**, **89r**) are shown in Figure E.2.

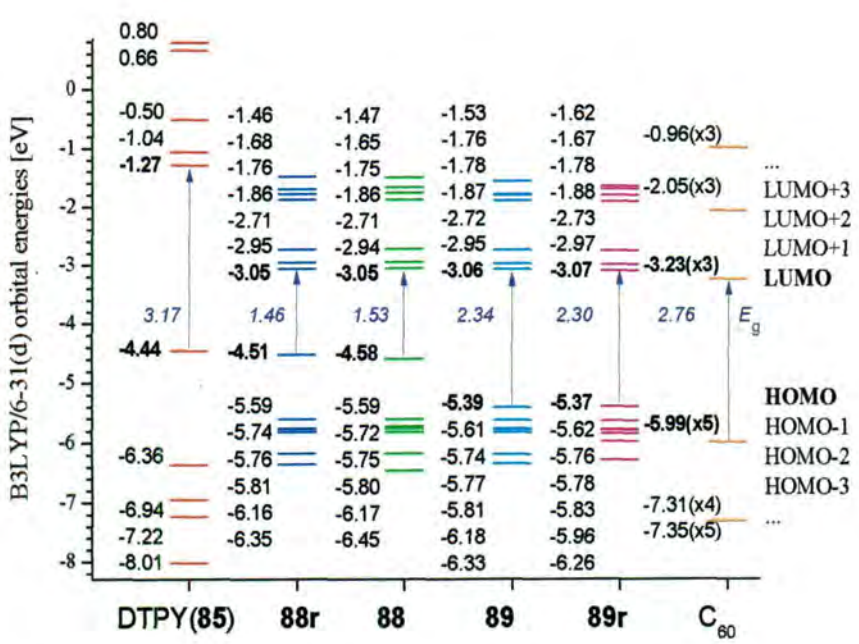


Figure E.1: Frontier orbitals energy levels of dyads **88** and **89** in comparison with those of DTPY (**85**) and $C_{60}$ from DFT B3LYP/6-31G* (d) calculations in gas phase.

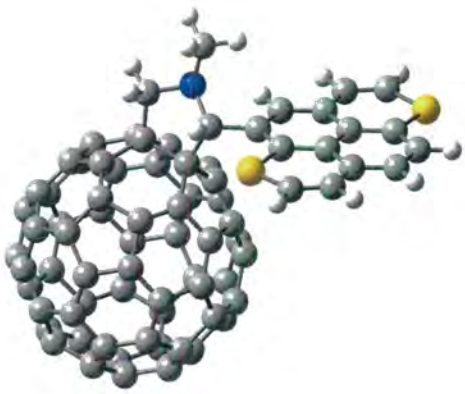

**88**

$E_{total}$ = -3792.9360598 Hartree

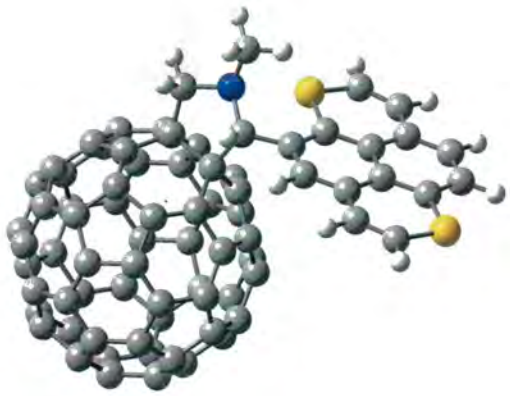

**88r**

$E_{total}$ = -3792.9313359 Hartree

$\Delta E$ (**88r** - **88**) = +2.96 kcal mol$^{-1}$

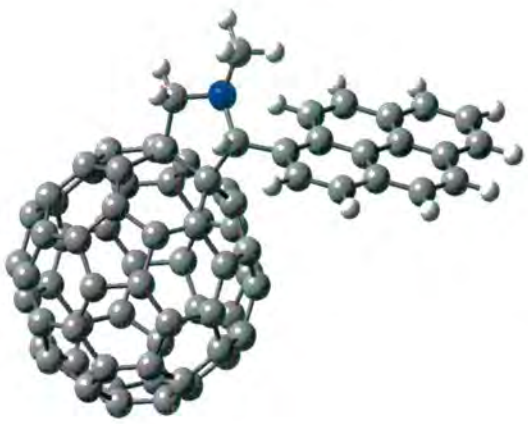

**89**

$E_{total}$ = -3074.0246028 Hartree

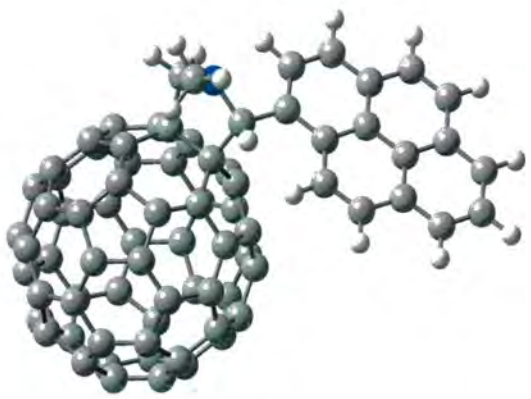

**89r**

$E_{total}$ = -3074.0144325 Hartree

$\Delta E$ (**89r** - **89**) = +6.38 kcal mol$^{-1}$

Figure E.2: B3LYP/6-31G* (d) optimised geometries for two rotamers of DTPY-$C_{60}$ (**88**, **88r**) and pyrene-$C_{60}$ (**89**, **89r**) dyads, their total energies and differences in the energies between the rotamers.

Both rotamers in DTPY-$C_{60}$ and pyrene-$C_{60}$ dyads have very close total energies in their optimised geometries, and similar frontier orbital energies (Figure E.1) and orbital coefficients (Figure E.3 shows orbital coefficients for the lowest energy rotamers, **88** and **89**). Turning the donor moieties in rotamers almost has no effect on the LUMO energy levels (as the LUMOs are localised on $C_{60}$ moiety), and slightly affect the HOMO energies

resulting in small differences in their HOMO–LUMO energy gaps (0.07 eV and 0.04 eV for DTPY-$C_{60}$ and pyrene-$C_{60}$ dyads, respectively; Figure E.1).

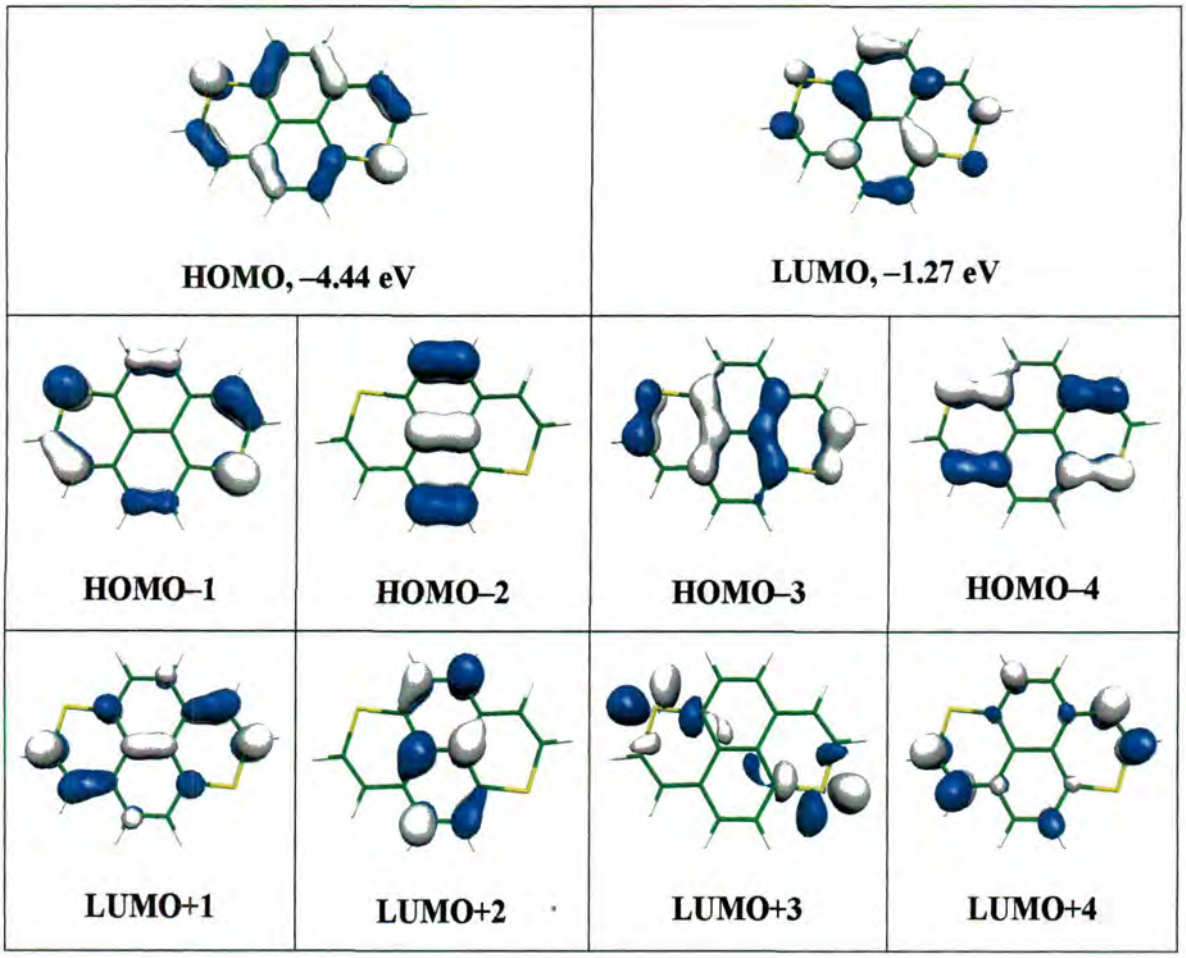


Figure E.3: Orbital contour plots for the five highest occupied MOs and the five lowest unoccupied MOs in DTPY (**85**).

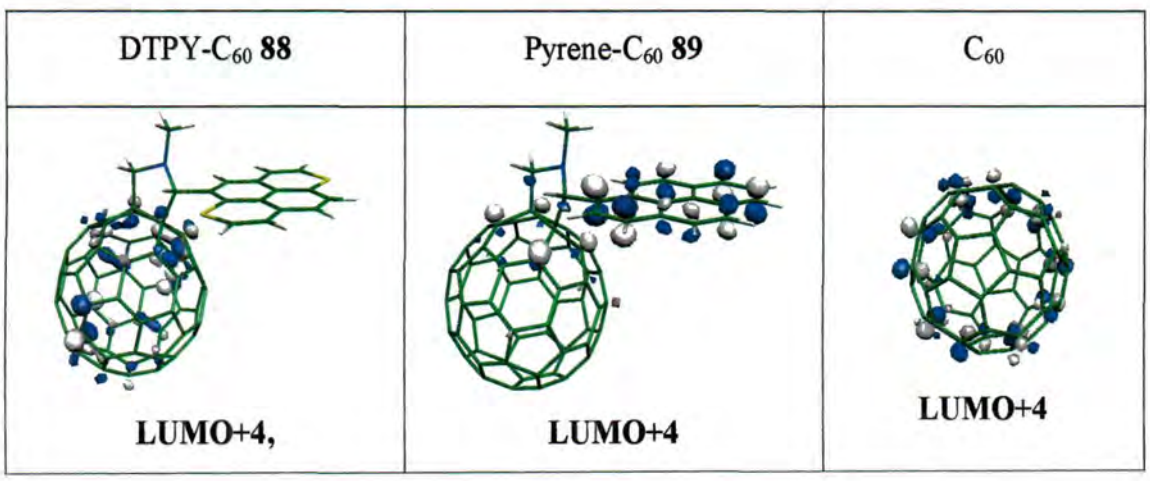

| | | |
|---|---|---|
| 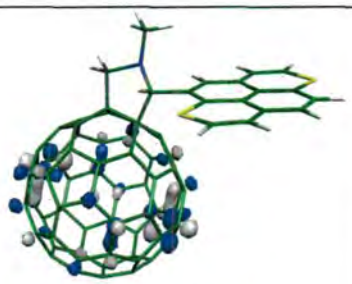 **LUMO+3** | 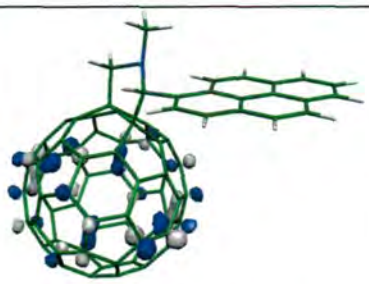 **LUMO+3** | 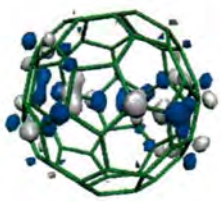 **LUMO+3** |
| 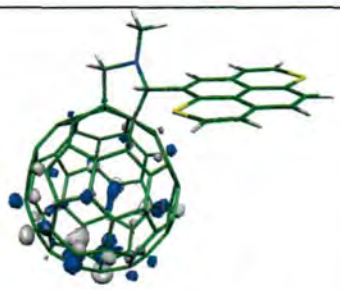 **LUMO+2** | 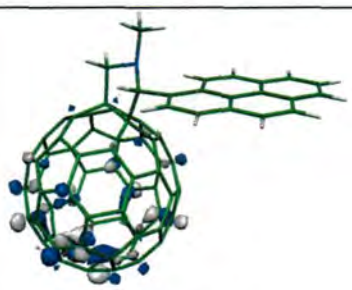 **LUMO+2** | 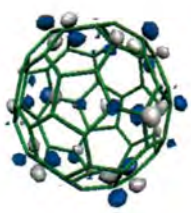 **LUMO+2** |
| 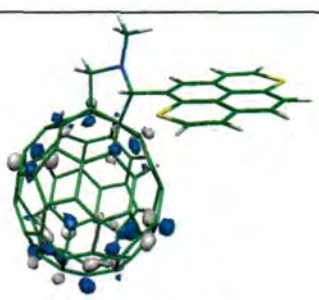 **LUMO+1** | 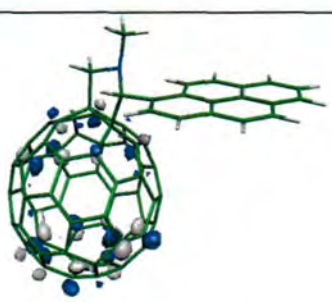 **LUMO+1** | 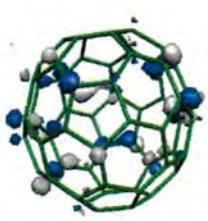 **LUMO+1** |
| 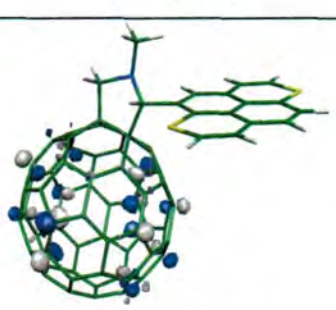 **LUMO, –3.05 eV** | 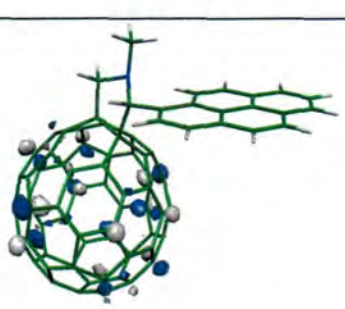 **LUMO, –3.06 eV** | 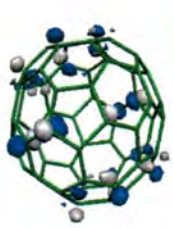 **LUMO, –3.23 eV** |
| 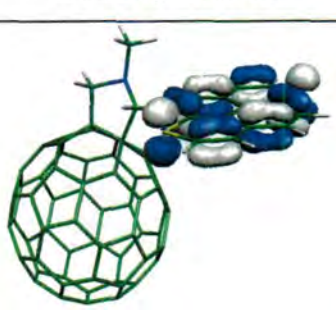 **HOMO, –4.58 eV** | 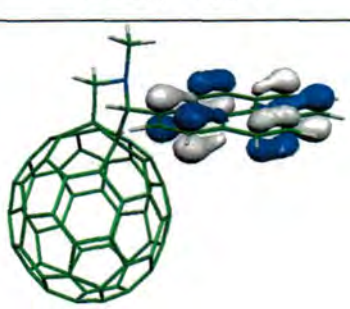 **HOMO, –5.39 eV** | 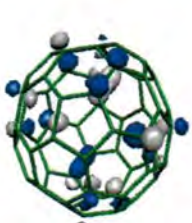 **HOMO, –5.99 eV** |

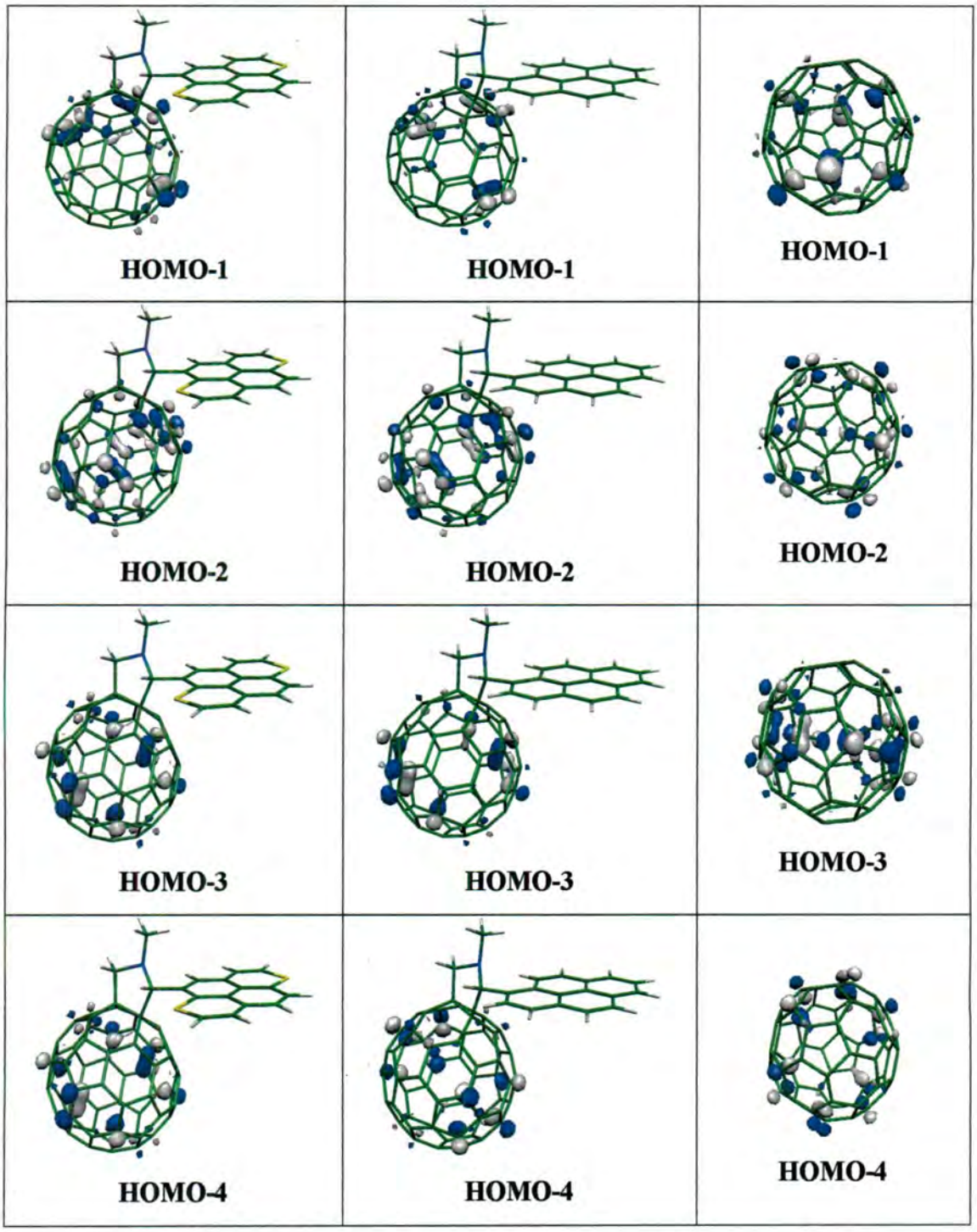


Figure E.4: Orbital contour plots for the five highest occupied MOs and the five lowest unoccupied MOs in dyads DTPY-$C_{60}$ (**88**) and pyrene-$C_{60}$ (**89**) and in $C_{60}$.

# Appendix F: CVs of DTPY-$C_{60}$ (88)

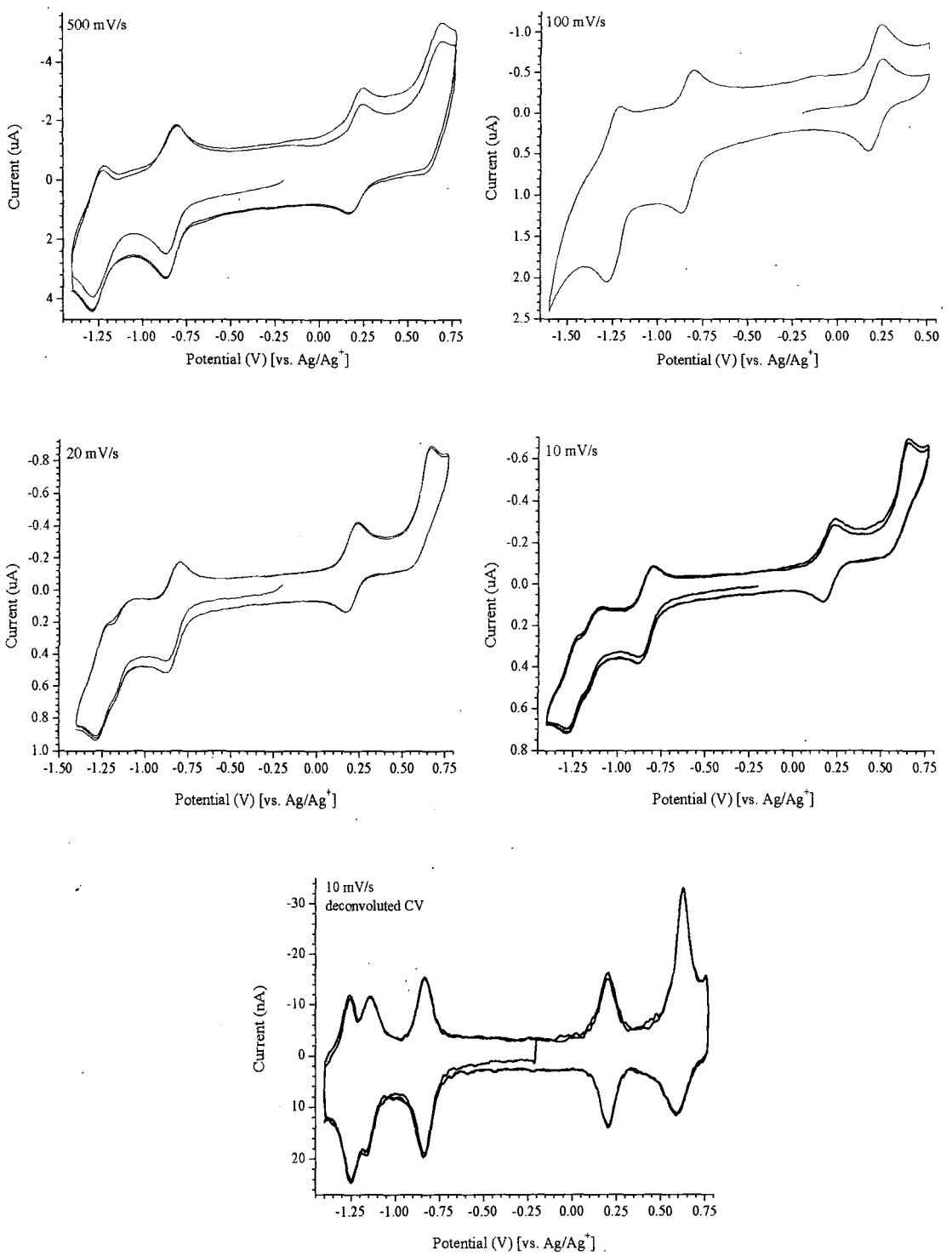


Figure F.1: CVs of dyad DTPY-C60 (88) in PhCN, 0.1 M $Bu_4NPF_6$, at different scan rates (500, 100, 20 and 10 mV $s^{-1}$) and deconvoluted CV ($E^1_{½,\,ox}$ = 0.204 V, $E^2_{½,\,ox}$ = 0.628 V, $E^1_{½,\,red}$ = -0.835 V, $E^2_{½,\,red}$ = -1.151 V, $E^3_{½,\,red}$ = -1.250 V).

# Appendix G: UV-Vis Spectra of DTPY-$C_{60}$ (88)

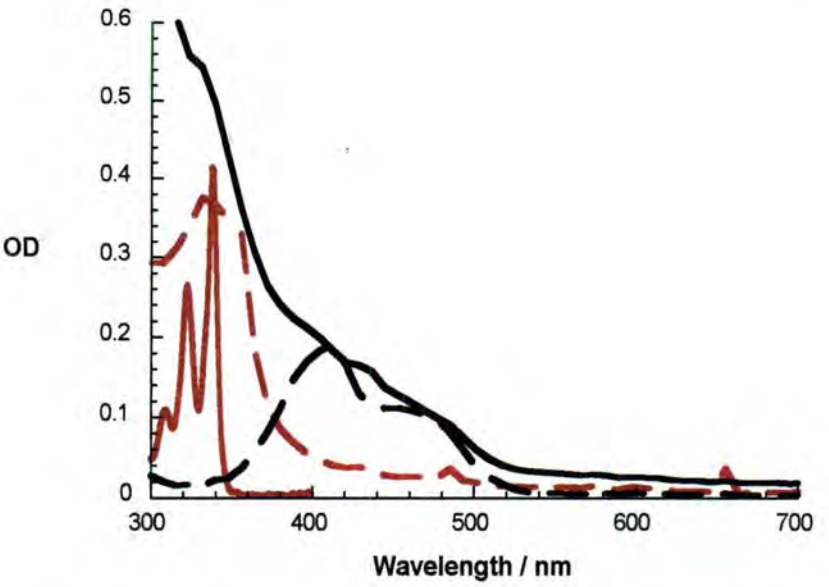


Figure G.1: UV-visible spectra of DTPY **85** (dashed black spectrum), DTPY-$C_{60}$ **88** (solid black spectrum), pyrene (solid red spectrum) and pyrene-$C_{60}$ **89** (dashed red spectrum) in toluene.

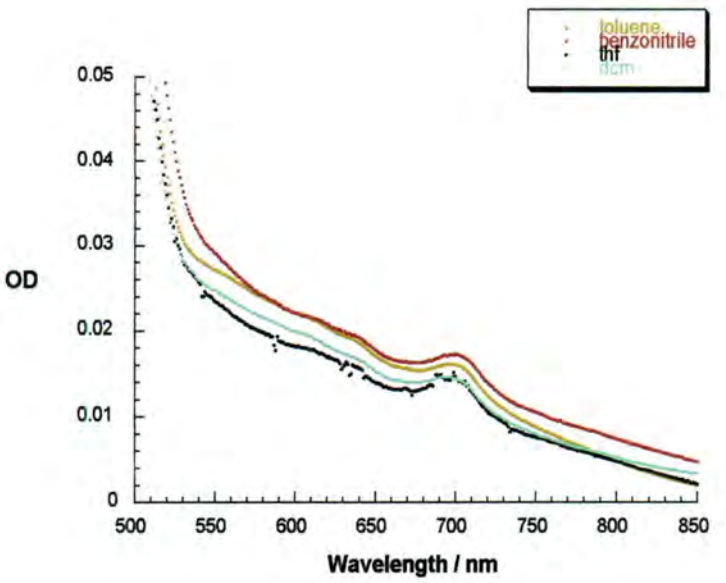


Figure G.2: Electronic absorption spectra of dyad **88** in different solvents (magnified Vis and near-infrared region is shown). The band at *ca.* 700 nm is consistent with an adduct at the more reactive [6,6]-ring junction with a closed transannular bond.

# Appendix H: Differential Absorption Spectra

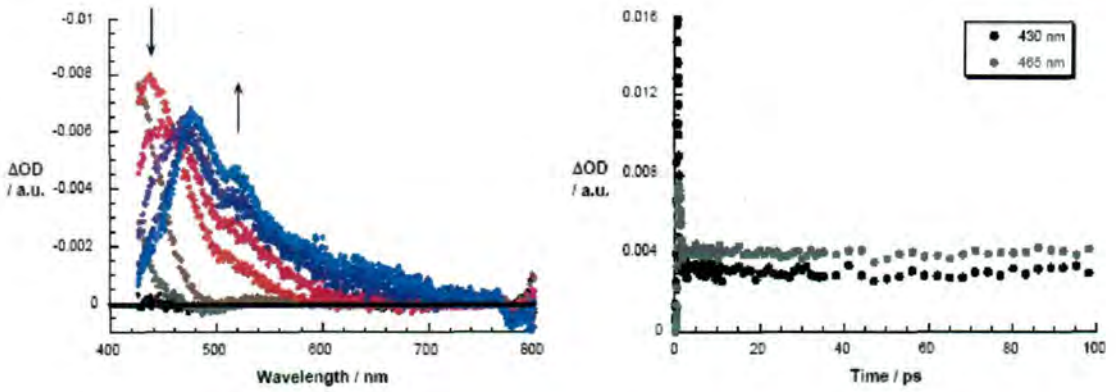


Figure H.1a (left): Differential absorption spectra (visible) obtained upon femtosecond flash photolysis (355 nm) of pyrene (~$1.0 \times 10^{-5}$ M) in nitrogen-saturated toluene solutions at different time delays between 0 and 10 ps at room temperature, indicating the pyrene singlet excited state formation. Figure H.1b (right): Time-absorption profiles of the spectra shown on the left at 430 and 465 nm, monitoring the excited state.

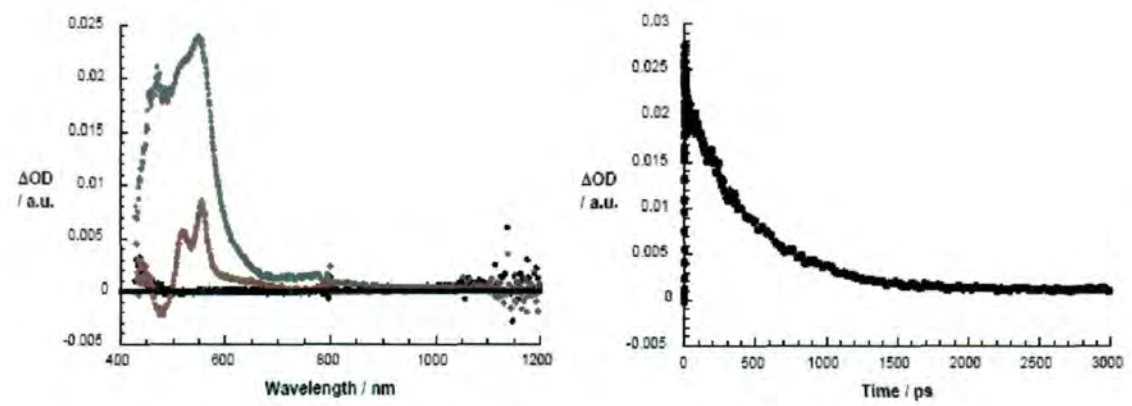


Figure H.2a (left): Differential absorption spectra (visible and near-infrared) obtained upon femtosecond flash photolysis (387 nm) of DTPY (~$1.0 \times 10^{-5}$ M) in nitrogen-saturated toluene solutions with time delays of 0 ps (black line), 5 ps (grey line) and 1500 ps (brown line) at room temperature, indicating the DTPY singlet and triplet excited state features. Figure H.2b (right): Time-absorption profiles of the spectra shown on the left at 590 nm, monitoring the singlet to triplet excited state transformation.

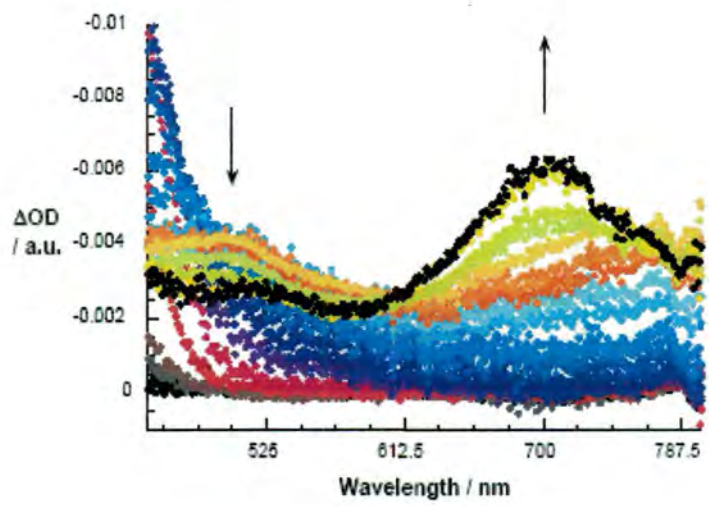


Figure H.3: Differential absorption spectra (visible and near-infrared) obtained upon femtosecond laser flash photolysis (380 nm) of ~$1.0 \times 10^{-5}$ M solutions of *N*-methyl pyrrolidinofullerene (**54**) in deaerated toluene at different time delays between 0 and 3000 ps at room temperature.

# References


1 The first transistor was invented by John Bardeen and Walter Brattain at Bell Labs.

2 R.L. Carroll, C.B. Gorman, *Angew. Chem. Int. Ed. Engl.* **2002**, *41*, 4378.

3 G.E. Moore, *Electronics* **1965**, *38*, 114.

4 G.E. Moore in *Digest of the 1975 International Electron Devices Meeting*, IEEE, New York, **1975**, pp. 1113.

5 R. Feynman presented a lecture entitled "There's Plenty of Room at the Bottom" on December 29th, 1959, at the annual meeting of the American Physical Society at the California Institute of Technology.

6 A. Aviram, M.A. Ratner, *Chem. Phys. Lett.* **1974**, *29*, 277.

7 C.R. Kagan, M.A. Ratner, *MRS Bull.* **2004**, *29*, 376.

8 A. Leger, J. Klein, M. Belin, D. Defourneau, *Thin Solid Films* **1971**, *8*, R51.

9 B. Mann, H. Kuhn, *J. Appl. Phys.* **1971**, *42*, 4398.

10 G. Binning, H. Rohrer, C. Gerber, E. Weibel, *Phys. Rev. Lett.* **1982**, *49*, 57.

11 Two news stories by R.F. Service ("Next-generation technology hits an early midlife crisis", (News Focus) *Science*, 24 Oct. **2003**, p. 556; "Nanodevices make fresh strides toward reality", (News of the Week) *Science*, 21 Nov. **2003**, p. 1310 sparked the discussion about the future of molecular electronics (*e.g.* (Letters) *Science*, 20 Feb **2004**, pp. 1136-1137).

12 *Nanoelectronics and Information Technology; Advanced Electronic Materials and Novel Devices* (Ed.: R. Waser), Wiley-VCH, Weinheim, **2003**.

13 V. Balzani, A. Credi, M. Venturi, *Molecular Devices and Machines*, Wiley-VCH, Weinheim, **2003**.

14 M.N. Paddon-Row in *Electron Transfer in Chemistry, Vol. 3* (Ed.: V. Balzani), Wiley-VCH, Weinheim, **2001**, pp. 181.

15 A.C. Benniston, A. Harriman, *Chem. Soc. Rev.* **2006**, *35*, 169.

16 *Electronic Materials: The Oligomer Approach* (Eds.: K. Müllen, G. Wegner), Wiley-VCH, Weinheim, **1998**.

17 *Fullerenes; Chemistry, Physics and Technology* (Eds.: K.M. Kadish, R.S. Ruoff), Wiley-VCH, Weinheim, **2000**.

18 *Electroanalytical Chemistry* (Eds.: A.J. Bard, I. Rubinstein), Dekker, New York, **1996**.

19 A.E. Kaifer, M.G. Gómez-Kaifer, *Supramolecular Electrochemistry*, Wiley-VCH, Weinheim, **1999**.

20 *Electron Transfer in Chemistry, Vol. 1* (Ed.: V. Balzani), Wiley-VCH, Weinheim, **2001**.

21 B.D. Wagner in *Handbook of Photochemistry and Photobiology, Vol. 3* (Ed.: H.S. Nalwa), American Scientific Publishers, Stevenson Ranch, **2003**, pp. 1.

22 *Functional Organic and Polymeric Materials* (Ed.: T.H. Richardson), Wiley-VCH, Weinheim, **2000**.

23 N.J. Turro, *Modern Molecular Photochemistry*, University Science Books, Sausalito, **1991**.

24 A. Gilbert, J. Baggott, *Essentials of Molecular Photochemistry*, Blackwell Scientific Publications, Oxford, **1991**.

25 C.J. Cramer, *Essentials of Computational Chemistry*, John Wiley & Sons Ltd, Chichester, **2002**.

26 *Handbook of Nanoscience, Engineering and Technology* (Eds.: W.A. Goddard, D.W. Brenner, S.E. Lyshevski, G.J. Iafrate), CRC Press, Boca Raton, **2003**.

27 F. Giacalone, J.L. Segura, N. Martín, J. Ramey, D.M. Guldi, *Chem. Eur. J.* **2005**, *11*, 4819.

28 P.F. Barbara, T.J. Meyer, M.A. Ratner, *J. Phys. Chem.* **1996**, *100*, 13148.

29 H.W. Kroto, J.R. Heath, S.C. O'Brien, R.F. Curl, R.E. Smalley, *Nature* **1985**, *318*, 162.

30 W. Krätschmer, L.D. Lamb, K. Fostiropoulos, D.R. Huffman, *Nature* **1990**, *347*, 354.

31 *Handbook of Organic Conductive Molecules and Polymers, Vol. 1* (Ed.: H.S. Nalwa), John Wiley & Sons Ltd, Chichester, **1997**.

32 S. Fukuzumi, D.M. Guldi in Electron Transfer in Chemistry, *Vol. 2* (Ed.: V. Balzani), Wiley-VCH, Weinheim, **2001**, pp. 270.

33 M. Fujitsuka, O. Ito in *Handbook of Photochemistry and Photobiology, Vol. 2* (Ed.: H.S. Nalwa), American Scientific Publishers, Stevenson Ranch, **2003**, p. 111.

34 M. Bühl, A. Hirsch, *Chem. Rev.* **2001**, *101*, 1153.

35 D.M. Guldi, M. Prato, *Acc. Chem. Res.* **2000**, *33*, 695.

63 N. Armaroli, F. Barigelletti, P. Ceroni, J.-F. Eckert, J.-F. Nicoud, J.-F. Nierengarten, *Chem. Commun.* **2000**, 599.

64 J.-F. Eckert, J.-F. Nicoud, J.-F. Nierengarten, S.-G. Liu, L. Echegoyen, F. Barigelletti, N. Armaroli, O. Ouali, V. Krasnikov, G. Hadziioannou, *J. Am. Chem. Soc.* **2000**, *122*, 7467.

65 J.-F. Nierengarten, J.-F. Eckert, J.-F. Nicoud, O. Ouali, V. Krasnikov, G. Hadziioannou, *Chem. Commun.* **1999**, 617.

66 E. Peeters, P.A. van Hal, J. Knol, C.J. Brabec, N.S. Sariciftci, J.C. Hummelen, R.A.J. Janssen, *J. Phys. Chem. B* **2000**, *104*, 10174.

67 N. Armaroli, G. Accorsi, J.-P. Gisselbrecht, M. Gross, V. Krasnikov, D. Tsamouras, G. Hadziioannou, M.J. Gómez-Escalonilla, F. Langa, J.-F. Eckert, J.-F. Nierengarten, *J. Mater. Chem.* **2002**, *12*, 2077.

68 M.J. Gómez-Escalonilla, F. Langa, J.-M. Rueff, F. Oswald, J.-F. Nierengarten, *Tetrahedron Lett.* **2002**, *43*, 7507.

69 M.J. Gómez-Escalonilla, J.-M. Rueff, T.M. Figueira-Duarta, J.-F. Nierengarten, V. Palermo, P. Samori, Y. Rio, G. Accorsi, N. Armaroli, *Chem. Eur. J.* **2005**, *11*, 4405.

70 T. Yamashiro, Y. Aso, T. Otsubo, H. Tang, Y. Harima, K. Yamashita, *Chem. Lett.* **1999**, *28*, 443.

71 M. Fujitsuka, O. Ito, T. Yamashiro, Y. Aso, T. Otsubo, *J. Phys. Chem. A* **2000**, *104*, 4876.

72 M. Fujitsuka, K. Matsumoto, O. Ito, T. Yamashiro, Y. Aso, T. Otsubo, *Res. Chem. Intermed.* **2001**, *27*, 73.

73 M. Fujitsuka, T. Makinoshima, A. Takamizawa, Y. Araki, O. Ito, Y. Obara, Y. Aso, T. Otsubo, *Bull. Chem. Soc. Jpn.* **2006**, *79*, 1860.

74 Y. Obara, K. Takimiya, Y. Aso, T. Otsubo, *Tetrahedron Lett.* **2001**, *42*, 6877.

75 P.A. van Hal, E.H.A. Beckers, S.C.J. Meskers, R.A.J. Janssen, B. Jousselme, P. Blanchard, J. Roncali, *Chem. Eur. J.* **2002**, *8*, 5415.

76 S.C.J. Meskers, P.A. van Hal, A.J.H. Spiering, J.C. Hummelen, A.F.G. van der Meer, R.A.J. Janssen, *Phys. Rev. B* **2000**, *61*, 9917.

77 J.L. Segura, R. Gómez, N. Martín, C. Luo, D.M. Guldi, *Chem. Commun.* **2000**, 701.

78 D.M. Guldi, C. Luo, A. Swartz, R. Gomez, J.L. Segura, N. Martín, C.J. Brabec, N.S. Sariciftci, *J. Org. Chem.* **2002**, *67*, 1141.

79 N. Bucci, T.J.J. Müller, *Tetrahedron Lett.* **2006**, *47*, 8329.

80 J.J. Apperloo, C. Martineau, P.A. van Hal, J. Roncali, R.A.J. Janssen, *J. Phys. Chem. A* **2002**, *106*, 21.

81 C. Martineau, P. Blanchard, D. Rondeau, J. Delaunay, J. Roncali, *Adv. Mater.* **2002**, *14*, 283.

82 P.A. van Hal, J. Knol, B.M.W. Langeveld-Voss, S.C.J. Meskers, J.C. Hummelen, R.A.J. Janssen, *J. Phys. Chem. A* **2000**, *104*, 5974.

83 N. Negishi, K. Takimiya, T. Otsubo, Y. Harima, Y. Aso, *Chem. Lett.* **2004**, *33*, 654.

84 K. Komatsu, Y. Murata, N. Takimoto, S. Mori, N. Sugita, T.S.M. Wan, *J. Org. Chem.* **1994**, *59*, 6101.

85 Y. Shirai, Y. Zhao, L. Cheng, J.M. Tour, *Org. Lett.* **2004**, *6*, 2129.

86 Y. Zhao, Y. Shirai, A.D. Slepkov, L. Cheng, L.B. Alemany, T. Sasaki, F.A. Hegmann, J.M. Tour, *Chem. Eur. J.* **2005**, *11*, 3643.

87 C. Atienza, B. Insuasty, C. Seoane, N. Martín, J. Ramey, G.M. Aminur Rahman, D.M. Guldi, *J. Mater. Chem.* **2005**, *15*, 124.

88 J.-F. Nierengarten, T. Gu, T. Aernouts, W. Geens, J. Poortmans, G. Hadziioannou, D. Tsamouras, *Appl. Phys. A* **2004**, *79*, 47.

89 T. Gu, D. Tsamouras, C. Melzer, V. Krasnikov, J.-P. Gisselbrecht, M. Gross, G. Hadziioannou, J.-F. Nierengarten, *ChemPhysChem* **2002**, 124.

90 T. Gu, J.-F. Nierengarten, *Tetrahedron Lett.* **2001**, *42*, 3175.

91 N. Zhou, L. Wang, D.W. Thompson, Y. Zhao, *Tetrahedron Lett.* **2007**, *48*, 3563.

92 D.M. Guldi, C. Luo, A. Swartz, R. Gómez, J.L. Segura, N. Martín, *J. Phys. Chem. A* **2004**, *108*, 455.

93 J.L. Segura, N. Martín, *Tetrahedron Lett.* **1999**, *40*, 3239.

94 F. Guo, K. Ogawa, Y.-G. Kim, E.O. Danilov, F.N. Castellano, J.R. Reynolds, K.S. Schanze, *Phys. Chem. Chem. Phys.* **2007**, *9*, 2724.

95 F. Giacalone, J.L. Segura, N. Martín, D.M. Guldi, *J. Am. Chem. Soc.* **2004**, *126*, 5340.

96 N. Martín, *Synth. Met.* **2004**, *147*, 57.

97 C. Atienza, N. Martín, M. Wielopolski, N. Haworth, T. Clark, D.M. Guldi, *Chem. Commun.* **2006**, 3202.

98 *Parasurf 07*, T. Clark, Jr-H. Lin, A.H.C. Horn © **2007** CEPOS InSilico Ltd.

99 H. Lanig, R. Koenig, T. Clark, *Tramp 1.1d* **2005**.

100 S. Handa, F. Giacalone, S.A. Haque, E. Palomares, N. Martín, J.R. Durrant, *Chem. Eur. J.* **2005**, *11*, 7440.

101 H. Kanato, M. Narutaki, K. Takimiya, T. Otsubo, Y. Harima, *Chem. Lett.* **2006**, *35*, 668.

102 H. Kanato, K. Takimiya, T. Otsubo, Y. Aso, M. Nakamura, Y. Araki, O. Ito, *J. Org. Chem.* **2004**, *69*, 7183.

103 M. Nakamura, H. Kanato, Y. Araki, O. Ito, K. Takimiya, T. Otsubo, Y. Aso, *J. Phys. Chem. A* **2006**, *110*, 3471.

104 F. Oswald, D.-M. Shafiqul Islam, Y. Araki, V. Troiani, P. de la Cruz, A. Moreno, O. Ito, F. Langa, *Chem. Eur. J.* **2007**, *13*, 3924.

105 J. Ikemoto, K. Takimiya, Y. Aso, T. Otsubo, M. Fujitsuka, O. Ito, *Org. Lett.* **2002**, *4*, 309.

106 M. Nakamura, M. Fujitsuka, Y. Araki, O. Ito, J. Ikemoto, K. Takimiya, Y. Aso, T. Otsubo, *J. Phys. Chem. B* **2004**, *108*, 10700.

107 M. Nakamura, J. Ikemoto, M. Fujitsuka, Y. Araki, O. Ito, K. Takimiya, Y. Aso, T. Otsubo, *J. Phys. Chem. B* **2005**, *109*, 14365.

108 M. Sun, P. Song, Y. Chen, F. Ma, *Chem. Phys. Lett.* **2005**, *416*, 94.

109 Y. Ie, T. Kawabata, T. Kaneda, Y. Aso, *Chem. Lett.* **2006**, *35*, 1366.

110 T. Oike, T. Kurata, K. Takimiya, T. Otsubo, Y. Aso, H. Zhang, Y. Araki, O. Ito, *J. Am. Chem. Soc.* **2005**, *127*, 15372.

111 G. de la Torre, F. Giacalone, J.L. Segura, N. Martín, D.M. Guldi, *Chem. Eur. J.* **2005**, *11*, 1267.

112 D.M. Guldi, F. Giacalone, G. de la Torre, J.L. Segura, N. Martín, *Chem. Eur. J.* **2005**, *11*, 7199.

113 D.M. Guldi, *Phys. Chem. Chem. Phys.* **2007**, *9*, 1400.

114 S.A. Vail, P.J. Krawczuk, D.M. Guldi, A. Palkar, L. Echegoyen, I.P.C. Tomé, M.A. Fazio, D.I. Schuster, *Chem. Eur. J.* **2005**, *11*, 3375.

115 S.A. Vail, D.I. Schuster, D.M. Guldi, M. Isosomppi, N. Tkachenko, H. Lemmetyinen, A. Palkar, L. Echegoyen, X. Chen, J.Z.H. Zhang, *J. Phys. Chem. B* **2006**, *110*, 14155.

116 D. Neher, *Macromol. Rapid Commun.* **2001**, *22*, 1365.

117 I.I. Perepichka, I.F. Perepichka, M.R. Bryce, L.-O. Pålsson, *Chem. Commun.* **2005**, 3397.

118 U. Scherf, E.J.W. List, *Adv. Mater.* **2002**, *14*, 477.

119 M. Svensson, F. Zhang, S.C. Veenstra, W.J.H. Verhees, J.C. Hummelen, J.M. Kroon, O. Inganäs, M.R. Andersson, *Adv. Mater.* **2003**, *15*, 988.

120 X. Wang, E. Perzon, F. Oswald, F. Langa, S. Admassie, M.R. Andersson, O. Inganäs, *Adv. Func. Mater.* **2005**, *15*, 1665.

121 F. Zhang, W. Mammo, L.M. Andersson, S. Admassie, M.R. Andersson, O. Inganäs, *Adv. Mater.* **2006**, *18*, 2169.

122 F. Zhang, E. Perzon, X. Wang, W. Mammo, M.R. Andersson, O. Inganäs, *Adv. Func. Mater.* **2005**, *15*, 745.

123 R.H. Goldsmith, L.E. Sinks, R.F. Kelley, L.J. Betzen, W. Liu, E.A. Weiss, M.A. Ratner, M.R. Wasielewski, *Proc. Nat. Acad. Sci.* **2005**, *102*, 3540.

124 N. Miyaura, T. Yanagi, A. Suzuki, *Synth. Commun.* **1981**, *11*, 513.

125 J. Hassan, M. Sevignon, C. Gozzi, E. Schulz, M. Lemaire, *Chem. Rev.* **2002**, *102*, 359.

126 A.L. Kanibolotsky, R. Berridge, P.J. Skabara, I.F. Perepichka, D.D.C. Bradley, M. Koeberg, *J. Am. Chem. Soc.* **2004**, *126*, 13695.

127 A. Suzuki, *J. Organomet. Chem.* **2002**, *653*, 83.

128 N. Miyaura, A. Suzuki, *Chem. Rev.* **1995**, *95*, 2457.

129 N.T.S. Phan, M.V.D. Sluys, C.W. Jones, *Adv. Synth. Catal.* **2006**, *348*, 609.

130 A. Suzuki, *J. Organomet. Chem.* **1999**, *576*, 147.

131 P. Fitton, E.A. Rick, *J. Organomet. Chem.* **1971**, *28*, 287.

132 T.I. Wallow, B.M. Novak, *J. Org. Chem.* **1994**, *59*, 5034.

133 J.C. Perrine, R.N. Keller, *J. Am Chem. Soc.* **1958**, *80*, 1823.

134 T. Ishiyama, J. Takagi, A. Kamon, N. Miyaura, *J. Organomet. Chem.* **2003**, *687*, 284.

135 S.P. Dudek, M. Pouderoijen, R. Abbel, A.P.H.J. Schenning, E.W. Meijer, *J. Am. Chem. Soc.* **2005**, *127*, 11763.

136 G. Hughes, C. Wang, A.S. Batsanov, M. Fearn, S. Frank, M.R. Bryce, I.F. Perepichka, A.P. Monkman, B.P. Lyons, *Org. Biomol. Chem.* **2003**, *1*, 3069.

137 B. Li, J. Li, Y. Fu, Z. Bo, *J. Am. Chem. Soc.* **2004**, *126*, 3430.

138 L. Zhu, J. Duquette, M. Zhang, *J. Org. Chem.* **2003**, *68*, 3729.

139 R. Anémian, J.-C. Mulatier, C. Andraud, O. Stéphan, J.-C. Vial, *Chem. Commun.* **2002**, 1608.

140 M. Prato, M. Maggini, *Acc. Chem. Res.* **1998**, *31*, 519.

141 M. Maggini, G. Scorrano, M. Prato, *J. Am. Chem. Soc.* **1993**, *115*, 9798.

142 P. Atkins, L. Jones, *Chemical Principles*, fourth ed., W.H. Freeman and Company, New York, **2008**.

143 F. Giacalone, J.L. Segura, N. Martín, *J. Org. Chem.* **2002**, *67*, 3529.

144 M.R. Bryce, A.J. Moore, *J. Chem. Soc. Perkin Trans. 1* **1991**, 157.

145 M.R. Bryce, A.J. Moore, M. Hasan, G.J. Ashwell, A.T. Fraser, W. Clegg, M.B. Hursthouse, A.I. Karaulov, *Angew. Chem. Int. Ed. Engl.* **1990**, *29*, 1450.

146 Y. Yamashita, Y. Kobayashi, T. Miyashi, *Angew. Chem. Int. Ed. Engl.* **1989**, *28*, 1052.

147 N. Martín, I. Pérez, L. Sánchez, C. Seoane, *J. Org. Chem.* **1997**, *62*, 870.

148 N. Martín, L. Sánchez, C. Seoane, C. Fernández, *Synth. Met.* **1996**, *78*, 137.

149 M.C. Díaz, M. Herranz, B.M. Illescas, N. Martín, N. Godbert, M.R. Bryce, C. Luo, A. Swartz, G. Anderson, D.M. Guldi, *J. Org. Chem.* **2003**, *68*, 7711.

150 M.C. Díaz, B.M. Illescas, C. Seoane, N. Martín, *J. Org. Chem.* **2004**, *69*, 4492.

151 P.K. Tsolakis, J.K. Kallitsis, *Chem. Eur. J.* **2003**, *9*, 936.

152 D.M. Guldi, L. Sánchez, N. Martín, *J. Phys. Chem. B* **2001**, *105*, 7139.

153 A.E. Jones, C.A. Christensen, D.F. Perepichka, A.S. Batsanov, A. Beeby, P.J. Low, M.R. Bryce, A.W. Parker, *Chem. Eur. J.* **2001**, *7*, 973.

154 *Electron Transfer: From Isolated Molecules to Biomolecules* (Eds.: M. Bixon, J. Jortner), Wiley, New York, **1999**.

155 *Photoinduced Electron Transfer* (Eds.: M.A. Fox, M. Chanon), Elsevier, Amsterdam, **1988**.

156 *The Porphyrin Handbook, Vol. 8* (Eds.: K.M. Kadish, K.M. Smith, R. Guilard), Academic Press, San Diego, **2000**.

157 *Porphyrins and Metalloporphyrins* (Ed.: K.M. Smtih), Elsevier Scientific, Amsterdam, **1975**.

158 P. Piotrowiak, *Chem. Soc. Rev.* **1999**, *28*, 143.

159 Y. Nakamura, N. Aratani, A. Osuka, *Chem. Soc. Rev.* **2007**, *36*, 831.

160 D. Holten, D.F. Bocian, J.S. Lindsey, *Acc. Chem. Res.* **2002**, *35*, 57.

161 A.D. Adler, F.R. Longo, J.D. Finarelli, J. Goldmacher, J. Assour, L. Korsakoff, *J. Org. Chem.* **1967**, *32*, 476.

162 J.T. Groves, R. Quinn, T.J. McMurry, M. Nakamura, G. Lang, B. Boso, *J. Am. Chem. Soc.* **1985**, *107*, 354.

163 J.S. Lindsey, I.C. Schreiman, H.C. Hsu, P.C. Kearney, A.M. Marguerettaz, *J. Org. Chem.* **1987**, *52*, 827.

164 Z. Fei, B. Li, Z. Bo, R. Lu, *Org. Lett.* **2004**, *6*, 4703.

165 C.A. Barker, X. Zeng, S. Bettington, A.S. Batsanov, M.R. Bryce, A. Beeby, *Chem. Eur. J.* **2007**, *13*, 6710.

166 L. Yu, J.S. Lindsey, *Tetrahedron* **2001**, *57*, 9285.

167 R.W. Wagner, Y. Ciringh, P.C. Clausen, J.S. Lindsey, *Chem. Mater.* **1999**, *11*, 2974.

168 R.W. Wagner, T.E. Johnson, F. Li, J.S. Lindsey, *J. Org. Chem.* **1995**, *60*, 5266.

169 G. Doisneau, G. Balavoine, T. Fillebeen-Khan, *J. Organomet. Chem.* **1992**, *425*, 113.

170 R. Chinchilla, C. Nájera, *Chem. Rev.* **2007**, *107*, 874.

171 H. Doucet, J.-C. Hierso, *Angew. Chem. Int. Ed. Engl.* **2007**, *46*, 834.

172 J.A. Marsden, M.M. Haley in *Metal-Catalyzed Cross-Coupling Reactions* (Eds.: A. de Meijere, F. Diederich), Wiley-VCH, Weinheim, **2004**, pp. 317.

173 K. Sonogashira, Y. Tohda, N. Hagihara, *Tetrahedron Lett.* **1975**, *16*, 4467.

174 W.-Y. Wong, G.-L. Lu, K.-F. Ng, C.-K. Wong, K.-H. Choi, *J. Organomet. Chem.* **2001**, *637-639*, 159.

175 D.M. Guldi, *Chem. Commun.* **2000**, 321.

176 D.M. Guldi, S. Fukuzumi in *Fullerenes: From Synthesis to Optoelectronic Properties* (Eds.: D.M. Guldi, N. Martín), Kluwer, Dordracht, **2003**, pp. 237.

177 D.M. Guldi, P.V. Kamat in *Fullerenes, Chemistry, Physics and Technology* (Eds.: K.M. Kadish, R.S. Ruoff), Wiley-Interscience, New York, **2000**, pp. 225.

178 D. Gust, T.A. Moore, A.L. Moore in *Electron Transfer in Chemistry, Vol. 3* (Ed.: V. Balzani), Wiley-VCH, Weinheim, **2001**, pp. 272.

179 T. Hasobe, S. Fukuzumi, P.V. Kamat, *Interface* **2006**, *15*, 47.

180 T. Hasobe, H. Imahori, P.V. Kamat, T.K. Ahn, D. Kim, T. Hanada, T. Hirakawa, S. Fukuzumi, *J. Am. Chem. Soc.* **2005**, *127*, 1216.

181 T. Hasobe, P.V. Kamat, V. Troiani, N. Solladié, T.K. Ahn, S.K. Kim, D. Kim, A. Kongkanand, S. Kuwabata, S. Fukuzumi, *J. Phys. Chem. B* **2005**, *109*, 19.

182 K. Nakasuji, H. Kubota, T. Kotani, I. Murata, G. Saito, E. T, K. Imaeda, H. Inokuchi, M. Honda, C. Katayama, J. Tanaka, *J. Am. Chem. Soc.* **1986**, *108*, 3460.

183 K. Nakasuji, J. Toyoda, K. Imaeda, H. Inokuchi, I. Murata, A. Oda, A. Kawamoto, J. Tanaka, *Synth. Metals* **1991**, *42*, 2529.

184 Y. Morita, E. Miyazaki, J. Toyoda, K. Nakasuji, *Bull. Chem. Soc. Jpn.* **2003**, *76*, 205.

185 Y. Morita, E. Miyazaki, J. Kawai, K. Sato, D. Shiomi, T. Takui, K. Nakasuji, *Polyhedron* **2003**, *22*, 2219.

186 Y. Morita, E. Miyazaki, H. Yamochi, G. Saito, K. Nakasuji, *Synth. Metals* **2003**, *135-136*, 581.

187 E. Miyazaki, Y. Morita, K. Nakasuji, *Polyhedron* **2005**, *24*, 2632.

188 M. Eiermann, R.G. Hicks, B.W. Knight, H. Neugebauer, F. Wudl, *Electrochem. Soc. Proceedings* **2004**, *22*, 407.

189 S. Mitsumori, T. Tsuri, T. Honma, Y. Hiramatsu, T. Okada, H. Hashizume, S. Kida, M. Inagaki, A. Arimura, K. Yasui, F. Asanuma, J. Kishino, M. Ohtani, *J. Med. Chem.* **2003**, *46*, 2446.

190 A.J. Seed, J.T. Kenneth, J.W. Goodby, M. Hird, *J. Mater. Chem.* **2000**, *10*, 2069.

191 M. Bendikov, F. Wudl, D.F. Perepichka, *Chem. Rev.* **004**, *104*, 4891.

192 M.T. Rispens, L. Sánchez, J. Knol, J.C. Hummelen, *Chem. Commun.* **2001**, 161.

193 T. Ohno, K. Moriwaki, T. Miyata, *J. Org. Chem.* **2001**, *66*, 3397.

194 K. Lee, Y.J. Choi, Y.-J. Cho, C.Y. Lee, H. Song, C.H. Lee, Y.S. Lee, J.T. Park, *J. Am. Chem. Soc.* **2004**, *126*, 9837.

195 F. Langa, P. de la Cruz, E. Espildora, A. de la Hoz, J.L. Bourdelande, L. Sanchez, N. Martín, *J. Org. Chem.* **2001**, *66*, 5033.

196 F. Langa, P. de la Cruz, E. Espíldora, A. Gonzalez-Cortés, A. de la Hoz, V. López-Arza, *J. Org. Chem.* **2000**, *65*, 8675.

197 M.Á. Herranz, J. C. T. Cox, L. Echegoyen, *J. Org. Chem.* **2003**, *68*, 5009.

198 F. Hauke, A. Hirsch, S.-G. Liu, L. Echegoyen, A. Swartz, C. Luo, D.M. Guldi, *ChemPhysChem* **2002**, *3*, 195.

199 R. Gómez, J.L. Segura, N. Martín, *Org. Lett.* **2005**, *7*, 717.

200 M. Carano, T.D. Ros, M. Fanti, K. Kordatos, M. Marcaccio, F. Paolucci, M. Prato, S. Roffia, F. Zerbetto, *J. Am. Chem. Soc.* **2003**, *125*, 7139.

201 S. Amriou, A. Mehta, M.R. Bryce, *J. Mater. Chem.* **2005**, *15*, 1232.

202 H. Imahori, K. Tamaki, D.M. Guldi, C. Luo, M. Fujitsuka, O. Ito, Y. Sakata, S. Fukuzumi, *J. Am. Chem. Soc.* **2001**, *123*, 2607.

203 A.S.D. Ssandanayaka, Y. Araki, O. Ito, G.R. Deviprasad, P.M. Smith, L.M. Rogers, M.E. Zandler, F. D'Soura, *Chem. Phys.* **2006**, *325*, 452.

204 R.A. Marcus, N. Sutin, *Biochim. Biophys. Acta* **1985**, *811*, 265.

205 R.A. Marcus, *Angew. Chem. Int. Ed. Engl.* **1993**, *32*, 1111.

206 R.A. Marcus, *Annu. Rev. Phys. Chem.* **1964**, *15*, 155.

207 D. Bonifazi, O. Enger, F. Diederich, *Chem. Soc. Rev.* **2007**, *36*, 390.

208 D. Hirayama, T. Yamashiro, K. Takimiya, Y. Aso, T. Otsubo, H. Norieda, H. Imahori, Y. Sakata, *Chem. Lett.* **2000**, *29*, 570.

209 D. Hirayama, K. Takimiya, Y. Aso, T. Otsubo, T. Hasobe, H. Yamada, H. Imahori, S. Fukuzumi, Y. Sakata, *J. Am. Chem. Soc.* **2002**, *124*, 532.

210 K. Kim, -S, M.-S. Kang, H. Ma, A.K.-Y. Jen, *Chem. Mater.* **2004**, *16*, 5058.

211 Y. Shirai, L. Cheng, B. Chen, J.M. Tour, *J. Am. Chem. Soc.* **2006**, *128*, 13479.

212 T. Pinault, F. Chérioux, B. Therrien, G. Süss-Fink, *Heteroatom Chem.* **2004**, *15*, 121.

213 R. Adams, A. Ferretti, *J. Am. Chem. Soc.* **1959**, *81*, 4927.

214 N. Stuhr-Hansen, *Synth. Commun.* **2003**, *33*, 641.

215 A. Blaszczyk, M. Elbing, M. Mayor, *Org. Biomol. Chem.* **2004**, *2*, 2722.

216 E. Janata, *Radia. Phys. Chem.* **1992**, *40*, 437.

217 M. J. Frisch, G. W. Trucks, H. B. Schlegel, G. E. Scuseria, M. A. Robb, J. R. Cheeseman, J. A. Montgomery, Jr., T. Vreven, K. N. Kudin, J. C. Burant, J. M. Millam, S. S. Iyengar, J. Tomasi, V. Barone, B. Mennucci, M. Cossi, G. Scalmani, N. Rega, G. A. Petersson, H. Nakatsuji, M. Hada, M. Ehara, K. Toyota, R. Fukuda, J. Hasegawa, M. Ishida, T. Nakajima, Y. Honda, O. Kitao, H. Nakai, M. Klene, X. Li, J. E. Knox, H. P. Hratchian, J. B. Cross, V. Bakken, C. Adamo, J. Jaramillo, R. Gomperts, R. E. Stratmann, O. Yazyev, A. J. Austin, R. Cammi, C. Pomelli, J. W. Ochterski, P. Y. Ayala, K. Morokuma, G. A. Voth, P. Salvador, J. J. Dannenberg, V. G. Zakrzewski, S. Dapprich, A. D. Daniels, M. C. Strain, O. Farkas, D. K. Malick, A. D. Rabuck, K. Raghavachari, J. B. Foresman, J. V. Ortiz, Q. Cui, A. G.

Baboul, S. Clifford, J. Cioslowski, B. B. Stefanov, G. Liu, A. Liashenko, P. Piskorz, I. Komaromi, R. L. Martin, D. J. Fox, T. Keith, M. A. Al-Laham, C. Y. Peng, A. Nanayakkara, M. Challacombe, P. M. W. Gill, B. Johnson, W. Chen, M. W. Wong, C. Gonzalez, J. A. Pople, *Gaussian 03*, *Revision B.04*, Gaussian, Inc.: Wallingford CT, **2004**.

218 A.D. Becke, *J. Chem. Phys.* **1993**, *98*, 5648.

219 A.D. Becke, *Phys. Rev. A* **1988**, *38*, 3098.

220 C. Lee, W. Yang, R.G. Parr, *Phys. Rev. B* **1988**, *37*, 785.

221 S. Portmann, H.P. Lüthi, *Chimia* **2000**, *54*, 766.

222 P. Flükiger, H.P. Lüthi, S. Portmann, J. Weber, *Molekel*, *Version 4.3*, Swiss Center for Scientific Computing, Manno (Switzerland), **2002**.